Polymer bioadhesives for drug delivery

PhD Thesis

Matthew Deacon

1999

Supervisors: Prof. S.E. Harding (Division of Food sciences)
Prof. S.S. Davis (School of Pharmaceutical sciences)

Industrial supervisor: Dr. R. White (Optokem Inst., Wrexham)

Table of Contents

List of Figures

Abstract

This study is a natural follow on from previous work by M.T. Anderson and I. Fiebrig. The goal of those latter and of the present study is to find a mucoadhesive system for improving the oral bioavailability of a number of drugs, for example bioactive peptides and proteins. This current work evaluates the adhesive properties of a cationic polymer and a cationic protein to mucus glycoproteins as a step towards the future development of a mucoadhesive drug delivery system.

Four different mucin populations were analysed in solution (a freshly purified sample PGM-MD, and three purified from different regions of the porcine stomach cardiac, antrum and fundus). Their interaction with two groups of chitosans differing in degree of deacetylation (F_A = 0.11 and 0.25) and a protein purified from the foot of the blue mussel *Mytilus edulis* foot protein-1 (Mefp-1) were studied. Interaction was determined using analytical ultracentrifugation and with the chitosan/mucin interaction specifically atomic force microscopy. The influence of ionic strength on the interaction was studied in detail studied as was the effect of the oligosaccharide composition of the mucin population on the interaction.

It was found that both groups of chitosans (F_A = 0.11 and 0.25) formed a large complex with a freshly purified mucin population (PGM-MD). Ionic strengths above 0.2 M were found to inhibit the interaction. The three mucin species differed in terms of their net charge, with cardiac being the most negatively charged and antrum the least negative. It was found that the cardiac species interacted the most and antrum the least, as would be expected for an ionic interaction. Increasing ionic strength was found to inhibit the interaction. There was also evidence for a hydrophobic interaction at high ionic strengths.

The atomic force microscopy results allowed the complex to be visualised under atmospheric conditions and to get away from the harsh sample preparation techniques

employed by electron microscopy. Large spherical complexes were seen as entanglements of mucin and chitosan strands.

Acknowledgements

To my supervisors, principally Prof. S.E. Harding, also to Dr. R. White and Prof. S.S. Davis, for their encouragement and support over the last 3 years.

Thanks go to Dr. Simon McGurk who collaborated with me on all of the AFM work. To Prof. Martyn Davies, Prof. Saul Tendler, Dr. Phil Williams, Dr. Clive Roberts and to Prof. X. Chen and all in the LBSA lab for their help.

To my girlfriend, Ellen, for reading countless drafts of this thesis and for keeping me sane over the last nine months.

For all the people in the lab who have answered all my questions specifically Connie, Neil, Arthur and of course Uncle Pete, Krim, Chris, and Gordon.

To all my friends at Food Science over the past three years principally Raj, Claire, Inger, Baltasar, Zoë and my flatmate Joe the rest, who have been responsible for many good evenings and quite a few bad mornings.

The BBSRC and Optokem Instruments for the funding of this PhD.

And last of all to my parents, sister Louise and brothers Neal and Peter and the rest of the family for all of their love and support both financial and emotional over the last 26 years.

Abbreviations

AFM	Atomic force microscopy
FFF	Field flow fractionation
HBS	Hydrodynamically balanced systems
MALLS	Multi angle laser light scattering
M_w	Weight average molecular weight
N.D.	Not determined
PGM	Pig gastric mucin
PMSF	Phenylmethanesulphonyl fluoride
RI	Refractive index
$S^0_{20,w}$	Sedimentation coefficient at 20°C in water extrapolated to zero concentration
SC210 +	Sea Cure 210 + a glutamate salt chitosan Pronova, Norway
SEC	Size exclusion chromatography
STM	Scanning tunneling microscopy
TEM	Transmission electron microscopy
$\bar{\nu}$	v-bar: partial specific volume (g/ml)

Chapter 1

Introduction

1.1 Drug delivery

The delivery of drugs into the body can take many forms; patches, injections, creams and, of course, the most favoured route - oral delivery. Oral delivery is the favoured route because of the ease of taking to the prospective patient. The administration of pharmaceutical dosage forms via the mouth is generally well accepted. It can easily be taken anywhere and is safe. In contrast invasive methods, injection for example, usually require the assistance of trained health care personnel and these procedures involve certain risks.

The oral administration of a drug begins with ingestion of the dosage form through the mouth. It then passes down the oesophagus into the stomach. Little drug is absorbed in the stomach due to its relatively small surface area. The major site for the absorption of most drugs is the small intestine. It is ideal because of its large surface area (~100 m^2 in a healthy adult) and near neutral pH (Davis, 1989). Theoretically, drug absorption can occur along the entire length of the small intestine, however the majority of drugs are actually absorbed from the proximal small intestine (Booth, 1967). However if the drug is poorly soluble or is in a controlled release dosage form then significant absorption can also take place in the large intestine (Davis, 1989) despite the fact that it has a limited surface area. Oral drug delivery ceases eventually with the faecal excretion of any unabsorbed drug.

There are however many barriers to delivery of oral drugs; chemical degradation in the stomach, gastric emptying, intestinal motility, solubility and metabolic breakdown during

passage through the mucosa and subsequent first-pass metabolism by the liver (Li *et al.*, 1987). Because of these the actual bioavailability of a drug can be much smaller than that ingested.

It is believed for many dosage forms that the critical factor in its absorption from the gut is its residence time in the small intestine. So a possible method for increasing bioavailability would be to increase the residence time of the dosage form in the gastrointestinal tract through adhesion to the mucous. An example of such a drug is hydrochlorothiazide a polar drug whose bioavailability is believed to be dependent on its residence time at or upstream of its small intestinal absorption window (Beermann *et al.*, 1976; Lynch *et al.*, 1987). It is also important in the case of controlled release drug delivery systems, which are designed to release drugs over an extended period of time (4-12 hours for example). Once these have passed the optimal site for absorption (i.e. the small intestine) they are delivering drug to a non-optimal site for absorption. (Davis, 1985). The ideal controlled release system should release drug at a constant rate to maintain a constant plasma level comparable to that of an intravenous infusion (Förster and Lippold, 1982).

Adhesion can be defined as when two or more molecules are attached to each other by interfacial features for what is defined as an 'extended' period of time (Duchêne *et al.*, 1988). Bioadhesion refers to adhesive phenomena where at least one of the adhesives is of biological nature, it is referred to as mucoadhesion when the biological substrate is a mucosal surface.

1.2 Methods to delay gastrointestinal transit

Many attempts have been made to delay gastrointestinal transit. These have involved pharmacological, physiological as well as pharmaceutical approaches. Pharmacological approaches involve the co-administration into the drug preparation of another drug that acts to delay gastrointestinal emptying such as antimuscarinics, for example

propantheline which is a smooth muscle relaxant (Beerman and Grochinsky-Grind, 1978). Another alternative is to use a drug that changes intestinal motility, for example opiate analgesics or derivatives such as loperamide (Minami and McCallum, 1984). There are of course potential side effects from regular use of these methods, which makes their regulatory approval doubtful.

A physiological approach is the use of natural materials or fat derivatives such as triethanolamine myristate (Gröning and Heun, 1984, 1989), which stimulate the duodenal or jejunal receptors to slow gastric emptying. The use of large amounts of a volume filling polymer such as polycarbophil (Harris *et al.*, 1990a,b) can induce a fed-like state and delay gastric emptying due to a blocking effect.

Pharmacological and physiological approaches thus set out to delay gastrointestinal transit by modification of the rate of gastric emptying using delaying agents. By contrast, pharmaceutical strategies attempt to achieve the same objective by actually retaining the dosage form at or upstream of its absorption site for as long as possible. This is achieved by a particular physical or physicochemical characteristic. Mucoadhesion is one method by which this can be achieved.

(i) Swelling balloon hydrogel. If large enough, the formulation will not be expelled from the fasted stomach even when the pyloric sphincter is in its non-contracted state. The size of such systems has to increase after ingestion to an extent that gastric emptying is totally inhibited (Moës, 1993). The size-related retention of a dosage form in the stomach has been studied with various systems to include systems such as swelling balloon hydrogels (Park and Park, 1987) or unfolding stratified medicated polymer sheets (BE Patent No. 867, 692) or non-erodible or erodible tetrahedron shaped devices (Cargill *et al.*, 1988, 1989). These have never passed beyond the experimental stage and clinical data are unavailable. In any case these gastric retention devices may not be safe. The hazard of lodging in the oesophagus (Kikendall *et al.*, 1983; Al-Dujaili *et al.*, 1983; Wilson, 1990) or permanent retention in the stomach with cumulative effects (Brahams, 1984; Vere, 1984) could lead to life-threatening problems.

Another approach uses dosage forms of moderately high density, based on the premise that high density formulations remain in the stomach longer than conventional formulations, since they would be localised in the lower part of the antrum provided the density exceeds that of the normal stomach contents, i.e. > 1.4 g/ml (Bechgaard and Ladefoged, 1978). The effectiveness of this approach has not been confirmed on a broad basis and the evidence remains controversial (Moës, 1993).

(ii) *Buoyant density/ flotation approach.* This approach uses buoyant dosage forms which float on the gastric contents as a result of their relatively low density. Floating dosage forms have been discussed extensively by Moës (1993): The first floating dosage forms (F forms) (Sheth and Tossounian 1984), also called 'hydrodynamically balanced systems' (HBS), were able to maintain their low density while a polymer hydrated and built a gelled barrier at the outer surface. Hoffmann-LaRoche produced patents for floating drug delivery systems and *in vivo* studies on diazepam HBS capsules such as Valium® CR and Valrelease® and the L-dopa plus benserazide containing formulation Madopar® HBS (Prolopa® HBS). Moës (1993) has attempted to clarify the conflicting views on the gastric retention capabilities of floating systems resulting from a number of *in vivo* trials by different authors (Müller-Lissner and Blum, 1981; Davis *et al.*, 1986; Timmermans and Moës, 1990; Kaus, 1987; Sangekar *et al.*, 1987).

(iii) Polymer mucoadhesion. This involves attachment or encapsulation of the drug with a polymer which interacts with either the mucosal epithelia/ glycocalyx lining of the gastrointestinal tract (this is called 'direct' mucoadhesion) or mucous surfaces (the gel and the sloughed mucus in the lumen) lining the gastrointestinal tract hence providing a macromolecular 'brake' to the movement of the drug. A good challenge for mucoadhesion is the delivery of orally administered polar drugs (and possibly peptides and proteins). These materials have low absorption characteristics (and for peptides and proteins have stability problems due to enzymatic degradation and biotransformation). A mucoadhesive alternative route to parenteral administration would be highly desirable (Wearley, 1991).

If the polymer carrier can access and interact directly with the surface mucosal epithelium or glycocalyx, the decrease in diffusion path from the oral drug delivery system to the absorbing biological membrane could be an additional advantage for improving absorption particularly in intestinal delivery of peptide drugs, at the same time minimizing dilution and possible degradation in the luminal fluids (Hayton, 1980). The further addition of penetration enhancers to an adhering dosage form could enable alteration of membrane permeability and inclusion of specific enzyme inhibitors could prevent early degradation of the peptide (Wearly, 1991) and consequently increase bioavailability. However, the epithelium may not be accessible: instead the indirect route of interaction with the ~ 40-450 μm thick mucosal surface/ gel lining the gastrointestinal tract provides the most likely strategy. It is also worth noting that mucus is also not a major barrier to absorption.

The adhesion of gastrointestinal retention dosage forms to the mucosa has been studied for over a decade, mainly by *in vitro* or *ex vivo* test with few *in situ* or *in vivo* studies and even fewer trials in man. Despite the fact that bioadhesion, or more specifically mucoadhesion, has led to some success in drug delivery for ocular, buccal, nasal, vaginal and cervical applications (Chen and Cyr, 1970; Schor *et al.*, 1983; Nagai *et al.*, 1984; Nagai, 1986; Duchêne *et al.*, 1988; Greaves and Wilson, 1993; Smart, 1993; Bouckaert, *et al.*, 1994), gastrointestinal mucoadhesive drug delivery systems have yet to be succesfully established (see, e.g., Helliwell, 1993; Fiebrig *et al.*, 1995a).

1.3 The mucosal lining

The last ten years has also seen a tremendous advance in our understanding of the structure and molecular biology of mucus, and in particular its major macromolecular component, mucin. Mucus is a viscoelastic substance with a characteristic stickiness and ability to stretch into strands. By weight mucus mostly consists of water (95%–99.5%) and exists in a gel or in a viscous solution. Its most important polymeric, gel-forming component is the mucus glycoprotein mucin (0.5%–5%) (Harding, 1989; Carlstedt and

Sheehan, 1988; Neutra and Forstner, 1987; Gibbons, 1972). Specialised cells secrete the adherent mucus layer in the gastrointestinal tract. They are surface epithelial cells found mostly in the stomach but also in other parts of the gut and the goblet cells of the small and large intestine, as well as Brunner's glands in the duodenum (Neutra and Forstner, 1987; Allen, 1989). Unlike other gastrointestinal secretions, mucus adheres to the mucosal epithelial surfaces as a water insoluble gel until degradation and erosion takes place (Allen, 1989) leaving a mucin solution or slough on the lumen side of the gel.

For monitoring the thickness of the mucin a novel method has been developed which for the first time enables the preservation and visualization of the full thickness of the adherent gastric mucus layer and the underlying mucosa (Jordan *et al.*, 1998). This involves a modified periodic acid Schiff/Alcian Blue staining technique for use on cryostat sections of gastric mucosa.

It is believed that the adherent mucus layer plays a major role in protection of the delicate underlying epithelium against endogenous and exogenous attack, such as acidic pH (providing a boundary layer), digestive enzymes (pepsin), pathogens (bacteria) and abrasion, while the soluble mucus may play an important role in acting as a lubricant for ingested food. The requirement for such a protective adherent gel layer is obvious since from a physiological point of view the luminal side of the gastrointestinal tract can still be considered as the outer side of the body. These and other aspects regarding the function of mucus have been extensively described by various authors e.g. Allen (1981, 1983, 1989), Silberberg and Meyer (1982) and Bhaskar *et al.*, (1992). Chemical analysis of the mucus gives evidence of a heterogeneous material which also contains small amounts of a variety of proteins, lipids, bacteria, sloughed-off epithelial cells and in some cases nucleic acids (Creeth, 1978). It becomes clear that mucoadhesion is a process that involves large amounts of water, where the mucins play a key role in maintaining the gel-like properties of the substrate for a potential drug delivery platform. The mucins themselves display considerable heterogeneity that has been well described elsewhere (e.g. Carlstedt and Sheehan, 1984; Neutra and Forstner, 1987; Allen, 1989; Sheehan and Carlstedt, 1989; Harding, 1984, 1989).

1.4 Mucin

Mucins are large molecules with molecular weights ranging from 0.5×10^6 to over 20×10^6 g/mol. They contain large amounts of carbohydrate (for gastrointestinal mucins 70%–80% carbohydrate, 12%–25% protein and up to ~5% ester sulphate). Undegraded mucins are made up of multiples of a basic unit (M~400,000–500,00), linked together into the macroscopic mucin molecule. Although originally thought to be arranged in a windmill type of structure (Allen, 1978), this model has since been shown to be incorrect: Instead the molecule is linked into linear arrays as shown by Creeth, Harding and coworkers (Harding *et al.*, 1983a,b) and by Carlstedt, Sheehan and coworkers (Carlstedt & Sheehan, 1984). Although linear, the mucin molecule in solution is loosely/ randomly coiled into a spheroidal, highly swollen domain as confirmed by molecular hydrodynamics. Examples from electron microscopy clearly showing both these features are presented in Figure 1.1 which shows the linear secondary structure (Figure 1.1a) and the highly glycosylated spheroidal domains (Figure 1.1b) (Fiebrig *et al.*, 1995b). The total architecture seems to be very similar for mucins from a variety of sources (for example gastric, respiratory or cervical). The basic units are linked together by regions of low or no glycosylation which are subject to trypsin digestion: the ~400-500 kDa digestion products are thus commonly referred to as 'T-domains' (see Sheehan and Carlstedt, 1989). Every third or fourth T-domain is linked by a disulphide bridge, itself susceptible to reductive disruption by thiols. The thiol reduction products (of molecular weight between 1.5 and 2.5 MDa) are commonly referred to as 'subunits'. One of the most recent examples of such architecture in a mucin is that of colonic mucin (Figure 1.2) (Jumel *et al.*, 1997). Even mucins produced externally by cell-lines appear to adopt this architecture, although they appear to be only up to one or two subunits in length (mol. wt < 5 MDa) (Dodd *et al.*, 1998). Mucins which are different are the submaxillary mucins, with a lower carbohydrate content and different structure, but these are not so relevant in terms of gastrointestinal adhesion strategies.

Figure 1.1 Electron micrographs of gastric mucin prepared by (a) air drying onto mica, x29,800; (b) critical point-drying, x69,230; followed in each case by rotary shadowing with platinum at an angle of 5°. In (a) a 2-dimensional 'plan' is seen of the protein backbone. In (b) the mucin is visualized with its 3-dimensional structure retained, the highly glycosylated spheroidal regions are clearly visible (taken from Fiebrig 1995).

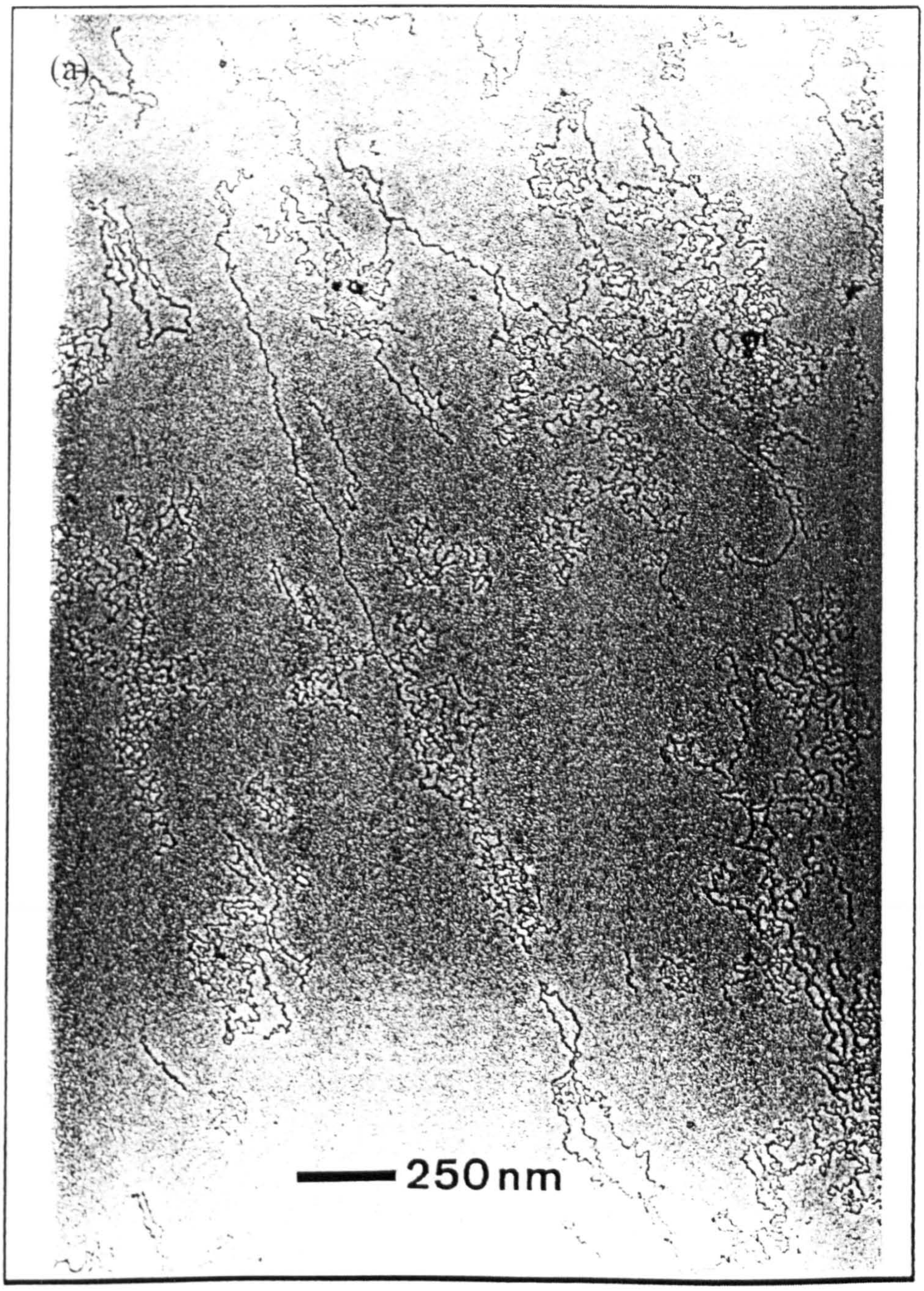

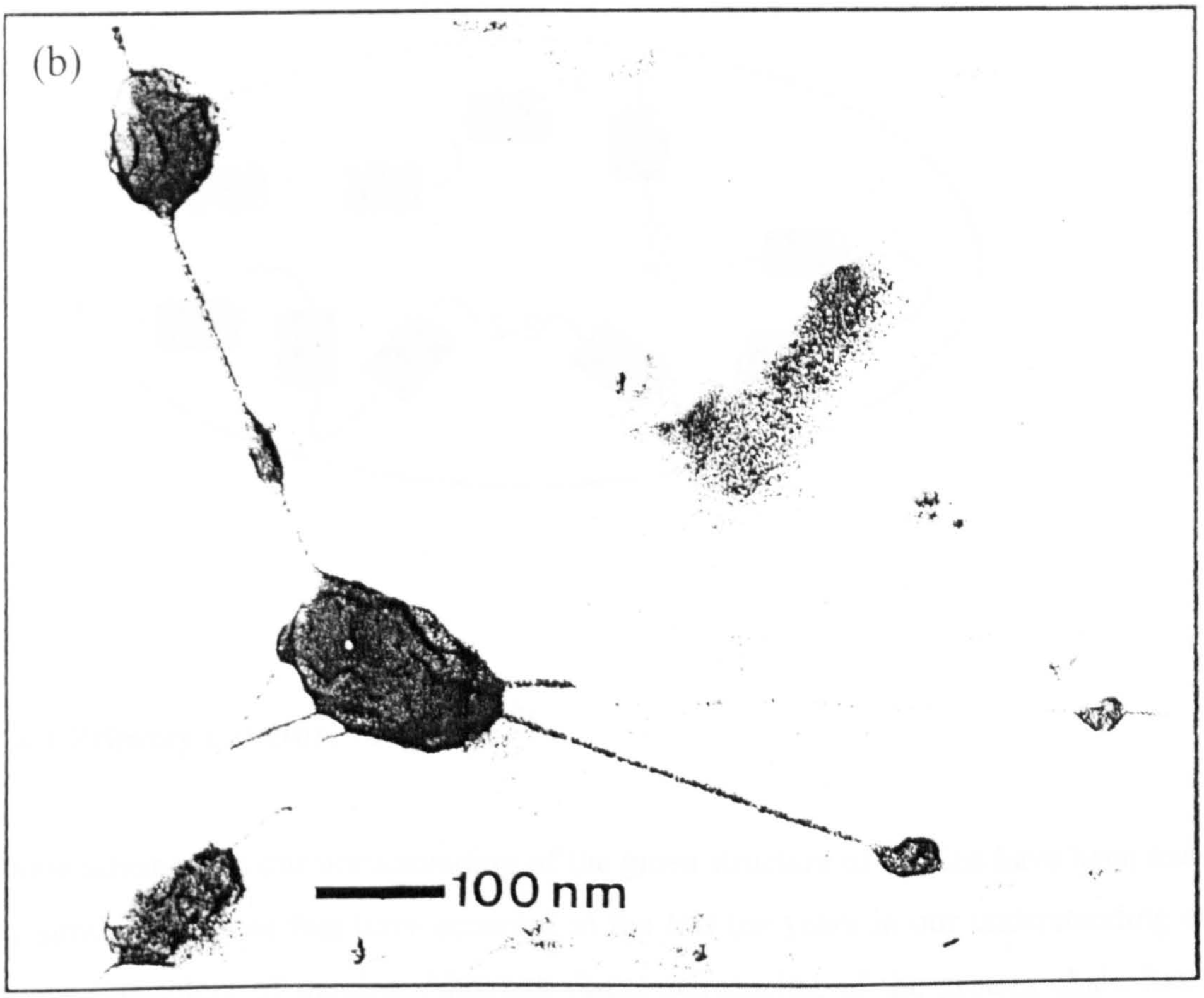
(b)
100 nm

Figure 1.2 The linear random coil model for the mucin macromolecule. (Taken from Jumel *et al.*, 1997).

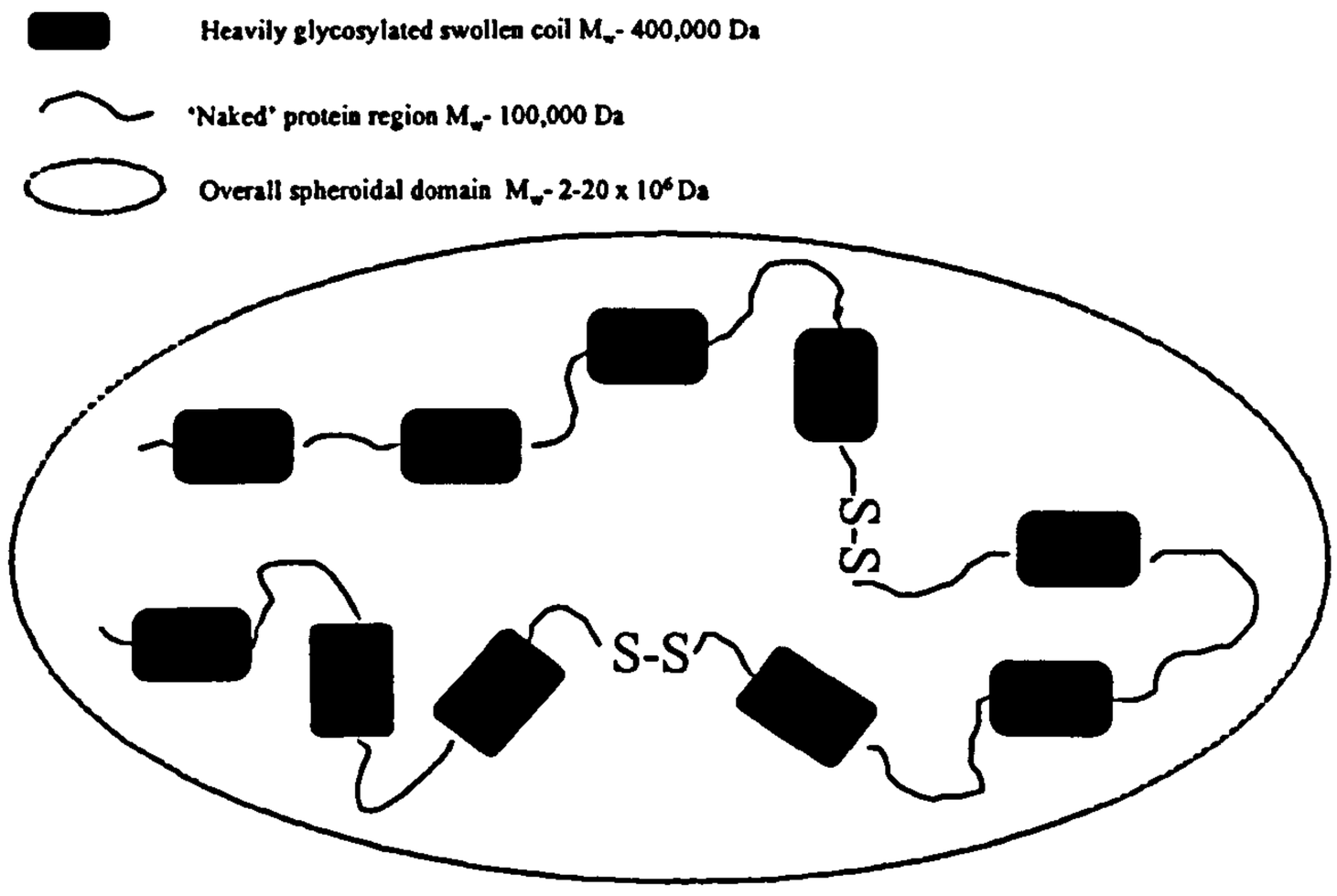

1.4.1 Primary structure of mucins

These advances in our understanding of the gross structure of mucins have been matched by similar advances that have occurred in the last ten years in our understanding of the primary structure of mucins. Although direct sequencing of the protein chain has been virtually impossible because of the insolubility of mucins stripped of their carbohydrate, at least nine different genes coding for mucin production have now been sequenced (see e.g., Hounsell *et al.*, 1997 & references therein). These are called 'MUC' genes and the ones known to date and the sources of mucin they code for are given in Table 1. The most important gene products as far as mucoadhesion are concerned appear to be MUC2 and MUC3 in the small intestine and colon, and MUC5AC, MUC5B and MUC6 from the stomach.

Table 1.1 Characterised mucin genes (from Hounsell *et al.*, 1997)

MUC gene	Location
MUC 1	Breast and colon cell surface episialin
MUC 2	Colon and small intestine goblet cell secretion
MUC 3	Intestinal tissue
MUC 4	Tracheobronchial tract
MUC 5AC	Respiratory tract and goblet cell secretion
MUC 5B	Submaxillary gland secretion
MUC 6	Gastric gland secretion
MUC 7	Salivary gland secretion
MUC 8	Respiratory tract

The protein sequences emerging from elucidating these genes confirm the presence of large amounts of serine and threonine, sites for the O-glycosylation, and also the large amounts of proline - which has been known for years (Harding *et al.*, 1983 a, b) to assist with the coiling of the mucin molecule. This knowledge of the genes has also revealed the concept of a tandem repeat of sequences of amino-acid throughout the linear polypeptide backbone Figure 1.3 shows a typical intestinal mucin gene product with highly glycosylated region and areas for either inter or intra molecular disulphide bridges.

The O-linked carbohydrate chains may contain up to five different monosaccharides; namely D-galactose, L-fucose, N-acetylglucosamine, N-acetylgalactosamine and sialic acid (Figure 1.4). As multi-branched oligosaccharides they are covalently attached via O-glycosidic linkages from N-acetylgalactosamine to serine and threonine residues of the protein core. The absence of uronic acid and only trace amounts of mannose (<1%) distinguish mucin glycoproteins from the proteoglycans of connective tissue and serum glycoproteins, respectively. Sialic acid residues, which belong to a family of acidic

sugars, are in gastrointestinal mucins usually either N-acetyl or N-glycollyl-neuraminic acid. They are usually in a terminal position on the carbohydrate chain, whereas ester sulphate residues occur in a more internal position, e.g. as N-acetylglucosamine-6-sulphate in pig gastric mucus (Allen, 1978; Slomiany and Meyer, 1972). They both contribute in giving the molecule a net negative charge, thought to be of importance in interactions with polycationic materials (Lehr *et al.*, 1992b; Fiebrig *et al.*, 1994). Other potential residues for mucoadhesive interaction are the carbonyl (hydrogen bonding) and methyl (hydrophobic bonding) groups on the N-acetyl residues and another methyl group on fucose.

Figure 1.3 Schematic of intestinal mucin. The amino terminus is on the left, carboxyl on the right. A cysteine-rich region occupies the last of the carboxyl end of the molecule. The heavily glycosylated area is boxed and contains mostly O-linked oligosaccharides (wavy lines) as well as a few N-linked (tridents). The disulphide bridges are also shown though it is unclear whether they are inter or intra molecular (Taken from Bansil *et al.*, 1995).

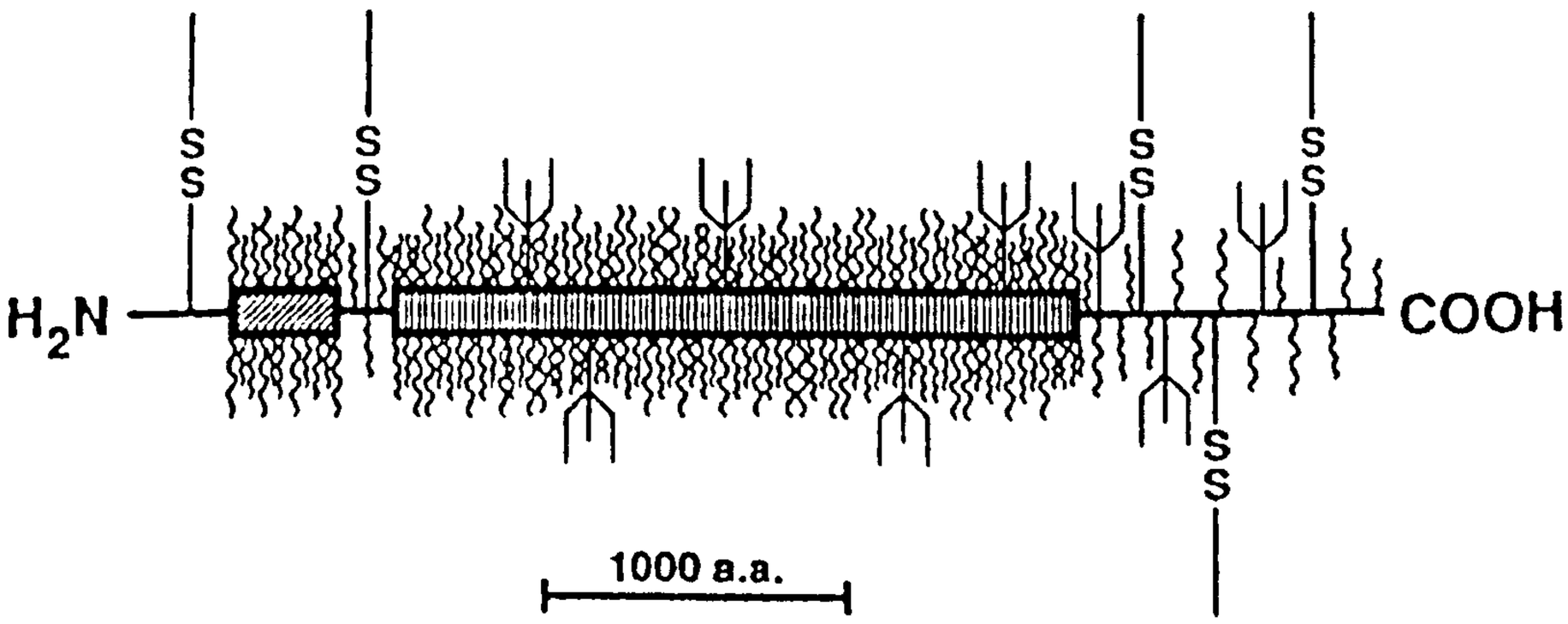

Figure 1.4 The principle sugars of gastrointestinal (also bronchial and cervical) mucins. The key ones, in terms of possible interaction sites for mucoadhesives are (4) galactose, (5) sialic acid ($-COO^-$ group for electrostatic interaction, R = H, $R_1 = COCH_3$, R_2 = H, R_3 = H, R_4 = H), (3) N-acetyl glucosamine and (2) N-acetyl galactosamine ($-COCH_3$ group, with the carbonyl for H-bonding) and the hydrophobic methyl residue of (1) fucose ($-CH_3$ group) (taken from Harding, 1989).

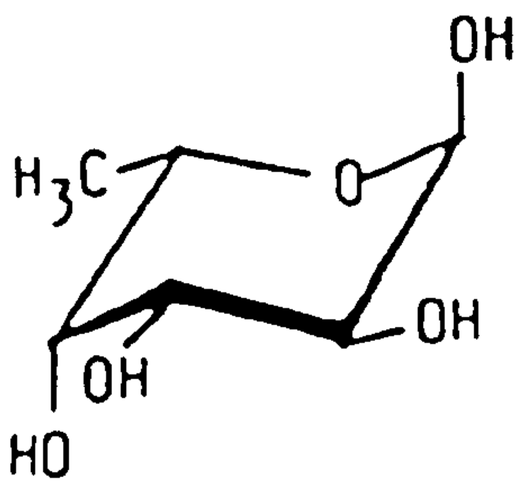

1

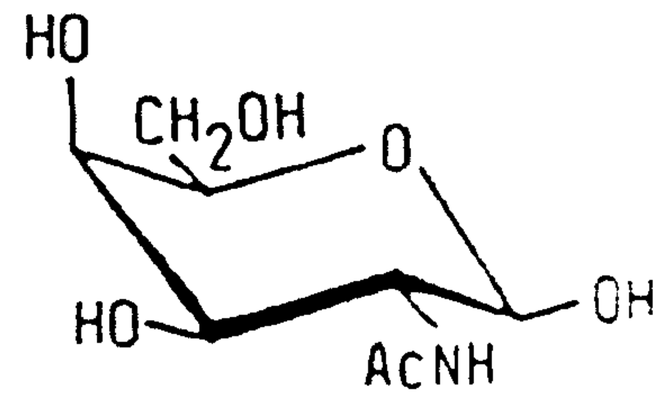

2

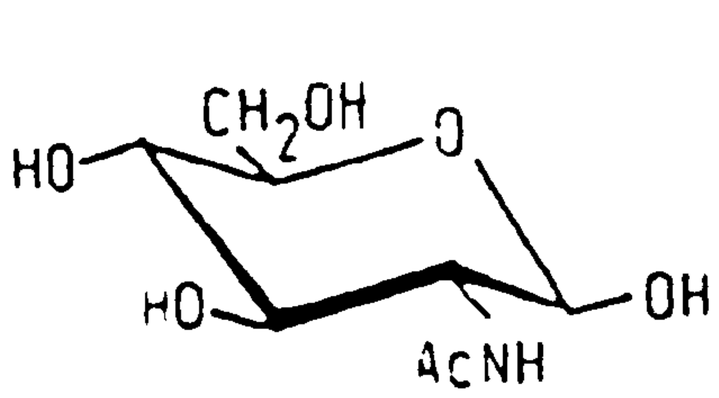

3

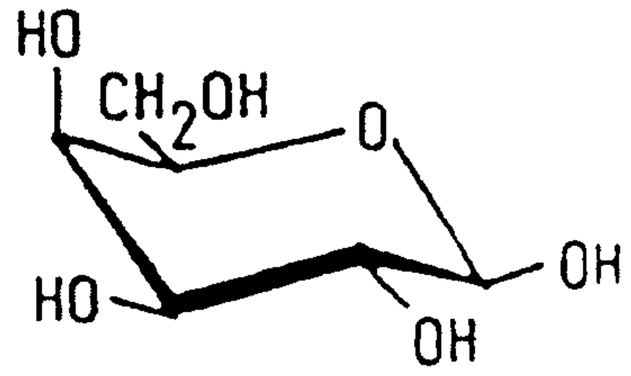

4

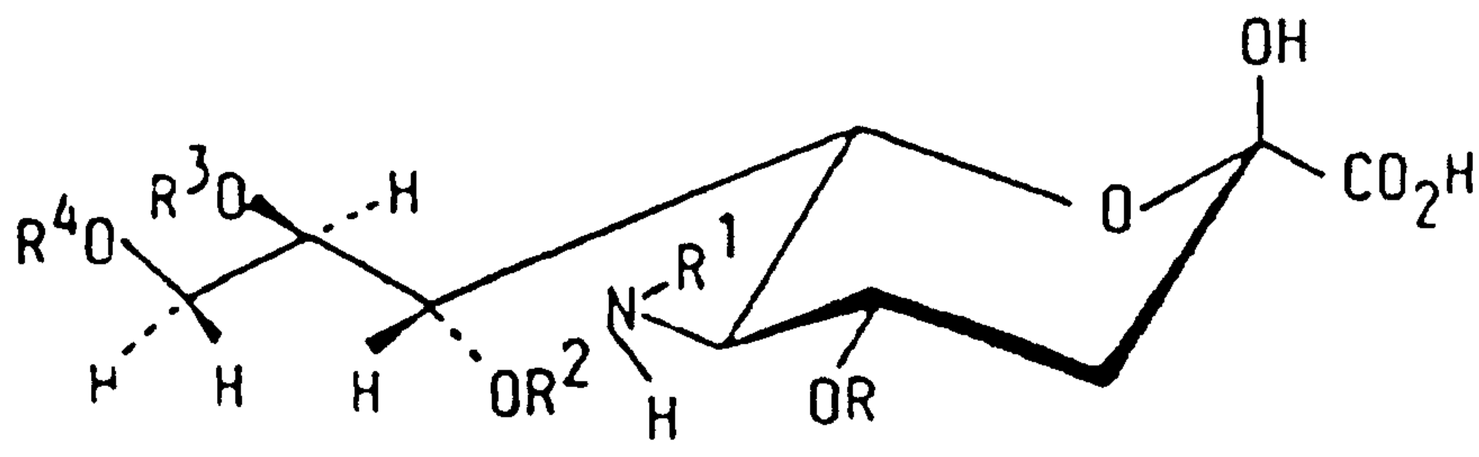

5

A recent development has been the discovery that mucins purified from different areas of the porcine stomach differ in terms of their oligosaccharide composition (Karlsson *et al.*, 1997). Karlsson *et al.* purified mucins from the antrum, fundus and cardiac regions (see Figure 1.5) and analysed them using mass spectrometry techniques. They found that the mucins purified from the cardiac region had the highest negative charge of the three. They postulate that this negative charge must be mostly due to sulphation of the oligosaccharides as only small amounts of sialic acid were found. They also found that the fundus mucin population had the longest average side chain length compared to the other two.

Figure 1.5 Anatomy of the porcine stomach. (A) Eusophagus, (B) Cardiac gland region, (C) Proventricular part, (D) Fundic gland region, (E) Antrum gland region, (F) Duodenum.

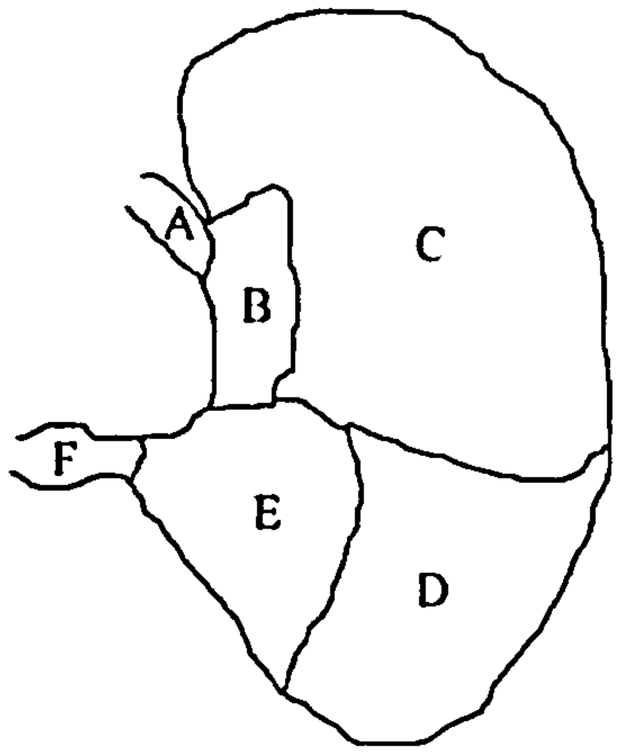

1.5 Is mucus an appropriate target?

There are three physiological aspects which remain critical for the concept of gastrointestinal mucoadhesion: (i) turnover of the adherent mucus layer, (ii) interactions

of the formulation with soluble, i.e. non-adherent mucus prior to adhesion and (iii) gastrointestinal motility.

1.5.1 Turnover of the adherent mucus layer

The mucus lining of the gastrointestinal tract is constantly being eroded by proteolysis and mechanical sloughing (Allen, 1981; Allen and Caroll, 1985). The most important of these is thought to be the latter caused by the ingestion of food and its digestion (Waldron-Edward, 1977). An equilibrium exists at the mucosal surface between mucus secretion and mucus erosion. If the mucus is not replaced by the secretion of new material then it will not be able to fulfill its protective role (Allen *et al.*, 1993). The difficulties in measuring mucus secretions *in vivo* has been outlined by Allen (1989). Studies on the turnover time of intestinal mucus gel layer in the rat *in situ* loop (Poelma and Tukker, 1987) by Lehr *et al.*, (1991) have attempted to shed some light on the limitations to gastrointestinal mucoadhesion. The maximal residence time of a bioadhesive drug delivery system at the site of adhesion is limited by the time it takes for the mucus gel layer to be renewed as determined by the steady state of synthesis, secretion and degradation of the mucins (Allen, 1981). Although the estimate for the mucus turnover time is relatively crude (47– 270 min), it is interesting to find that this time scale is similar to the mean residence time found for mucoadhesive microspheres (94±18 min) in earlier experiments using the same animal model (rat). Furthermore it has been observed that stimulating the mucus output, by perfusion with 10 mM sodium taurocholate, led to a significant shortening of the mean residence time of microspheres. Of even greater interest is the observation that the microspheres did not become detached from dead mucosal tissue *in vitro* when the system was stirred for more than 18 h. This leads to a further consideration; that of choosing an appropriate model system. This will be discussed in more detail below. Although mucus turnover in an *in situ* isolated gut loop in the rat (which has undergone surgery and has been removed from its normal function) may be different from mucus turnover in healthy humans or patients, this

physiological factor will limit potential adhesion to the adherent mucus in the gastrointestinal tract.

1.5.2 Competitive inhibitory interactions with soluble mucin

Any formulation entering the gastrointestinal tract interacting with the mucus gel is likely also to interact with soluble mucins of the "slough" or luminal material. This is an unavoidable complication that will reduce the efficiency of any adhesive system. That is any adhesive system targeted for groups on the mucus gel will also have the possibility of interacting with the soluble mucus present in the gastrointestinal lumen. Even if the epithelial cells are targeted, a 'competitive inhibition' for the mucoadhesive will recur as has been shown recently by Lehr *et al.*, (1992a). These authors used tomato lectin, a material that specifically binds to isolated pig enterocytes and monolayers of human Caco-2 cell cultures, that was proposed as a favourable candidate for specific bioadhesion to epithelial cells of the gastrointestinal tract. However, binding also occurred with crude pig gastric mucus. Other competitive inhibitors for mucoadhesion may also derive from other soluble components within the gastrointestinal tract, such as bile salts (Anderson, 1991).

1.5.3 Gastrointestinal motility

Gastrointestinal motility patterns and in particular the so called 'housekeeper wave' which involves strong gastrointestinal contractions, serves as a cleaning mechanism to clear all indigestible materials, including non-disintegrating dosage forms, from the stomach or proximal intestine (Code and Marlett, 1975; Grundy, 1985; Leung and Robinson, 1988). Thus, a good oral mucoadhesive drug delivery system also needs to resist the cleaning action of the 'housekeeper wave' and remain in the stomach or proximal small intestine.

1.6 Target for mucoadhesives

The target phase (in the stomach, small intestine and colon) most relevant to the concept of mucoadhesion is the water insoluble mucus gel lining the mucosa of the gastrointestinal tract. This mucus layer has a variable thickness, 50–450 μm, in man and about half that in the rat (Allen, 1978; Kerss *et al.*, 1982), with regional differences. In the colon the adherent gel is about mean 65 μm with something in the region of another 700 μm mobile viscous mucus that can be removed by suction. An important point is that in both cases the adherent gel barrier is continuous.

A variety of groups on the sugar residues on mucins provide potential sites for interaction of either an electrostatic, hydrogen bond or hydrophobic nature. This gives plenty of scope for potential mucoadhesives.

1.7 Mucoadhesives

The most important requirement of a mucoadhesive is that it must be non-toxic with no undesirable physiological or pharmacological actions, and should not be expensive. To this end, biopolymers, and in particular food grade polysaccharides are particularly attractive candidates (see Tombs and Harding, 1998). Other important criteria are that the mucoadhesive should have good wettability (and spreading ability) and high drug loading and a suitable unloading capacity. The following molecular properties are important considerations: charge, hydrogen-bonding, hydrophobicity, flexibility (ability to overcome steric hindrance problems) and molecular weight/ molecular weight distribution. The following molecular environmental factors are important: solubility, pH, ionic strength, presence of other salts (e.g. bile) and other macromolecules (antibodies, enzymes, polysaccharide etc.).

For bioadhesion to occur, an intimate contact between the adhesive and the substrate (mucus) is a prerequisite. Factors like good wettability as well as hydration are important

(Huntsberger, 1967; Chen and Cyr, 1970; Peppas and Buri, 1985). During the establishment of the adhesive bond the total surface energy between the two materials is diminished, eliminating two free surfaces and creating a new interface. This first step is believed to be followed by physical or mechanical bond formation obtained by deposition and inclusion of the adhesive material in the crevices of the mucus and chain entanglement between polymer chains of both phases (also referred to as inter-diffusion) (Boddé, 1990; Jabbari *et al.*, 1993). Lehr *et al.*, (1992b) have used electron microscopy in an attempt to visualize intermixing between a polyacrylic acid derivative (polycarbophil) and mucus. They were unable to observe intermixing in the micron range but did not exclude this phenomenon for the nanometre range. Sufficient chain flexibility is required to form secondary chemical bonds such as van der Waals forces as well as hydrogen bonding (Leung & Robinson, 1988; Duchêne *et al.*, 1988). The formation of primary (covalent) chemical bonds is important in hard tissue adhesion in orthopaedics and dentistry. However, for mucoadhesion, chemical reactions of this type have not been considered so far, since a long term attachment is not required (Peppas and Buri, 1985).

1.7.1 Polyanionic and neutral polymers

Polymers with hydroxyl or carboxyl groups on their surface had been earlier claimed as being the most desirable candidates for bioadhesion, rather than polymers with other functional groups or cationic moieties (Peppas and Buri, 1985). The synthetic polyacrylic acid derivatives known as polycarbophils (Carbopol® EX-55) and carbomer (Carbopol® 934) have to date been by far the most studied mucoadhesive polymers (Table 18.3 of Fiebrig *et al.*, 1995a). Both materials are polyanionic and interaction with mucus has largely been attributed to entanglement of the polymer chains. This is a result of swelling of the polymer when solvated and hydrogen bonding due to the carboxyl groups being in their unionised state at low pH (Robinson *et al.*, 1987; Leung and Robinson, 1988; Ponchel *et al.*, 1987a,b; Jabbari *et al.*, 1993). Polycarbophil is described as a water insoluble but swellable polymer of polyacrylic acid crosslinked with divinylglycol and used clinically in the treatment of diarrhoea and as a bulk laxative. Carbomer is a water-

soluble polymer of acrylic acid loosely crosslinked with allylsucrose. There have also been a wide range of polyanionic polysaccharides as possible biopolymer alternatives, such as alginate, pectin, carrageenan, xanthan and carboxy-methyl cellulose, but macroscopic (Lehr *et al.,* 1992c) and molecular studies (Anderson, 1991; Fiebrig, 1995) have yielded little or no mucoadhesion for these substances. This could possibly be due to the fact that both the mucoadhesive and the mucin are polyanionic, the results for polycarbophil are therefore rather surprising.

1.7.2 Polycations

According to Anderson *et al.*, (1989), Anderson (1991) and later Lehr *et al.,* (1992c), the need for hydrogen-bonding capabilities and negative charge in bioadhesive materials *should not be generalized.* These workers suggested that polycationic polymers might interact with the anionic sites on the mucins more favourably due to their opposite charges providing additional molecular attraction forces. For example, interactions between charged polymeric molecules have been employed in colloidal titration (Terayama, 1952). The method is based on the principle that positively charged macromolecules will react with negatively charged macromolecules. The neutralisation reaction will proceed stoichiometrically, allowing an estimation of either material if a standard colloid solution is used. Katayama *et al.,* (1978) used the method for the titration of heparin using polydiallyldimethyl ammonium chloride as a standard polycation. Van Damme *et al.,* (1992) measured the negative charge content in cartilage using polydiallyldimethyl ammonium chloride as well. Interactions between alginates and pectins with cationic polypeptides such as poly(L-lysine) and poly(Lys-Lys-Ala) have been studied using circular dichroism (Bystricky *et al.,* 1990). Differences in interaction efficiency between the polymers were attributed to differences in conformational flexibility of the polyanionic chains in solution. Takahashi *et al.*, (1990) studied the characteristics of polyion complexes of chitosan with sodium alginate and sodium polyacrylate using viscometry and Fourier transform infra-red spectroscopy (FT-IR). They found that chitosan and alginate reacted with a defined binding ratio that was found

to be relatively constant in media of various pH values. In contrast, for polyacrylate–chitosan interactions the unit molecular binding ratio was greatly affected by the pH. (*n.b.* chitosans are generally poorly soluble above a pH ~6).

1.8 Chitosans

Figure 1.6 The Chitin (a) and Chitosan (b) macromolecules.

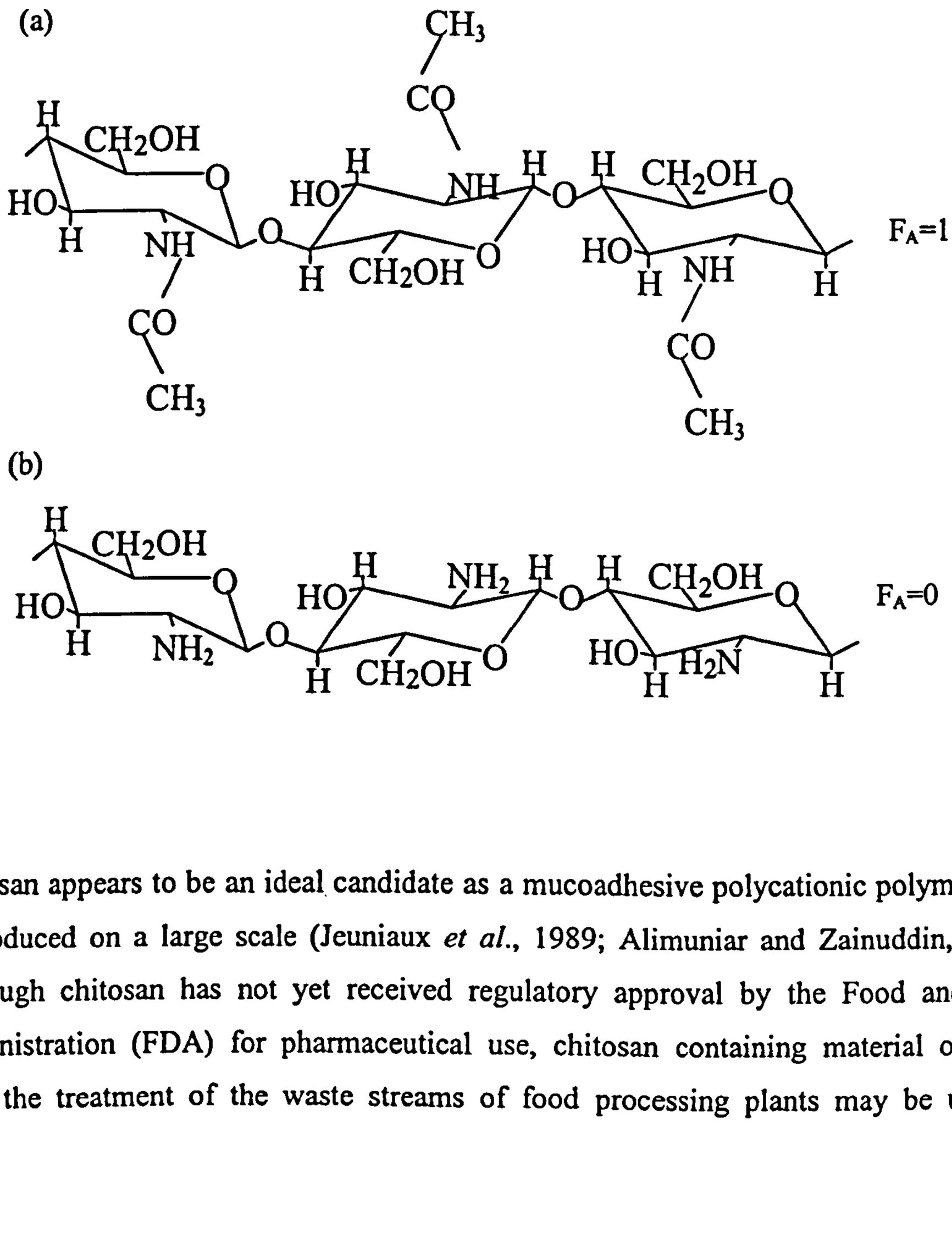

Chitosan appears to be an ideal candidate as a mucoadhesive polycationic polymer — it is produced on a large scale (Jeuniaux *et al.*, 1989; Alimuniar and Zainuddin, 1992). Although chitosan has not yet received regulatory approval by the Food and Drug Administration (FDA) for pharmaceutical use, chitosan containing material obtained from the treatment of the waste streams of food processing plants may be used as

livestock feed in the U.S.A. so long as the level of chitosan does not exceed 0.1% (Weiner, 1992). It is known to interact with other proteins such as lysozyme (Cölfen *et al.*, 1996). Its properties are quite different from polyanionic chitin derivatives, such as carboxy-methyl chitin (Korneeva *et. al,* 1996).

Chitosan (Figure 1.6) has been approved as a food additive in Japan since 1983 (and also in some European countries) and has been placed on the "*Japanese Natural Additive List*". It is used as a thickener and stabilizer (Weiner, 1992). It is a food ingredient in some dietary cookies and noodles from Hihon Kayaku Inc. and Tanami Foods Inc. as well as in vinegars of Nakano Inc., making use of its hypocholesterolaemic properties (Hirano, 1989). The food industry has also exploited the chelating properties of chitosan for the clarification of beverages such as apple and carrot juices (Imeri and Knorr, 1988; Soto Peralta *et al.*, 1989).

The lack of acute oral toxicity of chitosan has been supported by experiments in mice (Arai *et al.*, 1968) who determined an LD50 of > 10g/kg. However the literature lacks adequate scientific studies on long term and widespread human exposure through food and pharmaceutical products (McCurdy, 1992).

Chitosan is a derivative of chitin; the insoluble structural exoskeletal polysaccharide of the shells of crabs and lobsters and can be harvested very cheaply (see Tombs & Harding, 1998); the chief producers being Norway, Japan, China and Russia. Like cellulose it is a β(1→4)-D-glucan. Unlike cellulose the residue on the number 2 carbon atom in the ring is N-acetylated (Figure 1.6). In native chitin these residues are fully acetylated. However, after extraction the chitin molecule can be deacetylated to varying degrees to give a polycationic molecule. The degree of acetylation is represented by the parameter F_A, with F_A= 1 (fully acetylated) corresponding to pure chitin and F_A=0 to fully deacetylated chitosan.

Variations in molecular weight and degree of deacetylation together with the ability to form gels and films allow flexibility in formulation design (Acatürk, 1989; Miyayaki *et al.*, 1990; Errington *et al.*, 1993).

1.9 Strategies for studying mucoadhesion

There are two separate methods for studying mucoadhesion direct and molecular. Direct methods involve a study of a macroscopic interaction, usually involving whole mucus, whereas the molecular methods focus on the interactions and usually involve the purified mucin component.

The assay methods can either employ freshly excised tissue from various animals (frog, rat, rabbit, pig, cow, etc.), used either immediately as live or dead tissue or stored frozen and defrosted prior to use, or they use mucus or mucin at various degrees of degradation and purity either solubilised or as gel (usually from pig stomach or bovine submaxillary glands). Whatever model material is used, its relevance to the human mucus, whether in health or disease state, has to be considered (MacAdam, 1993). Dead mucosal tissue may well not produce any new mucus, while degradation of existing mucus will still take place. This will have a marked effect on the rheological characteristics of the substrate, considered to be highly relevant to adhesional phenomena. Mucus thickness may vary from species to species and intersubject, as well as intrasubject, variability of the mucosal tissue poses problems in terms of reproducibility. For the mucin based procedures, mucins, once extracted are subject to degradation by enzymes and mechanic disruption: they have to be handled with extreme care, and enzyme degradation must be kept to a minimum (e.g. by extraction in guanidine hydrochloride (Sheehan and Carlstedt, 1989) or with adequate protease inhibitors present). Mucin carbohydrate composition also varies within the gastrointestinal tract (Allen, 1989).

Small intestinal mucin is very difficult to solubilise and available in only small quantities. Gastric mucin from pigs appears to be an alternative since it is available in larger

quantities and although its sialic acid content is low, its carbohydrate composition is comparable to human gastric mucin. Purification methods allow the removal of other components present in mucus in order to obtain purified mucin which still shows the gel-forming characteristics of native mucus (Sheehan & Carlstedt, 1989; Bell *et al.*, 1985; Allen, 1989).

Commercially available pig gastric mucins or mucus are somewhat different in the detail of their composition when compared with freshly prepared and purified material. They may be rather degraded or the freeze drying procedure may have altered the structure in such a way that it becomes difficult to redissolve them completely. Commercially available 'submaxillary' mucins are quite different from the mucins secreted in the gastrointestinal tract. They are secreted in a viscous soluble form rather than as water-insoluble gels (for a discussion of these differences see Gottschalk *et al.*, 1972). Nevertheless, highly purified mucins can give more accurate information on the actual nature of the interaction of a putative mucoadhesive with the main mucin-forming component. The use of dilute mucin solutions also allows the study of mucin–bioadhesive polymer interactions on a fundamental level.

It has been recognized that the degree of hydration of the bioadhesive drug delivery system, as well as the amount of water available, plays an important role in determining the strength of adhesion or whether adhesion can take place at all (Leung and Robinson, 1988; Chen and Cyr, 1970). The hydration aspect can be controlled in local applications such as mouth or vagina by drying excess water in the area immediately prior to application (Deasy and O'Neill, 1989). In the gastrointestinal tract, however, excess water at the site of adhesion as well as excess in the amount of surrounding liquid cannot be controlled. Lehr *et al.*, (1992c) pointed out that numerous so-called mucoadhesive polymers adhere only under conditions where the amount of interstitial liquid is limited. This kind of dry-to-wet adhesion or "blotting adhesion" is due to the capillary forces drawing liquid from the mucus into the delivery system (Huntsberger, 1967; Lehr *et al.*, 1992c; Mortazavi and Smart, 1993). If the polymer involved offers no intrinsic ability to form a bond with the substrate (e.g. some cellulose derivatives), the initial adhesive

forces, although high at the beginning may become negligible as soon as the material is fully hydrated (Junginger and Lehr, 1990). Therefore, adhesion measurements in fully hydrated systems and over a period of time are necessary to avoid attributing a high adhesive force erroneously to intrinsic mucoadhesive properties. The adhesion mechanism of capillary attraction between a dry, water-absorbing polymer and a wet, mucosal surface being dehydrated is quite different to the interactions between two hydrogels (polymer and mucus) in equilibrium with a third liquid phase (Mortazavi and Smart, 1993).

1.10 Aims of this study

The experiments presented in this thesis are designed to try and determine the factors that effect the interaction between mucin and chitosan focussing on the effects of ionic strength, degree of acetylation, and source of mucin on the interaction. Also studied was *Mytilus edulis* foot protein 1 another potential mucoadhesive.

This work follows on from two previous studies conducted by Immo Fiebrig (1995) and Morag Anderson (1991). Anderson investigated the whether pig gastric mucin interacted with anionic polymers (sodium alginate, sodium carboxymethyl cellulose and xanthan) the interaction with a cationic polymer was also investigated (DEAE-dextran). No interaction was found between the polyanions using analytical ultracentrifugation but an interaction was measured between DEAE-dextran and mucin. Fiebrig (1995) followed on this work by studying the interaction of mucin with other polycationic materials, including a preparation of chitosan. He found a strong interaction between pig gastric mucin and chitosan and investigated it again using the technique of analytical ultracentrifugation but also used electron microscopy, turbidimetry and static light scattering.

Chapter 2 outlines the theoretical background of analytical ultracentrifugation and light scattering. These techniques with atomic force microscopy have been used to characterise

the mucin/chitosan complex. *Chapter 3* describes the materials used in this thesis, the purification of mucin the substrate for adhesion. Also described are the experimental conditions used to characterise the complex. The results of the characterisation of the three mucin substrates are presented in *Chapter 4*. The substrates were characterised using multi-angle laser light scattering linked on-line to size exclusion chromatography. *Chapter 5* contains the results for the determination of the sedimentation coefficient for the mucin/chitosan mixtures under varying conditions. The effects of ionic strength on the interaction are quantified using sedimentation velocity of control and mixture solutions. In *Chapter 6* the results from the Flow field flow multi-angle laser light scattering study on the complex are presented. The results from atomic force microscopy are presented in *Chapter 7*. The visualisation of the mucin macromolecule and the mucin/chitosan complex at different ionic strengths. Together with the results from chapter 5 these are used to determine the effect of ionic strength on the complex. *Chapter 8* contains the results for the characterisation of a new potential mucoadhesive *Mytilus edulis* foot protein 1. It is characterised in dilute solution and its interaction with mucin studied. Finally *Chapter 9* draws conclusions from the work presented in this thesis, and contains ideas for future work.

Chapter 2

Analytical Ultracentrifugation and Static Light Scattering

2.1 Introduction

Analytical ultracentrifugation and light scattering are absolute methods for the determination of molecular weight (i.e. they do not require standards or calibration). This parameter is of the utmost importance when characterising molecules in solution. However, it is difficult to determine for substances such as mucins and polysaccharides because of complications through non-ideality (caused by asymmetry, high solvent affinity and polyelectrolyte behaviour) and heterogeneity (polydispersity or association phenomena).

2.2 Analytical ultracentrifugation

Thé Svedberg is regarded as the grandfather of the analytical ultracentrifuge, it was his pioneering work at the beginning of this century that led to the development of this technique (see Rånby, 1987). The first ultracentrifuge was constructed in 1924 and by 1925 the first results with haemoglobin were obtained. Using the ultracentrifuge Svedberg demonstrated that proteins existed with molecular weights in the tens of thousands whereas previously proteins were thought to be reversible aggregates of much smaller molecules. Svedberg won the Nobel Prize for Chemistry in 1926 for his work on colloid chemistry (see Brohult, 1987). The analytical ultracentrifuge was subsequently developed and used to calculate the absolute molecular weight of molecules using sedimentation velocity and equilibrium. The basic theory of these is described below (for

a more detailed description see for example Van Holde, 1998, Harding *et al.*, 1992, Ralston, 1993).

2.2.1 Sedimentation velocity

Sedimentation velocity experiments are performed to calculate the sedimentation coefficient of the molecules/complexes under investigation. The material to be studied is placed in an ultracentrifuge cell and accelerated to a high angular velocity such that a sedimenting boundary forms. The boundary represents the difference between pure solvent of the depleted region and the uniform distribution of the sedimenting solute. The rate of movement of this boundary is then measured and the sedimentation coefficient, s, determined. The sedimentation coefficient has two components, the molecular weight and the shape (and hydration) of the molecule in solution. The shape of the sedimenting boundary can also give an indication as to the heterogeneity of a sample.

When a molecule is dissolved in a solvent and placed in a centrifugal field there are three main forces that act upon the molecule. Figure 2.1 illustrates these forces.

The sedimenting force, F_s, in a spinning rotor is a function of the mass, m (g), of the molecule, the square of the angular velocity, ω (in radians per second), and the distance of the particle from the axis of rotation, r (cm).

$$F_s = m\omega^2 r = \frac{M}{N}\omega^2 r \qquad 2.1$$

M is the molecular weight of the solute (g/mol) and N is Avogadro's number.

The buoyant force, F_b, is equal to the weight of fluid that is displaced by the particle as it sediments and opposes the sedimenting force.

$$F_b = -m_o\omega^2 r = -\frac{M}{N}\bar{\nu}\rho\omega^2 r \qquad 2.2$$

Where m_0 is the mass of fluid displaced by the particle (g), $\bar{\nu}$ is the partial specific volume of the solute (ml/g) and ρ is the solvent density (g/ml).

If the density of the particle is greater than that of the solvent, i.e. F_s is greater than F_b, the particle will sediment. As the particle sediments, its velocity increases due to an increase in radial distance.

Figure 2.1 Forces acting upon a molecule in solution in an ultracentrifuge cell (taken from Van Holde *et al.*, 1998).

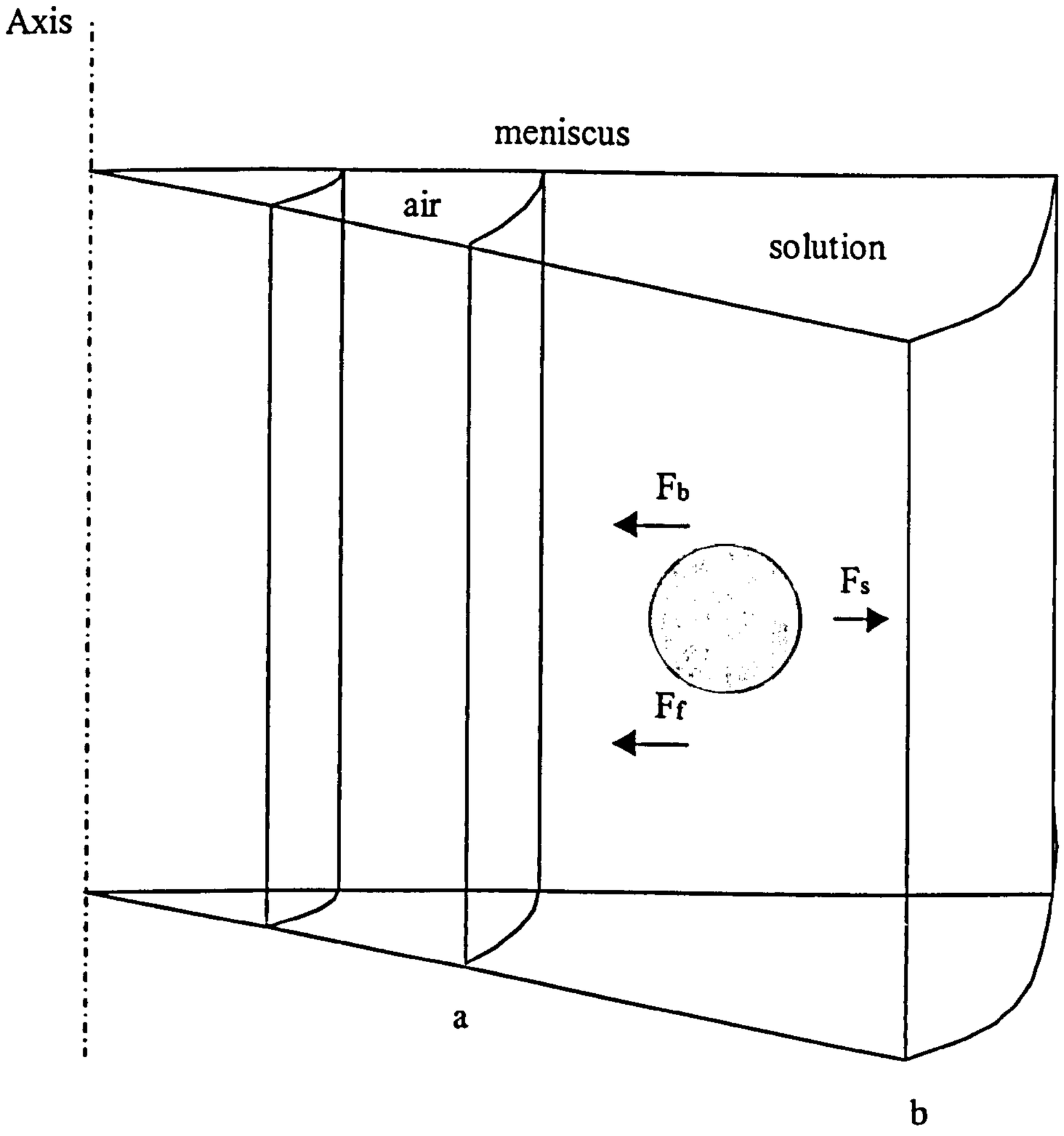

The frictional force, F_f, is the frictional resistance between the moving solute and the relatively stationary solvent molecules and also acts to oppose the sedimenting force.

$$F_f = -f\nu \qquad 2.3$$

Where ν is the velocity of the solute (m/s) and f is the frictional coefficient (g/s) which depends on the shape and size of the solute. Asymmetrical 'rough' molecules will sediment much slower than spherical 'smooth' molecules.

Although forces F_b and F_f act to oppose the sedimenting force F_s, once the centrifuge rotor has begun turning, after only a very short period of acceleration (typically less than 10^{-6} seconds), the three forces come to equilibrium resulting in a net zero accelerating force.

$$F_s + F_b + F_f = 0 \qquad 2.4$$

and therefore

$$\frac{M}{N}\omega^2 r - \frac{M}{N}\bar{\nu}\rho\omega^2 r - f\nu = 0 \qquad 2.5$$

rearranging gives

$$\frac{M}{N}\omega^2 r(1-\bar{\nu}\rho) = f\nu \qquad 2.6$$

and further

$$\frac{M(1-\bar{\nu}\rho)}{Nf} = \frac{\nu}{\omega^2 r} = s \qquad 2.7$$

The term $v/\omega^2 r$ corresponds to the velocity of the molecule per unit gravitational acceleration and is termed the sedimentation coefficient, s. As previously mentioned, the sedimenting force does not remain constant but increases proportionally with radial distance, so the boundary will increase in velocity as it moves towards the cell base. As a result of this the velocity must be expressed as a differential, $v = dr/dt$, and using the identity $(1/r)(dr/dt) = d\ln r/dt$, equation 2.7 becomes:

$$s = \frac{1}{\omega^2}\frac{d\ln r}{dt} \qquad 2.8$$

So during a sedimentation velocity experiment successive scans of the centrifuge cell at regular time intervals will show displacement of the boundary from the meniscus to the cell bottom. A plot of ln r against t should be linear and the gradient can be used to determine the sedimentation coefficient.

The sedimentation coefficient is also dependent on the concentration of the solute, C and on the temperature, viscosity and density of the solvent. It should, therefore, be measured at a number of different concentrations and corrected to standard conditions, i.e. those of water at 20°C, using equation 2.9 (Tanford, 1961)

$$s_{20,w} = s_{T,b}\left\{\frac{\eta_{T,b}}{\eta_{20,w}}\left(\frac{(1-\bar{\nu}\rho)_{20,w}}{(1-\bar{\nu}\rho)_{T,b}}\right)\right\} \qquad 2.9$$

where $s_{T,b}$ is the sedimentation coefficient at temperature, T, in buffer, b, η is the solvent viscosity and w refers to water. The $s_{20,w}$ values should then be corrected for radial dilution (Fujita, 1975) and plotted against concentration. Radial dilution occurs because the ultracentrifuge cell is sector shaped (to prevent convection (Ralston, 1993)) so as the solute migrates it enters a larger volume of solvent. The corrected sedimentation coefficients can then be extrapolated to infinite dilution (C = 0). The sedimentation coefficient is concentration dependent, due to the solvent having an increased viscosity at higher concentrations of solute and because the sedimenting solute particles must

displace solvent backwards as they sediment. At infinite dilution the $s^0_{20,w}$ value is obtained (Tanford, 1961). The sedimentation coefficient is usually quoted in Svedbergs, S, in honour of Thé Svedberg, where 1 S is equal to 1 x 10^{-13} seconds.

2.2.2 Sedimentation equilibrium

Sedimentation equilibrium experiments are performed to calculate the molar mass (g/mol) of the solute (numerically equal to the molecular weight in Da). A small volume of an initially uniform solution is centrifuged at a lower angular velocity than that required for sedimentation velocity. As the solute sediments towards the cell bottom the concentration at the bottom increases and the process of diffusion opposes that of sedimentation. After a period of time the two opposing forces reach an equilibrium (Figure 2.2) and the concentration of the solute increases exponentially towards the base of the cell. Measurement of the concentration at different points leads to the determination of the molar weight of the sedimenting solute.

For a single macromolecular species it can be shown that (Ralston, 1993):

$$M_{app} = \frac{2RT}{(1-\bar{\nu}\rho)\omega^2} \times \frac{d(\ln C)}{dr^2} \qquad 2.10$$

where M_{app} is the apparent molecular weight of the macromolecule (g/mol), T is the experimental temperature (Kelvin), R is the gas constant (8.314 J K^{-1} mol^{-1}) and C is the concentration of the macromolecule (g/ml). A plot of log concentration against r^2 for a single species at equilibrium will give a gradient proportional to the apparent molecular weight.

Figure 2.2 Representation of sedimentation equilibrium, the flow of solute due to sedimentation increases with radial distance (black arrows), this is balanced by the reverse flow from diffusion which increases with concentration gradient (open arrows)(from Ralston, 1993).

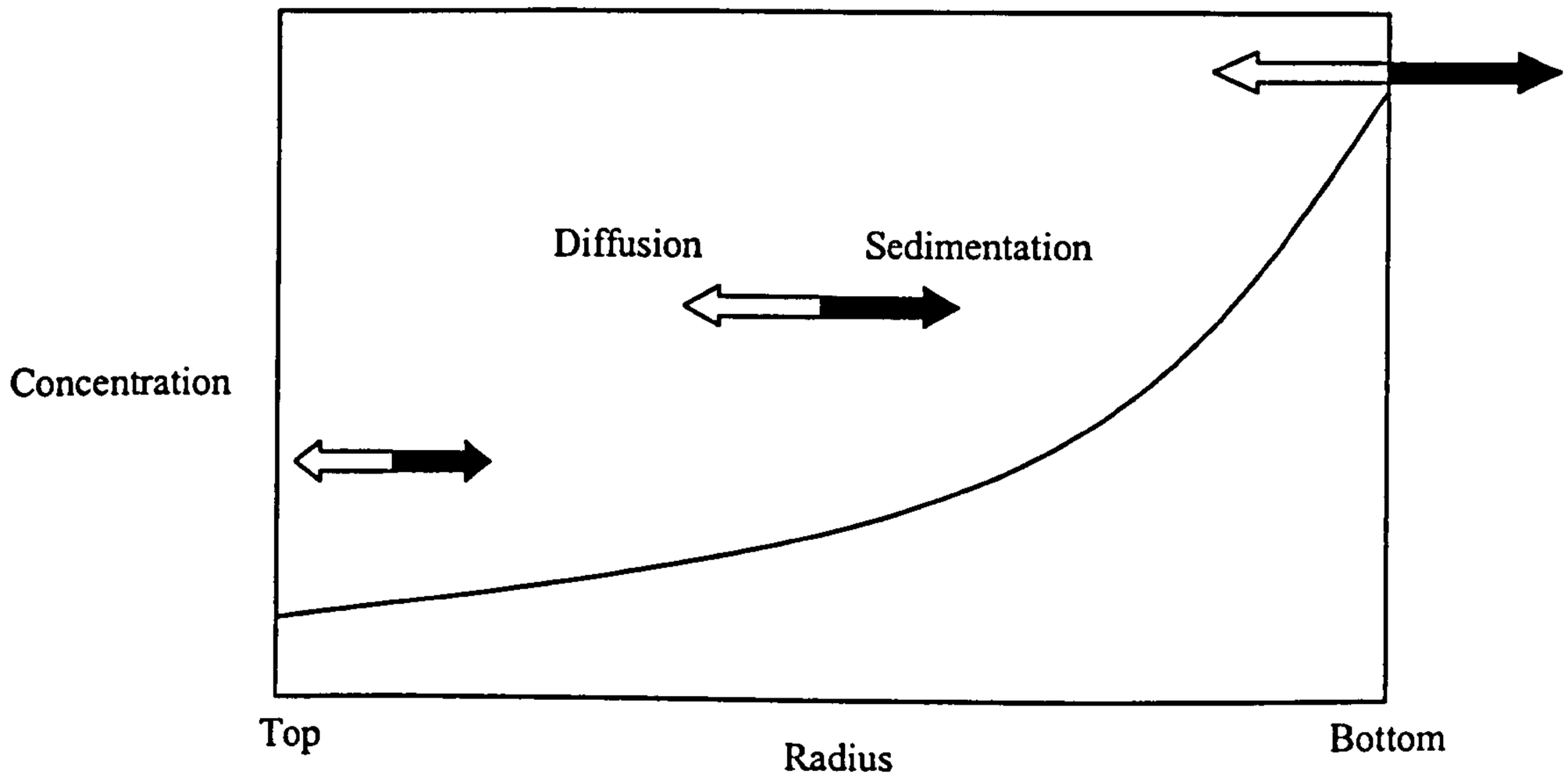

The apparent molecular weight is determined at a finite concentration while the true molecular weight is obtained through extrapolation to zero concentration to remove the effects of non-ideality. This means that the molecular weight should be measured at several concentrations. However, this can frequently be avoided by keeping the (loading) concentration low (<0.5 mg/ml), at which for *proteins* the effects of non-ideality can reasonably be ignored and the apparent molecular weight assumed to be equal to the ideal molecular weight.

If the macromolecular species being investigated are polydisperse (e.g. mucins) each molecular species will be distributed at sedimentation equilibrium according to equation 2.10. Higher molecular weight material will be selectively distributed towards the cell base, whilst the lower molecular weight material will be distributed at the meniscus (Yphantis, 1964). The molecular weight that is determined is, therefore, an average. If the

optical system gives a direct measurement of concentration (absorption or Rayleigh interference) then the molecular weight calculated will be the weight average apparent molecular weight ($M_{w,app}$). Substituting $M_{w,app}$ for M_{app} in equation 2.10, the $M_{w,app}$ that is calculated corresponds to the whole cell or whole distribution weight average apparent molecular weight. A convenient way of obtaining this is using the M* function, an operational point average molecular weight. When the M* function is extrapolated to the cell base it equals $M_{w,app}$ (Creeth and Harding, 1982). In addition to 'whole distribution' molecular weights, $M_{w,app}$, local or point average molecular weights $M_{w,app}(r)$ can also be obtained as a function of radial position, r, by sliding strip fits to the c vs r distributions (see Teller, 1973). The program MSTAR (Cölfen and Harding, 1997) evaluates both $M_{w,app}$ and $M_{w,app}(r)$.

2.3 Classical light scattering

There are three separate cases for light scattering of molecules, (i) scattering caused by small molecules (maximum radius < $\lambda/20$), (ii) Rayleigh-Gans-Debye scattering caused by larger molecules ($\lambda/20$ < maximum radius < λ) and Mie scattering by very large macromolecular assemblies (maximum radius > λ).

We have used light scattering to characterise mucins, which are in the Rayleigh-Gans-Debye range – i.e. (ii). But before we consider (ii) we need to consider the simplest case first, i.e. (i).

2.3.1 Light scattering by small molecules ('Rayleigh scattering')

The theory of light scattering has been reviewed at length by many authors, see for example Harding *et al.*, 1992b; Van Holde *et al.*, 1998. What follows is a brief description of the basic theory of classical light scattering.

If the solute molecules of an ideal dilute solution are considered as independent scatterers of light and it is assumed that they are small in comparison with the wavelength of the incident light in these conditions, then it can be seen from the ratio of the intensities of the incident light (I_0) and the scattered light (I_s), in equation 2.11, that the light scattered by each particle is dependent upon its polarizability (Tanford, 1961).

$$\frac{I_s}{I_0} = \frac{16\pi^4\alpha^2 \sin^2\theta_1}{\lambda^4 r^2} \qquad 2.11$$

Here θ_1 is the angle between the dipole axis (the dipole being induced in the particle by the incident light) and the line joining the point of observation to the dipole, r is the distance of the observer from the particle, λ is the *in vacuo* wavelength of the incident light and α is the molecular polarizability. Molecular polarizability is easily related to the excess refractive index of the solution (n) over that of pure solvent (n_0) by equation 2.12 where N is the number of solute particles per cm^3 (Van Holde, 1998).

$$n^2 - n_0^2 = 4\pi N\alpha \qquad 2.12$$

By rearranging and introducing the weight concentration, C (g/ml) equation 2.13 can be obtained which relates the polarizability of the molecule to the specific refractive index increment $(n-n_0)/C$. If this is linear for the system then this can be replaced by dn/dc to give equation 2.14.

$$\alpha = \frac{(n+n_0)}{4\pi}\frac{(n-n_0)}{C}\frac{C}{N} \qquad 2.13$$

$$\alpha = \frac{n_0}{2\pi}\frac{dn}{dC}\frac{C}{N} \qquad 2.14$$

C/N is equivalent to M/N_A, where N_A is Avogadro's number and M is the molecular weight. If we substitute all of this back into equation 2.11 then we obtain:

$$\frac{I_s}{I_0} = \frac{2\pi^2 n_0^2 (dn/dC)^2}{r^2 \lambda^4 N_A^2} CM(1+\cos^2\theta) \qquad 2.15$$

This equation tells us that the excess scattering produced by a solution containing a weight concentration, C, of particles of molecular weight, M, depends on the product CM. It also depends on the angle with respect to the incident beam, θ, but it is symmetrical with regards to forward and backward scattering, if the scattering particles are small compared to the wavelength of the light. For such scattering, which is called Rayleigh scattering, we can define a quantity, the Rayleigh ratio, R_θ, which corrects for the $1 + \cos^2\theta$ term, and is therefore independent of angle.

$$R_\theta = \frac{I_s}{I_0} \frac{r^2}{1+\cos^2\theta} \qquad 2.16$$

Substituting this into equation 2.15 we obtain:

$$R_\theta = \frac{2\pi^2 n_0^2 (dn/dC)^2}{N_A \lambda^4} CM = KCM \qquad 2.17$$

where

$$K = \frac{2\pi^2 n_0^2 (dn/dC)^2}{N_A \lambda^4} \qquad 2.18$$

These equations demonstrate that light scattering measurements can be used for the determination of molecular weights. With real solutions, the equations must be modified to take into account the non-ideality of the solution caused by, for example, excluded volume effects. A precise calculation can be made on the basis of the thermodynamic theory of Einstein (1910) and Debye (1944). Light scattering from a solution arises from local density fluctuations and from local fluctuations in the concentrations of the solute. If the scatter arising from density fluctuations is equal to that arising in the pure solvent,

then the excess scatter from the solution results entirely from concentration fluctuations (Billingham, 1977). The free energy required to create a concentration gradient in a solution is related to the osmotic pressure, π, of the solution and the treatment of Debye leads to equation 2.19 and for a non-ideal solution in equation 2.20, where A is the thermodynamic second virial coefficient.

$$\frac{KC}{R_\theta} = \frac{1}{RT}\left(\frac{d\pi}{dC}\right) \qquad 2.19$$

For a monodisperse polymer the osmotic pressure can be expressed in the form of a virial expansion so that equation 2.19 becomes:

$$\frac{KC}{R_\theta} = \frac{1}{M} + 2A_2C + 3A_3C^2 + \cdots \qquad 2.20$$

where A_2 and A_3 are the second and third virial coefficients etc.

Previously we have considered the case for a monodisperse solute, if we now consider that the solute is polydisperse there will be a mixture of *n* macromolecular components, of different individual molecular weights, M_i and concentrations, C_i. The total intensity of scattering is the sum of intensities from all components, i.e. R_θ is the sum of $R_{\theta i}$.

$$R_\theta = \sum_{i=1}^{n} R_\theta = \sum_{i=1}^{n} K_i C_i M_i \qquad 2.22$$

If the specific refractive index increment is the same for all different species then equation 2.22 can be rewritten as:

$$\frac{KC}{R_\theta} = \frac{\sum_{i=1}^{n} C_i}{\sum_{i=1}^{n} C_i M_i} = \frac{1}{M_w} \qquad 2.23$$

M_w is the weight average molecular weight, since each component is counted according to its weight concentration in taking the average. The second virial coefficient for a polydisperse solute is not a simple average, but depends upon the exact form of the molar mass distribution function. For this reason thermodynamic parameters can only be evaluated from light scattering data if the polymer is fractionated into near monodisperse fractions (Wyatt, 1992).

2.3.2 Light scattering by large molecules ('Rayleigh-Gans-Debye scattering')

Large molecules with respect to light scattering are those that have a molecular weight greater than 30,000 g/mol (Billingham, 1977). Molecules larger than this will give rise to scattering from different points of the molecule that will reach the detector in different phases. The beams scattered from different points of a particle are coherent and therefore capable of interference. If the beams are out of phase and interfere, the intensity of the resulting light is smaller than the sum of the intensities of the two beams. As this interference is caused by different points in the same particle it is termed internal interference. The consequence of this is that the scattered intensity at any angle to the forward direction of the beam is greater than at the corresponding angle to the backward direction and R_θ will be dependent on θ. The scattered intensity is reduced due to internal interference at all angles except for zero. It is possible to eliminate the effect by measuring at low angles and extrapolating to zero angle. However, as internal interference originates from the difference in distance between the scattering centres of the molecule the variation of scattering intensity with angle should yield information about the size and shape of the molecule.

The angular dependence of the scattering intensity for large particles can be defined as

$$P(\theta) = \frac{R_\theta}{R_0} \qquad 2.24$$

Where P(θ) is the scattering function, at zero angle the effect of internal interference is zero and so P(0) is equal to 1. The value for R_0 cannot be measured experimentally as most of the incident light is transmitted through the solution. R_0 is therefore determined by extrapolation to zero angle. Light scattered from different solute molecules can interfere, reducing the sum of the individual scattering intensities of the solute molecules, this effect is eliminated by extrapolation to zero concentration.

The particle scattering function can be related to the radius of gyration, R_G, of a molecule (see Tanford, 1961) without having to make assumptions about the shape of the molecule.

$$\lim_{\theta\to 0} P(\theta) = 1 - \frac{\mu^2 \langle R_G^2 \rangle}{3} \qquad 2.25$$

where $\mu = \left(\frac{4\pi}{\lambda}\right)\sin\frac{\theta}{2}$

This is unique because all other measurements of the radius of gyration require some assumption about the shape of the molecule. Equation 2.25 can be rearranged to give:

$$\lim_{\theta\to 0} P(\theta)^{-1} = 1 + \frac{16\pi^2}{3\lambda^2}\langle R_G^2 \rangle \sin^2\frac{\theta}{2} \qquad 2.26$$

and at zero concentration and zero angle $KC/R_\theta = 1/M$, therefore:

$$\lim_{(\theta\to 0),(c\to 0)} \frac{KC}{R_\theta} = \frac{1}{MP(\theta)} = \frac{1}{M}\left(1 + \frac{16\pi^2}{3\lambda^2}\right)\langle R_G^2 \rangle \sin^2\frac{\theta}{2} \qquad 2.27$$

The limits of the equation (extrapolation to zero angle/concentration) can be achieved using the method developed by Zimm (1948). Figure 2.3 shows an example of a Zimm plot where extrapolations to zero angle and zero concentration are plotted on the same

graph. The extrapolation to zero angle, a plot of KC/R_θ vs kC (where k is an arbitrary scale factor), yields 1/M as the intercept and the second virial coefficient as the gradient. The extrapolation to zero concentration, a plot of KC/R_θ vs $\sin^2(\theta/2)$, yields a direct measure of the R_G (limiting slope/intercept = $(16\pi^2/3\lambda^2)\langle R_G^2\rangle$).

Figure 2.3 A typical Zimm plot (taken from Kratochvil, 1987).

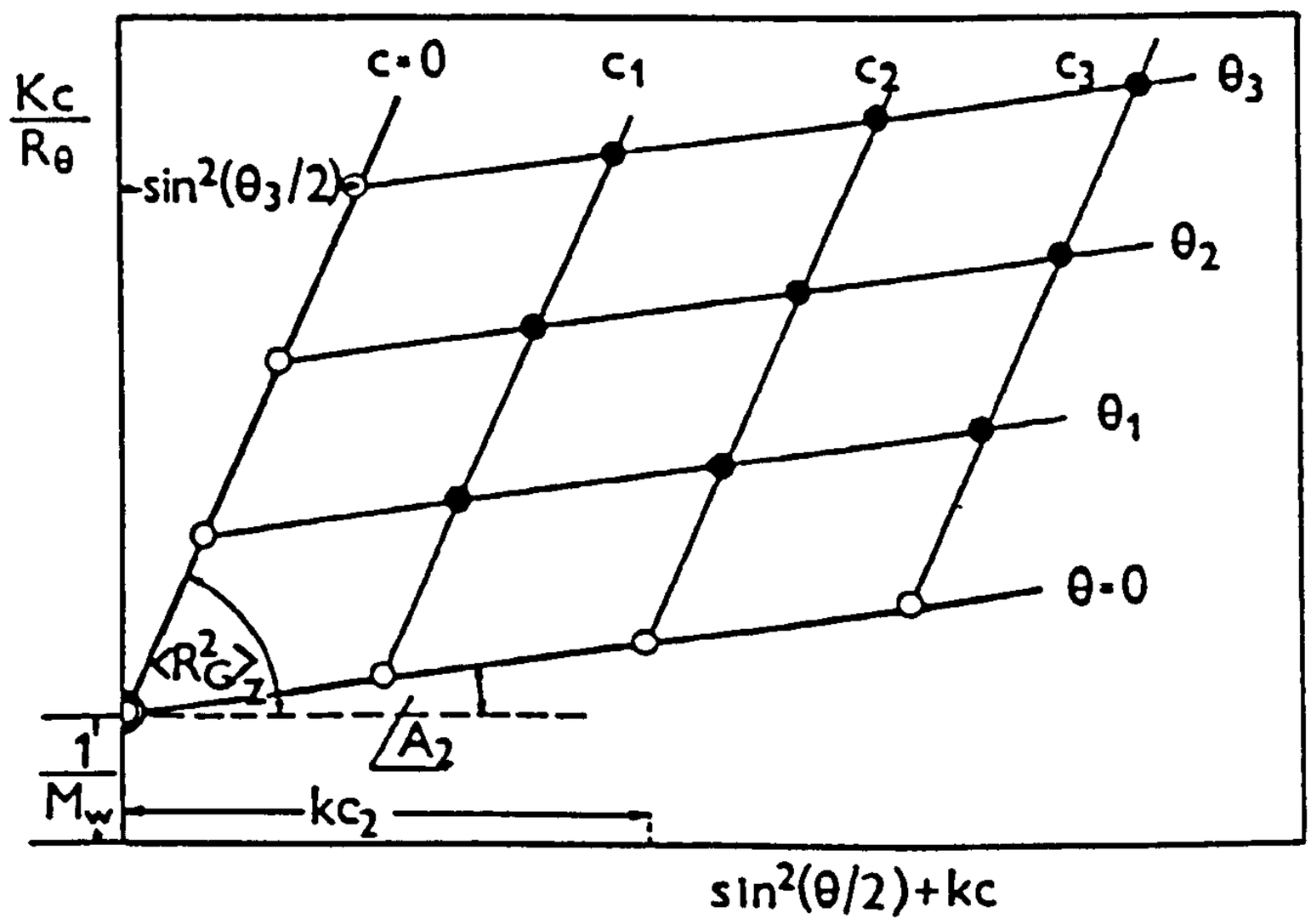

The particle scattering function can be derived for the three basic particle shapes, rod, sphere and random coil (see Kratochvil, 1987; Tanford, 1961) and are illustrated in Figure 2.4. It is recommended, however, to evaluate the particle size from the radius of gyration (Kratochvil, 1987). For the three basic shapes the following equations apply:

Rod $$\left\langle R_G^2 \right\rangle = \frac{L^2}{12} \qquad 2.28$$

Sphere $$\left\langle R_G^2 \right\rangle = \frac{3a^2}{5} \qquad 2.29$$

Random coil $$\left\langle R_G^2 \right\rangle = \frac{\left\langle r^2 \right\rangle}{6} \qquad 2.30$$

where L is the length of a rod, a is the radius of a sphere and r^2 is the mean square end-to-end distance of a random coil.

Figure 2.4 Particle scattering functions, $P(\theta)$ for the three basic particle shapes: (1) the linear random coil, (2) thin rods and (3) Spheres (x and $x^{1/2}$ are products from dimensional and angular factors and differ depending upon particle shape) (taken from Kratochvil, 1987).

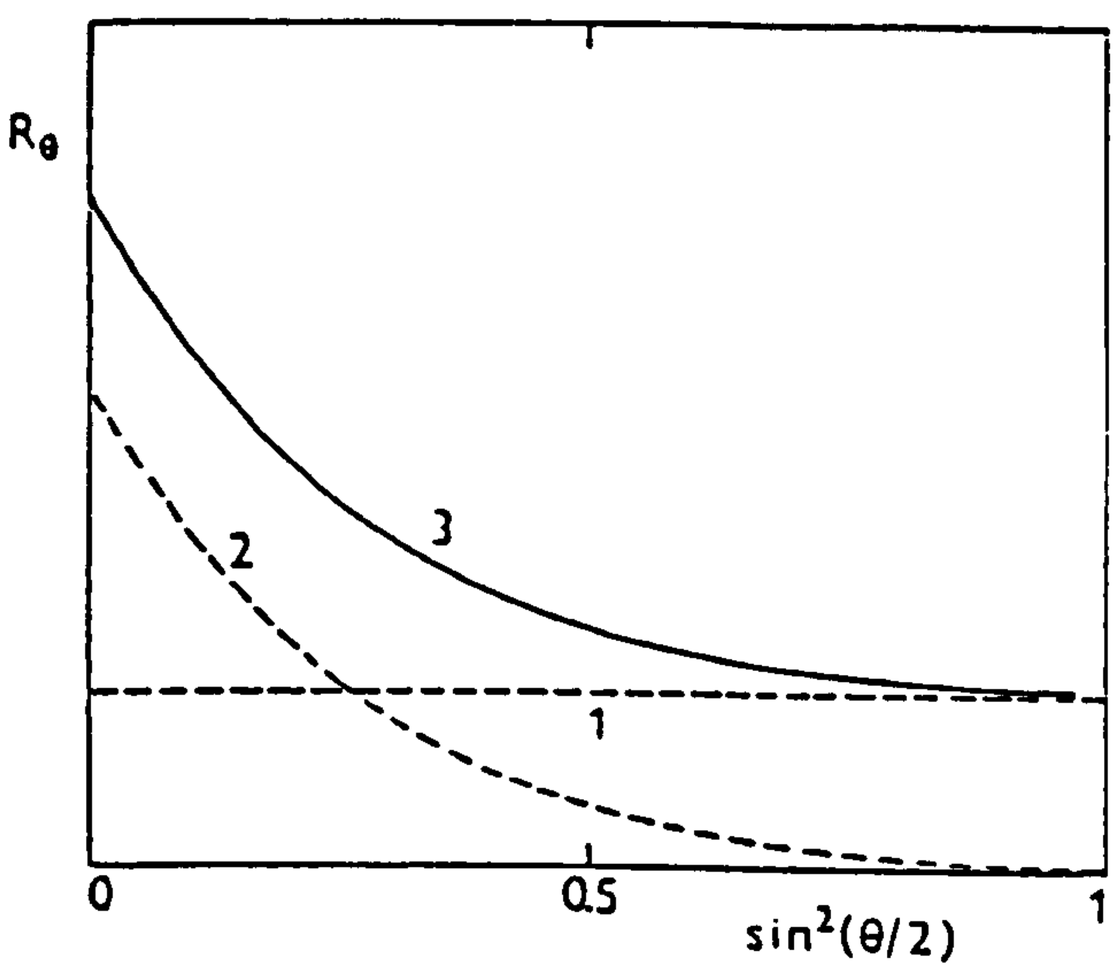

Information about particle size is a result of the angular dependence of the scattering intensity which is described by $P(\theta)$. To show this graphically, plots of $P^{-1}(\theta)$ vs $\sin^2(\theta/2)$ or a parameter proportional to $\sin^2(\theta/2)$ (for example $\mu^2\langle R_G^2\rangle = (16\pi^2/\lambda^2)\langle R_G^2\rangle\sin^2(\theta/2)$ are constructed. Similarly, KC/R_θ instead of $P^{-1}(\theta)$ can be plotted against $\sin^2(\theta/2)$, allowing elucidation of the weight average molecular weight. However, if angular dependencies of samples of different molecular weight are to be compared, it is

preferable to use a plot of $P^{-1}(\theta)$ vs $\sin^2(\theta/2)$. There are three typical shapes for $P^{-1}(\theta)$ shown in Figure 2.5. Line 1 corresponds to the angular dependence of small molecules where R_θ is independent of θ. For molecules with dimensions comparable to the wavelength of the incident light, line 2, the angular dependence may either be linear with a positive slope or moderately curved. Highly polydisperse solutions or those containing small amounts of large particles results in the strongly curved line 3. This can be explained by there being no angular dependence of R_θ for small particles. There is, however, high angular dependence for large particles where R_θ decreases with increasing angle of observation, resulting in a strong curvature at low angles which diminishes at higher angles. This is analogous to broad continuous distributions of molecular size and shape. For such systems it may be impossible to obtain any information from $P^{-1}(\theta)$ functions as the effect of polydispersity may outweigh the effect of particle shape.

Figure 2.5 Angular dependence of the Rayleigh ratio, R_θ, for a two component (large and small particles) system. Line A represents the contribution from the small particles, line B represents the contribution from the large particles and Line C the total excess Rayleigh ratio (taken from Kratochvil, 1987).

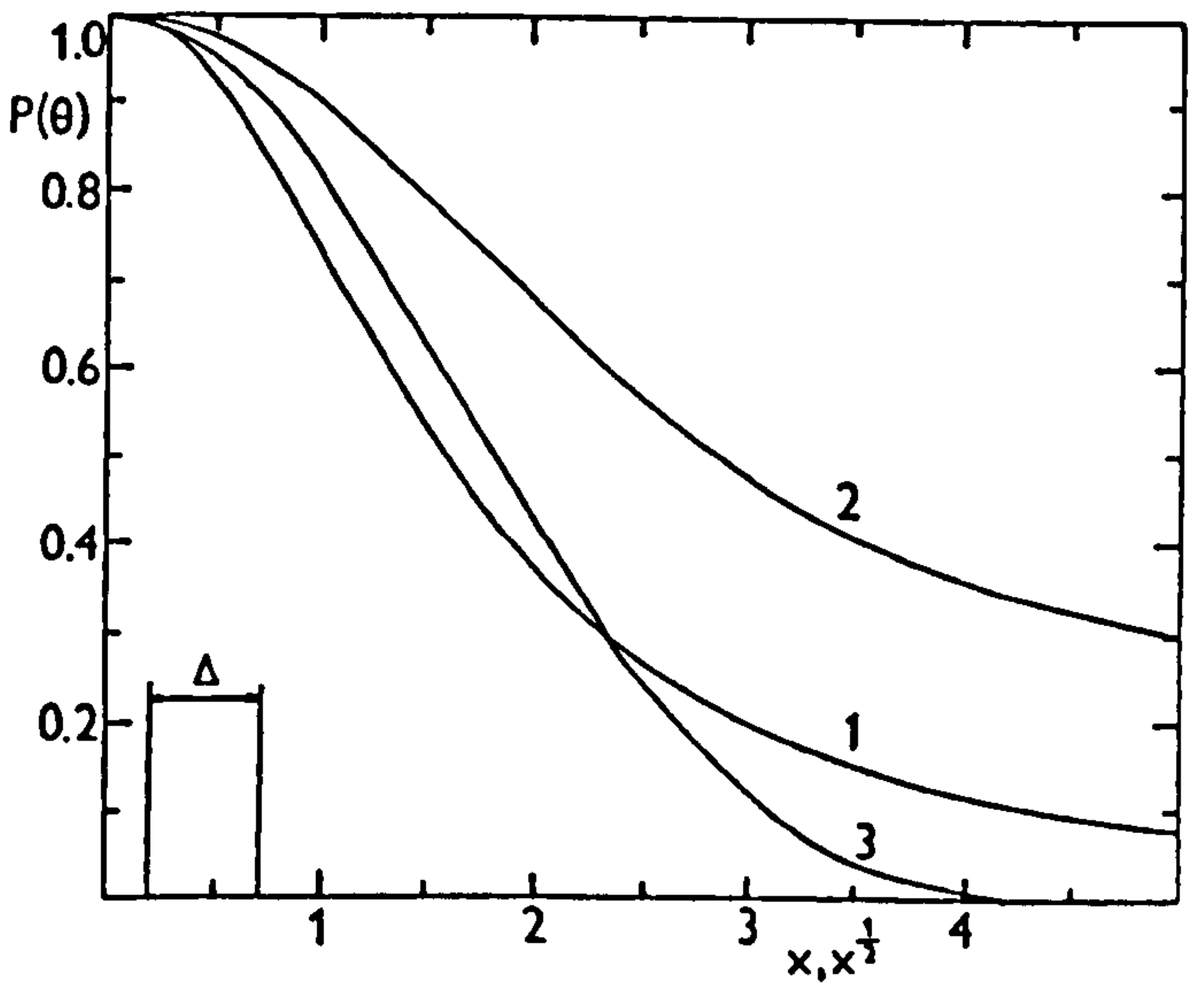

Chapter 3

Materials and Methods

3.1 Materials

3.1.1 Solvents

For most of the work in this study an acetate buffer pH 4.5 was used (Dawson *et al.*, 1986), although for sedimentation velocity analyses performed at 230 nm a phosphate buffer had to be used as acetate absorbs in this region (20 mM sodium dihydrogen phosphate and sodium chloride to an ionic strength of 0.1 M, adjusted to pH 4.5 using HCl). When necessary the ionic strength was adjusted using anhydrous sodium chloride. All buffers were prepared using deionised distilled water (dH_2O) and chemicals were all of Fisher Analytical Reagent grade (Fisher Scientific UK).

3.1.2 Samples

3.1.2.1 Chitosans

Sea Cure 210 + ('SC210 +'), a glutamate salt of chitosan was provided by Pronova Ltd. (Drammen, Norway). This is a preparation with a degree of acetylation of 11 % (i.e. of $F_A = 0.11$) and which has previously been well characterized (Errington, 1993). SC210 + chitosan solutions were prepared in acetate buffer to a concentration of 4 mg/ml; this was then left to dissolve overnight.

Chitosan A fractions 1-5 were a gift from Dr. G. Berth (Max Planck Institute, Teltow, F.R.G.). Chitosan A has a degree of acetylation of 25 % (i.e. of $F_A = 0.25$), determined by titration. Chitosan A has been characterised by Berth *et al.* (1998).

3.1.2.2 Mucins

The PGM ('PGM-MD') was purified according to the modified procedure of Hutton *et al.* (1990). Fresh pig stomachs were obtained from a local abattoir. The stomachs were cut open on the lesser curvature and emptied out. They were then washed gently to remove any remaining matter and mucus gel was scraped from the surface, using a microscope slide, into a proteinase inhibitor buffer chilled to 0°C (Sodium phosphate 67mM, Iodoacetamide 1mM, α(6) Aminocaproic acid 100mM, Benzamidine HCl 5mM, EDTA 10 mM, N-ethyl maleimide 10mM, Phenylmethylsulphonyl fluoride (PMSF) 1mM, pH 6.5). This was then solubilized by mild homogenization for 1 minute in a Waring blender. Insoluble material and tissue debris were removed by centrifugation for 1 hour at 2.4×10^4 g at 4°C. The supernatant was filtered through glass wool to remove any lipid etc. Caesium chloride was then added to adjust the density of the solution to 1.42 g/ml. This solution was then loaded into ultracentrifuge tubes and spun at 40,000 rpm at 4°C for 11 hours. The supernatant was taken off into 9 equal fractions and the fractions from each centrifuge tube pooled. The density from each fraction was measured using a pipette and balance (see Table 3.1). The fractions were then dialysed overnight in dH_2O to remove the caesium chloride.

Mucin was assayed colorimetrically using the periodic acid/Schiffs method (Mantle and Allen, 1978). Protein was assayed using the BioRad™ protein assay and any nucleic acid contamination from the ratio of A_{260nm} and A_{280nm} measurements (see Table 3.1). The fractions that were chosen were 4-7, these were further purified by running down a Sepharose Cl-2B column. Mucins were collected as the total

excluded volume from the column, fractions were assayed using A_{280nm}. A typical elution profile is shown in Figure 3.1.

Figure 3.1 Elution profile from 30 x 2.5 cm Sepharose Cl-2B column, V_t was approximately 150 ml. Void volume was determined using Blue Dextran (Mw = 2,000,000 Da, Sigma, Poole, Dorset), as 37ml. Fractions of 1ml were collected from 30ml onward. The dialysed mucin solution was loaded onto the column in 5 ml aliquots. A 0.1 M sodium acetate buffer, pH 4.5, was used as the elution buffer.

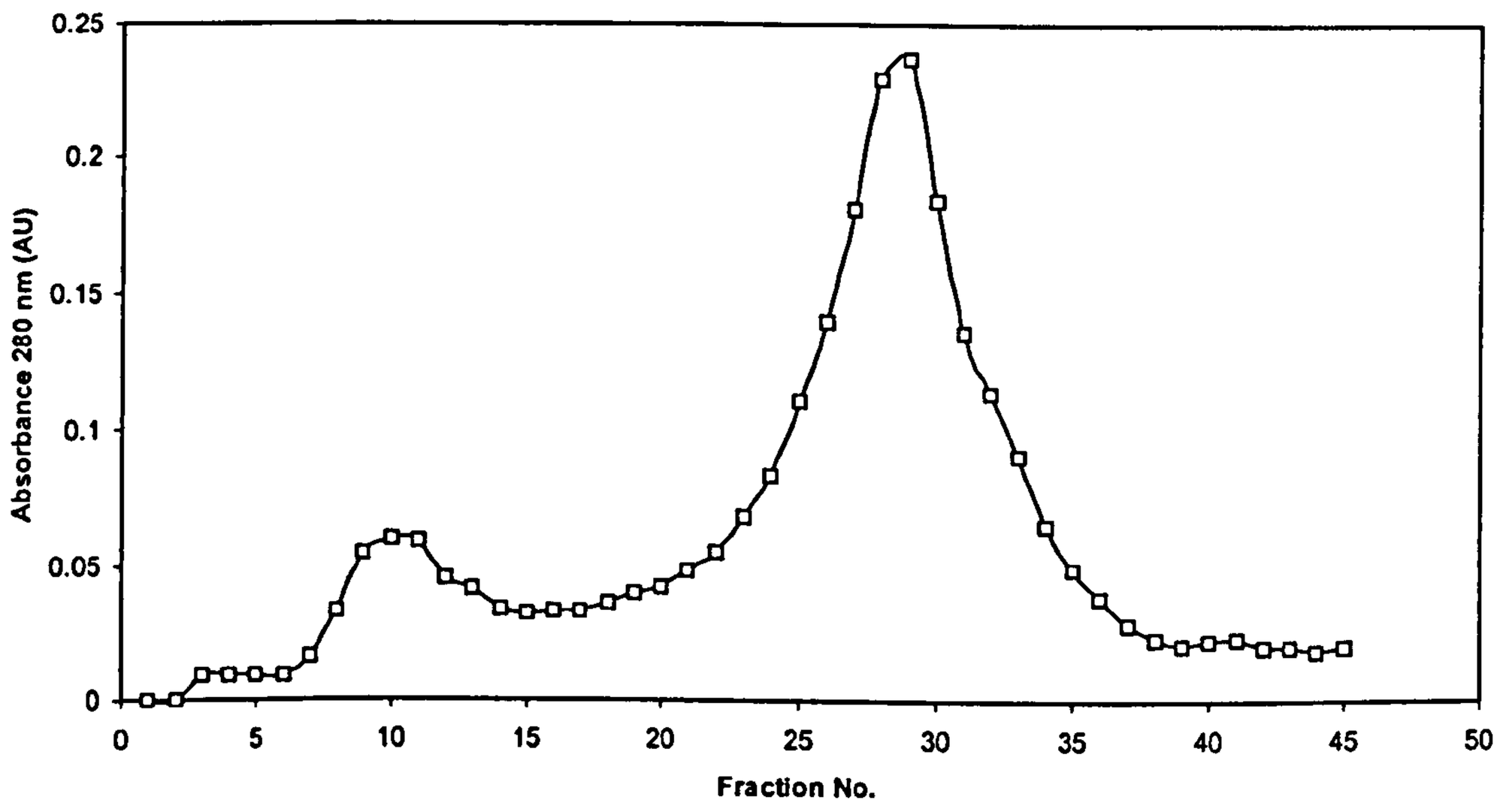

The fractions that were collected in this particular example were those from 9-12, which represent the absorbance of mucin at 280 nm. These fractions were pooled and then concentrated using an ultrafilter (Amicon Ultrafiltration cell Model 202).

An absorbance peak was also observed in fractions 22-35, this peak was due to sample impurities.

Table 3.1 Density of pooled fractions from the density gradient ultracentrifugation.

Fraction No.	Density (ml/g)	Glycoprotein content (mg/ml)	Protein content (mg/ml)	Nucleic acid content (mg/ml)
1	1.395	0.938	3.60	0.560
2	1.413	0.615	0.46	0.190
3	1.422	0.988	0.42	0.160
4	1.453	1.797	0.35	0.062
5	1.453	1.985	0.33	0.058
6	1.491	2.029	0.31	0.051
7	1.518	2.143	0.27	0.062
8	1.538	1.325	0.24	0.080
9	1.550	0.768	0.19	0.190

The cardiac, fundus and antrum mucins were a gift from Prof. I. Carlstedt (Institute for Medical Chemistry, Univ. Lund, Sweden). They were purified from different regions of the porcine stomach as described by Nordman *et al.* (1997). They have been characterised in terms of their polysaccharide composition using mass spectrometry, see Nordman *et al.* (1997); Karlsson *et al.* (1997).

All mucins were slowly defrosted and dialysed into buffer overnight at 4°C before use and all mucins had their molecular integrity checked by SEC/MALLS.

3.2 Methods

3.2.1 Light scattering

3.2.1.1 SEC/MALLS

The light scattering instrumentation that was used for molecular weight determination was the DAWN-F photometer (Wyatt Technology Ltd, Santa Barbara, USA). For a full description of the equipment see Wyatt, 1992, 1993. A representation of the Size Exclusion Chromatography/Multi-Angle Laser Light Scattering (SEC/MALLS) equipment is shown in Figure 3.2.

The light scattering cell and the geometry for a typical detector is shown in Figure 3.3, the cell is made of glass chosen to have a higher refractive index than that of the eluting phase. The solution passes through a channel in the cell, typically 1.25mm in diameter, in a direction parallel to the laser beam. The cell has 18 hybrid transimpedence type photodiodes which detect the scattered light.

As can be seen from Figure 3.2, size exclusion columns precede the cell and separate samples by size before entry into the light scattering cell (Figure 3.3). The columns used were an Ultrahydrogel Guard column plus a TSK G 4,000 PW, a TSK G 5,000 PW and a TSK G 6,000 PW 30mm x 7.5mm (Anachem, Beds., UK). There is also a refractive index detector, Wyatt Optilab 903 interferometric refractive index detector to measure concentration via dn/dc (the specific refractive index increment). Other equipment includes a Waters 590 HPLC pump (Waters, Millipore, Watford, UK) a degasser (Degasys, DG-1200, uniflow, HPLC Technology, Macclesfield, UK), and a Rheodyne Model 7125 injection valve (Rheodyne, Inc., Cotati, CA, USA) fitted with a 100µl injection loop. Degassing is important to remove air bubbles from the eluent, which could affect the pump,

columns and the light scattering detector. Data is acquired via a dedicated PC and analysed using the ASTRA™ software (Wyatt Technology, Santa Barbara, USA).

Figure 3.2 Schematic representation of the SEC/MALLS apparatus (Taken from Harding and Jumel, 1998).

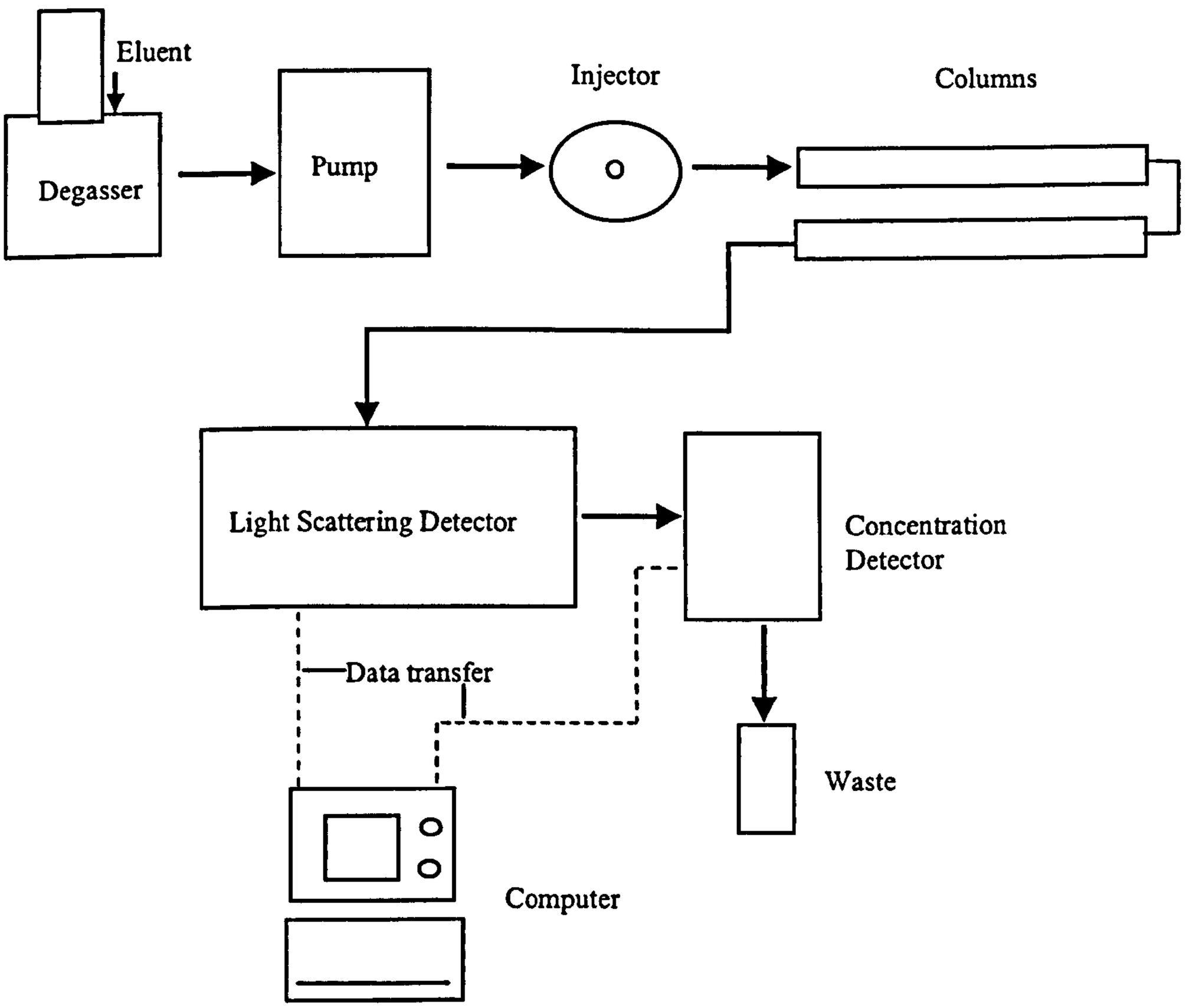

Figure 3.3 Geometry of a light scattering cell from the DAWN-F photometer.

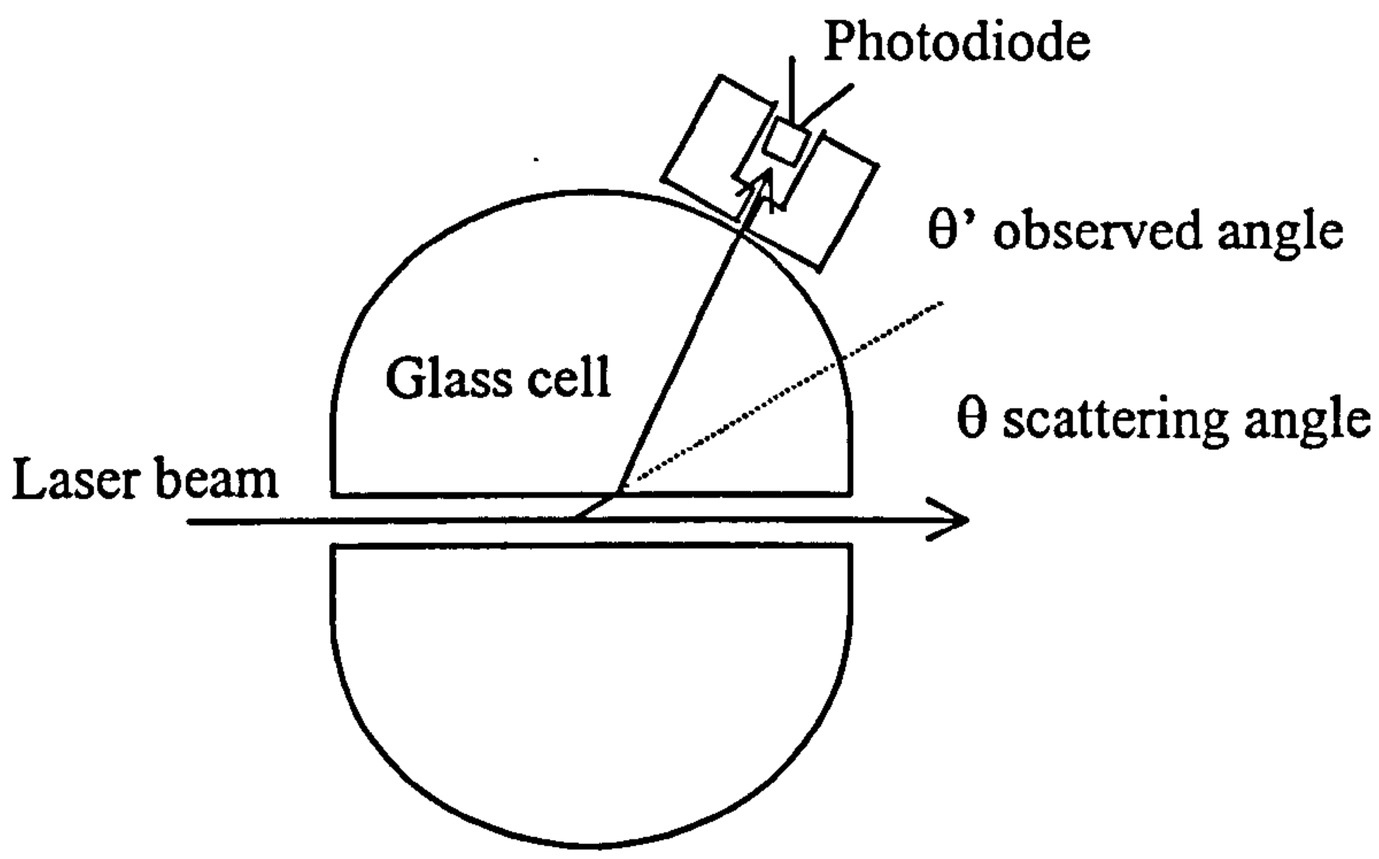

Molecular characterization of PGM-MD, cardiac, antrum and fundus mucins was performed using SEC/MALLS. Loading concentrations were 0.2, 0.98, 1.54 and 0.84 mg/ml for PGM-MD, cardiac, antrum and fundus mucins respectively. A flow rate of 0.8 ml/min was used for all SEC/MALLS measurements and all samples were filtered through a 0.45 μm filter before injection. Each injection was made through a 100 μl injection loop. An ionic strength of 0.1 M was present in all solutions, to prevent any charge effects. As SEC columns dilute the solute, the effect of non-ideality related to concentration can be assumed to be negligible.

3.2.1.2 Flow Field Flow Fractionation/MALLS

3.2.1.2.1 Mechanism of separation

The process by which field flow fractionation (FFF) achieves separation combines elements of chromatography and field-driven techniques such as ultracentrifugation, electrophoresis, etc. FFF is an elution technique with

underlying roots in differential flow displacement; like field-driven techniques, FFF requires a field or gradient. The field in FFF is applied at right angles to the direction of flow and drives different species into different flow laminae in a thin channel (50-300 μm). According to the different rates of flow, the species then become separated as they pass down the channel (see Figure 3.4). In Figure 3.4 the component bands X and Y are separated by flow in a thin ribbon-like channel, this is the preferred channel geometry for FFF (Giddings *et al.*, 1993). The channel is designed so that the flow profile is parabolic. The flow in the channel propels X and Y towards the outlet, however, the velocity at which X and Y travel in the channel depends upon the mean positions of the bands in the parabolic flow profile. The perpendicular field controls these positions and must be strong enough to drive the separate species into different regions of the parabolic flow profile. Generally the molecules are driven into equilibrium distributions close to one wall, termed the accumulation wall. The species that are forced closest to the accumulation wall (Y) will move the slowest due to the parabolic flow profile, and will become separated from those that are more highly elevated (X) and as such are moving faster. The accumulation wall consists of a membrane layered over a frit (see Figure 3.4 C), it is the pore size of the membrane that defines the lower size limit for separation. A spacer is used to form the channel. The spacer is placed between two large blocks and the channel is formed with the thickness of this spacer defining the channel height.

It is the viscous force exerted on a particle by the cross-flow stream that gives rise to separation. Stokes law gives (Ratanathanawongs and Giddings, 1993):

$$|F| = f|U| = 3\pi\eta|U|d = kT|U|/D \qquad 3.1$$

where the final term arises from the Stokes-Einstein relation, $D = kT/f$, d is the Stokes diameter of the particle, η is the viscosity, f is the frictional coefficient, D is the diffusion coefficient and U is the cross-flow velocity. Separation in the flow

FFF channel is therefore based on size alone (Giddings *et al.*, 1993), with retention time being approximately proportional to diameter.

Channel design is flexible, asymmetrical channels have been used in flow FFF with some success (Wittgren and Wahlund, 1997a). An asymmetrical channel narrows at the far end and it is this narrowing that forces solvent molecules through the membrane and creates the cross-flow. These channels have advantages over symmetrical channels as they act to concentrate the sample into a smaller volume as it passes through the channel and they do not require a separate pump to control the cross-flow.

3.2.1.2.2 Applications of Flow FFF

Flow FFF has been used to characterise proteins, e.g. Stevenson and Preston (1996) used Flow FFF to separate wheat proteins and Wahlund *et al.* (1996) used asymmetrical Flow FFF to separate high molecular weight glutenin proteins found in wheat flour. Wahlund *et al.* (1996) managed to fractionate proteins with hydrodynamic radii from 5-45 nm. Polysaccharides have been examined by Wittgren *et al.* (1998), who examined a nondegraded κ-carrageenan using asymmetrical Flow FFF/MALLS. Good separation was obtained and the effects of different buffers on the conformation was also investigated. Wittgren and Wahlund (1997b) used asymmetrical Flow FFF again to characterise a range of dextran and pullulan standards. Other macromolecules have also been characterised, see for example Jensen *et al.* (1996); Wittgren *et al.* (1996).

The same general experimental setup is used as shown in Figure 3.2, with the column system being replaced by the flow FFF cell. To provide the cross flow for the cell a Pharmacia Biotech P500 pump was used. The channel is supplied by FF fractionation, Inc. as was the cellulose membrane. All other procedures e.g. data collection, etc, are the same as those outlined previously.

Figure 3.4 (A) The narrow channel is usually created by cutting the channel volume from a thin spacer and placing the spacer between two appropriate walls. The thickness of the channel varies but is typically between 75-260 μm. Channel breadth is a few centimeters and length is in tens of centimeters. The outflow is linked to one or more detectors, for example ultraviolet, refractive index, light scattering, etc. **(B)** The exploded view shows the different distributions of two arbitrary components X and Y across the parabolic flow profile and the unequal flow displacement velocities that result. For normal mode operation, the X and Y clouds are distributed exponentially above the accumulation wall with characteristic (mean) elevations l_x and l_y. **(C)** Flow FFF, separation is driven by a "cross-flow" field (Taken from Giddings *et al.*, 1993).

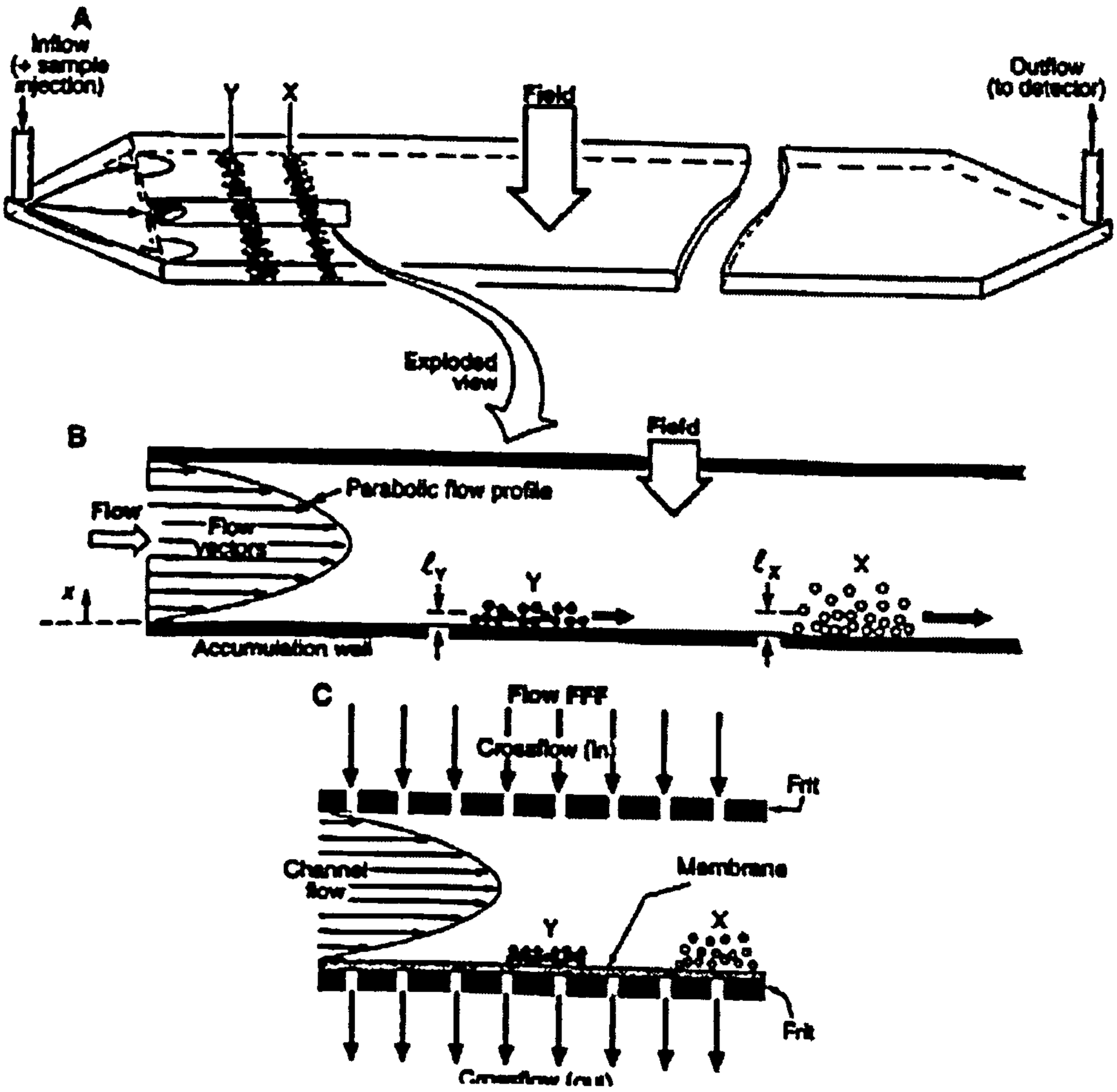

3.2.2 Analytical ultracentrifugation

Four analytical ultracentrifuges have been used in this study:

MSE Mk II	(for Schlieren optics)
Beckman Model E	(for Schlieren optics)
Beckman XL-A	(for Absorption optics)
Beckman XL-I	(for Absorption/Interference optics)

A description of the methods of detection and data collection can be found in Harding *et al.* (1992a). Data is collected as a record of solute concentration in a cell as a function of radial position, r. For absorption and interference optics this is against a reference solution (buffer only) contained in the same cell, double sector cells. The Schlieren optical system does not need a reference solution and uses single sector cells (see Figure 3.5).

Figure 3.5 Single and double sector analytical ultracentrifugation cells.

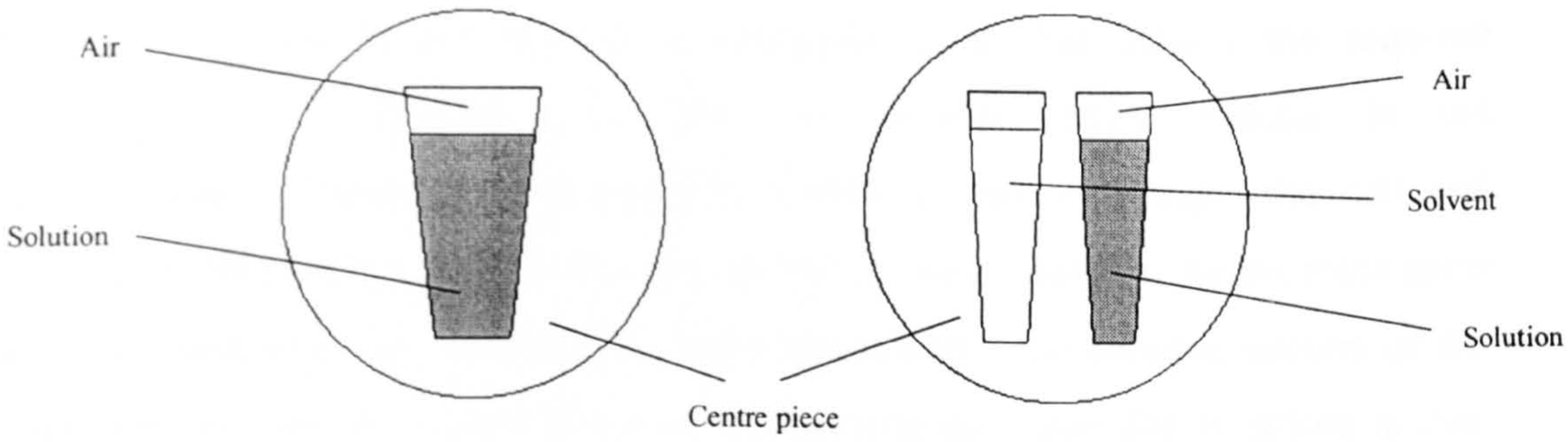

The MSE Mk II and the Beckman Model E are equipped with the Schlieren optical system and a phase plate. Schlieren optics are refractometric, i.e. they measure the concentration gradient, dC/dr, as a function of radial distance, r. These optics utilise the difference in the refractive index of the pure solvent and the solute because the

solution usually has a higher refractive index than that of the pure solvent. Light passing through the centrifuge cell where there is a change of concentration (and therefore refractive index) will be deviated radially, whereas light passing through regions of pure solvent or areas of uniform concentration will not be deviated. The light source on the Beckman Model E consists of a mercury lamp with a green filter, the MSE Mk II used a 500W green laser. A phase plate consists of a step and a hairline on a glass plate, the size of the step is equal to half the wavelength of the incident light. The phase plate causes destructive interference which produces a dark line on the image corresponding to the ultracentrifuge cell. Single sector cells with a pathlength of 20mm for the MSE Mk II and 12mm for the Beckman Model E were used. The advantage of this optical system is that the macromolecule does not need to contain a chromophore, e.g. chitosan which does not absorb except in the far UV, which cannot in general be accurately monitored. The disadvantage of this method is that the concentration has to be >2 mg/ml in order to produce a reasonable peak. Data collection is achieved by means of an online charge coupled device (CCD) camera that captured images at timed intervals.

The absorbance optical system of the Beckman XL-A and XL-I is illuminated by a high intensity xenon flash lamp that generates light at wavelengths between 190-800nm. The light passes through a monochromator that selects the required wavelength and collimates the light. An incident light detector in the monochromator measures light intensity before it passes through the cell and normalises the data for flash-to-flash variations in lamp intensity. As the rotor spins the light absorbance is measured for the reference and the solution sectors of the ultracentrifuge cell by a light detector. An absorbance value due to solute is then calculated on the basis of the difference between these two measurements. Absorbance optics are more sensitive than Schlieren optics and enable measurements to be made at much lower concentrations, providing that the macromolecule has a suitable chromophore. Data is collected, stored and processed on-line using a coupled PC and the Beckman data capture software (Giebeler, 1992).

The Rayleigh interference optical system is also based on refractive index, although unlike Schlieren it records concentration (relative to the meniscus) vs r rather than the concentration gradient vs r. Monochromatic light from a 30 MW diode laser passes through two parallel slits in the bottom of the laser housing just above the rotor, so that two parallel beams exit the laser housing. The system is aligned such that one beam passes through the reference sector and the other beam passes through the sample sector of the cell in the spinning rotor. The refractive index of the sample should be higher than that of the solution so the sample wave should be retarded relative to the reference wave. The light then passes through a series of lenses that overlap the two sector images at the CCD sensor, registering the interference pattern. A dedicated PC then acquires the image at specific time intervals and the data is analysed using the Beckman data capture software. The interference optics have the advantage of being able to provide better accuracy at high concentration, higher radial resolution, a greater concentration range and the ability to scan very steep gradients (see XL-I instruction manual, 1996). The disadvantage of this system is that it has an upper concentration limit of ~ 2 mg/ml.

Sedimentation velocity (on SC210 + chitosan, Chitosan A fractions 1-5, PGM-MD, cardiac, antrum and fundus mucins) was performed on the MSE (Crawley, U.K.) Mk II, Beckman (Palo Alto, U.S.A.) Model E, Optima XL-A and Optima XL-I at a temperature of 20°C and at various rotor speeds from 2,000-40,000 rpm..

Sedimentation equilibrium (on Mefp-1) was performed on the Optima XL-A analytical ultracentrifuge (Beckman Instruments, Palo Alto, CA) at a temperature of 20°C and at a rotor speed of 14,000 rpm.

Chapter 4

Conformation of structural integrity of mucins by SEC/MALLS

4.1 Introduction

As previously described in Chapter 2, light scattering is an absolute method for the determination of molecular weight, however, until molecules could be separated these measurements only produced averages over the whole distribution. The use of on-line light scattering detectors coupled to separation techniques, such as SEC and Flow FFF, enables the analysis of almost any sample no matter how polydisperse (Wyatt, 1993).

A Multi-Angle Laser Light Scattering (MALLS) photometer with simultaneous measurement across the angular intensity envelope was first developed by Wyatt (Wyatt *et al.*, 1988). A full description of this instrument has been given in Chapter 3. When it is coupled to a separation method it enables on-line characterisation of macromolecules giving separation and absolute measurement of molecular weight and radius of gyration.

4.2 Size Exclusion Chromatography (SEC)

Biological macromolecules rarely contain completely monodisperse solutions. Size exclusion chromatography is one of the most popular techniques for investigating whole molecular weight distributions. It separates molecules according to their size in solution and their molecular weight is then calculated using a set of standards.

The column matrix consists of a network of porous polymer beads. Large molecules cannot penetrate the pores in the gel matrix and are eluted in the void volume of the column (void volume is the volume between the packing particles). Smaller molecules can diffuse into the pores and are therefore retained on the column and elute after the void volume.

One of the problems with SEC is that the separation is based on the size of the molecule and not on its molecular weight. Molecular weight calculation relies on the use of calibration with standards. So, the molecular weight calculated is based on the assumption that the standards behave in the same way as the sample being investigated. A drawback of light scattering is that it calculates molecular weight on the basis of an average over a whole molecular weight distribution. Coupling the separation power of size exclusion chromatography to the ability of MALLS to calculate an absolute molecular weight is an ideal solution to these problems.

There are many extensive reviews on the uses and applications of SEC/MALLS especially in the field of biopolymers, see for example Jumel *et al.* (1992); Wyatt (1993), Williams *et al.* (1992).

4.3 Materials and Methods

4.3.1 Preparation of samples

Mucin, chitosan and mucin/chitosan mixture solutions were prepared as described in Chapter 3 in an acetate buffer pH 4.5, at concentrations of 0.2, 2 and 0.1/0.2 mg/ml respectively. Ionic strength was adjusted using NaCl. The dn/dc values used for the calculation of concentration from the refractive index detector were 0.160 ml/g for mucin, 0.150 ml/g for chitosan and 0.155ml/g for the complex (Huglin, 1972).

4.4 Results and Discussion

4.4.1 SEC/MALLS

4.4.1.1 PGM-MD at 0.1 M ionic strength

The chromatogram shows two traces, the trace from the MALLS experiment is taken from the 90° detector and also from the refractive index (RI) detector. The chromatogram produced by the 90° detector shows a narrow peak indicating that the sample is relatively monodisperse. The single peak in the refractive index chromatogram also confirms that no impurities are present in the sample, also that there are no high molecular weight aggregates or low molecular weight breakdown products.

4.4.1.2 Cardiac, Antrum and Fundus mucins at 0.1 M ionic strength

It was expected that all three traces would be similar as the mucin populations, isolated from the porcine stomach, were all purified using the same technique. The weight average molecular weights were slightly different (see Table 4.1), the antrum species having the lowest and fundus having the highest. It is interesting to note the difference in the signal trace between cardiac and the other two. Cardiac has the lowest light scattering signal of the three yet all three have similar concentrations (0.98, 1.54 and 0.84 mg/ml for cardiac, antrum and fundus respectively). However, cardiac is the most charged of the three so this could lead to some absorption onto the SEC columns thus reducing the light scattering signal.

Figure 4.1 PGM-MD in acetate buffer pH 4.5 at 0.1 M ionic strength. The y-axis on the left shows the scale of normalised voltage for the 90° detector and on the right the scale for the voltage of the RI detector.

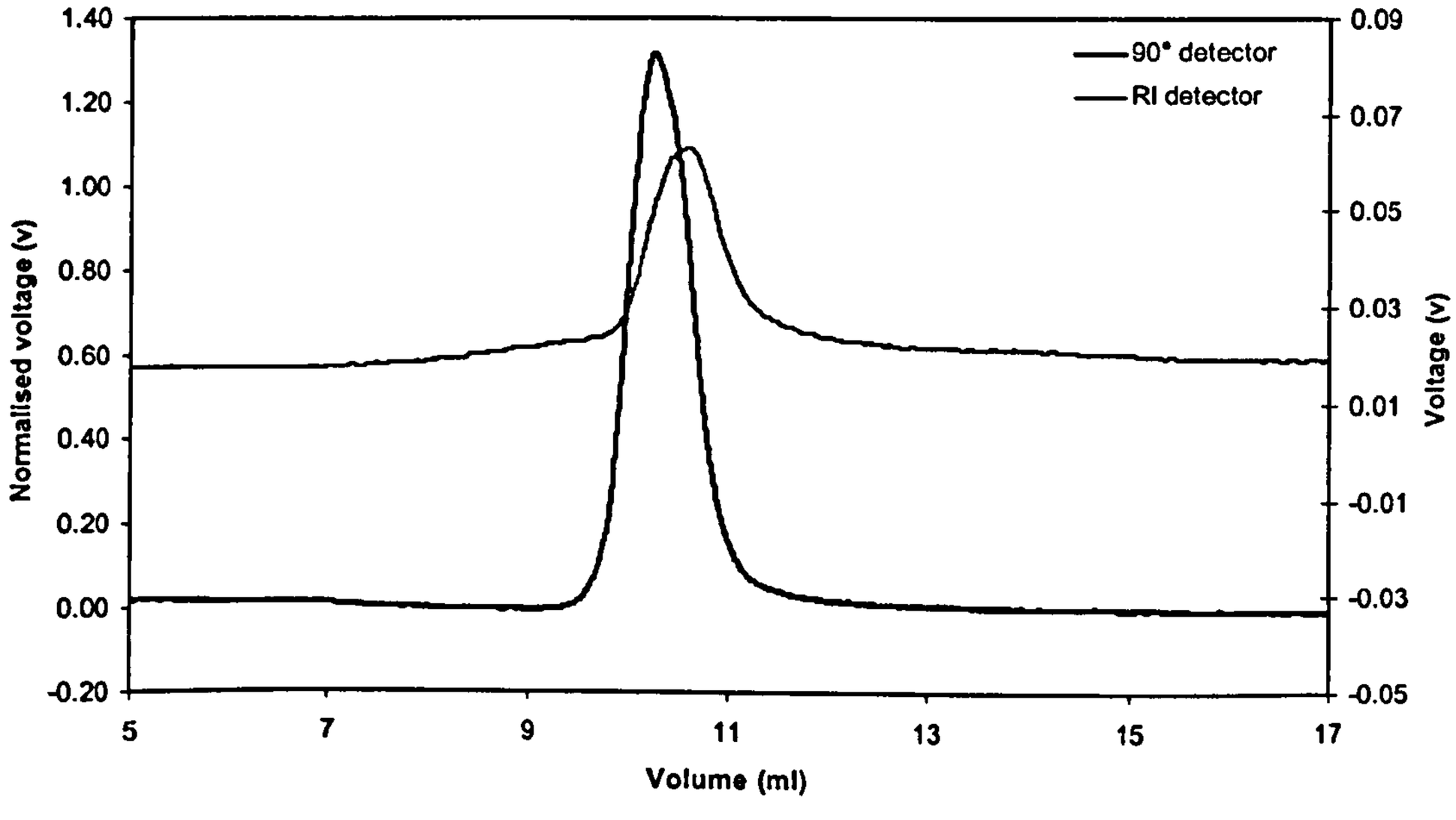

Figure 4.2 Cardiac mucin in acetate buffer pH 4.5 at 0.1 M ionic strength.

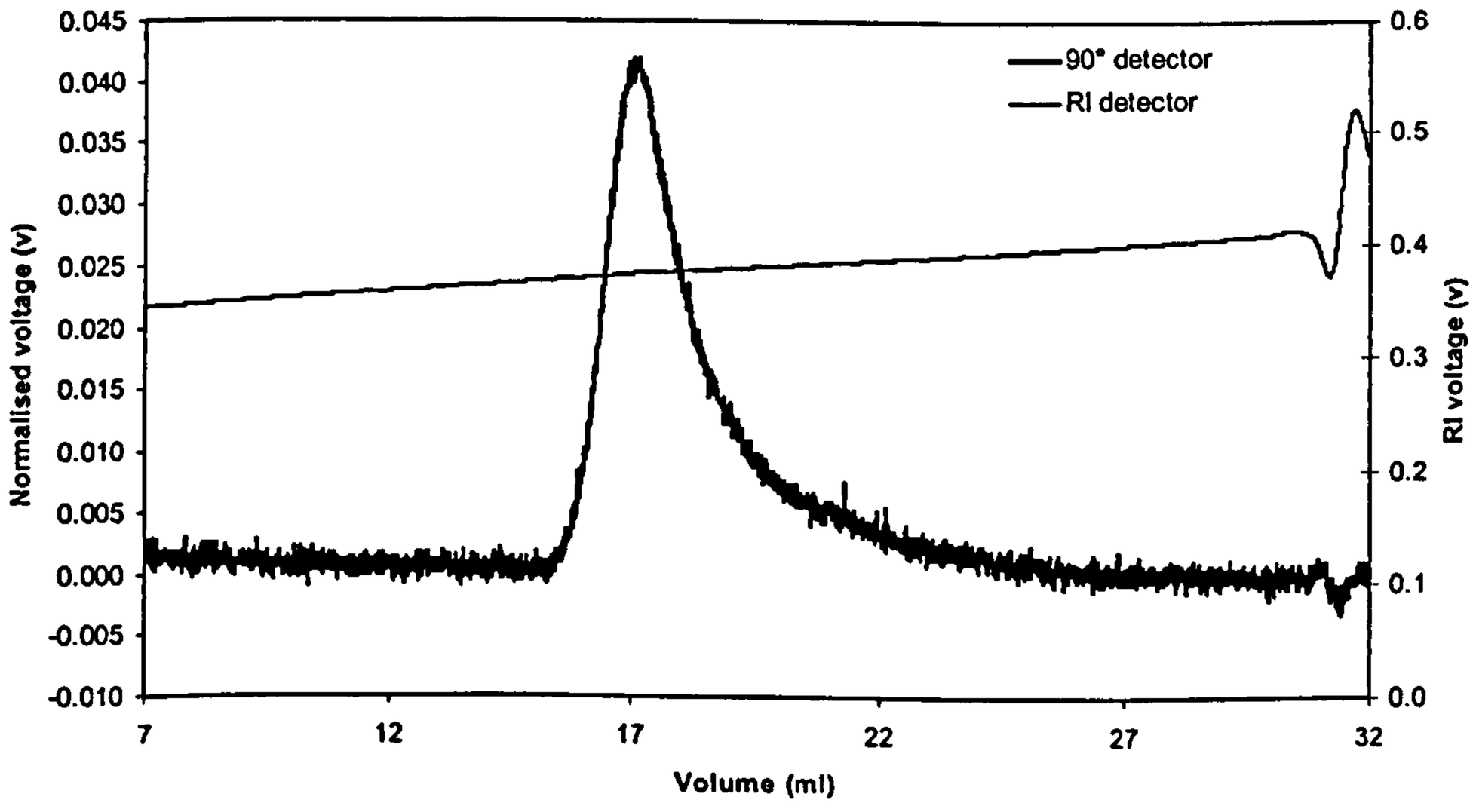

Figure 4.3 Antrum mucin in acetate buffer pH 4.5 at 0.1 M ionic strength.

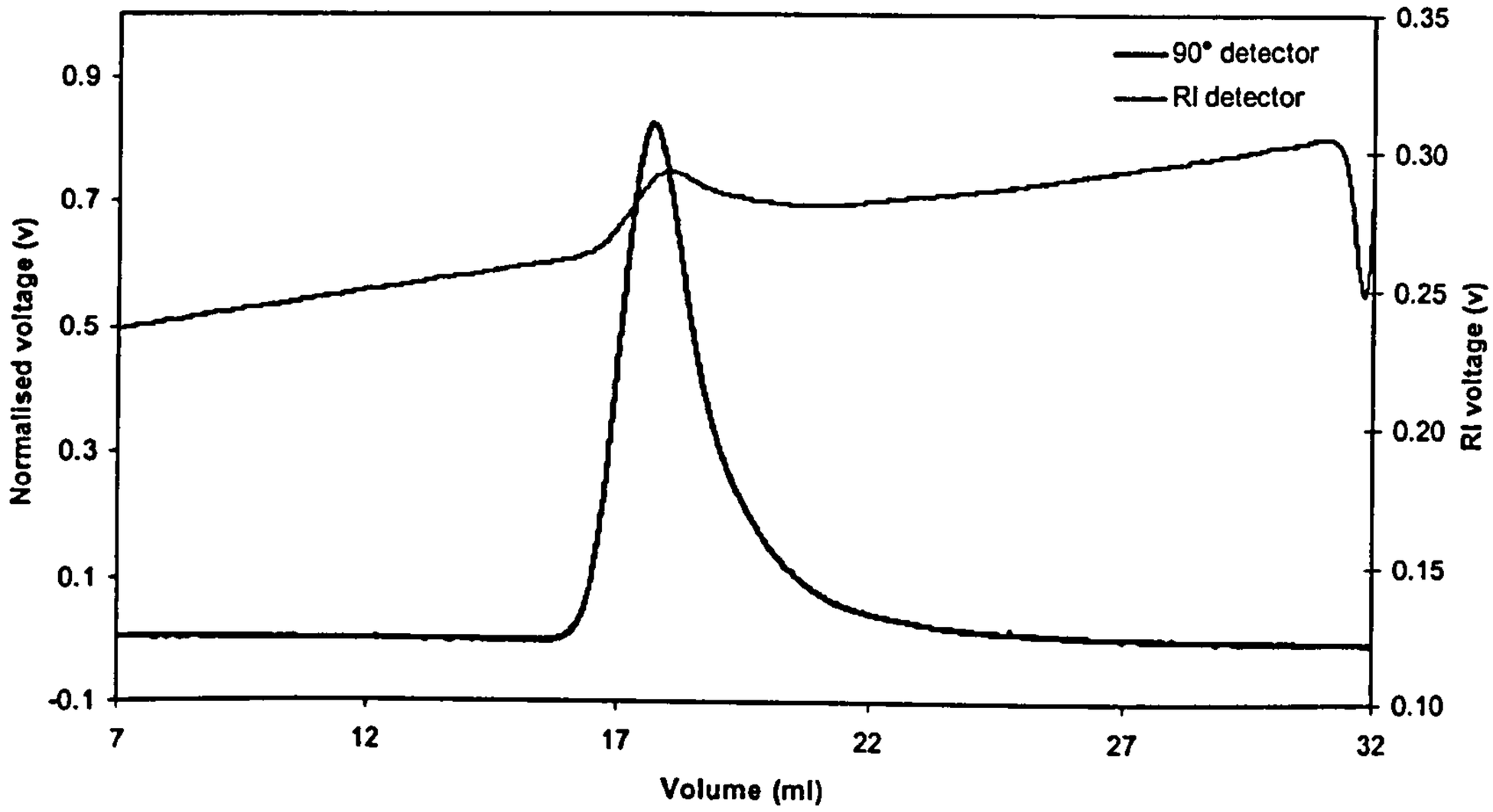

Figure 4.4 Fundus mucin in acetate buffer pH 4.5 at 0.1 M ionic strength.

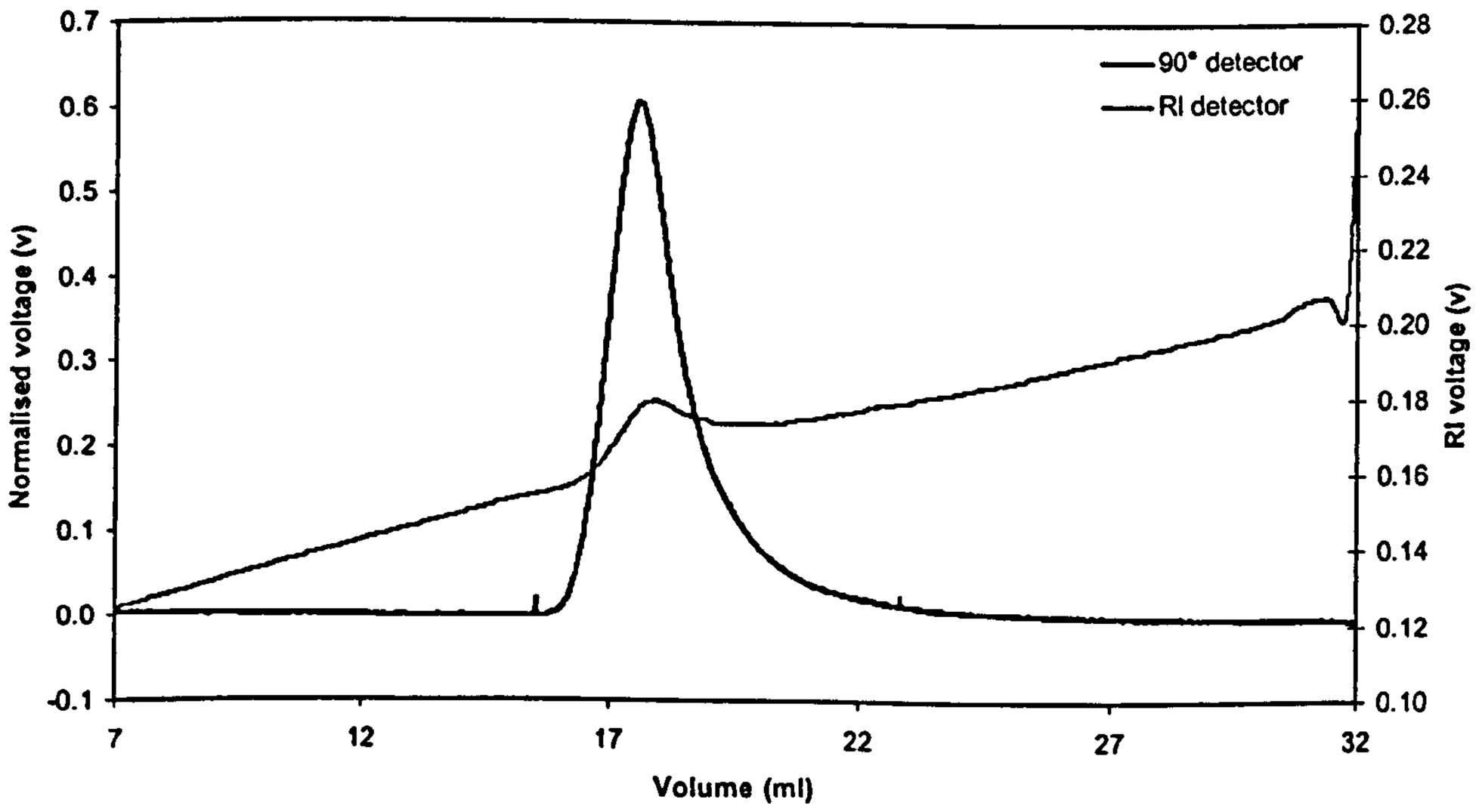

The Mark-Houwink-Kuhn-Sakarada coefficient c (MHKS c) is calculated by plotting the log of the molecular weight against the log of the root mean square (RMS) radius (Harding, 1995).

$$R_g = K^m M^c \qquad 4.1$$

For a compact sphere it has a value of 0.333, for a rigid coil 1.0 and for a random coil 0.5-0.6. By consulting Table 4.1 it can be seen that the value for all mucins measured indicates that they are all in a random coil conformation. Molecular weights are also consistent, with PGM-MD having a molecular weight of 10 x 10^6 g/mol and the others being around 6 x 10^6 g/mol, which are typical values for mucin glycoproteins (Jumel *et al.*, 1996).

Table 4.1 Characterisation of mucins by SEC/MALLS, weight average molecular weight calculated by SEC/MALLS and MHKS c coefficient from the gradient of the double log plot of weight average molecular weight and RMS radius.

Sample	Molecular weight (g/mol)	MHKS c coefficient
PGM-MD	9.6 (± 0.5) x 10^6	0.56
Cardiac	6.1 (± 1.0) x 10^6	0.52
Antrum	5.6 (± 0.2) x 10^6	0.52
Fundus	6.6 (± 0.2) x 10^6	0.57

4.5 Conclusions

PGM-MD are highly purified mucins with a molecular weight of 10 x 10^6 g/mol. There is no evidence of any of the smaller breakdown products (500,000 g/mol); there is only one species present. The MHKS c coefficient indicates that the PGM-MD sample is in a

random coil conformation. These results are in good agreement with those obtained by Jumel *et al.* (1996)

Cardiac, antrum and fundus mucins from the samples investigated have a relatively high molecular weight of approximately 6 x 10^6 g/mol, although this is not as high as that of PGM-MD. They also have a MHKS c coefficient that indicates a random coil conformation. The chromatograms from the light scattering show that there is a single species present and it is relatively monodisperse. In conclusion the mucins are all of good quality and suitable for interaction studies

Chapter 5

Analytical Ultracentrifugation characterisation of chitosan-mucin systems

5.1 Introduction

Previous work in this laboratory (see Fiebrig, 1995) has shown a strong interaction between Pig Gastric Mucin and SC210 + chitosan F_A = 0.11 (Errington *et al.*, 1993). Recently, mucins purified from different areas of the porcine stomach have been shown to differ in terms of their composition and net charge (Nordman *et al.*, 1997). How this affects the properties of these mucins is of great interest in terms of the specificity of mucoadhesion with chitosan.

Work has also been done on the interaction of a different chitosan with a different degree of acetylation (F_A = 0.25) which has previously been characterised by Berth *et al.* (1998). This chitosan has been separated into 5 fractions that differ in terms of molecular weight and the effect of molecular weight of this chitosan on the interaction with PGM-MD has been investigated.

5.2 Materials and Methods

The mixture solution was prepared by adding equal volumes of the chitosan and mucin solutions, which was then left for 30 minutes at room temperature. A control solution was prepared by adding equal volumes of chitosan solution and dH_2O.

For sedimentation velocity analyses on the XL-A a phosphate buffer pH 4.5 was used, all other experiments used an acetate buffer pH 4.5 (as described in Chapter 3) the ionic strength was adjusted using NaCl. Sedimentation velocity experiments were performed on the MSE Mk II, Beckman Model E and Beckman Optima XL-A/XL-I analytical ultracentrifuges equipped with a Schlieren optical system (Mk II and Model E) coupled on-line to a CCD camera or an absorbance optical system (XL-A/XL-I). For the experiments on the MSE Mk II, 700 µl of each solution was injected into 20 mm pathlength ultracentrifuge cells prior to being loaded into a four piece aluminium rotor. Experiments on the Beckman Model E used 300 µl injected into 12 mm pathlength ultracentrifuge cells which were then loaded into a four piece rotor. By calculating the area under the schlieren peak for each sedimenting species the solute concentration may be determined. Comparison of the Schlieren areas of the unbound chitosan in the mixture with the native chitosan control reveals quantitative information regarding the degree of interaction. The experiments on the Beckman Optima XL-I/XL-A used 320 µl of buffer and 280 µl of sample, injected into 12 mm double sector cells which were then loaded into a four piece rotor. Absorption optics were used to follow the sedimenting boundary, scans were then captured and analysed on-line using Beckman data capture and analysis software (XL-A instruction manual, 1991).

All sedimentation velocity measurements were made at 20°C and at rotor speeds of 2,000, 10,000 and 35-40,000 rpm, to trace the movement of the sedimenting complex, mucin and chitosan respectively.

5.3 Results and Discussion

5.3.1 Characterisation of PGM-MD mucin and SC210 + chitosan

PGM-MD was run in the Beckman XL-A ultracentrifuge to establish the sedimentation coefficient of the sample (Figure 5.1). Sedimentation was achieved at a rotor speed of 10,000 rpm, radial scans were captured at 10 minute intervals and analysed using the Beckman TRANSPORT software (XL-A instruction manual). A sedimentation coefficient of 22 (± 2) Svedbergs was calculated for the PGM-MD sample. This is typical for mucin glycoproteins which have sedimentation coefficients quoted in the region of 20 to 60 Svedbergs (Harding *et al.*, 1999). Due to the low concentration PGM-MD used (approximately 0.2 mg/ml) and considering that only 20 % of the molecular weight of mucins are accounted for by protein, there was significant noise in the profile. As a result no absorbance could be detected at 280 nm, so instead the peak at 230 nm is used. However, acetate buffers absorb in this region so a phosphate buffer had to be used. PGM-MD cannot be detected in the mixture due to the 50 % dilution, the signal is lost in noise.

The SC210 + chitosan sample was also analysed using sedimentation velocity on the Beckman XL-A (Figure 5.2). A value of 0.90 (± 0.03) Svedbergs was obtained for the sedimentation coefficient, calculated using the same method as above, which is in good agreement with Errington *et al.* (1993) who obtained an $S^0_{20,w}$ with a value of 1.41 (± 0.05) Svedbergs for SC210 + chitosan. The boundaries seen in Figure 5.2 are quite broad giving an indication that the sample is very polydisperse. This is confirmed by the Flow FFF/MALLS experiments. The concentration of SC210 + in Figure 5.2 is 4.0 mg/ml. The concentration that is present in the mixture solution of SC210 + and PGM is 2.0 mg/ml, at this concentration it is not possible to distinguish the chitosan boundary from noise. It is not possible to follow the sedimenting boundaries of the complex, PGM-MD and

Figure 5.1 Sedimentation profile of PGM-MD. Experimental conditions were 10,000 rpm, 20°C and scans were taken at 10 minute intervals. Absorbance was measured at 232 nm.

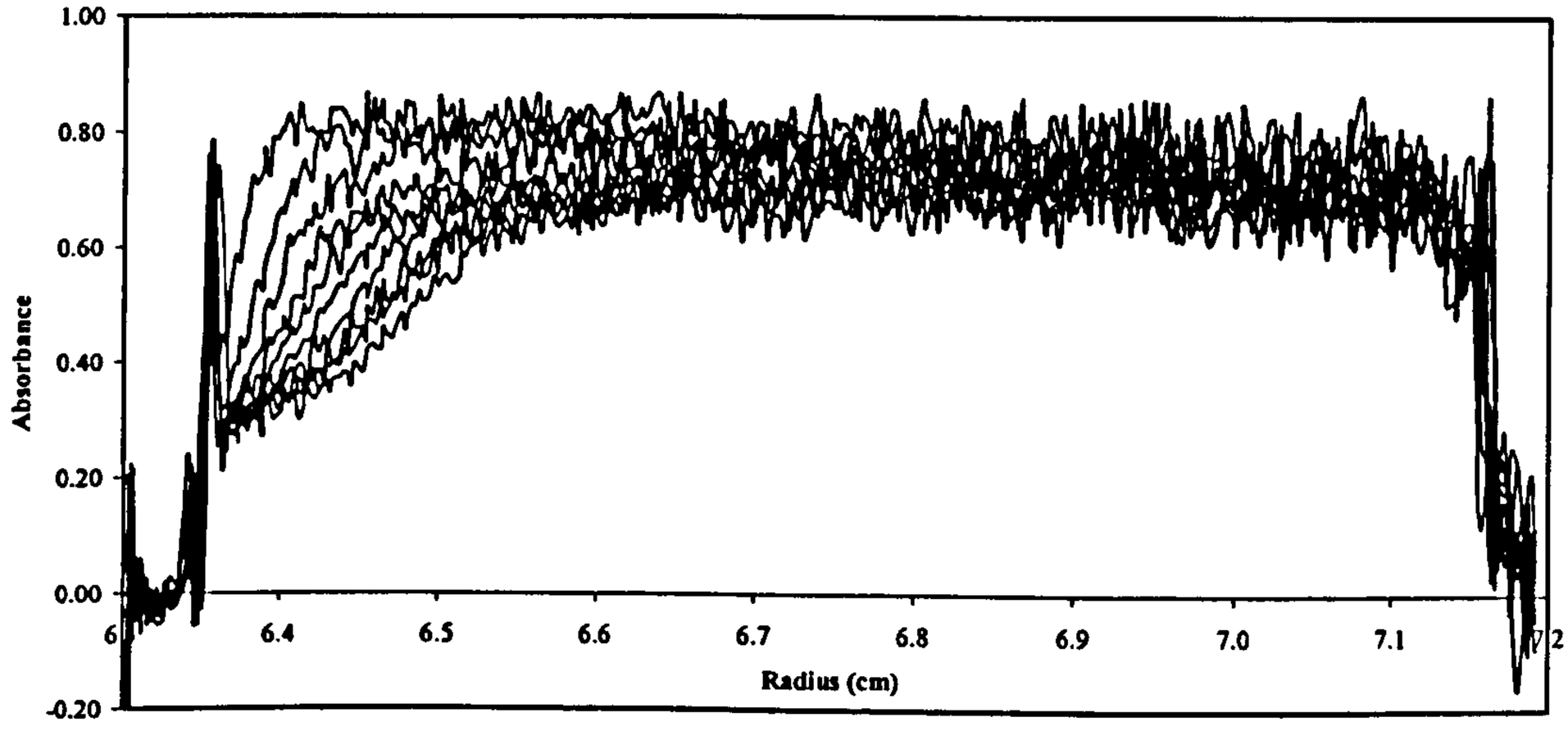

Figure 5.2 Sedimentation profile of SC210 + chitosan. Experimental conditions were 40,000 rpm, 20°C, scans were taken at 20 minute intervals. Absorbance was measured at 232 nm.

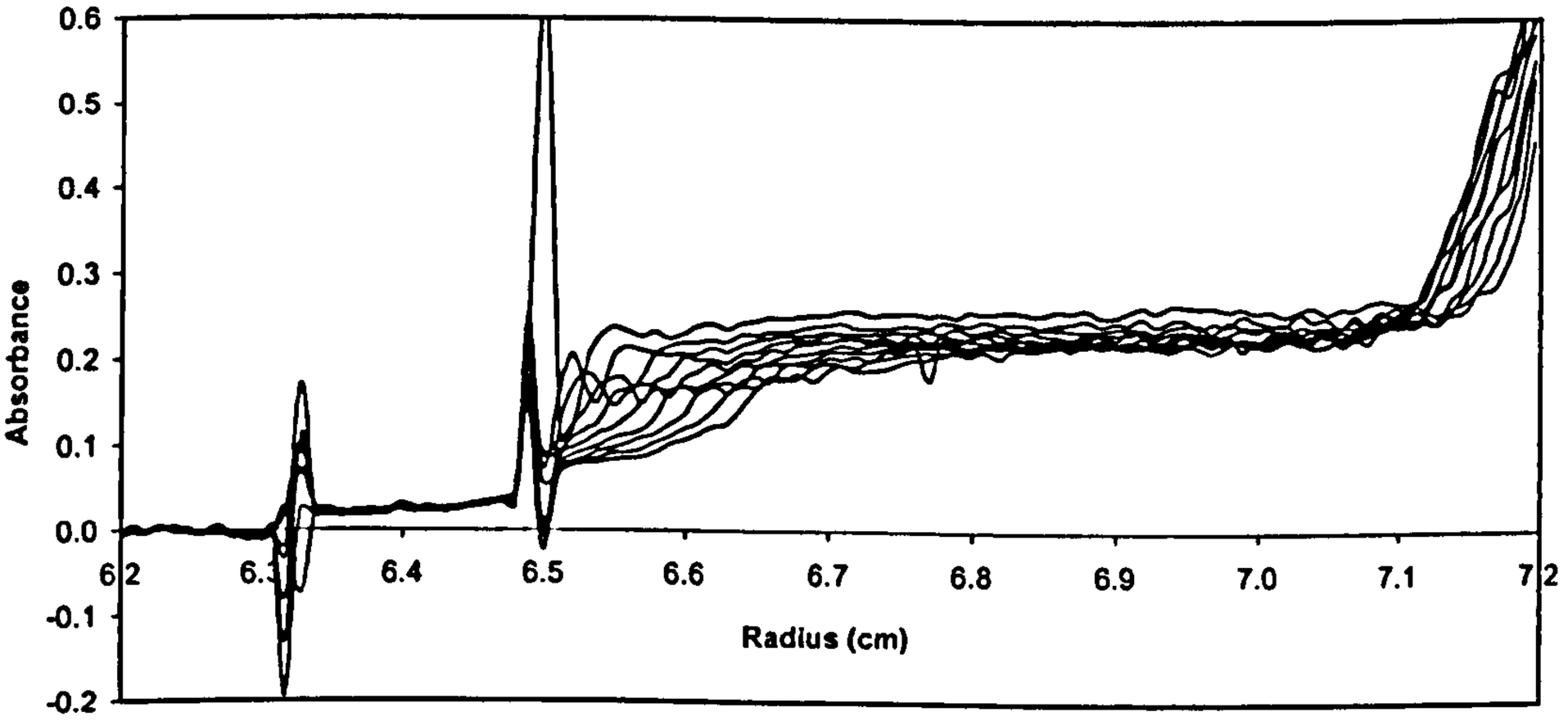

SC210 + using absorbance optics. Thus, a different optical system had to be used to characterise the complex.

5.3.2 PGM-MD and SC210 + complex

Schlieren optics do not need a chromophore but require a relatively high concentration (>1 mg/ml), in comparison to absorbance optics. This was not a problem for chitosan but mucins could not be observed. This was, however, the only possible alternative to the absorbance optical system. An example of a typical sedimentation profile is shown in Figure 5.3.

The differences in the areas under the Schlieren peaks for the control (left) and the mixture (right) are evident from Figure 5.3. The area under the peak is calculated, in terms of numbers of pixels, by following the Schlieren boundary and integrating under the curve, the NIH Image software, Version 1.55 (National Institutes of Health, USA) was used for all analyses. All scans were taken at 35,000 rpm to follow the movement of SC210 + chitosan in the ultracentrifuge. This is because the complex between SC210 + chitosan and mucin could not be detected due to its relatively low concentration (<1.0 mg/ml). The only method that could be used to quantify the complex was to calculate the percentage of chitosan that had interacted with mucin. The quantitative measurement of the amount of chitosan bound is determined by integrating the area under the Schlieren peak for the control and mixture samples and is an average of five measurements. The percentage of chitosan bound was calculated using equation 5.1.

$$\%\ bound = 100 - \left(\frac{area\ of\ mixture}{area\ of\ control} \times 100 \right) \qquad 5.1$$

Figure 5.3 Typical images captured by the on-line CCD camera coupled to the MSE Mk II analytical ultracentrifuge equipped with a schlieren optical system. SC210 + control is the left image it is at a concentration of 2.0 mg/ml, SC210 +/PGM-MD mixture is the right image, concentration of 2.0/0.1 mg/ml. A temperature of 20°C and a rotor speed of 35,000 rpm.

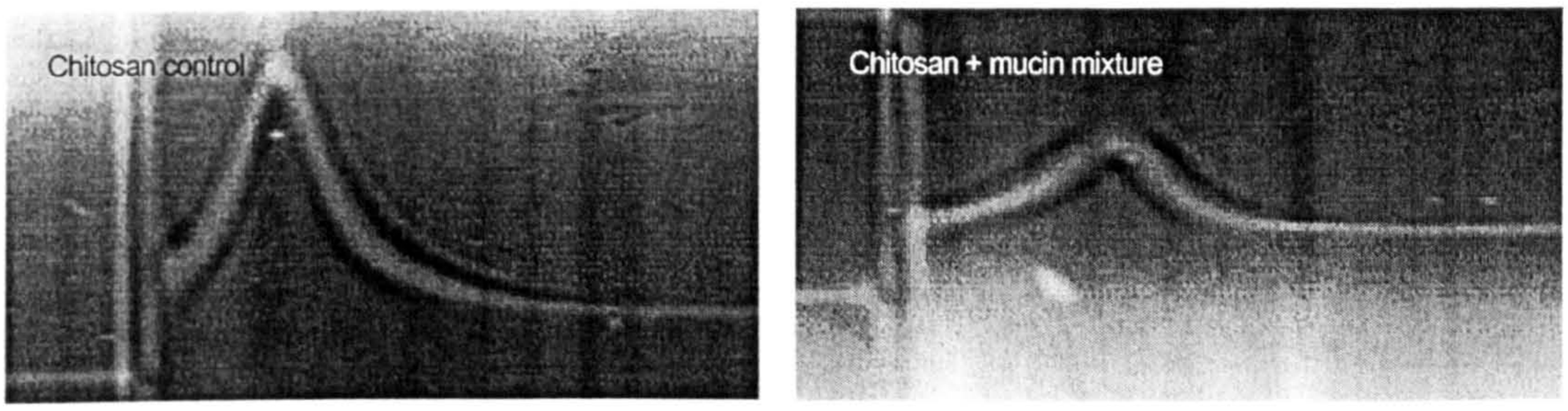

The effect of ionic strength on the interaction of PGM-MD and SC210 + was investigated and the results are shown in Figure 5.4. The interaction is almost completely inhibited above 0.3 M ionic strength. This can be explained by an ionic interaction between the positively charged amine groups present on SC210 + chitosan and the negatively charged sulphate groups present on PGM-MD mucin. As the ionic strength is increased the sodium/chloride ions form a shell around the charged group and effectively screen it from any other potential ion. As a result of this the chitosan and mucin molecules no longer interact to form the large complex seen at lower ionic strengths (<0.3 M). The interaction shows quite a steep dependence on ionic strength with a strong interaction at 0.2 M with 70 % of available SC210 + bound and at 0.3 M there is less than 20 % of the available SC210 + bound to the mucin. These results are important in the context of the ionic strength of the small intestine (0.1-0.2 M (Guyton, 1991)), which is the most probable site of action for a mucoadhesive drug delivery system. In the range of 0.1-0.2 M ionic strength SC210 + chitosan will interact with and bind readily to mucin to form the complex.

Figure 5.4 The effect of changes in ionic strength on the interaction of PGM-MD mucin with SC210 + chitosan. All experiments performed on the MSE Mk II analytical ultracentrifuge at 20°C scans were taken at 35,000 rpm.

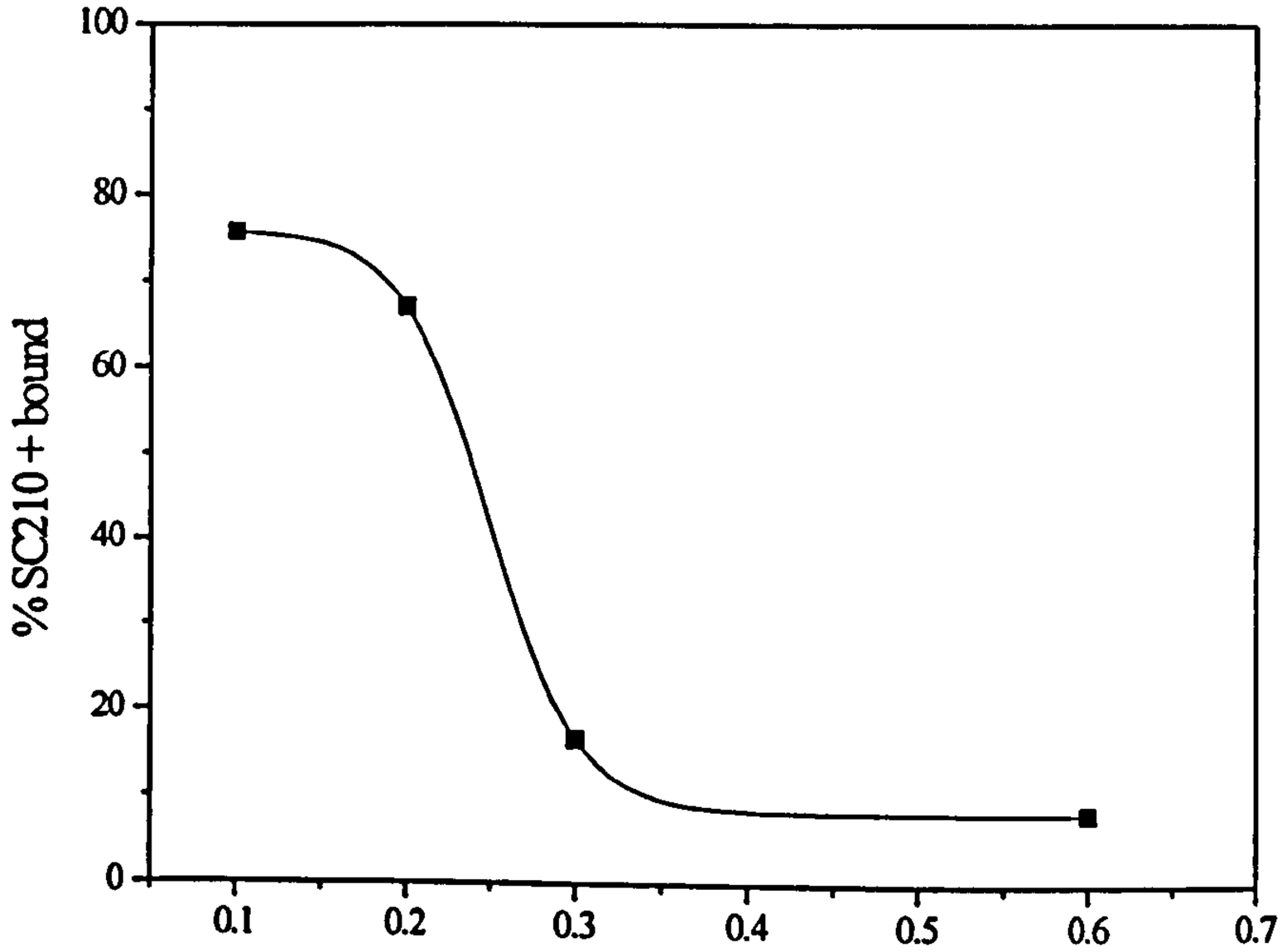

5.3.3 Cardiac, antrum, fundus mucins and SC210 + chitosan mixtures

The effect of mucins purified from different regions of the porcine stomach was also investigated. These mucins have been well characterised in terms of their oligosaccharide composition by matrix-assisted laser-desorption ionisation mass spectrometry (MALDI-MS) (Karlsson *et al.*, 1997; Nordman *et al.*, 1997). At 0.1 M ionic strength there is a strong interaction between SC210 + chitosan and the mucin population purified from the cardiac region of the porcine stomach (Figure 5.5).

A third of the SC210 + chitosan present in the solution had interacted to form the complex with the mucin population purified from the cardiac region of the porcine stomach. This mucin population has been shown by Karlsson *et al.* (1997) to

contain large amounts of sulphated oligosaccharides, which are thought to be responsible for the ionic interaction between mucins and chitosan. This seems to be confirmed by a much reduced interaction of the fundus mucin population (6 %) and no detectable interaction by the antrum mucin population, both of which have few sulphated oligosaccharides in comparison.

Figure 5.5 Effect of mucins purified from different regions of the porcine stomach on the binding of SC210 + chitosan in acetate buffer pH 4.5 at 0.1 M ionic strength.

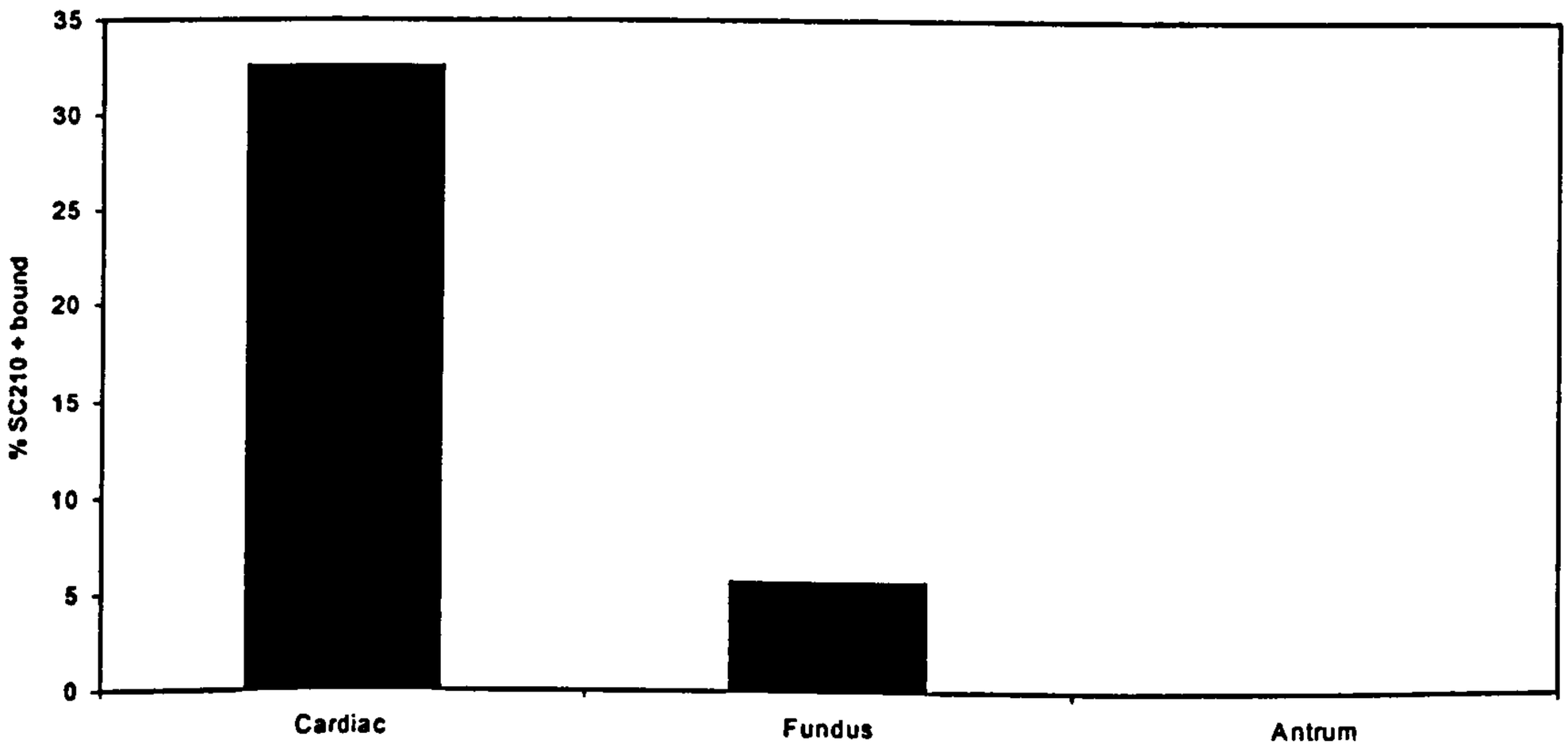

The interaction as the ionic strength increases is harder to account for. The cardiac mucin population shows no detectable interaction at 0.2 M ionic strength and a small interaction (9 %) at 0.3 M (Figure 5.6). This can be explained in terms of a 'charge screening effect' at 0.2 M ionic strength preventing the electrostatic interaction between side chains. At 0.3 M ionic strength it is possible that charges are screened to such an extent that hydrophobic interactions can now occur and cause some complexation.

The data for the antrum and fundus mucin populations is harder to rationalise, there is an increase in the interaction for both mucin species from 0.1 to 0.2 M ionic

strength, but then a decrease in the interaction at 0.3 M. It is possible that, as cardiac mucin has a much higher level of sulphation compared to antrum and fundus, it requires a higher ionic strength to shield charges sufficiently for there to be a hydrophobic interaction. Antrum and fundus mucin species, being less charged, require less charge screening, i.e. a lower ionic strength, for the hydrophobic interactions to occur.

The suppression of an electrostatic interaction by charge screening and an increase in hydrophobic interactions explains the increase in the percentage of SC210 + binding from 0.1 to 0.2 M ionic strength, but not the decrease from 0.2 to 0.3 M ionic strength. It is possible that at this higher ionic strength the structures of the molecules become more compact, due to charge screening effects, and thus interactions between SC210 + and PGM-MD are prevented.

Figure 5.6 The interaction of cardiac, antrum and fundus mucin species with SC210 + chitosan at three separate ionic strengths. All data collected on the Beckman Model E ultracentrifuge using the schlieren optical system. Images captured on-line using the CCD camera and analysed using NIH image (5.11).

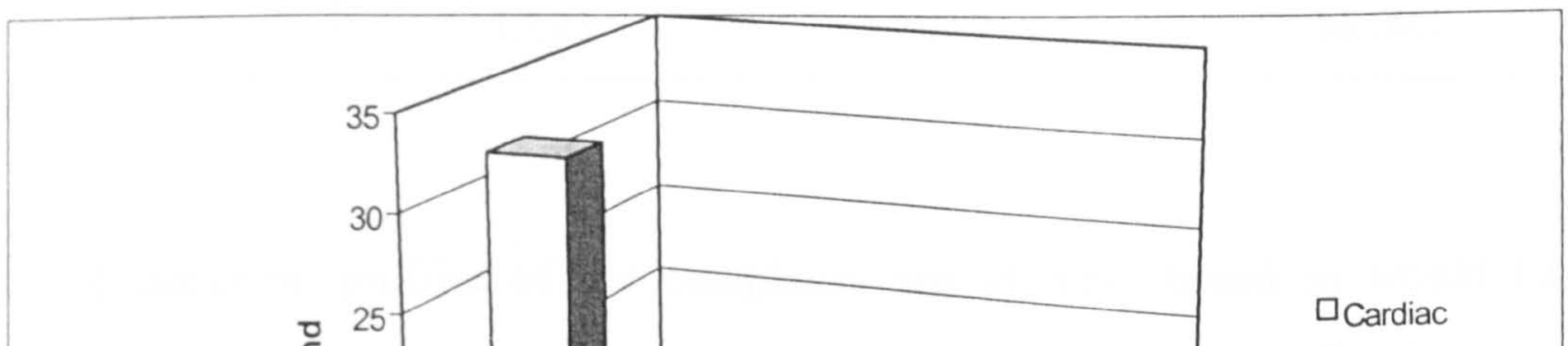

5.3.4 PGM-MD and Potsdam chitosans

The chitosan A fractions all have a degree of acetylation $F_A = 0.25$ (25 %) (Berth *et al.*, 1998) which means that they are less positively charged than the SC210 + chitosan. The effect of this difference in degree of acetylation on the complexation with PGM-MD is interesting to investigate. The effect of the different molecular weights of the fractions and how this affects the size of the complex was also investigated. Some hydrodynamic data for the fractions is displayed in Table 5.1.

Table 5.1 Hydrodynamic data for the chitosan A fractions, concentrations determined using dn/dc, molecular weights from light scattering (data from G. Berth personal communication).

Fraction No.	Concentration (mg/ml)	[η] (ml/g)	Molecular weight (g/mol)
1	0.12	120	N.D.
2	0.26	365	84,200
3	0.396	N.D.	58,000
4	0.714	223	35,300
5	1.143	212	36,000

The sedimentation profiles of the complexes are all very broad as would be expected from the interaction of two species that are initially highly polydisperse. All scans are taken at 2,000 rpm giving an indication as to the size of the complex. Fraction 1 has a very noisy profile with respect to the other fractions (Figure 5.7) which is due to the low concentration of this sample. It was not possible to analyse these samples using the Schlieren optical system because of the low concentration of all of the fractions.

All samples were run on the Beckman Optima XL-I. The chitosan A fractions had an absorbance maxima at 280 nm which was used to follow the interaction. Scans were taken using both the absorbance and interference optical systems. The sedimentation coefficient was calculated using the Beckman TRANSPORT software from an average of 5 measurements.

Figure 5.11 shows an interference profile for a chitosan control (Fraction 5) sample, this is a typical profile for all of the fractions. Due to the smaller size of fraction five, a rotor speed of 55,000 rpm was used to obtain sedimentation. A sedimentation coefficient for this fraction was calculated as 1.04 (± 0.05) Svedbergs.

Figure 5.7 Sedimentation velocity of the Chitosan Fraction 1/PGM-MD complex, a rotor speed of 2,000 rpm was utilised, the temperature was 20°C and radial scans were taken at 5 minute intervals. Absorbance was measured at 280 nm.

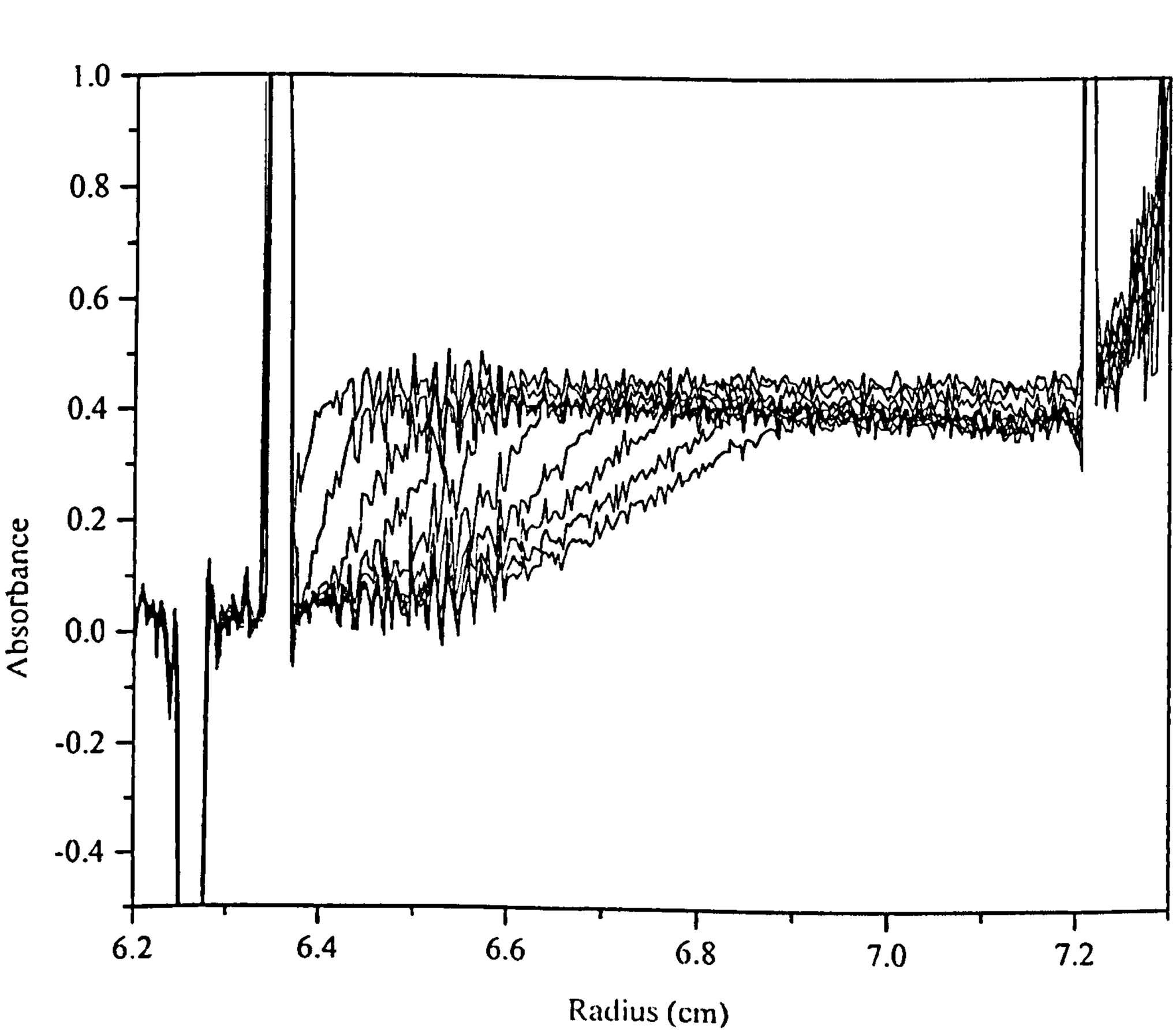

Figure 5.8 Sedimentation velocity of the Chitosan Fraction 2/PGM-MD complex, a rotor speed of 2,000 rpm was utilised, the temperature was 20°C and radial scans were taken at 5 minute intervals. Absorbance was measured at 280 nm.

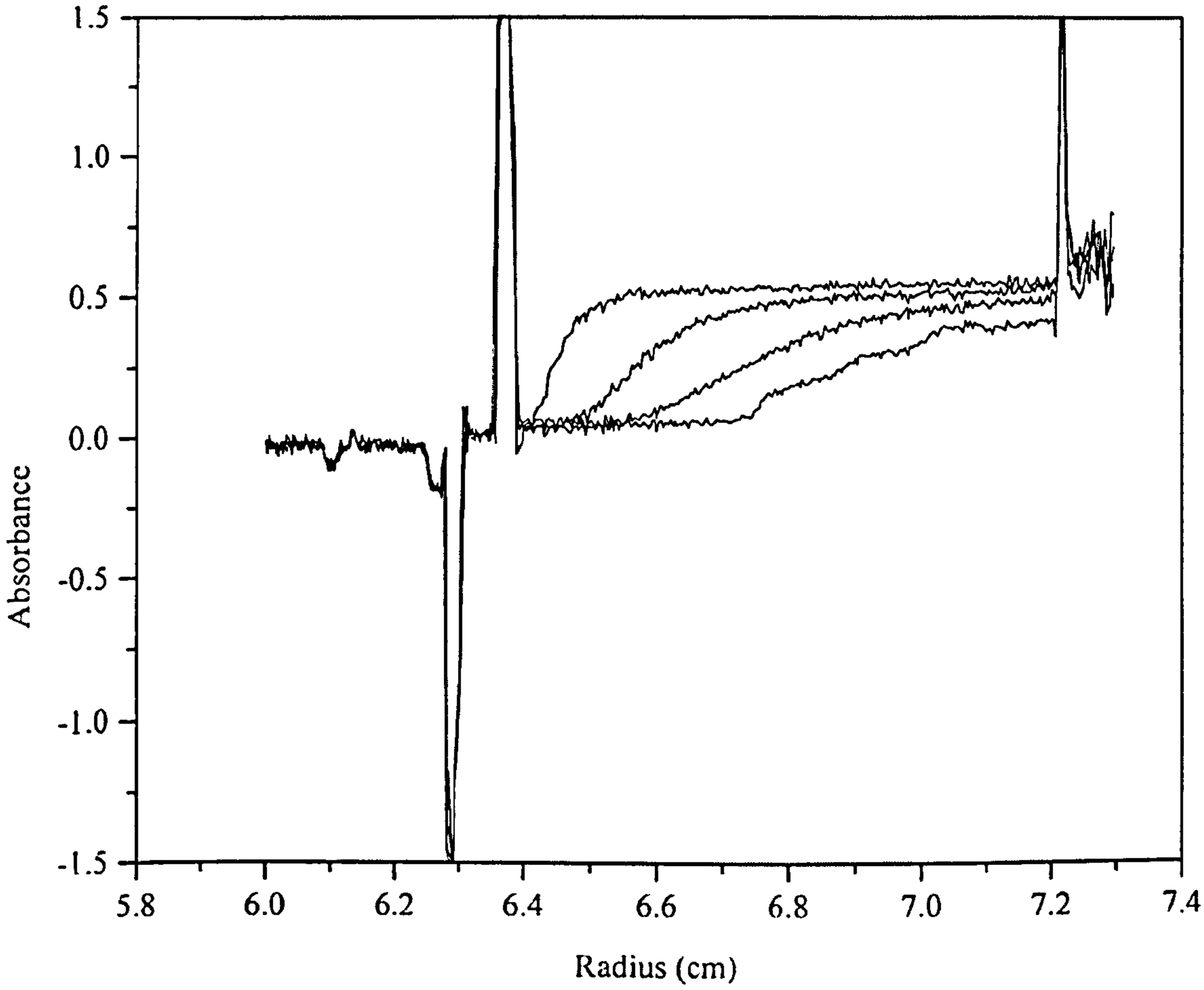

Figure 5.9 Sedimentation velocity of the Chitosan Fraction 3/PGM-MD complex, a rotor speed of 2,000 rpm was utilised, the temperature was 20°C and radial scans were taken at 5 minute intervals. Absorbance was measured at 280 nm.

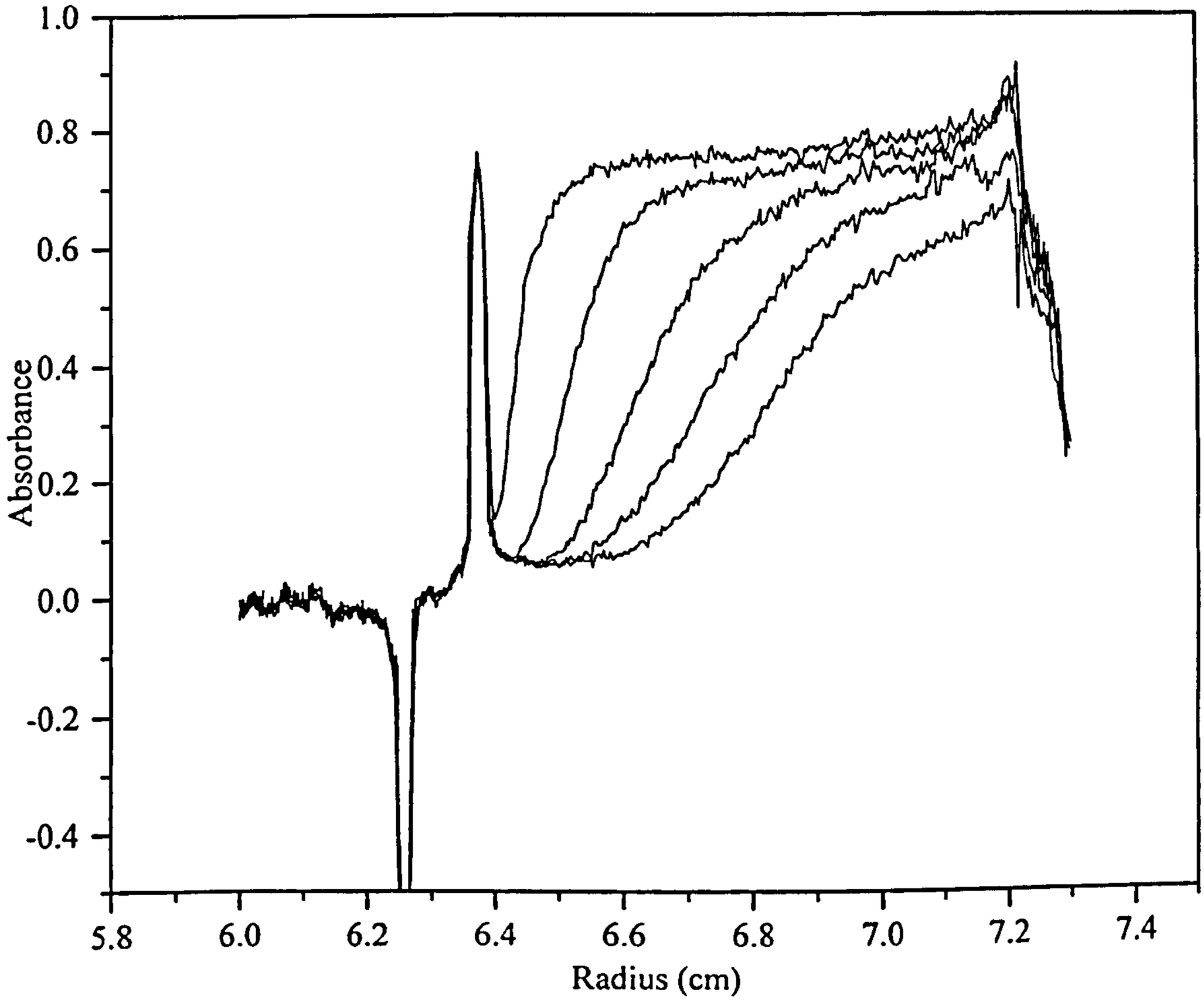

Figure 5.10 Sedimentation velocity of the Chitosan Fraction 4/PGM-MD complex, a rotor speed of 2,000 rpm was utilised, the temperature was 20°C and radial scans were taken at 5 minute intervals. Absorbance was measured at 280 nm.

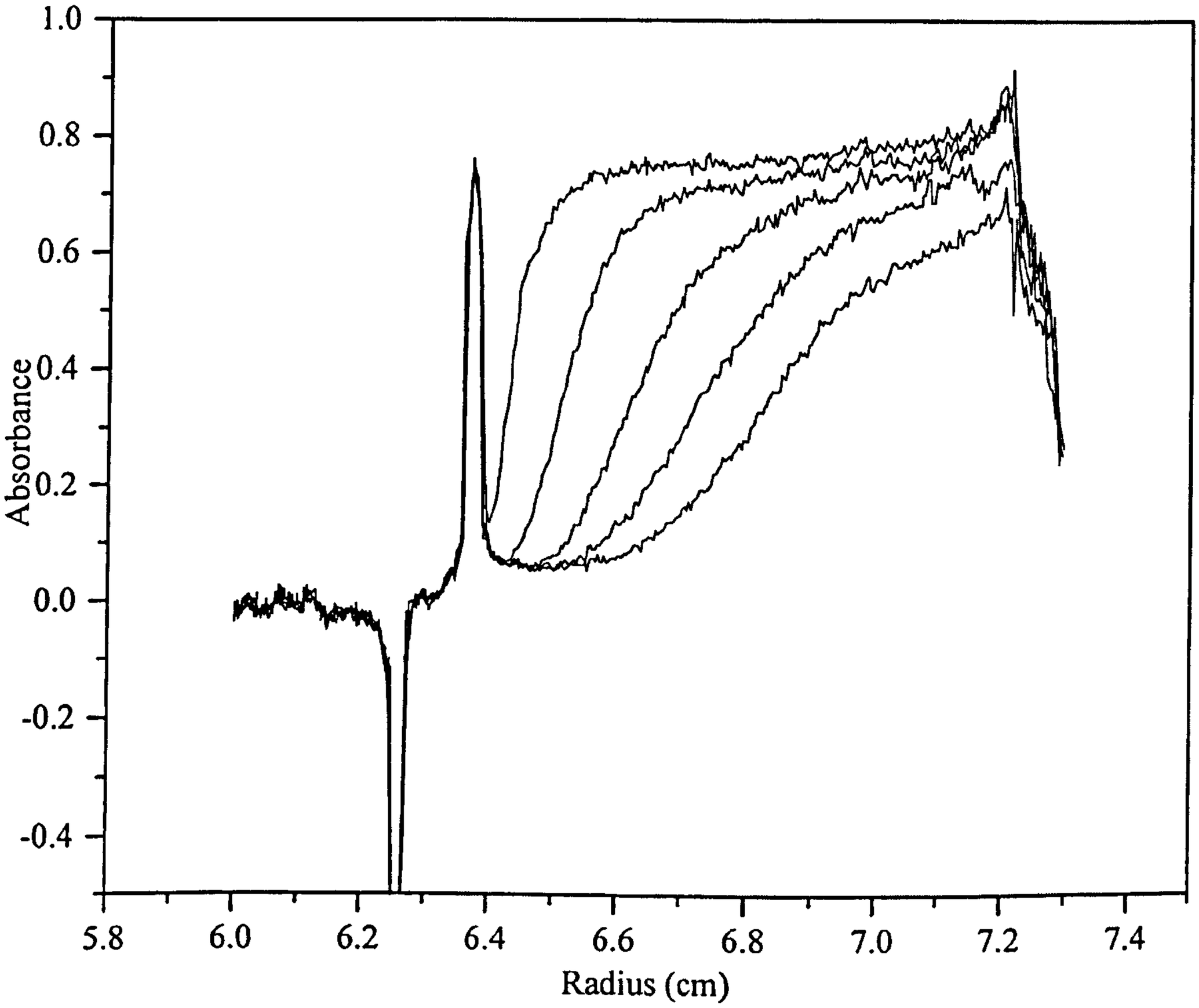

Figure 5.11 Sedimentation velocity of Chitosan Fraction 5, a rotor speed of 55,000 rpm was utilised, the temperature was 20°C and radial scans were taken at 20 minute intervals using interference optics.

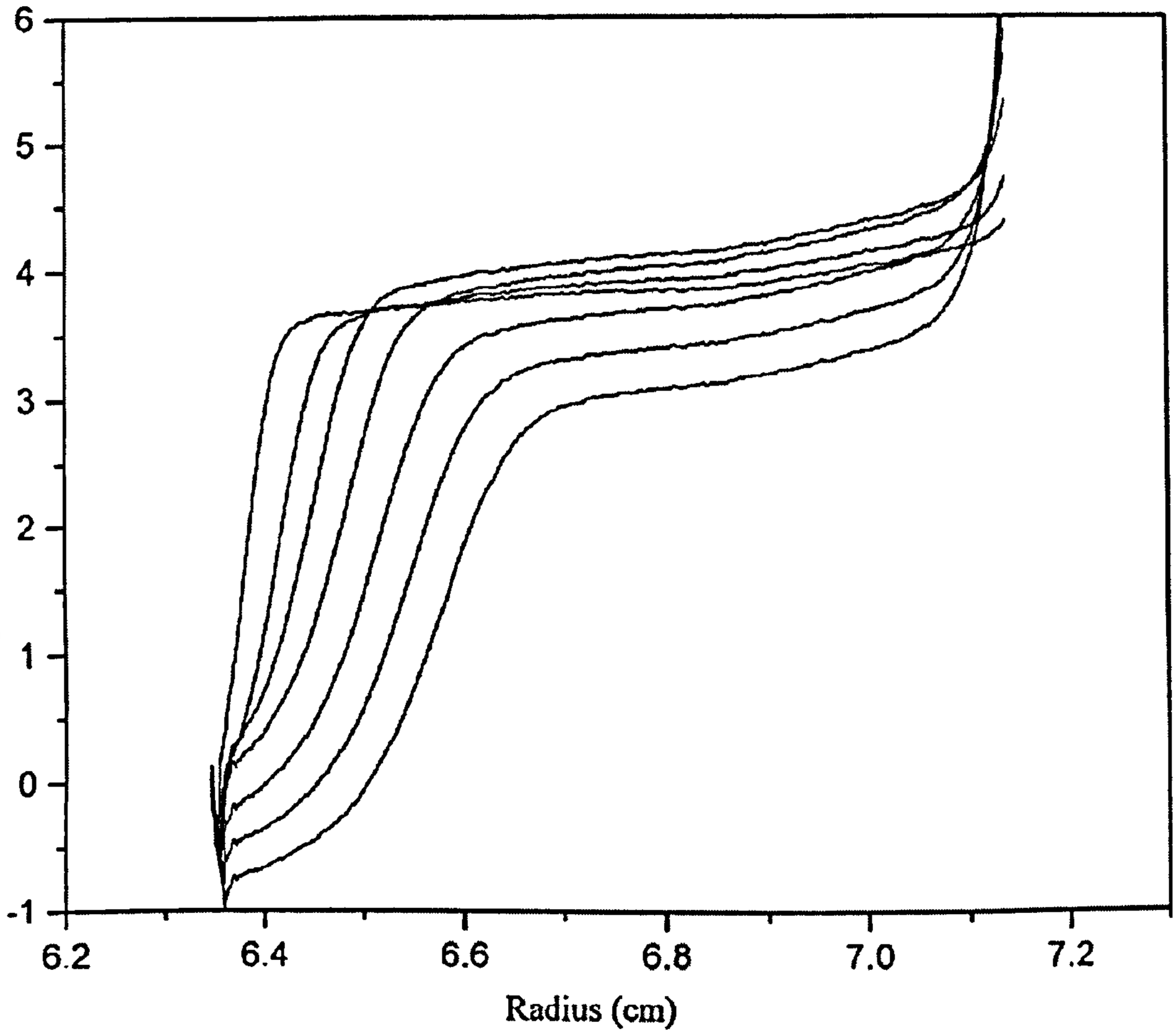

this size steric hindrance prevents the two molecules being able to come close enough for ionic interactions, therefore, no complex is formed between the two molecules.

Table 5.2 Sedimentation coefficients for the mucin complexes with various fractions of Chitosan A (degree of acetylation = 25 %).

Chitosan fraction	Sedimentation coefficient x 10^{13} (secs)
1 (M ~ 150,000)	3,572 ± 200
2 (M = 84,200)	16,659 ± 600
3 (M = 58,000)	16,033 ± 600
4 (M = 35,300)	12,342 ± 500
5 (M = 36,000)	12,705 ± 500

Figure 5.13 Molecular weight of chitosan fractions plotted against sedimentation coefficient of the complex illustrating the effect of chitosan molecular weight on the size of the complex (A molecular weight of 150,000 g/mol was used for fraction 5, which is an estimate of the molecular weight of this fraction, had not been determined by G. Berth).

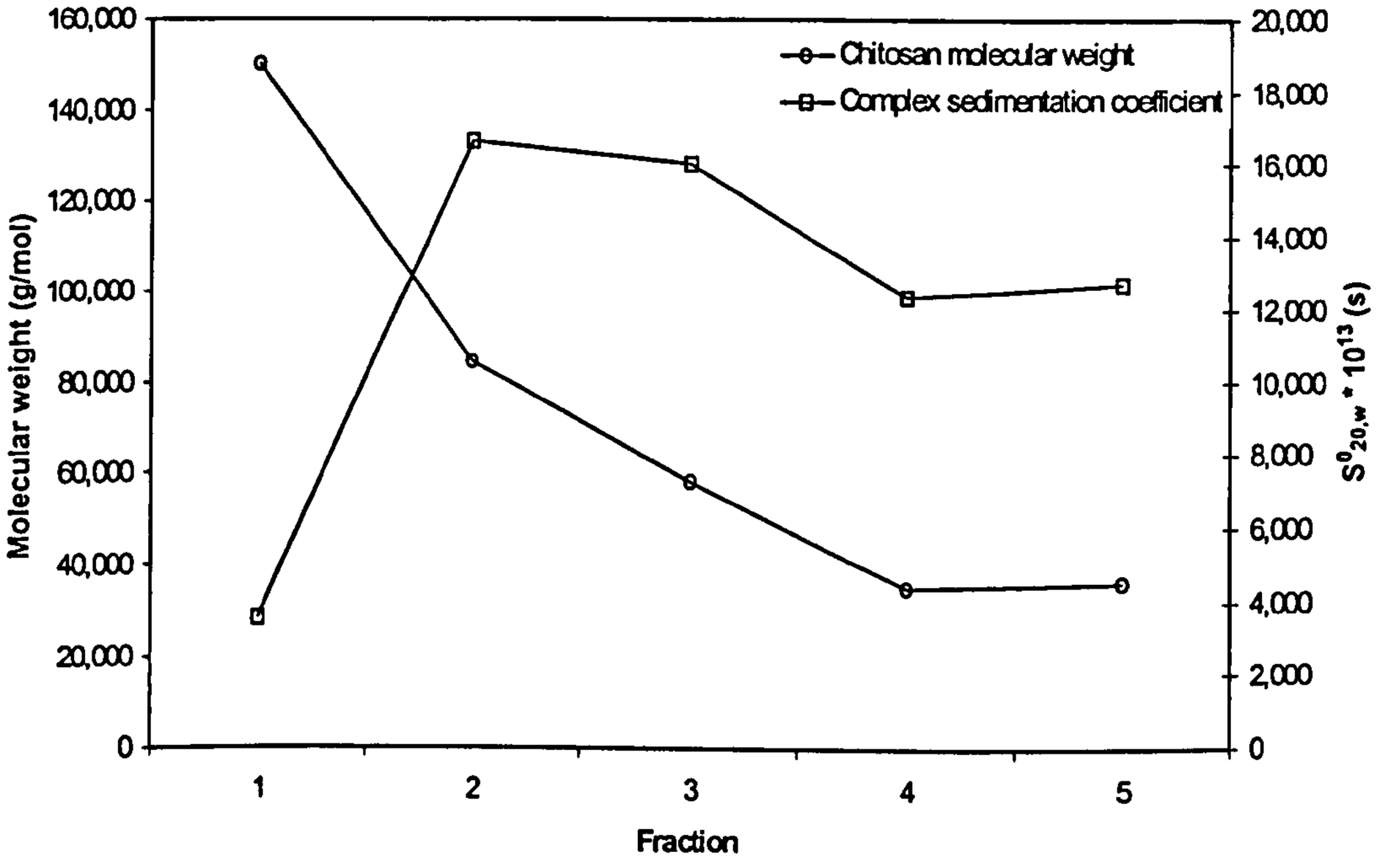

5.4 Conclusions

The results presented in this study are consistent with previous work performed in this laboratory. In the case of the interaction between chitosan and mucin, the size of the complex is so large that a sedimentation coefficient cannot be measured even at rotor speeds of less than 1,500 rpm. However, by comparing the peak areas of the free unbound chitosan with that of the control chitosan, a quantitative estimate of the degree of interaction can be made. The effect of ionic strength upon the interaction was also studied. It was found that at ionic strengths in excess of 0.25 M, no interaction was observed. These results can only be interpreted in terms of an

electrostatic interaction between chitosan and mucin. Above the critical ionic strength the charges on the polymers are effectively screened and thus limit association.

At 0.1 M ionic strength cardiac mucin binds more chitosan than fundus and antrum (see Figure 5.6.), which was expected because cardiac mucin is more negatively charged at pH 4.5 than fundus and antrum mucins and so should bind a larger amount of SC210 + chitosan which is positively charged at this pH. Also apparent from Figure 5.6. is that the amount of chitosan bound to mucin increases for fundus and antrum mucins at 0.2 M ionic strength. This can be explained in terms of charge screening of ionic groups and possible weak hydrophobic interactions.

Molecular weight was shown to have an effect on the interaction, using fractions of chitosan A (Berth *et al.*, 1998). There is evidently a sharp decrease in the size of the complex, measured by the sedimentation coefficient, when the molecular weight of chitosan A is above ~100,000 g/mol, indicating that steric effects may oppose the strong tendency for interactions through the electrostatic and/or hydrophobic groups.

Chapter 6

Field Flow Fractionation of chitosan-mucin systems

6.1 Introduction

Flow Field-Flow Fractionation (Flow FFF) is a relatively new technique designed to separate and probe the physical structure of complex macromolecular, colloidal, and particulate materials (Giddings *et al.*, 1993). Species can be separated in the range of $\approx 10^{-3}$ to 10^{2} μm, a much larger range than is currently available with any other technique. It is one of a family of methods for separating macromolecules others include thermal FFF, sedimentation FFF, electrical FFF and steric FFF. Due to the wide range of species that can be separated, flow FFF was used in conjunction with MALLS and a refractive index detector to characterise the complex formed between mucin and chitosan. This was impossible to do on the SEC/MALLS as chitosan adheres to the columns and is not eluted.

6.2 Materials and Methods

Chitosan SC210 + and PGMMD were used in the Flow-FFF studies at final concentrations of approximately 2.0 and 0.1 mg/ml respectively. All injections were made through a 20 μl injection loop. After trial runs a channel flow of 0.5 ml/min was chosen with a cross-flow decaying from 1 ml/min to 0.01 ml/min over 10 minutes (see Figure 6.1). A typical run lasted for 20 minutes by which time the entire sample had eluted through the channel.

Figure 6.1 Cross-flow rate during Flow FFF experiments, a decaying cross flow rate was found to give the best separation.

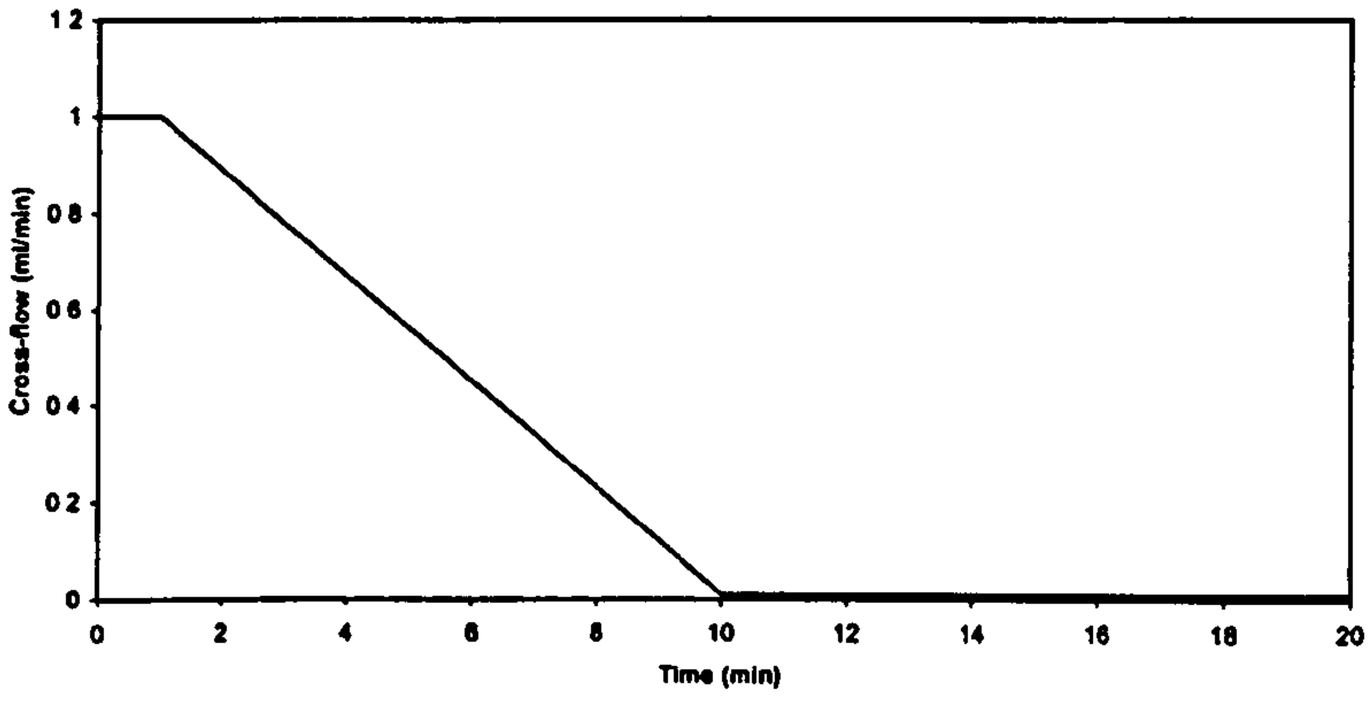

6.3 Results and Discussion

6.3.1 Control solution

It can be observed from Figure 6.2 that there is a drift in the baseline of the refractive index detector, it is likely that this is due to the decaying cross-flow that was used in the separation, it can also be noted that there is a similar slope in the light scattering trace.

Unfortunately due to the problem with the drifting baseline on the RI detector for the Flow FFF results it is impossible to obtain accurate representative molecular weights. However it is interesting to observe the results as an indication of the solution state of the sample.

Figure 6.2 Blank injection acetate buffer pH 4.5 at 0.1 M ionic strength.

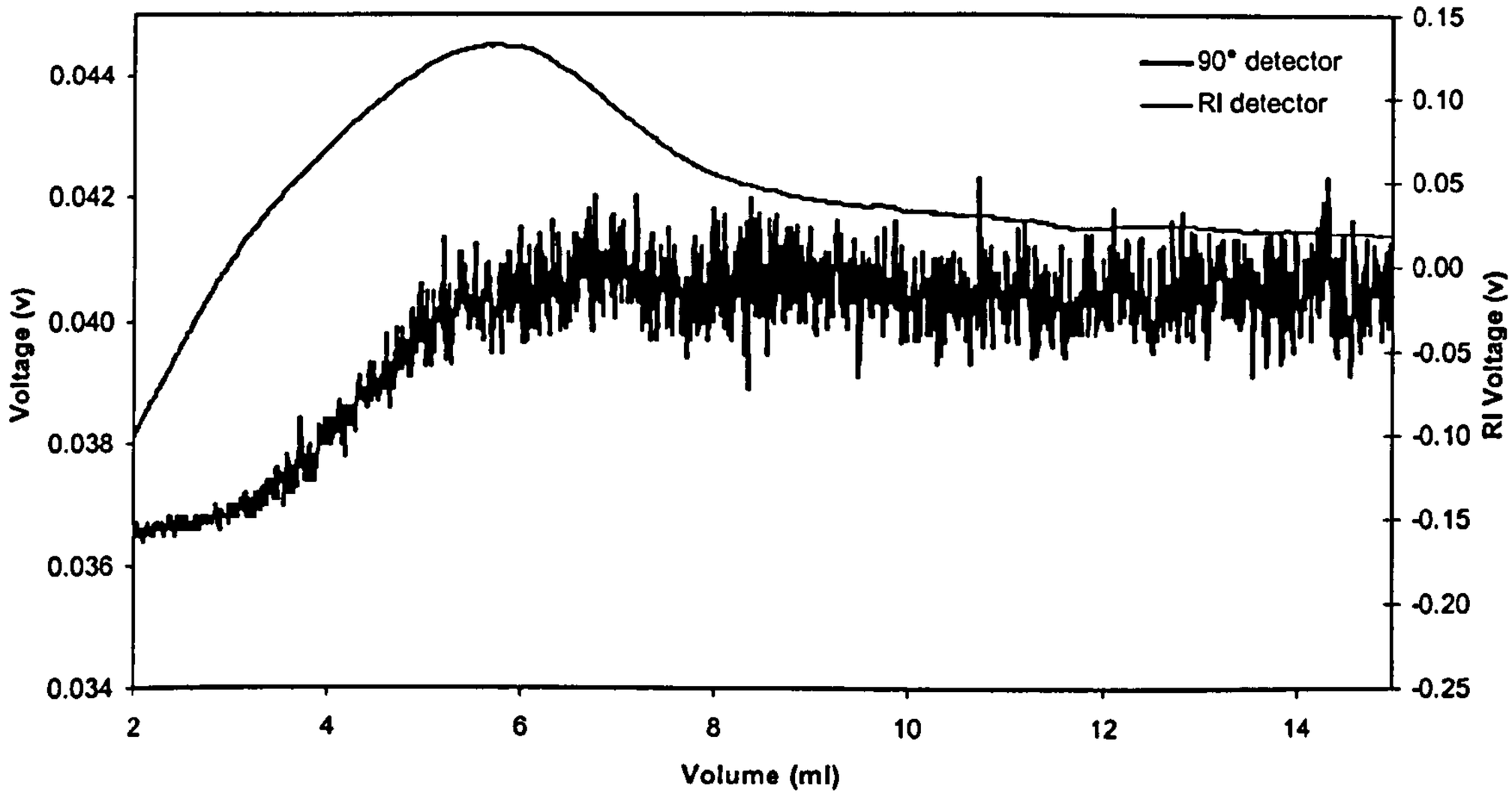

6.3.2 Chitosan solutions at 0.1-0.3 M ionic strength

From Figure 6.3 it can be seen that chitosan in an acetate buffer at 0.1 M ionic strength is very polydisperse it has a very broad chromatogram with a long tail indicating the presence of high molecular weight material. Polysaccharides are noted for their polydispersity due to the enzymatic nature of their formation and susceptibility to enzymatic breakdown. It is also significant to notice that there is no change in the shape of the chromatograms as the ionic strength is increased from 0.1-0.3 M (Figures 6.3-6.5). This confirms previous work by Errington (1993) who demonstrated, with viscosity measurements, that the chitosan chain is quite stiff and is not affected (by charge screening effects, for example) as ionic strength is increased.

Figure 6.3 SC210 + chitosan in acetate buffer pH 4.5 at 0.1 M ionic strength. Normalised voltage on the left axis for the light scattering signal, voltage on the right axis for the refractive index detector.

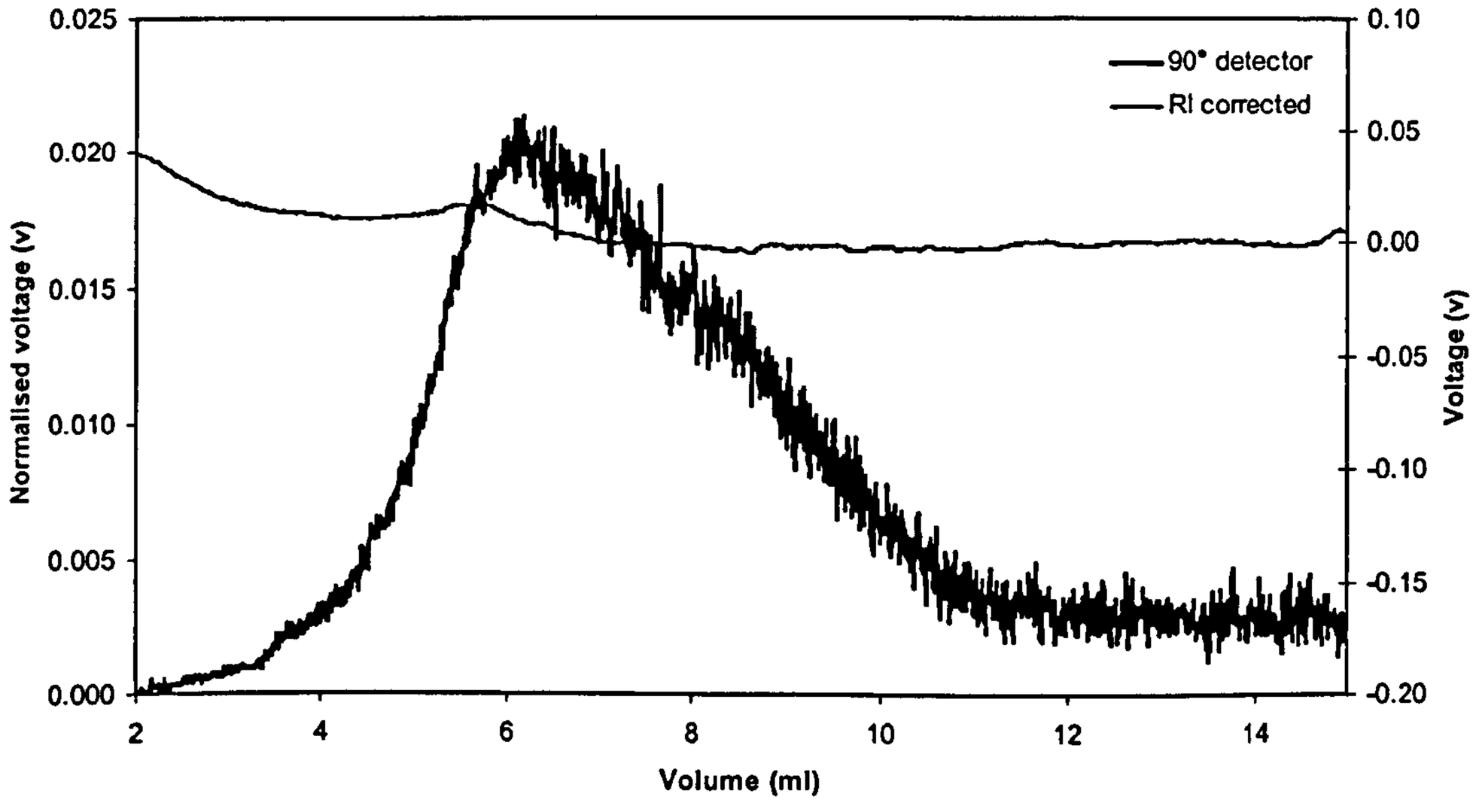

Figure 6.4 SC210 + chitosan in acetate buffer at 0.2 M ionic strength.

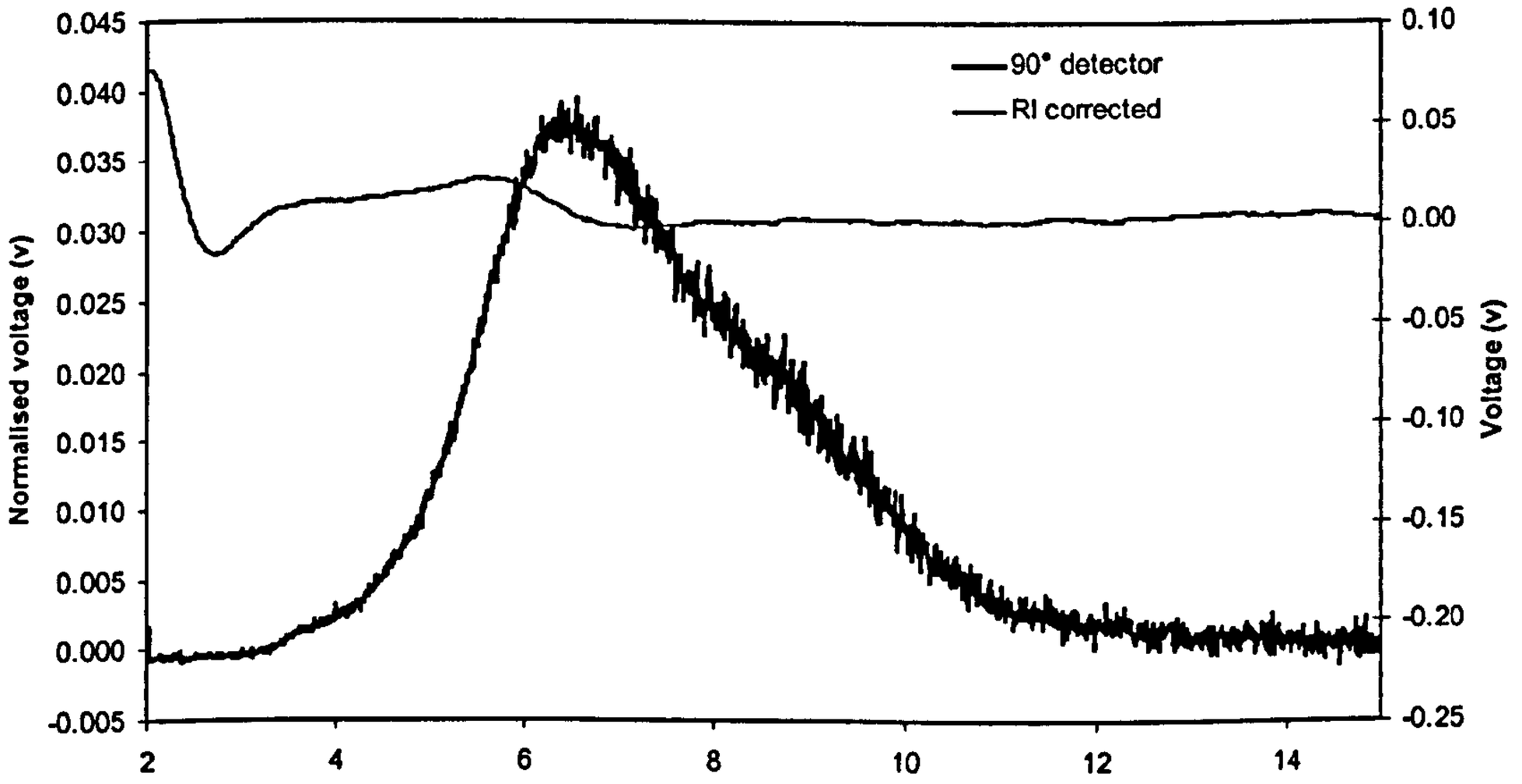

Figure 6.5 SC210 + chitosan in acetate buffer at 0.3 M ionic strength.

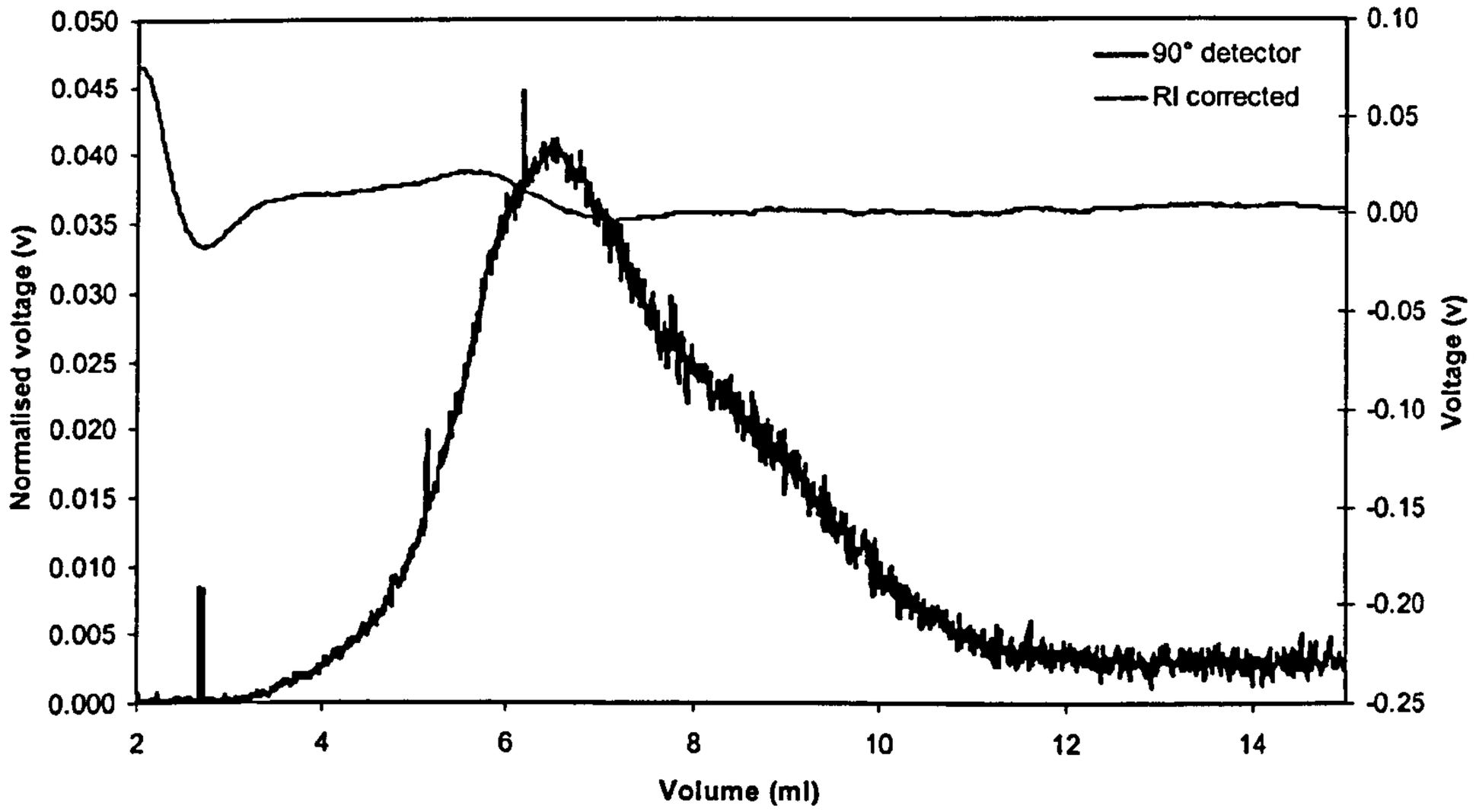

6.3.3 PGM-MD at 0.1 M ionic strength

The PGM-MD preparation gave a very low signal when injected into the Flow FFF channel in comparison to SC210 +, as shown in Figure 6.6 and Figure 4.1 respectively. It is apparent that there is a large difference in the size of the peaks observed, even when the smaller injection volume is taken into account (20 µl for Flow FFF to 100 µl for SEC) the peak height for SEC is 0.2 and for Flow FFF it is 0.008. This could be caused by dilution of the molecules as they pass down the Flow FFF channel.

Figure 6.6 PGM-MD in acetate buffer pH 4.5 at 0.1 M ionic strength.

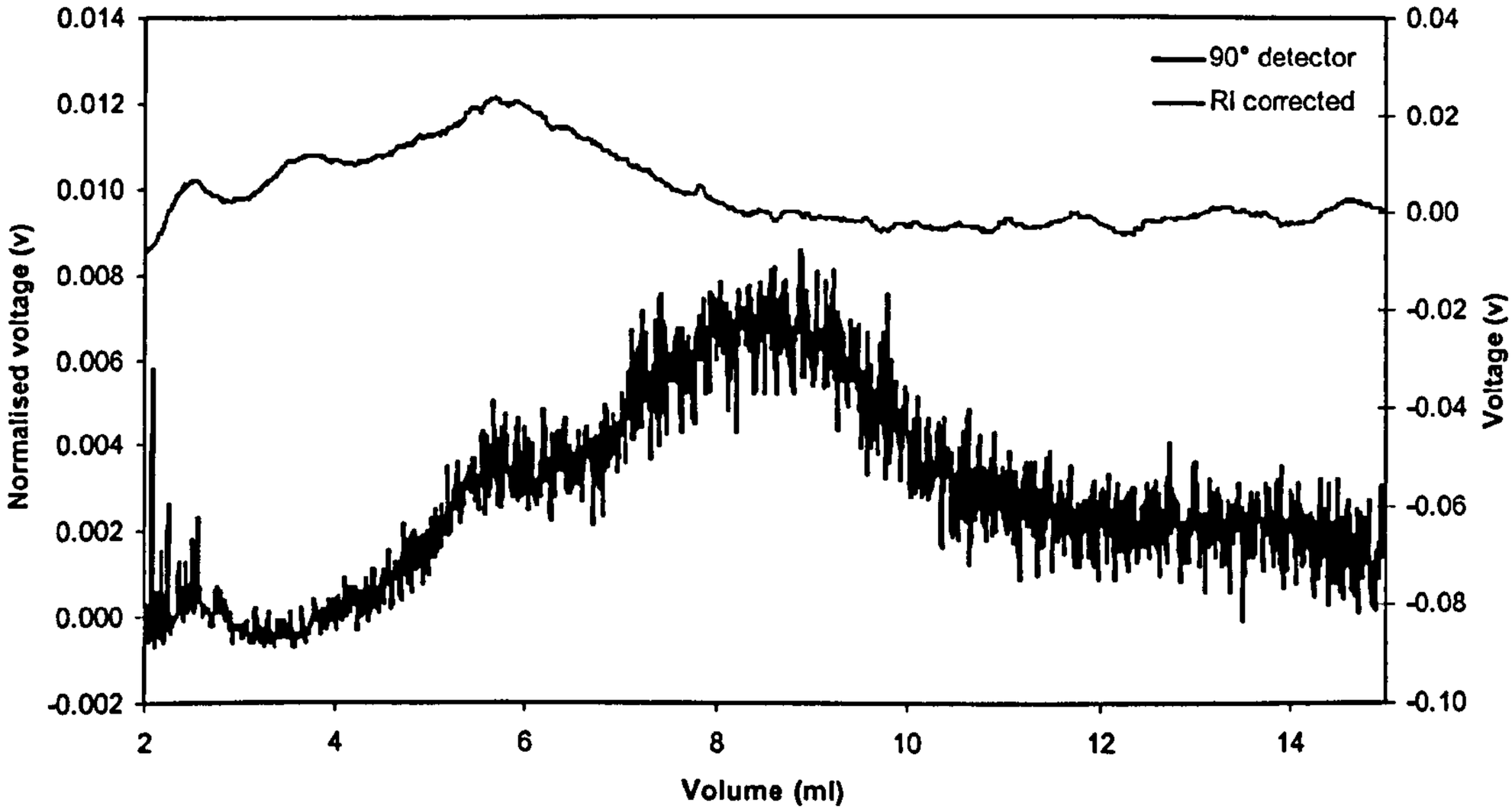

Figure 6.7 Mucin/Chitosan mixture in acetate buffer pH 4.5 at 0.1 M ionic strength.

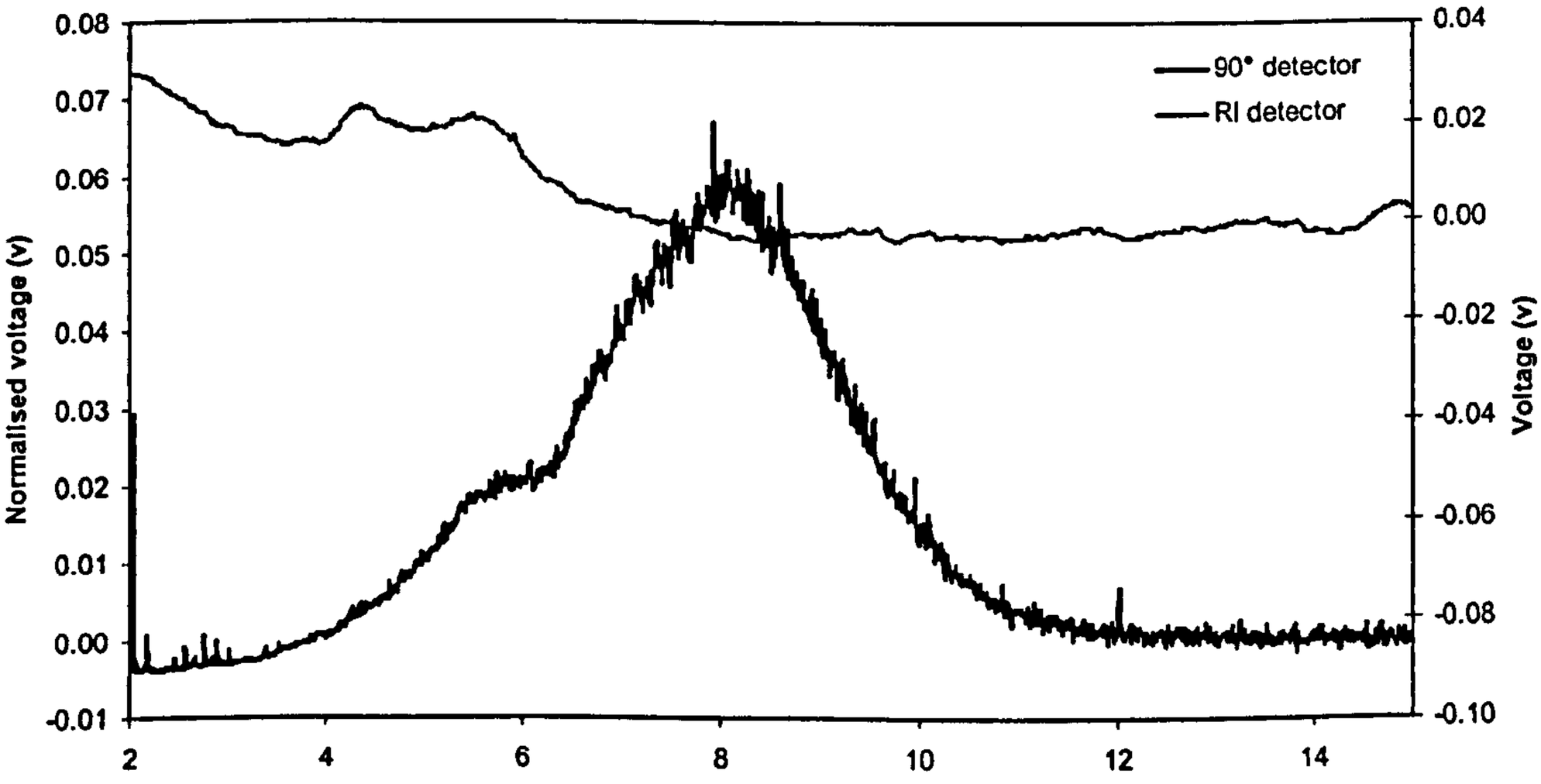

6.3.4 PGM-MD/SC210 + mixture solution at 0.1 M ionic strength

The peak in the chromatogram of the mucin/chitosan mixture is at a much higher voltage than all others indicating that higher molecular weight material is present. However, this cannot be confirmed due to the problem of the drifting baseline. The delay in the elution of the peak is not as large as expected considering the large size of the complex. This could be due to another effect that is seen with Flow FFF. Very large molecules/complexes display a "tumble weed" effect whereby they elute first. This is because they are so large that they cross several flow laminae in the channel, which gives rise to a reverse elution order.

6.4 Conclusions

Chitosans, as expected, are highly polydisperse (Figure 6.3-6.5) which is also confirmed by the broad boundaries seen with sedimentation velocity (Chapter 5). It is also apparent that there are no visible changes in the shape of elution profiles from 0.1-0.3 M ionic strength, thus confirming previous work by Errington (1993).

The results for the complex are inconclusive, there is an increase in the light scattering signal when compared to mucin alone. This indicates an increase in the molecular weight of the sample. However it is impossible to calculate a molecular weight because of the problem with the baseline. Further work with this method to solve the problem of the floating baseline would enable calculation of the molecular weight of the complex and enable Flow-FFF to become a useful tool in the characterisation of this interaction.

Chapter 7

Atomic Force Microscopy of chitosan-mucin systems

7.1 Introduction

Thus far the study of the interaction of chitosan and mucin using sedimentation and light scattering techniques has been described. However, it is useful to characterise these types of interactions using a range of techniques, preferably independent of each other. Atomic force microscopy (AFM) was used as an additional method for visualising the complex and to investigate the effect that changes in ionic strength have on the complex. Specifically, it was used to characterise the interactions between three mucin populations purified from the cardiac, antrum and fundus regions of the porcine stomach with chitosan at three different ionic strengths.

7.2 Atomic Force Microscopy

The atomic force microscope was developed by Binnig, Quate and Gerber in 1986 (Binnig *et al.*, 1986). It was advanced from Scanning Tunneling Microscopy (STM) in response to the needs for a dynamic imaging technique which did not require a conductive sample substrate. The advantages of AFM over many other microscopy techniques are derived from its ability to provide high resolution three-dimensional images in a multitude of environments. It does not require invasive and destructive sample preparation before analysis unlike most electron microscopic procedures (Kirby *et al.*, 1995) and generally achieves better resolution. Since AFM was invented, it has become one of the fastest growing and most versatile imaging techniques of this decade (Cohen, 1994).

Figure 7.1 illustrates a schematic of the main components and the general principle of the AFM. In essence, an AFM monitors the forces of interaction between the imaging probe and the sample surface. A laser beam is directed on the reverse side of a cantilever onto which an atomically sharp tip, normally constructed from silicon / silicon nitride, is formed. The tip is then brought into contact with, or within close proximity of, the sample surface and raster scanned over the surface. Most AFM instruments adopt the instrumental design outlined in Figure 7.1 where the sample sits on the scanning element, a piezoelectric tube. However, some instruments, termed "stand alone" AFMs, position the piezoelectric device above the tip. In this case, the tip is scanned over the surface rather than the sample rastering underneath a static tip.

Figure 7.1 Diagram illustrating the main components and the general principles of the AFM (Taken from McGurk, 1998).

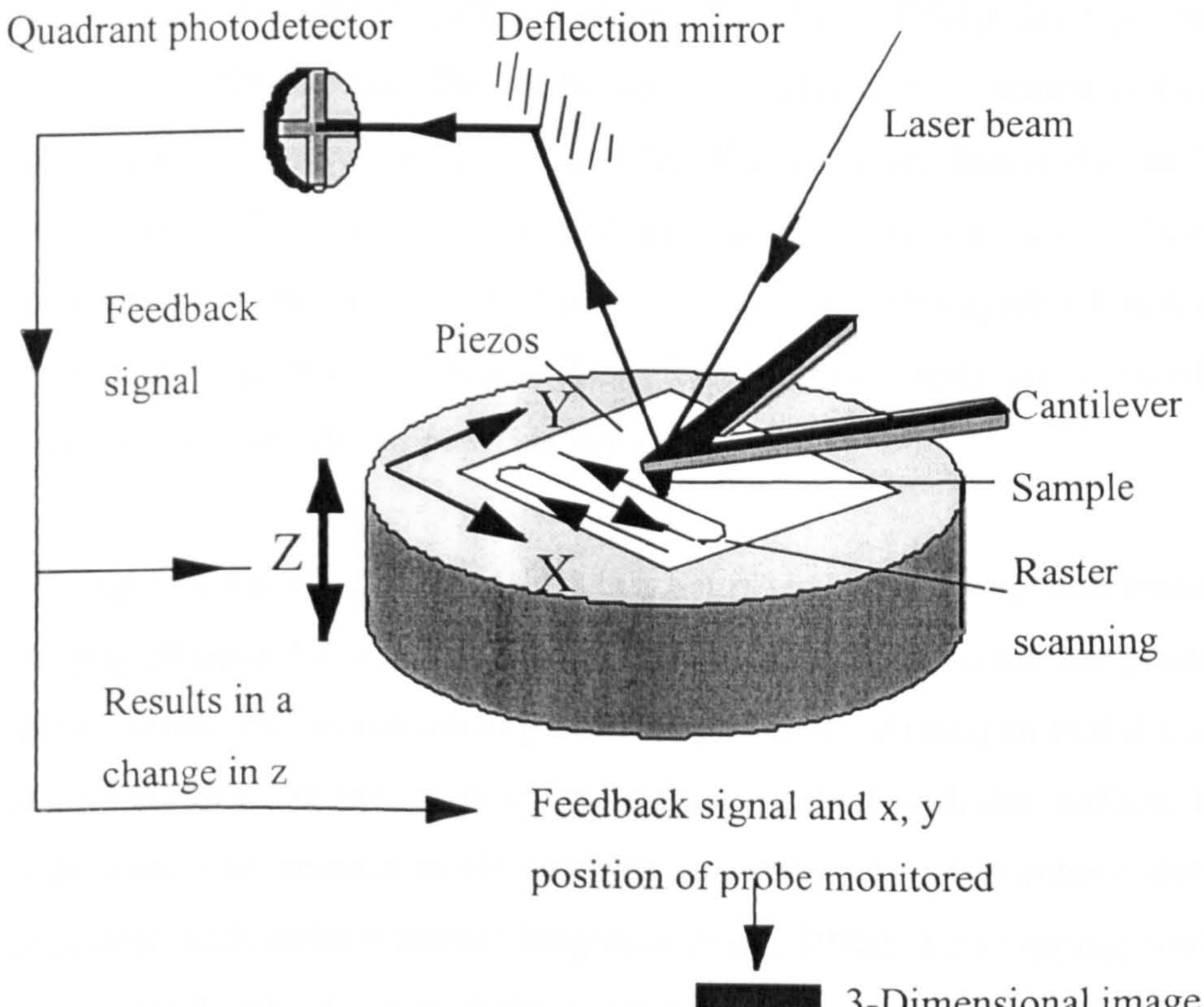

7.2.1 Imaging with AFM

The first and still most commonly used imaging technique with AFM is contact mode imaging (Figure 7.2 (a)). Contact mode monitors the repulsion forces between tip and surface as the probe raster scans over the surface. In this mode the probe is continuously in contact with the surface and maintains a constant force between probe and sample. This mode is extremely good for rigid samples and has traditionally offered the highest resolution. Lindsay (1993) reported that the interactional force between tip and sample to be in the order of nanoNewtons. This force is sufficient to disrupt and damage soft biological samples during imaging. Other AFM imaging modes have been developed which are less invasive, in order to overcome this limitation, such as non-contact and tapping modes.

In non-contact mode (Figure 7.2 (b) (Lüthi *et al.*, 1994)) the tip does not come into contact with the surface. The cantilever is oscillated in an attractive force regime where the long-range forces, mainly of van der Waals nature, distort the oscillatory motion of the cantilever. This mode of non-contact imaging overcomes some of the sample damage problems associated with contact imaging. However, this approach is much less sensitive to small topographical changes. Therefore, higher resolution is sacrificed in order to obtain images of soft samples (Hansma *et al.*, 1988).

Tapping mode (Zhong *et al.*, 1993) is a hybrid of both contact and non-contact modes of imaging (Figure 7.2 (c)). The cantilever is oscillated above the sample surface as in non-contact mode, but with a much greater amplitude (> 20 nm) so that the tip just strikes the sample surface. As the tip is in intermittent contact with the surface, the lateral forces associated with contact mode imaging are reduced, yet it retains the high resolution associated with contact mode (Magonov *et al.*, 1996). This tapping causes a decrease in the amplitude of vibration of the cantilever, with the magnitude of this reduction being dependent on the height of the surface features being probed. The feedback loop, shown in Figure 7.1, controls the position of the sample in the z direction in order to compensate for changes in vibrational amplitude. Therefore, the 3-dimensional images are recorded

by plotting the samples x, y and z dimensions. This type of imaging is termed amplitude-detection imaging (Chen *et al*, 1998). However, in addition to changes in the amplitude there are also changes in the phase of vibration. These changes have been utilized in a new form of tapping mode imaging called phase detection (Akari *et al*, 1996). The images produced in this imaging mode are created by plotting the phase lag of the cantilever vibration, relative to the z-piezo drive amplitude produced by the interaction with the surface and the x and y position. A study by Tamayo and Garcia (1996) showed that the dominant cause in the shifts of the phase of vibration were caused by probe-sample adhesion. Hence, this imaging mode offers great advantages in the analysis of polymeric materials as the tip-sample adhesion may be determined by many chemical and morphological polymeric factors.

Figure 7.2 A schematic summary of the different types of imaging modes with AFM; (a) contact mode, (b) non-contact mode and (c) tapping mode (Taken from McGurk (1998)).

7.3 Materials and Methods

7.3.1 Sample Preparation

Freshly cleaved mica sheet was silanized with aminopropyl-triethoxysilane (APTES). The mica pieces were placed into a glass petri-dish and three drops of APTES solution was placed on the inner side of the cover. The petri-dish was then sealed with Parafilm and the sheets were left for 2 hours at room temperature. Mucin, chitosan and mixture solutions were prepared in a pH 4.5 acetate buffer by pipetting 20 µl of sample into an eppendorff then adding glycerol solution (15-25 % v/v) to a volume of 0.5 ml and left for 30 minutes. Acetate buffer at pH 4.5, was chosen due to the insolubility of chitosan in most other liquids (Muzzarelli, 1995). The mica sheets were then coated with the sample solution for 30 seconds, rinsed with deionized water and then dried with argon. AFM investigation was performed immediately after sample preparation.

7.3.2 Atomic Force Microscopy

All imaging was performed in air with the Nanoscope IIIa (Digital Instruments, Santa Barbara, CA, USA). TappingMode™ was employed with a probe constructed from silicon with a length and resonant frequency of 125 M and 307-375 kHz respectively (Nanoprobe). All measurements made on the images of structures in this chapter such as RMS roughness, z displacement and size (width and diameter) were made utilizing the operating software provided with the Nanoscope IIIa AFM.

7.4 Results and discussion

7.4.1 Control surfaces

To show the thin filamentous nature of the mucin type structure previously shown with TEM (Sheehan *et al.*, 1986; Roberts *et al.*, 1995), and the unknown visual characteristics of chitosan, an extremely flat sample substrate is required. To this end, mica was chosen for this study. Figure 7.3 (a) and (b) show an AFM image, both topography and phase, of a clean mica surface. It is evident from this figure that the surface of this sample substrate is flat and featureless with a RMS roughness of 0.11 nm (compared to 13.36 nm for the silver surface plasmon resonance slide (Green *et al.*, 1997)) and a total movement of 0.9 nm (distance moved by the "z" piezoelectric in AFM), so any further adsorbed material in future sample preparation should be apparent against such a background. Figures 7.4 (c) and (d) show both topography and phase AFM images of the mica sheet that has been treated with APTES. Again, the sample substrate surface was flat and featureless with an RMS roughness of 0.14 nm and total z movement of 1.03 nm. APTES treatment was necessary to attach amino groups to the surface of the mica which attract the large mucin structures. This attraction has been attributed to a charge interaction between the positive amino terminus and the sialic acid or sulphate residues on the mucosal glycoproteins. Structural studies have indicated that the negative charge on this PGM-MD is thought to be attributed to the amount of sulphated O-linked oligosaccharide residues in the glycosylated region and not due to the amount of sialic acid present (Nordman *et al.*, 1997).

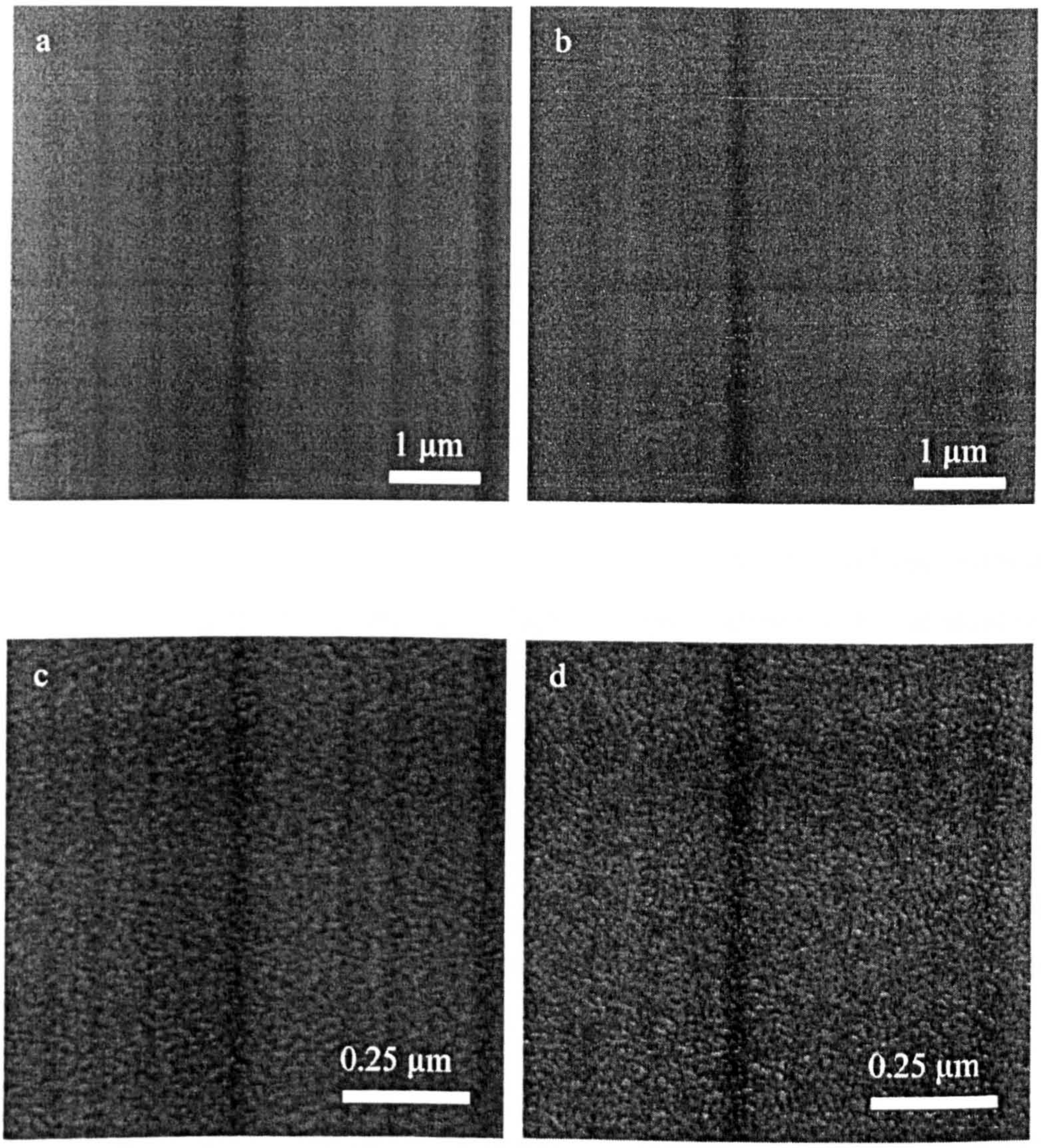

Figure 7.3 AFM images, both topography and phase, of the substrate mica and the APTES coated mica.

(a) Mica (topography)
(b) Mica (phase)
(c) APTES coated mica (topography)
(d) APTES coated mica (phase)

7.4.2 PGM glycoproteins

TEM and STM have been used in previous studies to produce visual information on the structure of PGM (Sheehan *et al.*, 1986; Roberts *et al.*, 1995, Fiebrig *et al.*, 1997). In those cases the sample surface had been coated with a thin layer of conductive material and the mucins themselves sprayed onto the substrate surface. The advantage of AFM over this is that the mucins may be adsorbed directly from solution and do not require further sample treatment prior to visualisation, such as surface metallic coatings.

In our present studies the characteristic naked and glycosylated segmented mucin glycoprotein structure is apparent. Figure 7.4 (a-d) shows both topography and phase images of PGM adsorbed from solution to the APTES treated mica surface. These two images were selected at random and are typical from a large library of images of these glycoproteins which portray similar structural information and surface coverage. The PGM adopts a long filamentous strand which is in good agreement with previous studies (Sheehan *et al.*, 1986; Roberts *et al.*, 1995, Jumel *et al.*, 1997). But, the characteristic expanded glycosylated areas which line the backbone shown in the TEM studies were not seen.

The average length of these PGM strands is approximately 2.00 (± 0.55) μm which agrees with studies performed with TEM and sedimentation equilibrium experiments (Harding, 1989). However, occasionally PGM filaments were seen to a maximum length of nearly 4 μm and a minimum of 0.5 μm reflecting the polydisperse nature of the material. The diameters of the filaments were approximately constant, giving values of approximately 16 nm. This width is wider than that seen for other filamentous molecules such as DNA when imaged with AFM. In a study by Delain *et al* (1992), the tapping mode was used in air to image DNA where they found the width of the strands to be approximately 10 nm. Since DNA does not have glycosylated regions protruding from its protein backbone structure, the increased width of the mucin filaments may be attributed to the glycosylation of the filament.

It was surprising that the AFM images did not reveal the characteristic glycosylated areas along the mucin backbone. One reason for this apparent lack of extensive glycosylation may be explained by work performed by Brown and Hoh (1997). In that study they showed how neurofilament sidearms provide entropic exclusion to adsorbing proteins, even though it is not possible to image such structures: the same scenario could well be applicable in this case. As the mucin glycoprotein remains partially hydrated (under atmospheric conditions), the glycosylated side chains may be in the form of an entropic brush, moving rapidly, thus unable to be imaged. This would also explain why the glycosylated areas were seen in TEM and STM studies. As the sample is completely dehydrated and immobilized when the surface is coated with a conductive layer, the hydrated side chains would no longer be mobile and hence, they would become imageable.

7.4.3 SC210 + Chitosan

To date there have been no imaging reports concerning the molecular structure of chitosan. Figure 7.5 illustrates AFM images of the chitosan molecules. It is possible to see from the larger 2.5 μm image (Figure 7.5 (a) and (b)) that the structure is extremely polydisperse with the polysaccharide chain lengths varying extensively. The average length of the polysaccharide was approximately 0.70 (± 0.27) μm, which is smaller than the average backbone length for the PGM. The widths of these polymer chains were very consistent, being approximately 11 nm, which is smaller than the values noted for PGM. Figure 7.5 (c) and (d) of a single chitosan chain reveal there are no real structural features to distinguish this from the mucin glycoprotein.

The immobilization strategy chosen for this study was aimed at immobilizing the much larger of the two molecules, namely the mucin. A positive surface potential was created to attract the slightly negatively charged mucin glycoproteins. Naturally, one would not expect any charge interaction between the positively charged chitosan molecule and the positively charged surface. Therefore, it is likely that the chitosan seen in these images is

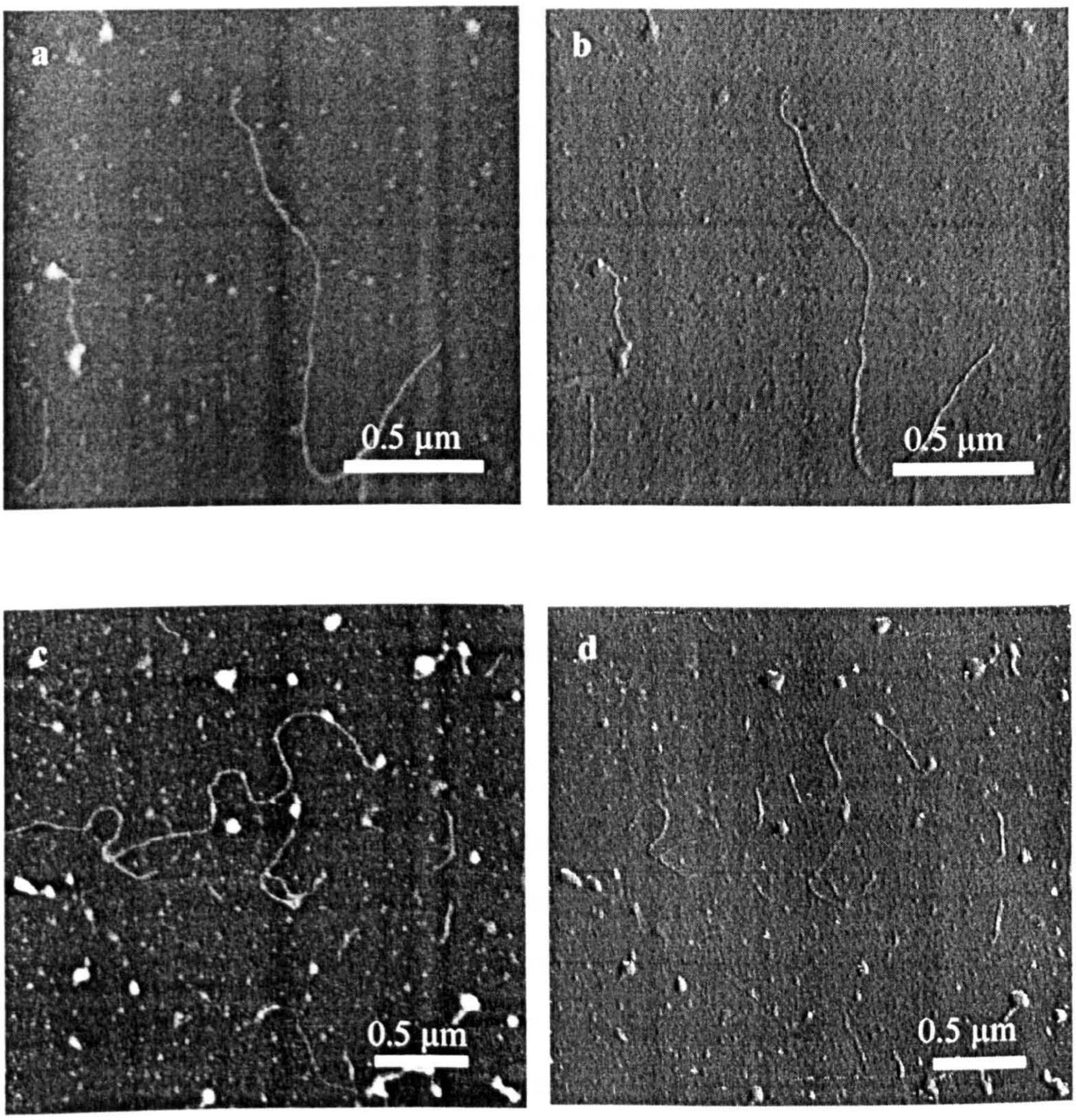

Figure 7.4 Sample AFM images, both topography and phase, of the purified pig gastric mucins in 0.1 M ionic strength acetate buffer.

(a) Mucin (topography)
(b) Mucin (phase)
(c) Mucin (topography)
(d)Mucin (phase)

merely lying on top of the APTES coated mica with very loose physical interaction. The effects of this charge repulsion were amplified when the ionic strength of the solution was increased from 0.1 M to 0.2 M and 0.3 M. At the high ionic strength, no chitosan was seen on the surface on the APTES coated mica. At low ionic concentrations repulsive forces between the positively charged deacetylated units situated along the polymer backbone keep the polymer in an extended linear arrangement. However, as the ionic concentration is increased this repulsion effect is reduced resulting in a more coiled arrangement of the polymer (Pronova Biopolymer Data Sheets, 1994). This may also contribute to the lack of chitosan observed on the surface at the elevated ionic concentrations.

7.4.4 Complexes of PGM and chitosan at 0.1 M ionic strength

As previously indicated, Deacon *et al.* (1998) and Chapter 5 of this study a significant interaction has been shown, with sedimentation velocity experiments, between the purified PGM and this form of chitosan. Considering now this interaction visualised by AFM, Figure 7.6 illustrates the difference in conformation for both the chitosan and mucin structures when mixed together in solution and then immobilized to the APTES coated substrate. Instead of the characteristic filamentous nature of both the chitosan and PGM, as previously indicated in Figures 7.4 and 7.5, large aggregates were noticed on the surface of the mica. The average diameter of these aggregates, determined by taking two diameter measurements (x and y) on many complexes, was approximately 0.70 (± 0.18) μm. However, complexes were seen with a range of diameters from 0.3 μm to 1.2 μm. Surrounding these aggregates was a tangled arrangement of filaments that seemed to emanate from the central aggregate. The diameter of these filaments was approximately 16 nm. This suggests that these filaments are strands of PGM radiating from the complex. There are also many chain ends of these filaments surrounding the central complex. This suggests that chitosan seems to have an aggregative effect on the PGM, causing many mucin filaments to interact. There have been many studies to investigate the nature of this interaction, however, to date there are only theories (Deacon *et al.*, 1998; Fiebrig *et al.*,

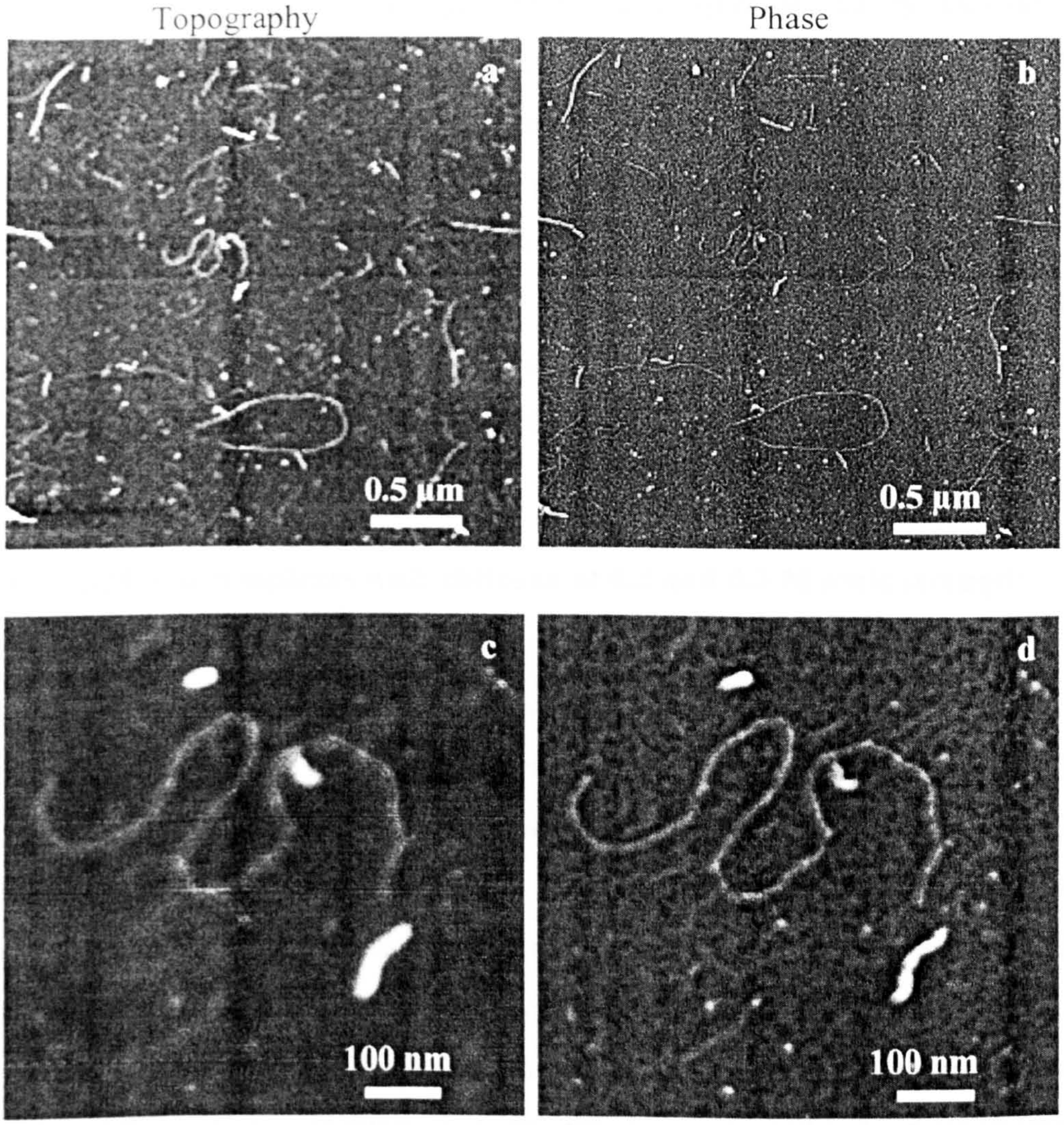

Figure 7.5 AFM images, both topography and phase, of the chitosan at 0.1 M buffer solution.

(a) Chitosan (topography)
(b) Chitosan (phase)
(c) Chitosan - close up (topography)
(d) Chitosan - close up (phase)

1995a; Illum *et al.*, 1994; Lehr *et al.*, 1992). The most recent theory (Deacon *et al.*, 1998) describes the charge interaction between the positive (NH_3^+) groups on the chitosan and the negative sulphated (SO_3^{2-}) groups known to be present on the mucin (see Karlsson *et al.*, 1997). As each molecule has many potential sites for interaction, (chitosan mediated by the degree of deacetylation, Pronova Biopolymer Data Sheets, 1994) and mucin (through its backbone structure, Fogg *et al.*, 1996), the possibility of intermolecular interactions is high. These intermolecular interactions would promote aggregation as considered in detail by Fiebrig *et al.* (1995a) and Deacon *et al.* (1998).

7.4.5 PGM and complexes with chitosan at 0.2 and 0.3 M ionic strength

Figure 7.7 (a)-(d) shows the characteristic mucin (a and c) and complex (b and d) structures at 0.2 M and 0.3 M ionic strength respectively. It is apparent that the structure of the mucin at 0.2 M and 0.3 M ionic strength is quite different to that 0.1 M ionic strength. At 0.2 M (Figure 7.7 a), the long filamentous structure seen at 0.1 M is no longer present and instead, the characteristic mucin structures observed in TEM of areas of glycosylation and naked protein (or region of very low glycosylation) areas are prevalent (Sheehan *et al.*, 1986). It was difficult to measure the average length of the mucins at this molar concentration as the structures seemed to be formed from a number of mucin filaments. However, where an individual filament was evident, the average width was equivalent to that in the 0.1 M solution, approximately 16 nm. This mucin interaction effect became more pronounced at the higher 0.3 M ionic strength solution, shown in Figure 7.7 (c). At this ionic strength there seemed to be many filaments interacting to form more complex aggregates of mucin. The only mucins available for analysis of dimensions were those which emanated from the complex. The average diameter was again 16 nm, but the average length was impossible to determine due to the extent of interaction. If the number of mucin strands which emanate from the mucin complex are counted it shows that, on average over many complexes imaged, at 0.2 M there are 3-4 mucins and at 0.3 M there are 10-11 interacting to form the complex.

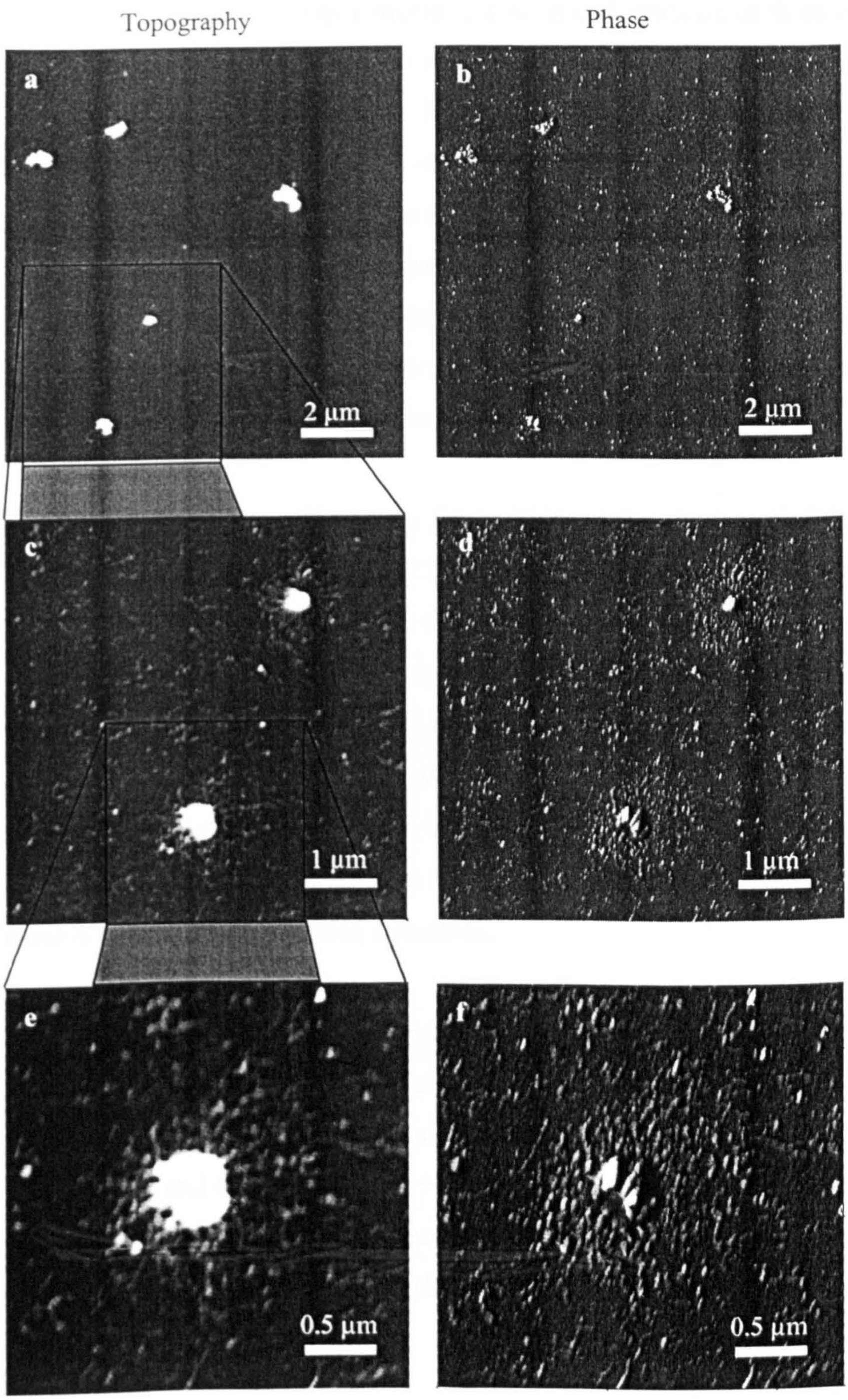

Figure 7.6 AFM images, both topography and phase, of the purified pig gastric mucin/chitosan complex in 0.1 M ionic strength acetate buffer solution.
(a, b) Complex- 10 µm (topography and phase)
(c, d) Complex- 5 µm (topography and phase)
(e, f) Complex- 2.5 µm (topography and phase)

As previously stated, the experimentally determined structure of these mucins in liquid is a long chain protein with attached side chains and it is these charged side chains which cause the mucin to remain in a linear structure (due to charge repulsion along its backbone) (Harding, 1989). The addition of salt to the solution may cause a charge-shielding effect on the charged areas of the mucin backbone. This process is likely to neutralize the mucin. The neutralization of the backbone would reduce the interactional charge repulsion and allow neighbouring mucins to entwine and increase the aggregating effect. This effect may be the reason for the increased number of mucins seen interacting as the concentration of salt increases.

The images presented in Figure 7.7 (b) and (d) are the structures of the complexes from the mucin chitosan interactions at 0.2 M and 0.3 M ionic strength respectively. These also display some differences from the structures observed at 0.1 M (Figure 7.6): there still appears to be some degree of complexation between the mucin and chitosan, however, the size of the complexes is greatly reduced. At 0.1 M, large aggregates formed that had an average diameter of 0.7 μm, whilst at 0.2 M and 0.3 M the smaller aggregate structures visualised had an average diameter of approximately 150 nm (visualised in the same way as those structures at 0.1 M). It can also be noticed that there is a greater number density of the complex structures.

A reason for this behaviour may also be described by the presence of charged ions in the buffer causing a charge shielding effect between the interaction of the chitosan and the mucin. Sedimentation velocity results discussed in chapter 5 showed the interaction of these PGM's and the same SC210 + chitosan at two different ionic strengths, 0.1 M and 0.2 M (same acetate buffer). These results are in agreement showing a reduction in interaction between the mucin and chitosan as the ionic strength increases.

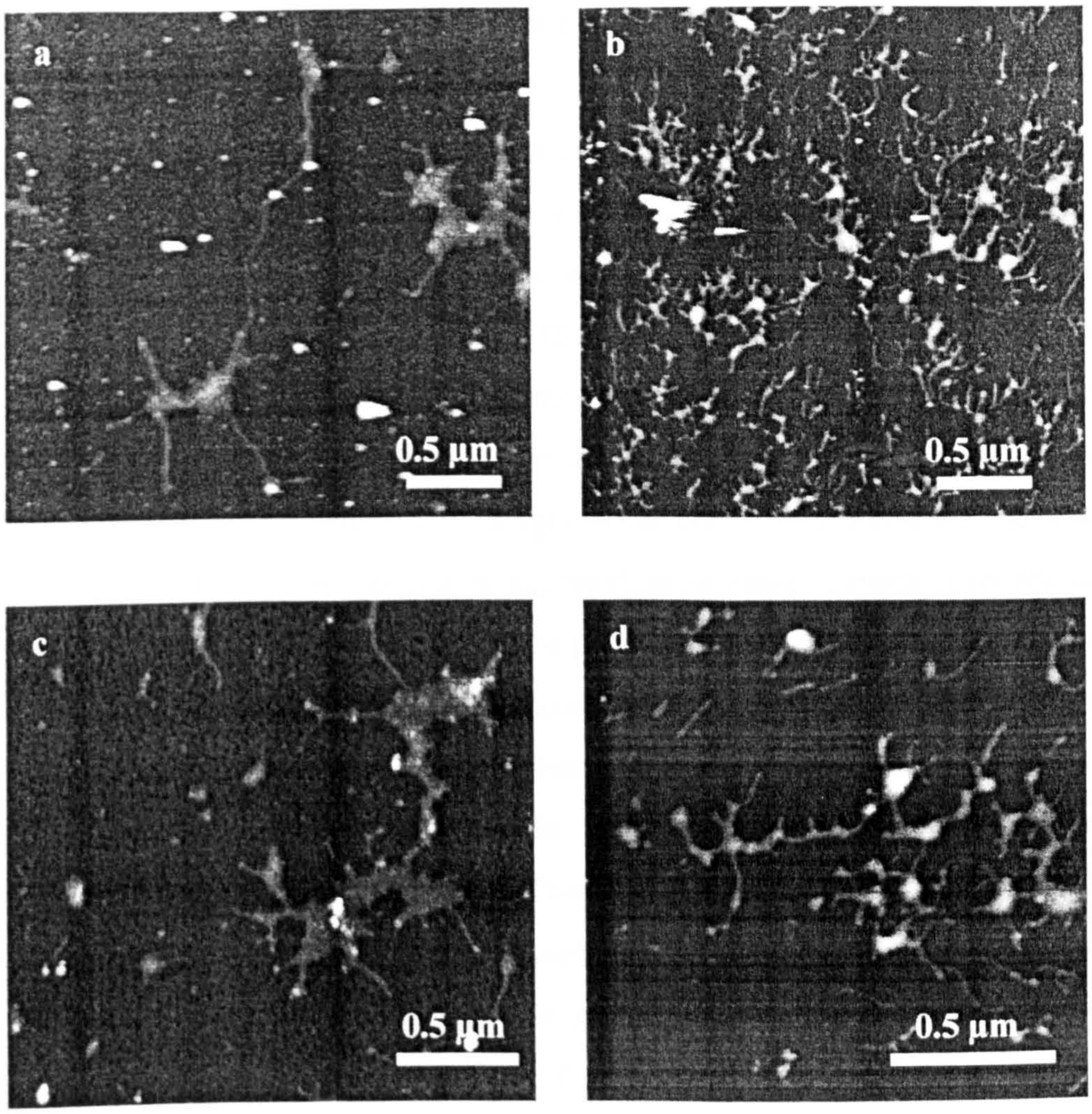

Figure 7.7 AFM topography images of the pig gastric mucin and mucin/chitosan complex in 0.2 M and 0.3 M ionic strength acetate buffer solution.
(a) Mucin at 0.2 M (topography)
(b) Complex at 0.2 M (topography)
(c) Mucin at 0.3 M (topography)
(d) Complex at 0.3 M (topography)

7.4.6 Images of three different mucin populations (Cardiac, Antrum and Fundus)

Also imaged were three mucin populations that had been purified from different areas of the porcine stomach. They have been well characterised by Nordman *et al.* (1998) and Karlsson *et al.* (1998). The mucin populations have been shown to differ in terms of their net charge and glycosylation. The effect of this on the interaction with chitosan is obviously of great interest with reference to a possible drug delivery system. Figure 7.8 shows topographic images of cardiac mucin and cardiac mucin chitosan mixtures at 0.1, 0.2 and 0.3 M ionic strength. The images of cardiac mucins alone are the same as those of PGM in that there is an increase in aggregation as ionic strength is increased, suggesting a possible charge screening effect of the polar side chains enabling entanglements. This is seen in all of the mucin images taken (see also Figures 7.9 and 7.10). The images for the mixtures of cardiac mucin and chitosan (Figure 7.8 a, c and e) show a decrease in complexation with increasing ionic strength, which agrees with results from sedimentation velocity experiments. The mucins purified from the cardiac region are the most charged of the three different populations (Nordman *et al.*, 1997, Karlsson *et al.*, 1997) so on the basis that electrostatic interactions are the dominant feature they would be expected to show the highest level of interaction. This is what is seen when comparing Figures 7.8b, 7.9b and 7.10b. The mucins alone show no real difference in structure or size between the different populations, although Karlsson *et al.* (1997) found differences in the average length of side chains and in molecular weight. It is unlikely, with the polymorphic nature of these materials, that it would be possible to visualize these. The antrum mucin populations demonstrate no real evidence of complex formation with chitosan at 0.1, 0.2 or 0.3 M ionic strength (Figure 7.9a-f). Antrum mucins are not as highly charged as the mucins purified from the cardiac region of the stomach as mentioned above so these results are not surprising; however from the sedimentation velocity experiments some interaction would have been expected at the higher ionic strengths. The lack of complex might be due to the higher ionic strength decreasing the interaction between the APTES on the surface and the side chains of the mucins. Fundus mucins (Figure 7.10a-f) show very little evidence of complexation; this is, perhaps, not surprising as these mucins have the lowest level of sulphation (Nordman *et al.*, 1997).

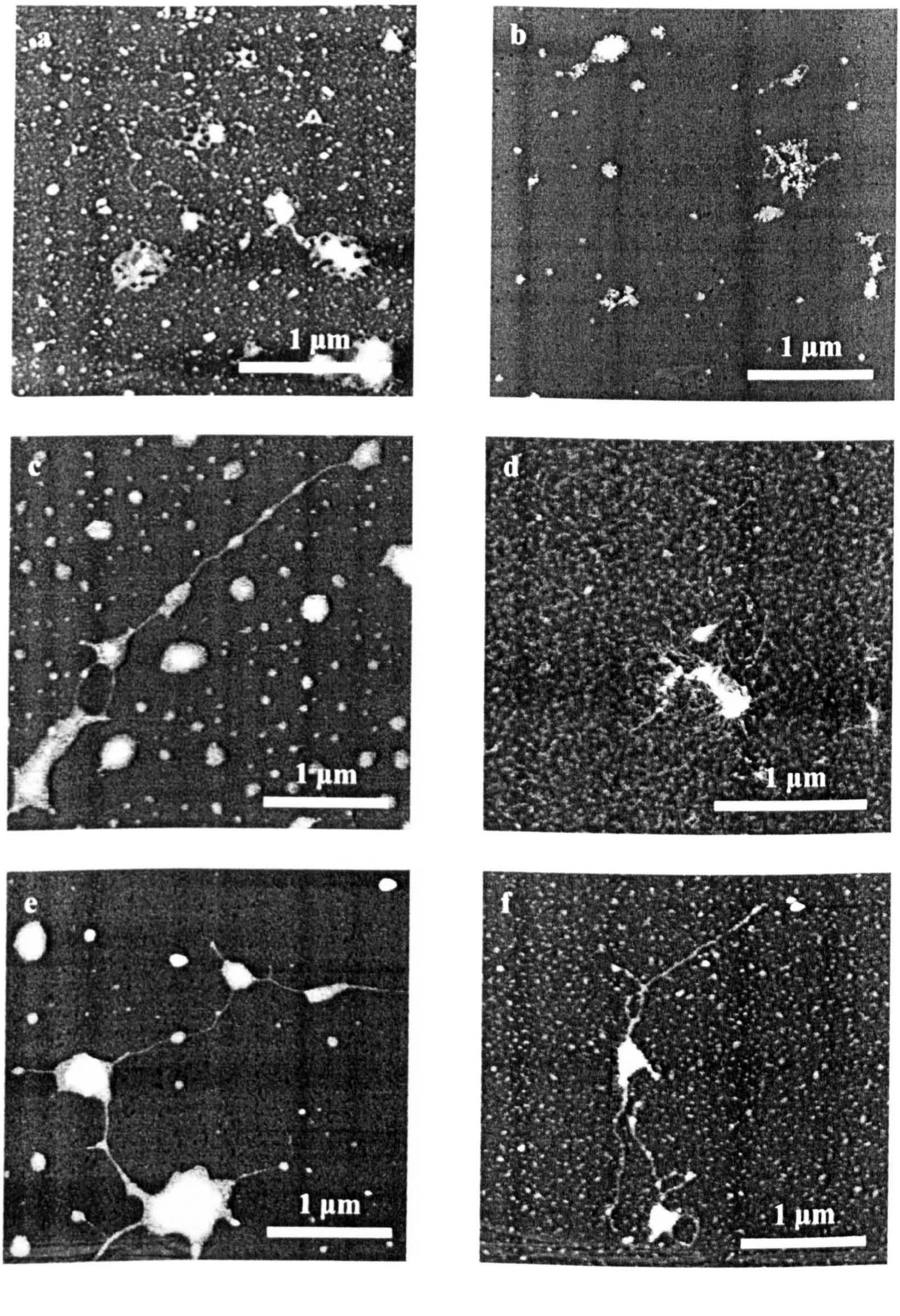

Figure 7.8 AFM topography images of cardiac mucins and the complexes of these mucins with chitosan (SC210+) in three acetate buffers at different ionic strength.
(a) Mucin at 0.1 M (b) Complex at 0.1 M
(c) Mucin at 0.2 M (d) Complex at 0.2 M
(e) Mucin at 0.3 M (f) Complex at 0.3 M

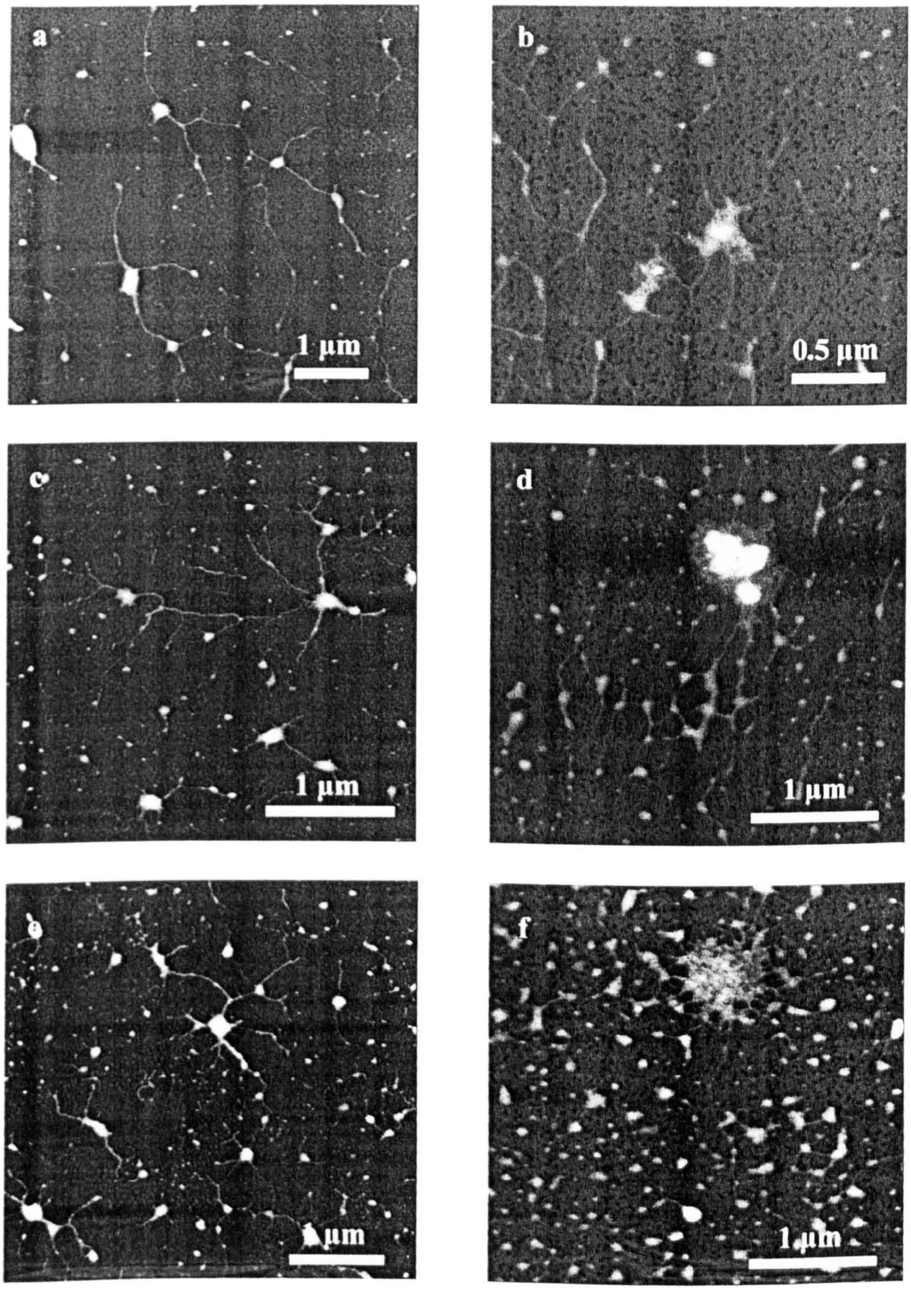

Figure 7.9 AFM topography images of antrum mucins and the complexes of these mucins with chitosan (SC210+) in three acetate buffers at different ionic strength.

(a) Mucin at 0.1 M (b) Complex at 0.1 M
(c) Mucin at 0.2 M (d) Complex at 0.2 M
(e) Mucin at 0.3 M (f) Complex at 0.3 M

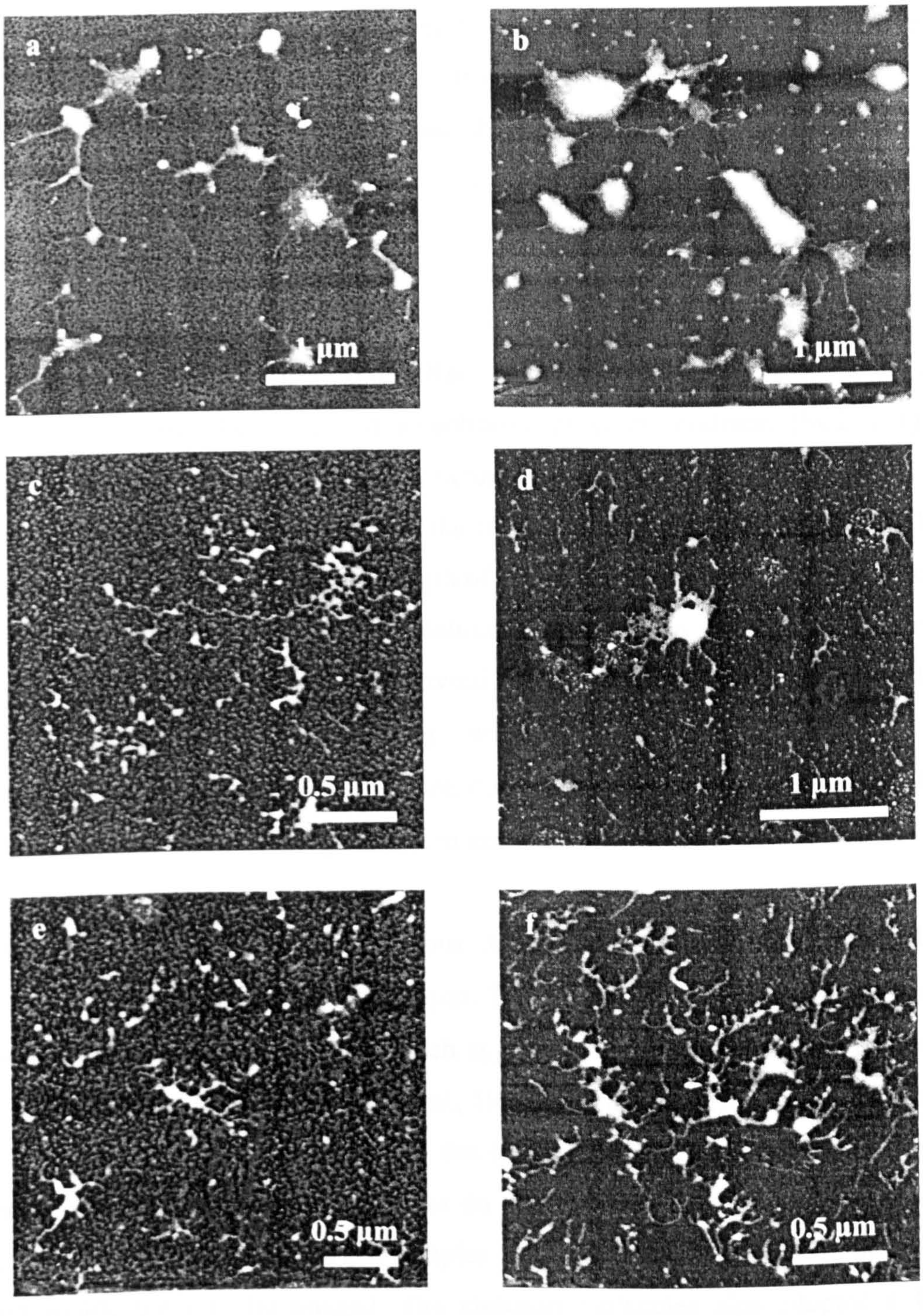

Figure 7.10 AFM topography images of fundus mucins and the complexes of these mucins with chitosan (SC210+) in three acetate buffers at different ionic strength.

(a) Mucin at 0.1 M (b) Complex at 0.1 M
(c) Mucin at 0.2 M (d) Complex at 0.2 M
(e) Mucin at 0.3 M (f) Complex at 0.3 M

There is little or no difference between the images of the fundus mucins alone and those of these mucins in the presence of chitosan. Again this agrees well with results from sedimentation velocity experiments (see Chapter 5).

7.5 Conclusions

In this chapter the AFM has been utilized to probe, at a molecular level, the interaction between purified PGM and a mucoadhesive polymer, chitosan (SC210 +). Initially, images were produced detailing the structures of both PGM and chitosan in 0.1 M acetate buffer (pH 4.5), then the complex of the two structures obtained in the same buffer was investigated. The effect of ionic strength of the buffer on the structure of the complex was studied and finally three mucin populations from different areas of the porcine stomach (cardiac, fundus and antrum) were investigated. The AFM enabled the structures to be observed without surface coating with a conductive material. In addition, TappingMode™ AFM was used which does not produce lateral forces on the surface, appropriate for the soft biological mucin samples.

The mucin adopted a long filamentous structure in 0.1 M acetate buffer, the average length of which was approximately 2 μm. The average diameter was 16 nm. Surprisingly, the expanded glycosylated areas which appear intermittently along the mucin backbone in previous TEM studies (Harding *et al.*, 1983, Sheehan *et al.*, 1986) were not apparent in this AFM study. This may have been due to the partial hydration of the sample allowing the carbohydrate side chains to act as an unimageable entropic brush. The subsequent drying in the preparation of TEM samples would, in effect, immobilize these side chains and enable them to be imaged. The chitosan molecules also adopted a filamentous structure in the 0.1 M acetate buffer, however, this molecule was much more polydisperse and had a smaller average length and diameter than the mucin of, 0.7 μm and 11 nm respectively.

When the mucin and chitosan were mixed in 0.1 M ionic strength acetate buffer, large complexes were formed with an average diameter of 0.7 μm. Interestingly, the complexes formed did not interact at a 1:1 level between the mucin and the chitosan but appeared as a multiple interaction. Surrounding the central complex emanated filaments with an average width of 16 nm. This suggests that these filaments were strands of mucin radiating away from the complex. The interaction between mucin and chitosan is not fully characterized or understood, however, one mechanism describes a charge interaction between the negatively charged mucin and the positively charged chitosan. The positive charge on the chitosan is created by the deacetylation process leaving positive amino termini (Pronova Datasheet, 1994). The negative charge on the PGM has been attributed to the sulphated carbohydrate side chains (Karlsson *et al*, 1997) and not the sialic acid residues as previously thought (Lehr *et al*, 1992).

When the mucins were imaged at 0.2 and 0.3 M ionic strength acetate buffer, the structure seemed to change from the long filamentous nature observed at 0.1 M to a more aggregated appearance. This effect increased with increasing ionic strength. The average number of mucin strands emanating from the mucin complex was estimated. It was found that as the ionic concentration increased the properties of mucins self-interacting also increased from approximately 1 at 0.1 M, 3 at 0.2 M and then 10 at 0.3 M. This may have been due to charge-shielding, effectively neutralizing the mucin filaments. This neutralization would reduce the repulsive forces between the strands and allow them to interact and intertwine resulting in the observed complexes.

At the elevated ionic concentrations of 0.2 and 0.3 M there was still some evidence of complexation between the mucin and chitosan. Small aggregates were formed in both the 0.2 and 0.3 M solution with an average diameter of approximately 150 nm. This is much smaller than the 0.7 μm complexes formed at 0.1 M. The complexes also seemed much more disperse over the sample substrate. Again, this reduction in size of the complex formation may be related to the effect of the salt ions in the buffer leading to neutralization of the mucin and chitosan molecules through charge-shielding.

The results for the three different mucin populations show that there is no visible difference in the structure of the three (cardiac, antrum and fundus) either in the length of the molecules or in their width (ie length of side chains). The only species that showed a visible interaction with chitosan was the cardiac population at 0.1 M ionic strength, there was no evidence of any interaction at the higher ionic strengths. The other two mucins showed no interaction at all. This can be explained in terms of a difference in the levels of sulphation between the three populations, the cardiac species having the highest (60%) and the antrum and fundus the lowest (20%) (Nordman *et al.*, 1997).

In this chapter, the AFM has provided qualitative information, on a molecular level, detailing the structure of PGM, chitosan and their complexes at 0.1, 0.2 and 0.3 M ionic strength in pH 4.5 acetate buffer. The AFM technique used in conjunction with sedimentation velocity in the analytical ultracentrifuge (Chapter 4) has also been shown to provide powerful quantitative information about such interaction phenomena. It is hoped in the future that SPR and AFM *f/d* measurements could yield additional quantitative information about the interactional kinetics and forces of adhesion between mucosal glycoproteins and chitosan.

Chapter 8

Characterisation of Mefp-1 and its mucoadhesion

8.1 Introduction

Having considered the mucoadhesive properties of a highly promising cationic polysaccharide in detail – chitosan, for comparison we now report on an investigation on the mucoadhesive properties of a highly cationic protein: the mussel foot glue protein Mefp-1.

8.1.1 Adhesion of the mussel

The blue mussel *Mytilus edulis* has evolved an opportunistic and permanent adhesive strategy in seawater. It attaches itself to surfaces by means of one or more byssal threads (byssus) and a combination of adhesive proteins secreted into an adhesive plaque between the distal end of the byssus and the surface. The byssus is a collagenous thread, which is attached to the animal at one end and to the surface at the other (Waite, 1983a, Bendict and Waite, 1986). The distal end of the byssus is flattened into a round disk, which is glued to the surface by the adhesive plaque. The byssal thread and disk are formed by the secretion of collagen from the accessory glands into a groove in the foot. At the same time the phenol glands secrete the adhesive proteins which not only cover the disk but also the thread, acting as a sort of protective coating (Laursen, 1992). When the mussel wants to make a thread it extends the foot and presses it to the surface, which it cleans using a scrubbing action (Tamarin *et al.*, 1976). The adhesive proteins are then secreted and the foot is retracted from the surface leaving the insoluble thread.

8.1.2 The adhesive proteins

Characterisation of mussel adhesive proteins began with the work of Waite (Waite and Tanzer, 1981). They isolated a highly basic protein, using acid extraction of phenol glands from the feet of *Mytilus edulis*, with an apparent molecular weight of 130 kDa measured by electrophoresis. This protein was referred to as *Mytilus edulis* foot protein-1 (Mefp-1). Using amino-acid analysis they found that Mefp-1 contained approximately 10% dihydroxyphenylalanine (DOPA) as well as significant amounts of 3- and 4-hydroxyproline. Lysine was the most abundant amino-acid (21%) but also present in large amounts were threonine, serine and tyrosine (Waite and Tanzer, 1981). The presence of DOPA was thought to be significant because it is rarely found in proteins and yet accounts for 10% of Mefp-1. Further work by Waite and coworkers demonstrated that Mefp-1 consists largely of a linear tandem array of decapeptide repeats, the consensus of which is Ala-Lys-Pro-Ser-Tyr-Hyp-Hyp-Thr-Dopa-Lys (Waite, 1983a, Waite *et al.*, 1985). The entire sequence for Mefp-1 has now been determined from cDNA (Ou, 1990) and is shown in Figure 8.1. The apoprotein has a signal sequence of 24 amino-acids which is cleaved to give the native protein. The molecular weight calculated from the sequence is 106,000 Da (Laursen, 1992) which is significantly lower than the original molecular weight (calculated from electrophoresis in the presence of cetylpyridinium chloride, migrating between the α and β chains of type I collagen) reported by Waite and Tanzer (1981) of 130,000 Da. It is possible that this could be due to the high basic charge on the molecule or that it has a highly extended structure in solution, which would increase the rate of progress in electrophoresis. There are 71 repeats of the decapeptide and 13 of the hexapeptide in Mefp-1. The sequence is similar to that obtained for *Mytilus galloprovincialis* (Inoue and Odo, 1994), they found that Mefp-1 and the adhesive protein from *M. galloprovincialis* were very similar, but there was no hexapeptide motif in *M. galloprovincialis* instead they found a tetradecapeptide repeat. Overall there appears to be a high level of homology between all the high molecular weight mussel foot proteins from different species (Laursen, 1992). Recent work has shown that there are at least four families of mussel plaque proteins, which differ in terms of their molecular weight (6, 46, 70 and 130 kDa, Papov *et al.*, 1995). The 46 kDa protein family (Mefp-2) contains about

2-3 mol % of DOPA, which is restricted to the C and N termini, with most of the protein consisting of 11 tandem repeats of an epidermal growth factor motif 37-41 residues in length (Papov et al., 1995, Rzepecki et al., 1992). Mefp-2 differs from Mefp-1 in that it has higher levels of the amino-acid cystine, 6-7 mol % (Rzepecki *et al.*, 1992). It is thought that the high levels of cystine may act to cross link Mefp-2 molecules in the adhesive plaque. Mefp-2 is exclusively found in the adhesive plaque contributing up to 25% to the plaque protein which would seem to confirm this role (Rzepecki *et al.*, 1992). Mefp-3 is the 6 kDa family that has recently had its structure determined by Papov *et al.* (1995) using matrix-assisted laser desorption ionization time-of-flight mass spectrometry

Figure 8.1 Amino-acid sequence of *Mytilus edulis* foot protein-1 deduced from cDNA sequence (Ou, 1990). The underlined portion is the signal sequence. Numbers to the right indicate the number of repeats, numbers in parentheses indicate the position in the sequence. **Y** = 100% conversion to DOPA, Y ≤ 50% conversion to DOPA, **P** = 100% conversion to trans-2,3-cis 3,4 dihydroxyproline, P ≤ 50% conversion to conversion to trans-4 hydroxyproline, P = 100% conversion to trans-4 hydroxyproline.

MEGIKLNLCLLCIFTFDVLGFSNGNIYNAHVSSYAGASAGAYKKLPNAYPYGTKP
EPVYKPVKTSYSAPYKPPTYQPLKKKVDYRPTKSYPPTYGSKTNYLPLAKKLSSY
KPIKTTYN (94)

AKTNYPPVYK 1(104)	AKPSYPPTYK
PKMTYPPTYK	AKPSYPPTYK
PKPSYPPTYK	AKPSYPPTYK
SKP TYK	AKP TYK
PKITYPPTYK	VKPTYPSTYK
AKPSYPPTYK	AKPSYPPTYK
PKKTYPPTYK	AKPSYPPTYK 50(566)
PKLTYPPTYK	AKPSYPPTYK
PKPSYPPTYK	AKPSYPPTYK
SKP TYK 10(186)	AKPSYPPTYK

PKITYPPTYK
AKPSYPPTYK
PKKTYPPTYK
PKLTYPPTYK
PKPSYPPTYK
PKPSYPPSYK
TKKTYPPTYK
PKLTYPPTYK
PKPSYPPSYK
PKKTYPPTYK 20(286)
PKLTYPPTYK
AKPSYPPTYK
AKPSYPPTYK
AKPSYPPTYK
AKPSYPPTYK
AKP TYK
AKPTYPSTYK
AKPTYPPTYK
AKPSYPPTYK
AKPSYPPTYK
AKP TYK
AKL TYK 30(378)
AKPSYPPTYK
AKPSYPPTYK
AKPSYPPTYK
AKPSYPPTYK
AKPSYPPTYK
VKP TYK
AKPTYPSTYK
AKPSYPPTYK
AKPSYPPTYK
AKPSYPPTYK
AKPSYPPTYK 40(474)
AKPSYPPTYK

AKPSYPPTYK
AKP TYK
AKPTYPSTYK
AKPSYPPTYK
AKP TYK
AKPTYPSTYK
AKPTYPSTYK
AKPSYPPTYK
PKISYPPTYK
AKPSYPSTYK
AKSSYPPTYK
AKP TYK 70(746)
AKPTYPSTYK
AKP TYK
AKPTYPPTYK
AKPSYPPTYK
PMPSYPPTYK
SKSSYPSSYK
PKKTYPPTYK
PKLTYPPTYK
PKPSYPASYK
PKITYPSTYK 80(842)
LKPSYPPTYK
SKTSYPPTYN
KKISYPSSYK
AKTSYPPAYK 84

AKPTYPSTYK PTNRY* C-terminus (887)

AKP TYK

(MALDI-TOF-MS). It was found to contain high levels of DOPA in common with Mefp-1 and 2, but also 4-hydroxyarginine which has not been found present in any other (naturally occurring) proteins. This may have a role to play as Arg-DOPA is cleaved by trypsin but HOArg-DOPA is not, suggesting some kind of bond formation (Papov *et al.*, 1994). Mefp-3 and 4 are both known to be found in the cold shocked adhesive plaque but as yet no firm role for them has been proposed (Papov *et al.*, 1995).

8.1.3 Mechanism of adhesion

The mechanism by which Mefp-1 binds to surfaces has been the subject of much speculation, although it is thought that DOPA plays an important role. DOPA has strong dehydration and hydrogen bonding properties, which would make it ideal for attachment to underwater surfaces (Olivieri *et al.*, 1992a, Olivieri *et al.*, 1992b, Hansen *et al.*, 1994). Ionic interactions between the amine terminals of the lysine residues are likely to be involved in cell binding to Mefp-1 through cell surface-Mefp-1 interactions either protein-protein or protein-polysaccharide. Using a molecular model composed of the decapeptide repeat sequence of Mefp-1, Olivieri *et al.* (1992a) describes how L-DOPA provides the initial adsorption to the surface, with the neighbouring hydroxyprolines providing the conformational rigidity that presents the polar side chains of the lysine residues to the outside.

8.1.4 Applications of mussel adhesive proteins

Many attempts have been made to find an application for the adhesive properties of these molecules. Hansen *et al.* (1994) demonstrated that Mefp-1 has a very high affinity for stainless steel and significantly lowered the amounts of metal ions present in solution. Cellular attachment has been investigated by Robin *et al.* (1988), using rabbits they investigated whether Mefp-1 would improve the success of corneal transplants. They found that when 10 µl of a solution of Mefp-1 and a cross linking agent, were placed on the cornea and the eyeball there was a success rate of 73%, compared to a control where none of the transplants succeeded. In addition, the improved attachment of osteoblasts and cartilage has been shown by Fulkerson *et al.* (1990). When Mefp-1 was first coated onto a culture plate surface, 83.6 % of cells were lost from a suspension compared to 30 % lost on an uncoated surface. It is also important to note that in comparison to other cellular adhesives (cyanoacrylates) Mefp-1 is nontoxic; cells continued to grow and multiply on surfaces that had been coated with Mefp-1. Notter (1988) also demonstrated an enhancement of attachment of hypothalamic cells and cells of the tissue culture line N_2AB-1 when using Mefp-1 (in a cellular adhesive, Cell-Tak) compared to tissue-culture plastic.

8.1.5 Our Work

Because of their adhesive properties and basic charge it is thought that these molecules could be used as a mucoadhesive for drug delivery as an alternative to chitosans for example. However, before any interaction can be studied it is important to study the solution conformation and oligomerisation state. In this chapter the conformation and state of the molecule is established using sedimentation velocity and sedimentation equilibrium techniques and the interaction of Mefp-1 with pig gastric mucin assessed.

8.2 Materials and Methods

8.2.1 Preparation of solutions

Mefp-1 was prepared according to the method of Waite (1983a) from material supplied by the Sigma Chemical Company (St. Louis, MO) and was recovered as a freeze-dried mat. This mat was dissolved for 2 hours in buffer before use. Pig gastric mucin (PGM) was isolated and purified as described in Chapter 3. All solution measurements were performed in an acetate buffer, pH 4.5 and I = 0.10 M (Dawson *et al.*, 1986).

8.2.2 Sedimentation equilibrium

An Optima XL-A ultracentrifuge (Beckman Instruments, Palo Alto, CA) was used at a rotor speed of 14,000 rpm at a temperature of 20°C. Standard 12 mm optical path length aluminium filled epoxy double sector cells were employed, filled to 100 µl (giving approximately 2.8 mm solution and solvent columns). Three loading concentrations were used, 0.4, 0.8 and 1.0 mg/ml. Equilibrium was established within 48 hours and confirmed by successive overlay of scans separated by 10 hours. A partial specific volume, $\bar{\nu}$, was calculated from the amino-acid sequence (see Figure 7.1), according to the consensus of Perkins (1986).

Equilibrium solute distributions were captured as an ASCII data set of concentration (expressed as ultraviolet absorbance at a wavelength of 265 nm) versus radial displacement from the rotor centre, r (cm), using the M* procedure (Creeth and Harding, 1982) incorporated into the PC routine MSTARA (Cölfen and Harding, 1997). The M* procedure yields the apparent weight average molecular weight (for the whole distribution of macromolecular solute in the ultracentrifuge cell), $M_{w,app}$, from the identity $M_{w,app} = M^*(r = \text{cell base})$. MSTARA additionally, produces plots of point average molecular data sets of $M_{w,app}(r)$ versus local concentrations, c(r) expressed in absorbance

units (A(r)), at different radial positions, r, in the ultracentrifuge cell. These were obtained for all loading concentrations (to check for the presence of associative phenomena).

8.2.3 Sedimentation velocity

The Optima XL-A ultracentrifuge was also used for sedimentation velocity experiments at a rotor speed of 40,000 rpm and temperature of 20°C, using the 12 mm optical path length cells. Loading concentrations of 0.2, 0.3, 0.4, 0.6, 0.66 and 0.8 mg/ml were used corrected for radial dilution. Sedimentation coefficients $s_{T,b}$ (where T,b represents at room temperature and in buffer b) were evaluated using the routine XLA-VEL (Cölfen et al, 1997). All sedimentation coefficient measurements were performed in triplicate to minimise errors and then corrected to standard conditions of solvent density (ρ) and viscosity (η), i.e. those of water at 20°C, by means of the expression (Tanford, 1961)

$$s_{20,w} = \left\{\frac{(1-\bar{\nu}\rho)_{20,w}}{(1-\bar{\nu}\rho)_{T,b}}\right\}\left\{\frac{\eta_{T,b}}{\eta_{T,b}}\right\}s_{T,b} \qquad 7.1$$

8.3 Results and Discussion

8.3.1 Characterisation of Mefp-1 in dilute solution

8.3.1.1 Sedimentation equilibrium

The apparent weight average molecular weight, $M_{w,app}$, was determined from the extrapolation of the 'M*' function to the cell base for the data-set for the lowest loading concentration (0.4 mg/ml), where it is reasonable to assume $M_w = M_{w,app}$. Using this procedure, M_w = 114,000 (± 5,000) Da. Since the molecular weight of the monomer is

known to be 106,000 from the sequence (Laursen, 1992), it can reasonably be inferred that the Mefp-1 protein is monomeric in dilute solution, at least under these conditions (pH 4.6, I = 0.10 M). This observation is strengthened when the plots of point apparent molecular weight, $M_{w,app}(r)$, as a function of local concentration (expressed as absorbance units A(r) at radial positions r from the rotor centre) are considered (Figure 8.2). This clearly demonstrates that for the loading concentrations of 0.4, 0.8 and 1.0 mg/ml there is no evidence of associative behaviour, which is further confirmed by the single symmetric nature of the boundaries from sedimentation velocity experiments (Figure 8.3).

Figure 8.2 Plot of point weight average molecular weights, $M_{w,app}(r)$, versus local concentration [expressed as absorbance units at 265 nm, A(r)] at various radial positions r in the ultracentrifuge cell for different loading concentrations (0.4, 0.8, 1.0 mg/ml).

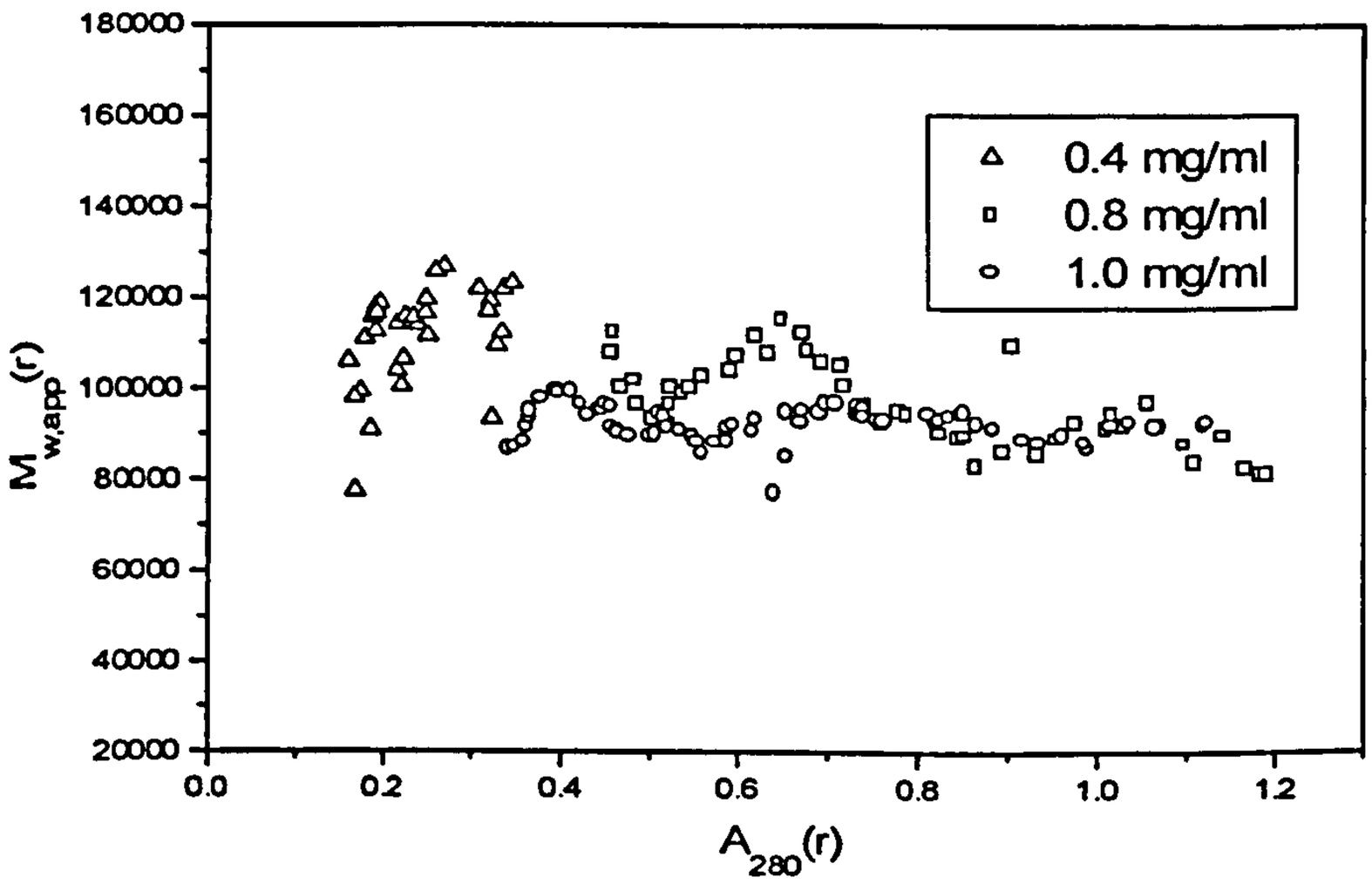

Figure 8.3 Sedimenting boundary for Mefp-1. Rotor speed = 40,000 rpm, temperature = 20°C, loading concentration of 0.8 mg/ml.

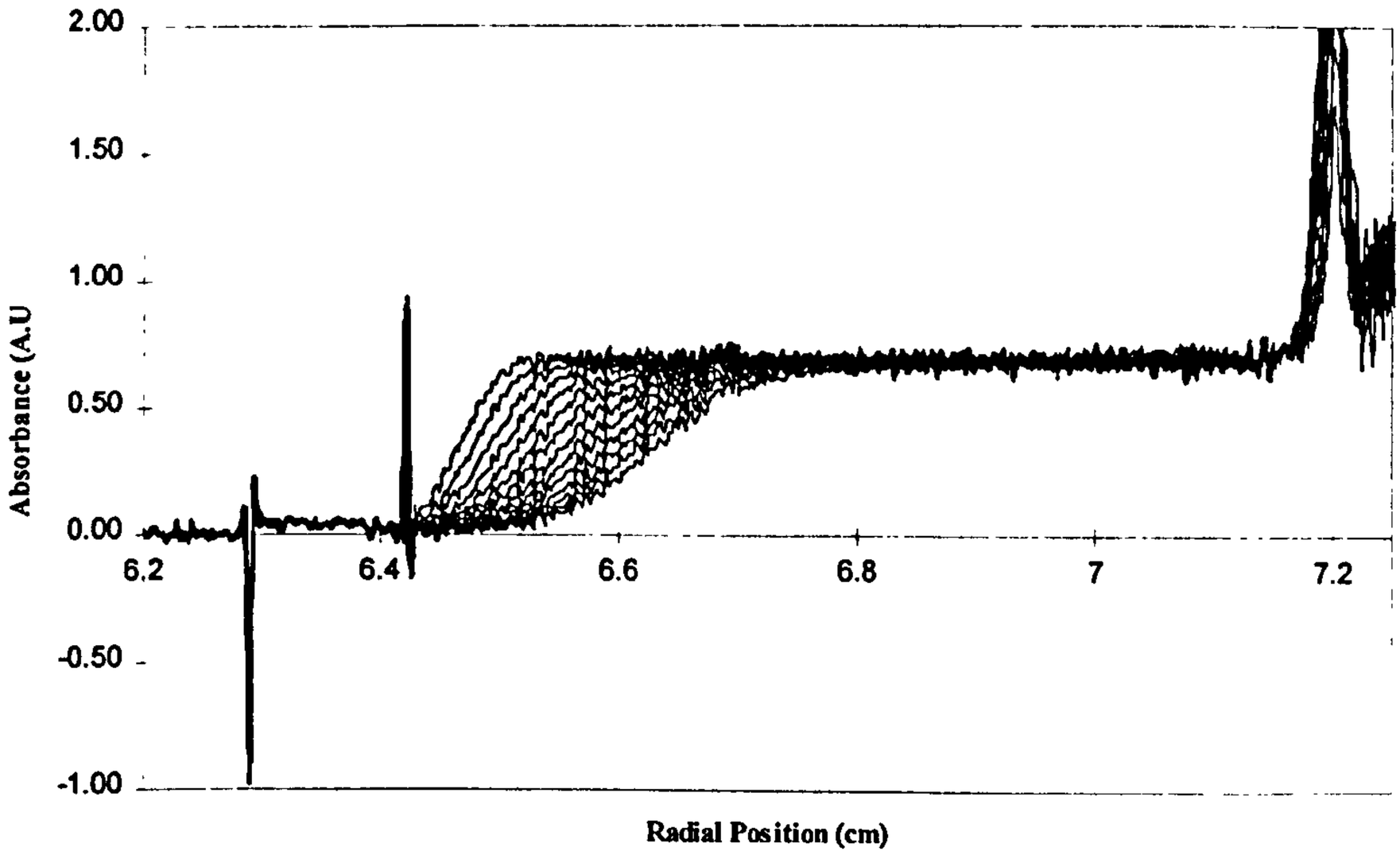

8.3.1.2 Sedimentation velocity

From the plot of $s_{20,w}$ versus sedimenting concentration (i.e. corrected for radial dilution), C (Figure 8.4), a value of $s^0_{20,w}$ of 2.34 (± 0.17) S is obtained by linear regression analysis. This is quite low for a protein of molecular weight equal to 110,000 Da and suggests an asymmetric and/or highly hydrated form for the macromolecule in solution. This was investigated further by calculation of the frictional ratio f/f_0 and the corresponding Perrin function, P for the hydrodynamically equivalent prolate ellipsoid of revolution. f/f_0 is the ratio of the translational frictional coefficient of a macromolecule to the corresponding coefficient for a spherical particle of the same mass and (anhydrous) volume, and is given by

$$\frac{f}{f_0} = \left[\frac{M(1-\bar{\nu}\rho_0)}{N_A(6\pi\eta_0 s^0_{20,w}}\right]\left(\frac{4\pi N_A}{3\bar{\nu}M}\right)^{\frac{1}{3}} \qquad 8.2$$

where N_A is Avogadro's number and ρ_0 (g/ml) and η_0 (P) are the density and viscosity of water at 20°C. Using the values of M = 110,000 Da, $s^0_{20,w} = 2.34 \pm 0.17$ S, $\bar{\nu} = 0.753$ ml/g, $\rho_0 = 0.9982$ g/ml and $\eta_0 = 0.01$ P, f/f_0 was calculated as 3.2 ± 0.3.

Table 8.1 Summary of the solution properties of Mefp-1

Physical property	Value
Monomer molecular weight, M_1(Da)	110,000
Weight average molecular weight, M_w (Da)	114,000 ± 5,000
Sedimentation coefficient, $s^0_{20,w}$ (S)	2.34 ± 0.17
Partial specific volume, $\bar{\nu}$ (ml/g)	0.753
Translational frictional ratio, f/f_0	3.2 ± 0.3

The frictional ratio is related to two macromolecular parameters describing the molecule in solution: shape and the molecular expansion of the molecule in solution through (aqueous) solvent association. The shape contribution is represented by the Perrin function, P (Perrin, 1936), and the molecular expansion through solvent association is popularly represented by the 'apparent hydration', δ (the mass of aqueous solvent chemically or physically associated with the protein per unit dry mass of protein). P is given by (see for example Harding *et al.*, 1997)

$$P = \left(\frac{f}{f_0}\right)\left(\frac{\delta}{\bar{\nu}\rho_0} + 1\right)^{-1/3} \qquad 8.3$$

It is possible to consider two cases one in which the hydration (δ) is assumed to be a typical value for a protein and the other where the hydration is calculated if the protein is assumed to be a sphere.

(1) *Calculation of the axial ratio of the hydrodynamically equivalent prolate ellipsoid of revolution for a "typical" value of δ.* From the shape function P, the overall asymmetry

of the protein can be represented in terms of the axial ratio a/b (where a is much greater than b) of the hydrodynamically equivalent prolate ellipsoid of revolution, for specified values of δ:

$$P = \frac{(1-b^2/a^2)^{1/2}}{(b/a)^{2/3}\ln\left\{\dfrac{1+(1-b^2/a^2)^{1/2}}{b/a}\right\}} \qquad 8.4$$

a/b can be found for a specified P by simple numerical inversion of the above equation, using the PC routine ELLIPS1 (Harding *et al.*, 1997). Considering a range of plausible values for δ from 0.2-0.5 according to Squire and Himmel (1979), we see from Table 8.2 that Mefp-1 is hydrodynamically equivalent to an extended rod shape in solution. Allowing for experimental error in the frictional ratio, the limits of the axial ratio for Mefp-1 are within the range 30:1 to 60:1. This would compare, for example with a value of ~80:1 for myosin and myosin rods (Harding, 1987).

Table 8.2 Perrin function, P and axial ratio a/b for Mefp-1 for various values of molecular hydration, δ.

δ	P	a/b
0.2	3.0	50
0.35	2.8	45
0.5	2.7	40

(2) *Calculation of the maximum value possible of the apparent hydration, δ, if the overall domain of the molecule is assumed to be a sphere.* The axial ratio could, of course, be lower if the apparent hydration was unexpectedly higher (i.e.greater than 0.5), and any molecular flexibility would increase the apparent hydration. For the case where molecular expansion is the sole contribution to the frictional ratio (i.e. P = 1), an f/f_0 of

approximately 3.2 corresponds to a δ of approximately 25. This relates to a molecular expansion (i.e. volume occupied by hydrated molecule/volume of anhydrous molecule) of approximately 35 times, a value more typical for heavily glycosylated systems such as mucin glycoproteins which have more coil-like properties (Harding *et al.*, 1983, Jumel *et al.*, 1997).

Both cases are consistent with the results from sedimentation equilibrium where the effects of thermodynamic non-ideality are relatively small (and that at the loading concentration used effects can be assumed to be negligible). This can be shown with the routine, COVOL (Harding *et al.*, 1997, Harding *et al.*, 1998), which, based on the Rallison-Harding (Rallison and Harding, 1985) exclusion volume theory for general ellipsoids, predicts the second thermodynamic virial coefficient B for a macromolecule based on its shape (as specified by its semi-axial dimensions a, b, c or axial ratios a/b, b/c), its molecular weight, and its molecular hydration or expansion. The routine also provides for calculation of the polyelectrolyte contribution to B, where appropriate. To a first approximation, if we assume that the ionic strength is sufficient to suppress this latter contribution, the predicted values of B are 5.97×10^{-4} ml·mol^{-1}·g^{-2} for case 1 above and 9.82×10^{-4} ml·mol^{-1}·g^{-2} for case 2. The apparent weight average molecular weight $M_{w,app}$ at a finite concentration, C (g/ml) is, to first order non-ideality (Tanford, 1961):

$$1/M_{w,app} = (1/M_w)(1+2BM_wC) \qquad 8.5$$

For a concentration of 1 mg/ml and M_w = 110,000 Da, the equation above predicts a value of 91,900 Da for case 1 and 83,100 for case 2. In both cases there is a drop in molecular weight, ~20% for case 1 and ~30% for case 2 as the concentration is varied from 0-1.5 mg/ml (corresponding to the concentration range of Figure 8.2). Unfortunately, both cases are consistent with the data and it is not possible to compare this result with an X-ray crystallographic structure as Mefp-1 is yet to be crystallised.

The solution conformations of Mefp-1 and a recombinant analogue with 20 repeats of the consensus decapeptide (AKPSYPPTYK) have, however, been studied using far-UV

circular dichroism (CD) and enzyme-directed modification (Williams *et al.*, 1989). Although the conditions differ from those used here (0.6 M NaCl with 0.1 M phosphate at pH 7.0), it is useful to compare these results. The CD data suggested that the secondary structure in Mefp-1 and the recombinant analogue were limited to no more than 5% α-helix, 10% β-sheet and 20% β-turns. The remainder was attributed to 'random coil' as it was minimally perturbed by temperature variations or the addition of 6 M guanidine hydrochloride. This interpretation of the results contrasts with those from the tyrosinase-directed modification of tyrosines in the recombinant analogue. Tyr-9 of each consensus repeat was at least an order of magnitude more reactive than Tyr-5 (Williams et al., 1989). Taken together, these results suggest an overall extended and flexible Mefp-1 structure that is punctuated by regions of rigidity, somewhere in between case 1 and case 2. This is presented as the 'consensus model' of Figure 8.5 for the structure of Mefp-1 in dilute solution.

Figure 8.4 Concentration dependence of the sedimentation coefficient, $s_{20,w}$, for Mefp-1 in acetate buffer (pH = 4.5, I = 0.10 M) at 20°C.

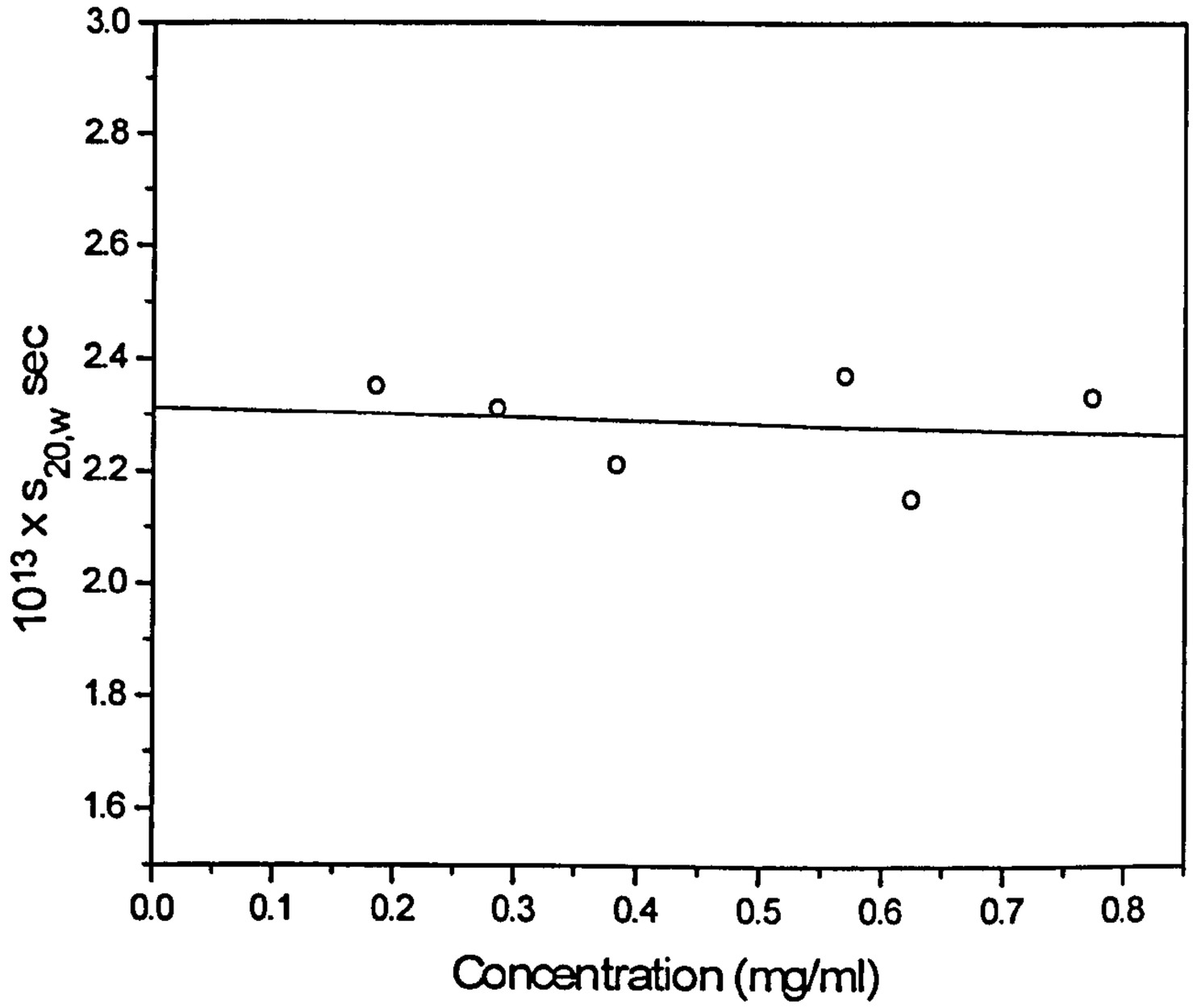

Figure 8.5 Consensus semi-flexible rod model for Mefp-1. This model takes into account the linear flexible properties consistent with larger values for hydration ($\delta > 0.5$), earlier CD studies (Laursen, 1992), and the ability to adhere and hydrate at surfaces (Baty *et al.*, 1997). The model consists of a globular region with a nonrepetitive amino-acid sequence and an extended region consisting of repeat sequences of amino-acids with alternating stiff and flexible segments. Except at high pH (>7) and ionic strength, the chain will be relatively stiff due to electrostatic repulsion of segments.

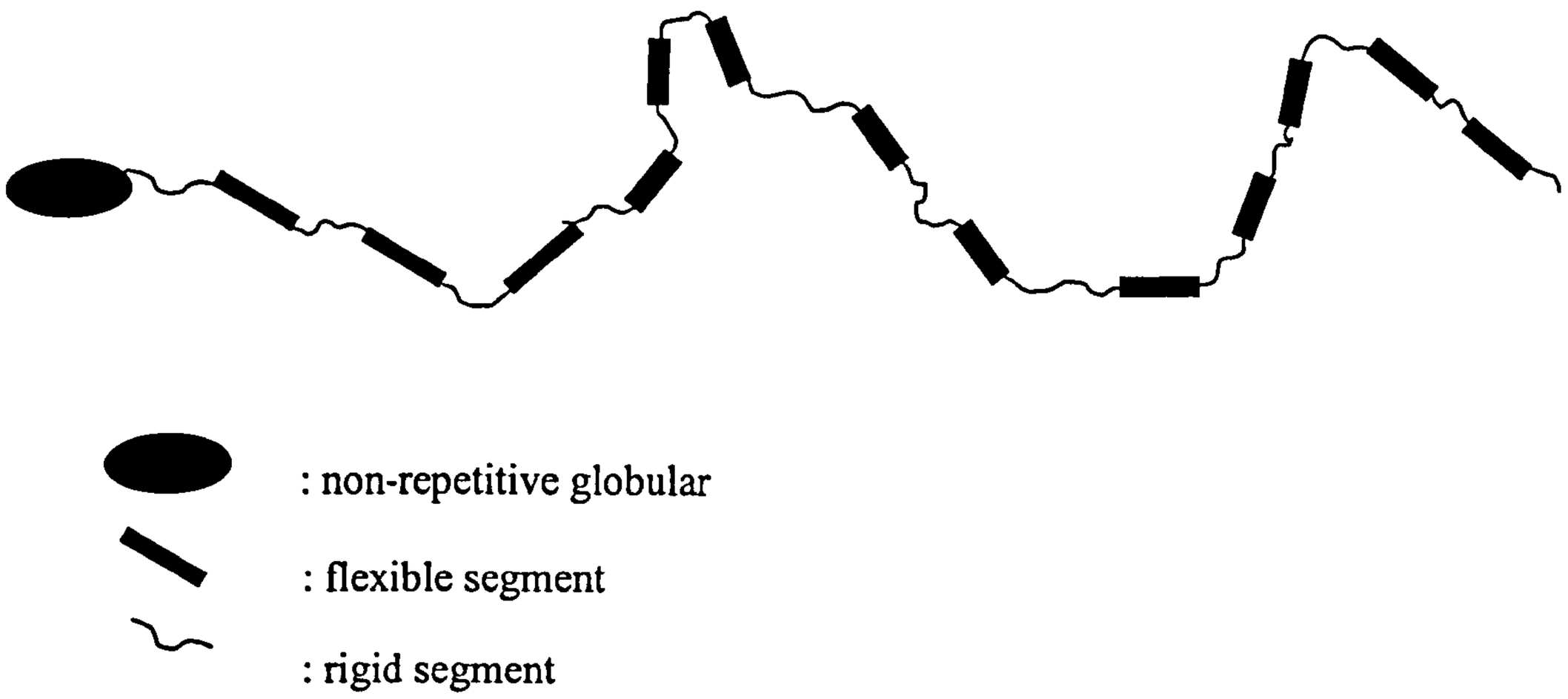

8.3.2 Interaction with Pig gastric Mucin (PGM)

8.3.2.1 Sedimentation velocity

By using the solution conditions at which Mefp-1 is known to be present, essentially as the monomer (pH 4.5, 0.1 M I), the interactions between Mefp-1 and other molecules can be measured without any of the complications of self-association or aggregation. The interaction between Mefp-1 and PGM was studied using velocity sedimentation, Figure

8.6 shows the sedimentation scans obtained. Comparison of these scans with those in Figure 8.3 indicates that there is a huge increase in the size of the macromolecule. This can only be explained in terms of an interaction between Mefp-1 and PGM. Mefp-1 has a sedimentation coefficient of 2.34 S and PGM of approximately 60 S, whereas the analysis of the sedimentation scans using the Beckman TRANSPORT method (XL-A instruction manual, 1991) gives a sedimentation coefficient of 7,000 S. When rotation velocity was increased to 40,000 rpm, it was also observed that there were no longer any sedimentation profiles visible, indicating that there was no measurable unbound Mefp-1 present in the ultracentrifuge cell. The complex is so large that it makes the measurement of its molecular weight by sedimentation equilibrium impossible. However, by assuming a roughly spheroidal random coil conformation for both Mefp-1 and PGM-MD, the Mark-Houwink-Kuhn-Sakurada relation (for example, Harding, 1995) $s \sim M^{0.6}$, (0.6 was chosen because it is intermediate between the limits for coil (0.667) and sphere (0.5)). To estimate the size of the complex, a molecular weight of $\sim 2.5 \times 10^{10}$ is predicted. It should be noted that the sedimenting boundaries are quite broad and strongly indicate considerable heterogeneity of the complexes formed.

Figure 8.6 Sedimenting boundaries for the PGM-Mefp-1 complex. Rotor speed = 2,000 rpm, temperature = 20°C, scan interval = 10 min, concentration of mucin after mixing = 0.1 mg/ml, concentration of Mefp-1 after mixing = 0.4 mg/ml.

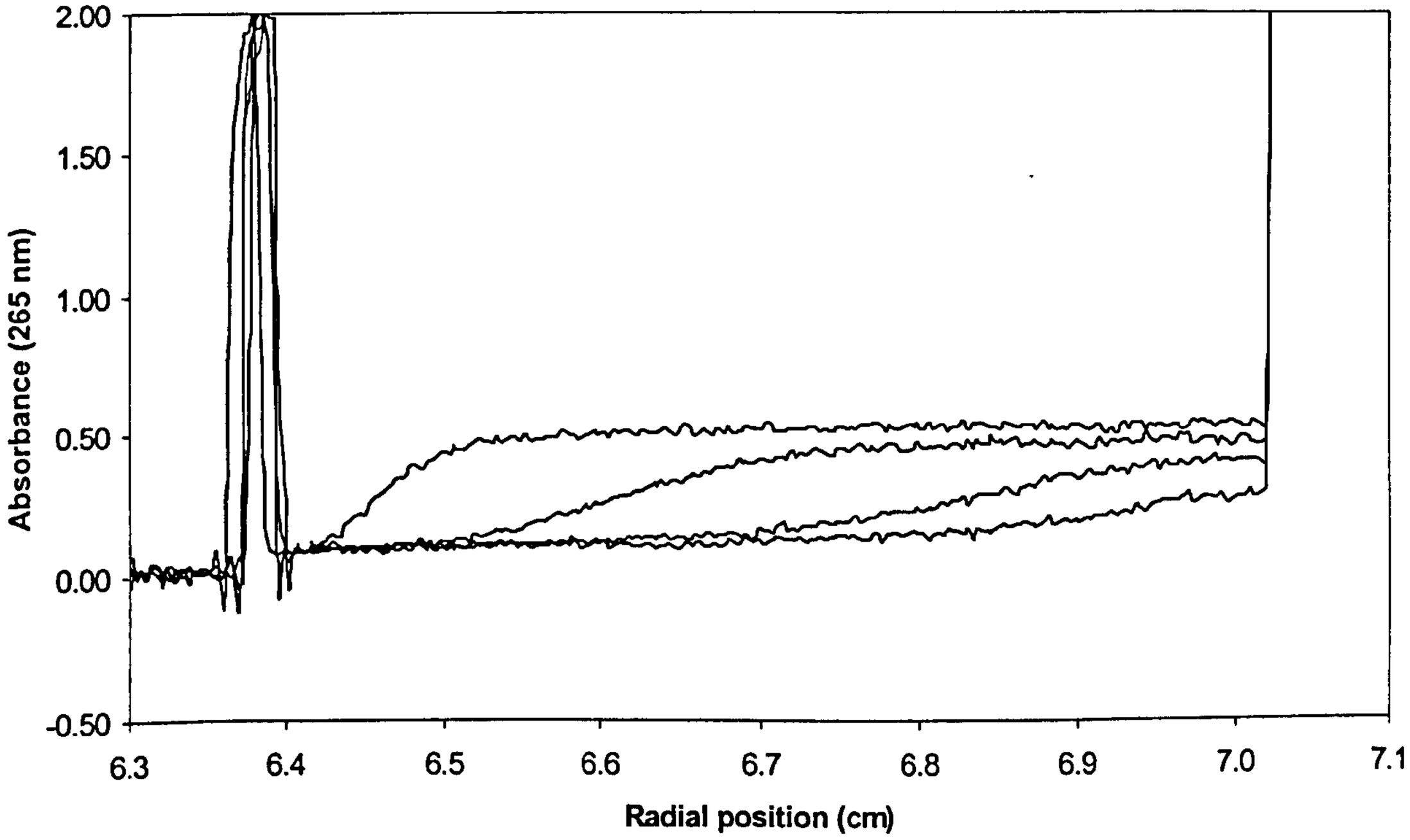

Chapter 9

Conclusions

This work has focussed on the interaction between fully hydrated independent macromolecules in dilute solution. A variety of mucins have been characterised by SEC/MALLS and their interactions with different preparations of chitosan and a protein purified from the foot of the blue mussel have been measured. The techniques of sedimentation velocity, sedimentation equilibrium, atomic force microscopy and multi-angle laser light scattering (linked to size exclusion chromatography and flow field flow fractionation) have all been used to characterise both the substrates and the complex.

The mucin populations were characterised using SEC/MALLS and shown to be single species relatively monodisperse with molecular weights in the region of 10 x 10^6 Daltons. The chitosan SC210 + had been previously characterised by Errington *et al.* (1993), chitosan A fractions have been characterised by Berth *et al.* (1998). *Mytilus edulis* foot protein 1 was characterised using sedimentation velocity and equilibrium and shown to be monomeric in dilute solution with a molecular weight of 114,000 Daltons.

This work has demonstrated that the interaction between chitosan and mucin is the product principally of an ionic interaction between pig gastric mucin and chitosan. The results from sedimentation velocity experiments and from atomic force microscopy show a decline in the number and size of complexes formed as the ionic strength of the solution is increased from 0.1 to 0.3 M and beyond. The critical point appears to be around 0.25 M above this ionic strength there is very little interaction between SC210 + and PGM-MD. The sedimentation velocity results also suggested that at the higher ionic strengths (>0.3M) there may be a weak hydrophobic interaction.

Sedimentation velocity was also used to measure the effect of a chitosan with a higher degree of deacetylation (25%) which was found to form a large complex with pig gastric mucins. The effect of molecular weight of this chitosan was investigated with

sedimentation velocity and it was found that there was a sharp reduction in the interaction when the chitosan molecular weight was above 80,000 Daltons.

The interaction between the pig gastric mucins purified from different regions of the porcine stomach also confirmed the ionic nature of the interaction. The cardiac mucin population showed the highest interaction with SC210 + chitosan, as measured by sedimentation velocity and atomic force microscopy. The antrum and fundus mucin populations showed a much lower level of interaction measured by the same methods. Mefp-1 has also been shown to form a strong interaction with pig gastric mucin which was likely to be due to interactions between positively charged lysine groups and the negatively charged sulphated sugar residues present on the mucin macromolecule.

Chitosan shows much promise as a vehicle for drug delivery to the gastrointestinal tract. Other work has shown (Illum *et al.*, 1994) that not only does chitosan have mucoadhesive properties but it also has the ability to open the epithelial tight junctions. This gives it a dual function in a drug delivery system. The interaction that has been measured in this thesis is one that occurs in dilute solutions. However, the interaction in the gastrointestinal tract would not be between substrates that are free in solution as the mucus forms a gel like coating on the surface that reduces the number of sites available for interaction. The interaction of Mefp-1 with pig gastric mucin is also interesting but as this is a protein it is a target of proteolysis. The protein would therefore need to be protected within the drug delivery vehicle until arrival in the small intestine.

Further work in this field should include the use of model drugs in the system to see what effect they have on the formation of the complex. *In vivo* studies with trial formulations could also be undertaken. The results from flow field flow fractionation are promising but further work needs to be undertaken in refining this technique so that full characterisation of the complex can be obtained.

Since the elucidation of such interactions as those between mucins and chitosans a doorway has been opened to the possibility of succesful delivery of peptides and other problem drugs.

Chapter 10

References

Acatürk, F. (1989). Preparation of a prolonged-release tablet formulation of diclofenac sodium. Part 1: Using chitosan. *Pharmazie*, **44**, 547–549.

Akari, S.O., van der Vegte, E.W., Grim, P.C.M., Belder, G.F., Koutsos, V., ten Brinke, G. and Hadziioannou, G. (1996) Imaging of single polymer chains based on their elasticity. *Applied Physics Letters* **65**, 1915.

Al-Dujaili, H., Salole, E.G. and Florence, A.T. (1983) Drug formulation and oesophageal injury. *Adverse Drug Reactions and Acute Poisoning Reviews* **2**, 235–256.

Alimuniar, A. and Zainuddin, R. (1992) An economical technique for producing chitosan. In *Advances in Chitin and Chitosan*, Ed. C.J. Brine, P.A. Sandford and J.P. Zikakis, pp627-632. London: Elsevier Applied Science.

Allen, A. (1978) Structure of gastrointestinal mucus glycoproteins and the viscous and gel-forming properties of mucus. *British Medical Bulletin* 34, 28–33.

Allen, A. (1981) Structure and function of gastrointestinal mucus. In *Physiology of the Gastrointestinal Tract*, ed. L.R. Johnson, pp 617-639. New York: Raven Press.

Allen, A. (1983) Mucus – a protective secretion of complexity. *Trends in Biochemical Sciences*, 8, 169–173.

Allen, A. (1989) Gastrointestinal mucus. In *Handbook of Physiology – The Gastrointestinal Physiology. Salivary, Gastric and Hepatobiliary Secretions*, Ed. M.D. Bethesda, Section 6, Vol. III, pp 359–382. USA: American Physiological Society.

Allen, A. and Caroll, N.J.H. (1985) Adherent and soluble mucus in the stomach and duodenum. *Digestive Diseases and Sciences* **30**, 55S–62S.

Allen, A., Flemström, G., Garner, A. and Kivilaakso, E. (1993) Gastroduodenal mucosal protection. *Physiological Reviews* **73**, 823–857.

Anderson, M.T. (1991) The interaction of mucous glycoproteins with polymeric materials, *Ph.D. thesis*, University of Nottingham, U.K.

Anderson, M.T., Harding, S.E. and Davis, S.S. (1989) On the interaction in solution of a candidate mucoadhesive polymer, diethylaminoethyl-dextran, with pig gastric mucus glycoprotein. *Biochemical Society Transactions* 631st meeting Guildford, **17**, pp 1101–1102.

Arai, K., Kinumaki, T. and Fujita, T. (1968) Toxicity of chitosan. *Bulletin of the Tokai Regional Fisheries Research Laboratory*, **56**, 89–94.

Bansil, R., Stanley, E. and LaMont, J.T. (1995) Mucin biophysics. *Annual Rev. Physiol.* **57**, 635-657.

Baty, A.M., Leavitt, P.K., Siedlecki, C.A., Tyler, B.J., Suci, P.A., Marchant, R.E. and Geesey, G.G. (1997) Adsorption of adhesive proteins from the marine mussel, Mytilus edulis, on polymer films in the hydrated state using angle dependent X-ray photoelectron spectroscopy and atomic force microscopy. *Langmuir* **13**, 5702-5710.

Bechgaard, H. and Ladefoged, K. (1978) Distribution of pellets in the gastrointestinal tract. The influence on transit time exerted by the density and diameter of pellets. *J. Pharm. and Pharmacol.* 30, 690–692.

Beermann, B., Groschinsky-Grind, M. and Rosen, A. (1976) Enhancement of the gastrointestinal absorption of hydrochlorothiazide by propantheline. *European J. of Clin. Pharm.* **13,** 385-387.

Beermann, B., Groschinsky-Grind, M. and Rosen, A. (1978) Absorption metabolism and excretion of hydrochlorothiazide. *Clin. Pharm. And Ther.* **19,** 718-721.

Bell, A.E., Sellers, L.A., Allen, A., Morris, E., Ross-Murphy, S. (1985) Properties of gastric and duodenal mucus: effects of proteolysis, disulphide reduction, bile, acid, ethanol and hypertonicity on mucus gel structure. *Gastroenterology* **88**, 269–280.

Benedict, C.V. and Waite, J.H. (1986) Location and analysis of byssal structural proteins of *Mytilus edulis*. *J. Morphol.* **189,** 171-181.

Berth, G., Dautzenberg, H. and Peter, M.G. (1998) Physico-chemical characterization of chitosans varying in degree of acetylation. *Carb. Pol.* **36,** 205-216.

Bhaskar, K.R., Garik, P., Turner, B.S., Bradley, J.D., Bansil, R., Stanley, H.E. and Lamont, J.T. (1992) Viscous fingering of HCl through gastric mucin. *Nature* **360**, 458–461.

Billingham, N.C. (1977) Light scattering. *In: Molar mass measurements in polymer science.* pg 105-145. Kogan Press Ltd.

Binnig, G., Quate, C.F. and Gerber, C.H. (1986) Atomic force microscope. *Phys. Rev. Lett.* **56**, 930-933.

Boddé, H.E. (1990) Principles of Bioadhesion. In *Bioadhesion – Possibilities and Future Trends*, ed. R. Gurny and H.E. Junginger, Wissenschaftliche Verlagsgesellschaft mbH Stuttgart, APV, Vol. 25, pp 44–64

Booth, C.C. (1967) Sites of absorption in the small intestine. *Federation Proceedings*, **28**, 1583–1588.

Bouckaert, S., Temmerman, M., Dhont, M. and Remon, J.P. (1994) The treatment of bacterial vaginosis with a bioadhesive vaginal slow-release tablet with metronidazole. *Proceedings of the International Symposium on Controlled Release of Bioactive Materials* **21**, 585–586.

Brahams, D. (1984) Death of a patient participating in trial of oral morphine for relief of postoperative pain. *Lancet* **1**, 1083–1084.

Brohult, S. (1987) Svedberg as a scientist. *In*: *Physical chemistry of colloids and macromolecules.* pg 9-13. Rånby, B. (Ed.) Blackwell Scientific Publications, Oxford, UK.

Brown, H.G. and Hoh, J.H. (1997) Entropic exclusion by neurofilament side arms: A mechanism for maintaining interfilament spacing. *Biochemistry* **36,** 15035-15040.

Bystricky, S., Malovíková, A. and Sticzay, T. (1990) Interaction of alginates and pectins with cationic polypeptides. *Carbohydrate Polymers* **13**, 283–294.

Cargill, R., Caldwell, I.J., Engle, K., Fix, J.A., Porter, P.A. and Gardner, C.R. (1988) Controlled gastric emptying. I. Effects of physical properties on gastric residence times of non-disintegrating geometric shapes in beagle dogs. *Pharm. Res*. **5**, 533–536.

Cargill, R., Engle, K., Gardner, C.R., Porter, P., Sparer, R.V. and Fix, J.A. (1989) Controlled gastric emptying. II. *In vitro* erosion and gastric residence times of an erodible device in beagle dogs. *Pharm. Res.* **6**, 506–509.

Carlstedt, I. and Sheehan, J.K. (1984). Is the macromolecular architecture of cervical, respiratory and gastric mucins the same? *Biochem. Soc. Trans.* **12**, 615–617.

Carlstedt, I. and Sheehan, J.K. (1988). Structure and macromolecular properties of mucus glycoproteins. *Monographs in Allergy*, Basel, **24**, 16–24.

Chen, J.L. and Cyr, G.N. (1970) Compositions producing adhesion through hydration. In *Adhesion in Biological Systems*, Ed. R.S. Manly, pp 163-181. New York: Academic Press.

Chen, X., McGurk, S.L., Davies, M.C., Roberts, C.J., Shakesheff, K.M., Tendler, S.J.B. and Williams, P.M. (1998) Chemical and morphological analysis of polymer surfaces by phase-detection imaging SFM. *Macromolecules* **31**, 2278-2283.

Code, C.F. and Marlett, J.A. (1975). The interdigestive myo-electric complex of the stomach and small bowel of dogs. *J. Phys.* **246**, 289–309.

Cohen, S.R. (1994) Recent advances in scanning force microscopy. *Heterogen. Chem. Rev.* **1**, 135-144.

Cölfen, H. and Harding, S.E. (1997) MSTARA and MSTARI : interactive PC algorithms for simple, model independent evaluation of sedimentation equilibrium data. *Eur. Biophys. J.* **25**, 333-346.

Cölfen, H., Harding, S.E. and Rowe, A.J. (1997) unpublished results.

Cölfen, H., Harding, S.E., Vårum, K.M., and Winzor, D.J. (1996) A study by analytical ultracentrifugation on the interaction between lysozyme and extensively deacetylated chitin (chitosan). *Carbohyd. Polym.* 30, 45-53.

Creeth, J.M. (1978) Constituents of mucus and their separation. *British Medical Bulletin*, **34**, 17–24.

Creeth, J.M. and Harding, S.E. (1982) Some observations on a new type of point average molecular weight. *J. of Biochem. and Biophys. Methods* **7**, 25-34.

Davis, S.S. (1985) The design and evaluation of controlled release systems for the gastrointestinal tract. *J. Controlled Rel.* **2**, 27-38.

Davis, S.S. (1989) Small intestine transit. In*: Drug delivery to the Gastrointestinal Tract.* By: Hardy, J.G., Davis, S.S., Wilson, C.G. (Eds.), Ellis Horwood Ltd., Chichester, pg. 49-61.

Davis, S.S., Stockwell, A.F., Taylor, M.J., Hardy, J.G., Whalley, D.R., Wilson, C.G., Bechgaard, H. and Christensen, F.N. (1986) The effect of density on gastric emptying of single- and multiple-unit dosage forms. *Pharm. Res.* **3**, 208–213.

Dawson, M.C., Elliot, D.C., Elliot, W.H. and Jones, K.M. (Eds.) (1986*) Data for Biochemical Research*, Clarendon Press, Oxford, pg. 429.

Deacon, M.P., Davis, S.S., White, R.J., Nordman, H., Carlstedt, I., Errington, N., Rowe A.J. and Harding S.E. (1998) Are chitosan-mucin interactions specific to different regions of the stomach? Velocity Ultracentrifugation offers a clue. Accepted for publication in *Carbohydrate Polymers*.

Deasy, P.B. and O'Neill, C.T. (1989) Bioadhesive dosage form for peroral administration of timolol base. *Pharmaceutica Acta Helvetiae* **64**, 231–235.

Delain, E., Fourcade, A., Poulin, J-C., Barbin, A., Coulaud, D., Le Cam, E. and Paris, E. (1992) Comparative observations of biological specimens, especially DNA and filamentous actin molecules in atomic force, tunnelling and electron microscopes. *Microsc. Microanal. Microstruct.* **3**, 457-470.

Duchêne, D., Touchard, F. and Peppas, N.A. (1988) Pharmaceutical and medical aspects of bioadhesive systems for drug administration. *Drug Development and Industrial Pharmacy*, **14**:283-381.

Errington, N. (1993) Hydrodynamic characterisation of novel polysaccharides for pharmaceutical and food use. Thesis Nottingham University.

Errington, N., Harding, S.E., Vårum, K.M., Illum, L. (1993) Hydrodynamic characterization of chitosans varying in degree of acetylation. *International Journal of Biological Macromolecules* **15**, 113–117.

Fiebrig, I. (1995) Solution studies on the mucoadhesive potential of various polymers for use in gastrointestinal drug delivery systems. PhD Thesis, University of Nottingham, UK.

Fiebrig, I., Harding, S.E., Davis, S.S. (1995a) Methods used to develop mucoadhesive drug delivery systems: Bioadhesion in the gastrointestinal tract. *Biopolymer Mixtures*, Eds Harding, S.E., Hill, S.E. and Mitchell, J.R., Nottingham University Press.

Fiebrig, I., Harding, S.E., Rowe, A.J., Hyman, S.C. and Davis, S.S. (1995b) Transmission electron microscopy studies on PGM and its interactions with chitosan. *Carbohydrate Polymers* **28**, 239-244.

Fiebrig, I., Vårum, K.M., Harding, S.E., Davis, S.S., Stokke, B.T. (1997) Colloidal gold and colloidal gold labelled wheat germ agglutinin as molecular probes for identification in mucin/chitosan complexes. *Carbohydrate Polymers* **33,** 91-99.

Fogg, F.J.J., Hutton, D.A., Jumel, K., Pearson, J.P., Harding, S.E. and Allen, A. (1996) Characterization of pig colonic mucins. *Biochemical Journal.* **316**:937-942.

Forster, H. and Lippold, B.C. (1982) Conception of peroral sustained-release dosage forms: calculation of initial and maintenance dose with consideration of accumulation. *Pharmaceutica Acta Helvetiae* **57,** 345-349.

Fujita, H. (1975) *Foundations of ultracentrifugal analysis.* John Wiley and Sons, NY, USA.

Fulkerson, J.P., Norton, L.A., Gronowicz, G., Picciano, P., Massicotte, J.M. and Nissen, C.W. (1990) Attachment of epiphyseal cartilage cells and 17/28 rat osteosarcoma osteoblasts using mussel adhesive protein. *J. Orthop. Res.* **8,** 793-798.

Gibbons, R.A. (1972) Physico-chemical methods for the determination of the purity, molecular size and shape of glycoproteins. In*: Glycoproteins: Their Composition, Structure and Function*. Gottschalk, A. (Ed.) Elsevier Publishing Company, Amsterdam, pg. 31-141.

Giddings, J.C. (1993) Field-flow fractionation: Analysis of macromolecular, colloidal, and particulate materials. *Science* **260,** 1456-1465.

Giebeler, R. (1992) The Optima XL-A: A new analytical ultracentrifuge with a novel precision absorption optical system. *In: Analytical ultracentrifugation in biochemistry and polymer science.* Harding, S.E., Rowe, A.J. and Horton, J.C. (Eds.), Royal Society of Chemistry, Cambridge, UK. pg. 16-25.

Gottschalk, A., Bhargava, A.S. and Murty, V.L.N. (1972) Submaxillary gland glycoproteins. In *Glycoproteins: Their Composition, Structure and Function*. Ed. A. Gottschalk, pp. 810-829. Amsterdam: Elsevier Publishing Company.

Greaves, J.L. and Wilson, C.G. (1993) Treatment of diseases of the eye with mucoadhesive delivery systems. *Adv. Drug Delivery Revs.* **11**, 349–383.

Green, R.J., Tasker, S., Davies, J., Davies, M.C., Roberts, C.J. and Tendler, S.J.B. (1997) Adsorption of PEO-PPO-PEO triblock copolymers at the solid/liquid interface: A surface plasmon resonance study. *Langmuir*, **13**, 6510-6515.

Grundy, D. (1985) *Gastrointestinal Motility*, Lancaster: MTP Press Ltd.

Gum, J.R. (1995) Human mucin glycoproteins: varied structures predict diverse properties and specific functions. In: Mucins Their Structure and Biology. Sheehan, J. (Ed.) *Biochemical Society Transactions.* **23**:795-799.

Guyton, A.C. (1991) Textbook of Medical Physiology Eighth edition. W.B. Saunders Company, Philadelphia, USA.

Hansen, D.C., Luther, G.W. and Waite, J.H. (1994) The adsorption of the adhesive protein of the blue mussel Mytilus edulis L onto type 304L stainless steel. *J. Coll. Int. Sci.* **168**, 206-216.

Hansma, P.K., Elings, V.B., Marti, O. and Bracker, C.E. (1988). Scanning tunneling microscopy and atomic force microscopy: Application to biology and technology. *Science* **242**, 209-216.

Harding, S.E. (1984). An analysis of the heterogeneity of mucins. No evidence for a self-association. *Biochem. J.* **219**, 1061-1064.

Harding, S.E. (1987) A general method for modelling macromolecular shape in solution a graphical (II-G) intersection procedure for triaxial ellipsoids. *Biophys. J.* **51,** 637-680.

Harding, S.E. (1989) The macrostructure of mucus glycoproteins in solution. *Advances in Carb. Chem. and Biochem.* **47**:345-381.

Harding, S.E. (1995) On the hydrodynamic analysis of macromolecular conformation. *Biophys. Chem.* **55,** 69-93.

Harding, S.E., Rowe, A.J., and Creeth, J.M. (1983a) Further evidence for a flexible and highly expanded model for mucus glycoproteins in solution. *Biochem. J.* **209,** 893-896.

Harding, S.E., Creeth, J.M. and Rowe, A.J. (1983b) Modelling the conformation of mucus glycoproteins in solution. In *Proceedings of the 7th International Glucoconjugates Conference,* Eds. A. Chester, D. Heinegard, A. Lundblad and S. Svensson, pp. 558-559. Sweden: Olsson-Reklambyra

Harding, S.E., Davis, S.S., Deacon, M.P. and Fiebrig, I. (1999) Biopolymer mucoadhesives (submitted for publication).

Harding, S.E., Horton, J.C. and Cölfen, H. (1997) The ellips suite of macromolecular conformation algorithms. *Eur. Biophys. J.* **25,** 347-360.

Harding, S.E., Horton, J.C., Jones, S., Thornton, J.M. and Winzor, D.J. (1998) (submitted for publication)

Harding, S.E., Jumel, K. (1998) Light scattering In: Current Protocols in Protein Science 7.8.1-7.8.14. John Wiley & Sons, Inc.

Harding, S.E., Rowe, A.J. and Horton, J.C. (1992a) *Analytical ultracentrifugation in biochemistry and polymer science.* Royal Society of Chemistry, Cambridge, UK.

Harding, S.E., Sattelle, D.B. and Bloomfield, V.A. (1992b) *Laser light scattering in biochemistry.* Royal Society of Chemistry, Cambridge, UK.

Harris, D., Fell, J.T., Sharma, H.L. and Taylor, D.C. (1990a) GI transit of potential bioadhesive formulations in man: a scintigraphic study. *Journal of Controlled Release.* **12**, 45–53.

Harris, D., Fell, J.T., Taylor, D.C., Lynch, J. and Sharma, H.L. (1990b) GI transit of potential bioadhesive systems in the rat. *Journal of Controlled Release.* **12**, 55–65.

Hayton, W.L. (1980). Rate-limiting barriers to intestinal drug absorption: A review. *J. Pharm. Biopharm.* **8**, 321–334.

Helliwell, M. (1993) The use of bioadhesives in targeted delivery within the gastrointestinal tract. *Adv. Drug Delivery Revs.* **11**, 221–251.

Hirano, S. (1989) Production and application of chitin and chitosan in Japan. In *Chitin and Chitosan*, Ed. G. Skjåk-Bræk, T. Anthonsen, T. and P. Sandford, P., pp37-43 London: Elsevier Applied Science.

Hounsell, E.F. (1997) Glycosylation targets for drug design. *Carb. Res.* **300,** 47-48.

Huglin, M.B. (Ed.) (1972) Specific refractive index increments. In*: Light scattering from polymer solutions* Academic Press, London and New York. pg 166.

Huntsberger, J.R. (1967) Mechanisms of adhesion. *Journal of Paint Technology*, 36, 199–211.

Hutton, D.A., Pearson, J.P., Allen, A. and Foster, S.N.E. (1990) Mucolysis of the colonic mucus barrier of faecal proteinases : inhibition by interacting polyacrylate. *Clin. Sci.* 78, 265-271.

Illum, L., Farraj, N.F. and Davis, S.S. (1994) Chitosan as a novel nasal delivery system for peptide drugs. *Pharm. Res.* **11,** 1186-1189.

Imeri, A.G. and Knorr, D. (1988) Effects of chitosan on yield and compositional data of carrot and apple juice. *Journal of Food Science*, **53**, 1707–1709.

Inoue, K. and Odo, S. (1994) The adhesive protein cDNA of Mytilus galloprovincialis encodes decapeptide repeats but no hexapeptide repeat. *Biol. Bull.* **186,** 349-355.

Jabbari, E., Wisniewski, N. and Peppas, N.A. (1993). Evidence of mucoadhesion by chain interpenetration at a poly(acrylic acid)/mucin interface using ATR-FTIR spectroscopy. *Journal of Controlled Release*, **26**, 99–108.

Jensen, K.D., Williams, S.K.R. and Giddings, J.C. (1996) High-speed particle separation and steric inversion in thin flow field-flow fractionation channels. *J. Chromat. A* **746,** 137-145.

Jeuniaux, C., Voss-Fouchart, M.-F., Poulicek, M. and Bussers, J.-C. (1989) Sources of chitin, estimated from new data on chitin biomass and production. In *Chitin and Chitosan*, Ed. G. Skjåk-Bræk, T. Anthonsen and P. Sandford, pp 3-11. London: Elsevier Applied Science.

Jordan, N., Newton, J., Pearson, J. and Allen, A. (1998) A novel method for the visualization of the in situ mucus layer in rat and man. *Clinical Science*, **95,** 97-106.

Jumel, K. Browne, P. and Kennedy, J.F. (1992) *The use of low angle laser light scattering with gel permeation chromatography for the molecular weight determination of biomolecules.* In: Laser light scattering in biochemistry. Harding, S.E., Satelle, D.B. and Bloomfield, V.A. (Eds.), Royal Society of Chemistry, Cambridge. pg 23-34.

Jumel, K., Fiebrig, I. and Harding, S.E. (1996) Rapid size distribution and purity analysis of gastric mucus glycoproteins by size exclusion chromatography/multi angle laser light scattering. *Int. J. Biol. Macromol.* **18,** 133-139.

Jumel, K., Fogg, F.J.J., Hutton, D.A., Pearson, J.P., Allen, A. and Harding, S.E. (1997). A polydisperse linear random coil model for the quaternary structure of pig colonic. *European Biophys. J.* **25,** 477-480

Junginger, H.E., Lehr, C.-M., Bouwstra, J.A., Tukker, J.J. and Verhoef, J. (1990) Site specific intestinal absorption using bioadhesives: Improved oral delivery of peptide drugs by means of bioadhesive polymers. In *Bioadhesion – Possibilities and Future Trends*, Eds. R. Gurny and H.E. Junginger *Wissenschaftliche Verlagsgesellschaft mbH* Stuttgart, APV, Vol. 25, pp 177–190

Karlsson, N.G., Nordman, H., Karlsson, H., Carlstedt, I. and Hansson, G.C. (1997) Glycosylation differences between pig gastric mucin populations: A comparative study of the neutral oligosaccharides using mass spectroscopy. *Biochem. J.* **326,** 911-917.

Katayama, T., Takai, K.-I., Kariyama, R. and Kanemasa, Y. (1978) Colloid titration of heparin using cat-floc (polydiallyldimethyl ammonium chloride) as standard polycation. *Analytical Biochemistry* **88,** 382–387.

Kaus, L.C. (1987) The effect of density on the gastric emptying and intestinal transit of solid dosage forms: comments on the article by Davis *et al.*, *Pharm. Res.* 4, 78.

Kerss, S., Allen, A., Garner, A. (1982) A simple method for measuring thickness of the mucus gel layer adherent to rat, frog and human gastric mucosa: influence of feeding, prostaglandin, N-actylcysteine and other agents. *Clinical Science* **63,** 187–195.

Kikendall, J.W., Friedman, A.C., Oyewole, M.A., Fleischer, D. and Johnson, L.F. (1983) Pill-induced esophageal injury. *Digestive Diseases and Sciences* **28,** 174–181.

Kim, Y.S., Gum, J.R., Byrd, J.C., and Toribara, N.W. (1991) The structure of human intestinal apomucins. *Am. Rev. Respir. Dis.* **144:**S10-S14.

Kirby, A.R., Gunning, A.P. and Morris, V.J. (1995) Atomic force microscopy in food research: a new technique comes of age. *Trends in Food Sci. and Rheol.* **6,** 359-365.

Korneeva, G.A., Vichoreva, G.A., Harding, S.E. and Pavlov, G.M. (1996) Hydrodynamic study of carboxymethyl chitin. *Abstrcats American Chemical Society* **212** (part 1) 75-cell.

Kratochvil, P. (1987) Classical light scattering from polymer solutions. Jenkins, A.D. (Ed.), Polymer Science Library 5, Elsevier, Amsterdam.

Laursen, R.A. (1992) Reflections on the structure of mussel adhesive proteins. In: Results and Problems in Cell Differentiation 19 Biopolymers. Case, S.T. (Ed) Springer-Verlag Berlin, pg 55-74.

Lehr, C.-M., Bouwstra, J.A., Kok, W., de Boer, A.G., Tukker, J.J., Verhoef, J.C., Breimer, D.D. and Junginger, H.E. (1992a) Effects of the mucoadhesive polymer polycarbophil on the intestinal absorption of a peptide drug in the rat. *J. Pharm. Pharmacol.* 44, 402–407.

Lehr, C.-M., Bouwstra, J.A., Schacht, E.H. and Junginger, H.E. (1992c) *In vitro* evaluation of mucoadhesive properties of chitosan and some other natural polymers. *International Journal of Pharmaceutics* 78, 43–48.

Lehr, C.-M., Bouwstra, J.A., Speis, F., Onderwater, J., van het Noordeinde, J., Vermeij-Keers, C., van Munsteren, C.J. and Junginger, H.E. (1992b). Visualization studies of the mucoadhesive interface. *Journal of Controlled Release*, **18**, 249–260.

Lehr, C.-M., Poelma, F.G.J., Junginger, H.E. and Tukker, J. (1991) An estimate of turnover time of intestinal mucus gel layer in the rat *in situ* loop. *Int. J. Pharm.* **70,** 235–240.

Leung, S.S.-H. and Robinson, J.R. (1988). The contribution of anionic polymer structural features to mucoadhesion. *Journal of Controlled Release* **5,** 223–231.

Li, V.H.K., Robinson, J.R., Lee, V.H.L. (1987) Influence of drug properties on design. In: *Controlled Drug delivery: fundamentals and applications*. By: Robinson, J.R. and Lee, V.H.L. (Eds.), Marcel Dekker Inc., New York, pg. 1-94.

Lindsay, S.M. (1993) Biological applications of scanning probe microscopy. *Scanning Tunneling Microscopy and Spectroscopy Theory, Techniques and Applications* (Ed. by Bonnell, D.A.), VCH Publishers Inc., NewYork.

Lüthi, R., Meyer, E., Howald, I., Haefke, H., Anselmetti, D., Dreier, M., Ruetsche, M., Bonner, T., Overney, R.M., Fromer, J. and Güntherodt, H.J. (1994) Progress in non-contact dynamic force microscopy. *J. Vac. Sci. Tech. B.* **12,** 1673-1676.

Lynch, J., Pownall, R.E. and Taylor, D.C. (1987) Site-specific absorption of hydrochlorothiazide in the rat intestine. *J. Pharm. and Pharmacol.* **39,** 55P.

Magonov, S.N. and Renecker, D.H. (1997) Characterization of polymer surfaces with atomic force microscopy. *Annu. Rev. Mater. Sci.* **27,** 175-222.

Magonov, S.N. and Whangbo, M-H. (1996) Scanning probe microscopes. *Surface Analysis with STM and AFM*, 21-49, VCH Publishers, NewYork.

Mantle, M. and Allen, A.A. (1978) A colorimetric assay for glycoproteins based on the periodic acid/Schiff stain. *Biochem. Soc. Trans.* **6,** 607-609.

McCurdy, J.D. (1992). FDA and the use of chitin and chitosan derivatives. In *Advances in Chitin and Chitosan*, Eds. C.J. Brine, P.A. Sandford and J.P. Zikakis, pp 659-662. London: Elsevier Applied Science.

McGurk, S. (1998) Thesis, Nottingham University.

Minami, H. and McCallum, R.W. (1984) The physiology and pathophysiology of gastric emptying in humans. *Gastroenterology* **86**, 1592-1610.

Miyayaki, S., Yamaguchi, H., Takada, M., Hou, W.-M., Takeichi, Y. and Yasabuchi, H. (1990) Pharmaceutical application of biomedical polymers. *Acta Pharmaceutica Nordica* **2**, 401–406.

Moës, A.J. (1993) Gastroretentive dosage forms. *Critical Reviews in Therapeutic Drug Carrier Systems* **10**, 143–195.

Mortazavi, S.A., Carpenter, B.G. and Smart, J.D. (1993) A comparative study on the role played by mucus glycoproteins in the rheological behaviour of the mucoadhesive/mucosal interface. *International Journal of Pharmaceutics* **94**, 195–201.

Müller-Lissner, S.A. and Blum, A.L. (1981) The effect of specific gravity and eating on gastric emptying of slow-release capsules. *New England Journal of Medicine* **304**, 1365–1366.

Muzzarelli, R.A.A. (1995) Naturally Chelating Polymers: Alginic Acid, Chitin and Chitosan. Plenum Press, N.Y., U.S.A.

Nagai, T. (1986) Topical mucosal adhesive dosage forms. *Medicinal Research Reviews* **6**, 227–242.

Nagai, T., Nishimoto, Y., Nambu, N., Suzuki, Y., Sekine, K. (1984) Powder dosage form of insulin for nasal administration. *Journal of Controlled Release* **1**, 15–22.

Neutra, M.R. and Forstner, J.F. (1987) Gastrointestinal mucus: Synthesis, secretion and function. In: *Physiology of the Gastrointestinal Tract.* By: Johnson, L.R. (Ed.), Raven Press, New York, pg. 975-1009.

Nordman, H., Davies, J.R., Herrmann, A., Karlsson, N.G., Hansson, G.C. and Carlstedt, I. (1997) Mucus glycoproteins from pig gastric mucosa: identification of different mucin populations from the surface epithelium. Biochem. J. **326,** 903-910.

Notter, M.F.D. (1988) Selective attachment of neural cells to specific substrates including Cell-Tak, a new cellular adhesive. *Exp. Cell Res.* **177,** 237-246.

Ohara, S., Ishihara, K., Hotta, K. (1993) Regional differences in pig gastric mucins. *Comp. Biochem. Physiol.* **106B,**153-158.

Olivieri, M.P., Baier, R.E. and Loomis, R.E. (1992a) Surface properties of mussel adhesive protein component films. *Biomaterials* **13,** 1000-1008.

Olivieri, M.P., Rittle, K.H., Tweden, K.S. and Loomis, R.E. (1992b) Comparative biophysical study of adsorbed calf serum, fetal bovine serum and mussel adhesive protein films. *Biomaterials* **13,** 201-208.

Ou, J-J. (1990) Cloning and sequencing of the complementary DNA encoding the polyphenolic adhesive protein from Mytilus edulis. Thesis, Boston University.

Papov, V.V., Diamond, T.V., Bieman, K. and Waite, J.H. (1995) Hydroxyarginine containing polyphenolic proteins in the adhesive plaques of the marine mussel *Mytilus edulis*. *J. Biol. Chem.* **270,** No. 34 20183-20192.

Park, K. and Park, H. (1987) Enzyme-digestible balloon hydrogels for long-term oral drug delivery: synthesis and characterization. *Proceedings of the International Symposium on Controlled Release of Bioactive Materials*. **14**, 41–42.

Peppas, N.A. and Buri, P.A. (1985) Surface, interfacial and molecular aspects of polymer bioadhesion on soft tissues. *Journal of Controlled Release* **2**, 257–275.

Perkins, S.J. (1986) Protein volumes and hydration effects- the calculations of partial specific volumes, neutron scattering matchpoints and 280 nm absorption coefficients for proteins and glycoproteins from amino-acid sequences. *Eur. J. Biochem.* **157,** 169-180.

Perrin, F. (1936) *J. Phys. Radium* **7,** 1-11.

Poelma, F.G.J. and Tukker, J.J. (1987) Evaluation of a chronically isolated internal loop in the rat for the study of drug absorption kinetics, *J. Pharm. Sci.* **76**, 433–436.

Ponchel, G.F., Touchard, F., Duchêne, D. and Peppas, N.A. (1987a) Bioadhesive analysis of controlled-release systems. I. Fracture and interpenetration analysis in poly(acrylic acid)-containing systems. *Journal of Controlled Release* **5**, 129–141.

Ponchel, G.F., Touchard, F., Wouessidjewe, D., Duchêne, D. and Peppas, N.A. (1987b) Bioadhesive analysis of controlled-release systems. III. Bioadhesive and release behaviour of metronidazole-containing poly(acrylic acid)-hydroxypropyl methylcellulose systems. *International Journal of Pharmaceutics* **38**, 65–70.

Pronova Biopolymer Data Sheets (1994) Pronova Biopolymer, Inc., 1725 Ocean Avenue, Raymond, W.A., U.S.A.

Rallison, J.M. and Harding, S.E. (1985) Excluded volume for pairs of triaxial ellipsoids at dominant brownian-motion. *J. Colloid Interface Sci.* **103,** 284-289.

Ralston, G. (1993) *Introduction to analytical ultracentrifugation.* Beckman Instruments, Inc., USA.

Rånby, B. (Ed.) (1987) *Physical chemistry of colloids and macromolecules.* Blackwell Scientific Publications, Oxford, UK.

Ratanathanawongs, S.K. and Giddings, J.C. (1991) *ACS Symposium Series* **521,** 13.

Roberts, C.J., Shivji, A., Davies, M.C., Davis, S.S., Fiebrig, I., Harding, S.E., Tendler, S.J.B. and Williams, P.M. (1995) A study of highly purified pig gastric mucin by scanning tunneling microscopy. *Protein and Peptide Letters* **2,** 409-414.

Robin, J.B., Picciano, P., Kusleika, R.S., Salazar, J. and Benedict, C. (1988) Preliminary evaluation of the use of mussel adhesive protein in experimental epikeratoplasty. *Arch. Opthalmol. (Chicago)* **106,** 973-977.

Robinson, R., Longer, M.A., Veillard, M. (1987) Bioadhesive polymers for controlled drug delivery. In *Annals New York Academy of Science*, ed. R.L. Juliano, R.L., Vol. 507, pp 307-314.

Rzepecki, L.M., Hansen, K.M. and Waite, J.H. (1992) Characterization of a cystine-rich polyphenolic protein family from the blue mussel *Mytilus edulis* L. *Biol Bull.* **183,** 123-137.

Sangekar, S., Vadino, W.A., Chaudry, I., Parr, A., Beihn, G. and Digenis, G. (1987) Evaluation of the effect of food and specific gravity of tablets on gastric retention time. *Int. J. Pharm.* **35,** 187–191.

Schachter, H. and Williams, D. (1982) Biosynthesis of mucus glycoproteins. In: *Mucus in health and disease-II.* Chantler, E.N., Elder, J.B. and Elstein, M. (Eds.) Plenum Press, New York. pg. 3-28.

Schnurrer, J. and Lehr, C.-M. (1996) Mucoadhesive properties of the mussel adhesive protein. *Int. J. Pharmaceutics* **141**, 251-256

Schor, J.M., Davis, S.S., Nigalaye, A. and Bolton, S. (1983) Susadrin transmucosal tablets (nitroglycerin in synchron controlled release base). *Drug Develop. Ind. Pharm.* **9**, 1359–1377.

Sheehan, J.K. and Carlstedt, I. (1989) Models for the macromolecular structure of mucus glycoproteins. *Dynamic Properties of Biomolecular Assemblies* (Eds. Harding S.E. and Rowe A.J.), Royal Society of Chemistry, Chap. 17, Cambridge, U.K.

Sheehan, J.K., Oates, K. and Carlstedt, I. (1986) Electron microscopy of cervical, gastric and bronchial mucus glycoproteins. *Biochem J.* **239**, 147-153.

Sheth, P.R. and Tossounian, J. (1984) The hydrodynamically balanced system (HBS®): a novel drug delivery system for oral use. *Drug Development and Industrial Pharm.* **10**, 313–339.

Silberberg, A. and Meyer, F.A. (1982) Structure and function of mucus. In *Mucus in Health and Disease-II,* Eds. E.N. Chantler, J.B. Elder and M. Elstein, pp 53-74. New York: Plenum Press.

Skaugrud, O. (1995) Drug Delivery Systems with Alginate and Chitosan. In: Excipients and Delivery Systems for Pharmaceutical Formulations. By: Karsa, D.R. and Stephenson, R.A. (Eds), Royal Society of Chemistry, Cambridge, pg. 96-107.

Smart, J.D. (1993) Drug delivery using buccal-adhesive systems. *Adv. Drug Delivery Revs.* **11**, 253–270.

Soto Peralta, N.V., Müller, H. and Knorr, D. (1989). Effects of chitosan treatments on the clarity and colour of apple juice. *Journal of Food Science*, **54**, 495–496.

Squire, P.G. and Himmel, M. (1979) *Arch. Biochem. Biophys.* **196,** 165-177.

Stevenson, S.G. and Preston, K.R. (1996) Flow field-flow fractionation of wheat proteins. *J. Cereal Sci.* **23,** 121-131.

Takahashi, T., Takayama, K., Machida, Y. and Nagai, T. (1990) Characteristics of polyion complexes of chitosan with sodium alginate and sodium polyacrylate. *International Journal of Pharmaceutics* **61,** 35–41.

Tamarin, A., Lewis, P. and Askey, J. (1976) The structure and formation of the byssus attachment plaque in Mytilus edulis. *J. Morphol.* **149,** 199-222.

Tamayo, J. and Garcia, R. (1996) Deformation, contact time, and phase contrast in Tapping mode scanning force microscopy. *Langmuir* **12,** 4430-4435.

Tanford, C. (1961) *Physical chemistry of macromolecules*. John Wiley and Sons, NY, USA.

Taylor, S.W., Herbert, J.H., Ross, M.M., Shabanowitz, J. and Hunt, D.F. (1994) trans-2,3-cis-3,4-Dihydroxyproline a new naturally occurring amino acid, is the sixth residue in the tandemly repeated consensus decapeptides of an adhesive protein from *Mytilus edulis*. *J. Am. Chem. Soc.* **116,** 10803-10804.

Teller, D.C. (1973) Characterisation of proteins by sedimentation equilibrium in the analytical ultracentrifuge. Methods in Enzymology **27,** 346-441. Eds C.H.W. Hirs and S.N. Timasheff. Academic Press, New York.

Terayama, H. (1952) Method of colloid titration (a new titration between polymer ions). *Journal of Polymer Science* **8,** 243–253.

Timmermans, J. and Moës, A.J. (1990) How well do floating dosage forms float? *Int. J. Pharm.* **62**, 207–216.

Tombs, M.P. and Harding, S.E. (1998) *An Introduction to Polysaccharide Biotechnology*, Taylor & Francis, London, UK.

Van Damme, M.-P.I., Blackwell, S.T., Murphy, W.H. and Preston, B.N. (1992) The measurement of negative charge in cartilage using a colloid titration technique. *Analytical Biochemistry* **204**, 250–257.

Van Holde, K.E, Johnson, W.C. and Ho, P.S. (1998) *Principles of Physical Biochemistry.* Prentice Hall Inc., Upper Saddle River, New Jersey, USA.

Vere, D. (1984) Death from sustained release morphine sulphate. *Lancet* **1**, 1477.

Wahlund, K.-G., Gustavsson, M., MacRitchie, F., Nylander, T. and Wannerberger, L. (1996) Size characterization of wheat proteins, particularly glutenin, by asymmetrical flow field-flow fractionation. *J. Cereal Sci.* **23**, 113-119.

Waite, J.H. (1983a) Evidence for a repeating 3,4-dihydroxyphenylalanine- and hydroxyproline-containing decapeptide in the adhesive protein of the mussel, *Mytilus edulis L. J. Biol. Chem.* **258** No. 5 2911-2915.

Waite, J.H. (1983b) Adhesion in byssally attached bivalves. *Biol. Rev.* **58**, 209-231.

Waite, J.H. and Tanzer, M.L. (1981) Polyphenolic substance of *Mytilus edulis*: Novel adhesive containing L-Dopa and hydroxyproline. *Science* **212**, 1038-1040.

Waite, J.H., Housley, T.J. and Tanzer, M.L. (1985) Peptide repeats in a mussel glue protein: theme and variations. *Biochem.* **24**, 5010-5014.

Waldron-Edward, D. (1977) The turnover of mucin glycoprotein in the stomach. In *Mucus in Health and Disease*, Ed. M. Elstein and D.V. Parke, pp 301-307. Plenum Press, New York.

Wearley, L.L. (1991). Recent progress in protein and peptide delivery by noninvasive routes. *Crit. Revs. Ther. Drug Carrier Systems* 8, 331–394.

Weiner, M.L. (1992). An overview of the regulatory status and of the safety of chitin and chitosan as food and pharmaceutical ingredients. In *Advances in Chitin and Chitosan* Eds. C.J. Brine, P.A. Sandford and J.P. Zikakis, pp 673-672. London: Elsevier Applied Science.

Williams, T., Marumo, K., Waite, J.H. and Henkens, R.T. (1989) Mussel glue protein has an open conformation. *Arch. Biochem. Biophys.* **269,** 415-422.

Wilson, (1990) In vivo testing of bioadhesion. In *Bioadhesion – Possibilities and Future Trends*. Eds R. Gurny and H.E. Junginger, Wissenschaftliche Verlagsgesellschaft mbH Stuttgart, APV, Vol. **25,** pp 93–108

Wittgren, B. and Wahlund, K.-G. (1997a) Effects of flow-rates and sample concentration on the molar mass characterization of modified celluloses using asymmetrical flow field-flow fractionation-multiangle light scattering. *J. Chromat. A* **791,** 135-149.

Wittgren, B. and Wahlund, K.-G. (1997b) Fast molecular mass and size characterization of polysaccharides using asymmetrical flow field-flow fractionation-multiangle light scattering. *J. Chromat. A* **760,** 205-218.

Wittgren, B., Borgstrom, J., Piculell, L. and Wahlund, K.G. (1998) Conformational change and aggregation of kappa-carrageenan studied by flow field-flow fractionation and multiangle light scattering. *Biopolymers* **45,** 85-96.

Wittgren, B., Wahlund, K.-G., Dérand, H. and Wesslén, B. (1996) Aggregation behaviour of an amphiphilic graft copolymer in aqueous medium studied by asymmetrical flow field-flow fractionation. *Macromol.* **29,** 268-276.

Wyatt, P.J. (1992) Combined differential light scattering with various liquid chromatography separation techniques. *In: Laser light scattering in biochemistry.* Harding, S.E., Sattelle, D.B. and Bloomfield, V.A. (Eds.), Royal Society of Chemistry, Cambridge, UK.

Wyatt, P.J. (1993) Light scattering and the absolute characterisation of macromolecules. *Anal. Chim. Acta* **272,** 1-40.

Wyatt, P.J., Jackson, C. and Wyatt, G.K. (1988) Part I. Absolute GPC determination of molecular weights and sizes from light scattering. *Am. Lab.* **20,** 86-91.

XL-A instruction manual (1991) Beckman Instruments, Inc, USA.

XL-I instruction manual (1996) Beckman Instruments, Inc, USA.

Yphantis, D.A. (1964) Equilibrium ultracentrifugation in dilute solution. *Biochemistry* **3,** 297-317.

Zhong, Q., Innes, D., Kjoller, K. and Elings, V.B. (1993) Fractured polymer silica fiber surface studied by tapping mode atomic force microscopy. *Surf. Sci. Lett.* **290,** L688-L692.

Zimm, B.H. (1948*) J. Chem. Phys.* **16,** 1099.

Appendix I

Table of specific refractive index increments

FOREWORD

We present here a modern collection of specific refractive index increments d*n*/d*c* for use by scientists using principally light scattering and analytical ultracentrifuge probes for the size, structure and interactions of macromolecules in what for many is their natural state: a solution. This list essentially updates a classical list published by M.B. Huglin over a quarter of a century ago (Huglin, M.B., *Light Scattering from Polymer Solutions*, Academic Press, London, Chapter 6, 1972). The proliferation of light scattering instrumentation (including multi-angle laser photometers coupled on-line to size exclusion chromatography columns, field-flow-fractionation and viscosity equipment) and a re-surgence of interest in analytical ultracentrifugation using refractive index based optical detection systems means there is a wide a user base as ever.

Unfortunately it is not possible to calculate d*n*/d*c* values on the basis of molecular composition (unlike density increments or partial specific volumes so widely used in analytical ultracentrifugation). Of course a light scattering or ultracentrifuge user can make his own measurements using appropriate instrumentation for which there are high-precision refractometers now available (in particular the Optilab DSP, Wyatt Technology Corp., Santa Barbara, USA). However, the accuracy with which these measurements can be made is not necessarily dependent on refractive index measurement but on concentration measurement, a parameter for which despite painstaking care, an accuracy better than 1% is rare. It is therefore useful to the scientist if he/she has access to earlier data recorded by some other user.

dn/dc values are not only highly dependent on the solvent, but also on temperature and they can show a dispersion with the wavelength, λ, of the incident light used for the measurement. Care has been taken to specify those parameters if available from the original reference, so that the reader can choose a value most appropriate for his/her application.

A. Theisen, C. Johann, M.P. Deacon and S.E. Harding.
Frankfurt and Nottingham, January 1999.

Specific Refractive Increments of Macromolecules

Substance	Solvent	Wavelength (nm)	Temperature	dn/dc (mL/g)	Remarks	Reference
Actin	0.5M KI (aq.)	?	?	0.227		1
Actin	$MgCl_2$	436		0.18	pH 8.0	2
Actin	Aqueous solution	436	?	0.17	pH 7.8-8.0	3
Actomyosin	Water	436	?	0.193	pH 4.26	4, 5
Actomyosin	Water	578	?	0.191	pH 4.26	4, 5
Actomyosin	Water	546	?	0.195	pH 4.26	4, 5
Actomyosin	Water	546	?	0.193	pH 4.26	4, 5
Actomyosin	Water	546	23 °C	0.200		6
Adenylate kinase	Imidazole buffer (aq.)	633	25 °C	0.187	in presence of 0.1% octaethyleneglycol n-dodecylether	7
Alginate (magnesium)	MgCl2 (aq.)	546	20-25 °C	0.158		8
Alginate (potassium)	Aqueous	546	20-25 °C	0.16	in presence of KCl	8
Alginate (sodium)	Aqueous	546	20-25 °C	0.165	in presence of NaCl	8
Amandin	1.7M NaCl (aq.)	546	25 °C	0.1697	pH 5.6	9
Amandin	1.7M NaCl (aq.)	589	25 °C	0.1674	pH 5.6	9
Amandin	1.7M NaCl (aq.)	436	25 °C	0.1686	pH 5.6	9
Amandin	1.7M NaCl (aq.)	653	25 °C	0.1678	pH 5.6	9
Ammodytes Viper venom	0.15M NaCl (aq.)	546	25 °C	0.195		10
β-Amyloid Peptide (1-40)	0.14M NaCl (aq.)	?	?	0.112	0.01M Potassium phosphate 0.02% NaN_3 (pH 7.4)	11
Amylopectin	Aqueous solution	?	?	0.146		12
Amylopectin	DMSO/water	632.8	25 °C	0.074	90/10 (w/w) vol.	13

Substance	Solvent	Wavelength / nm	Temperature	dn/dc / mL/g	Remarks	Reference
Amylopectin	DMSO/Water	546	?	0.110	0.2 N NaOH, 50/50 vol.	14
Amylopectin	DMSO/water	632.8	25 °C	0.074	90/10 (w/w)	13
Amylopectin	Water	546	?	0.152		14
Amylopectin	4.2M GHCl	436	?	0.14		15
Amylopectin	1 N KOH	546	?	0.142		16
Amylopectin	0.2 N NaOH	546	?	0.142		17
Amylopectin	Water	546	?	0.156		17
Amylopectin	8 M urea (aq.)	546	?	0.106		18
Amylopectin acetate	Acetone	546	?	0.118		17
Amylopectin acetate	Acetonitrile	546	?	0.128		17
Amylose	DMSO	436	?	0.0676		14
Amylose	DMSO/water	546	25 °C	0.112	DMSO/water (50/50 vol.)	19
Amylose	DMSO/water	546	25 °C	0.062	DMSO/water (90/10 vol.)	19
Amylose	KOH (aq.)	?	?	0.146		20
Amylose	4.2 M GHCl	546	25 °C	0.118		21
Amylose	Kcl (aq.)	?	?	0.146		22
Amylose acetate	Nitromethane	436	20 °C	0.0835		23
Amylose tributyrate	Ethyl acetate	546	25 °C	0.098		24
Amylose tricarbanilate	Acetone	546	27 °C	0.2279		25
Amylose tripropionate	Ethyl acetate	546	25 °C	0.092		24
Araban	2 M NaCl	?	?	0.13		26
Arachin	Phosphate buffer (aq.)	?	?	0.192		27
Arachin	Water	436	?	0.192		28

Substance	Solvent	Wavelength / nm	Temperature	dn/dc / mL/g	Remarks	Reference
ATPase	Imidazole-buffer (aq.)	?	25 °C	0.255 +/- 0.033	alpha-beta-diprotomer solubilized with C12E8	29
ATPase	Imidazole-buffer (aq.)	?	25 °C	0.202 +/- 0.038	alpha-beta-(6-8)-oligomer, solubilized with C12E8	29
ATPase	Imidazole-buffer (aq.)	?	25 °C	0.254 +/- 0.027	alpha-beta-(12-16)-oligomer, solubilized with C12E8	29
ATPase	Imidazole-buffer (aq.)	?	25 °C	0.264 +/- 0.027	alpha-beta-protomer, solubilized with	29
ATPase	NaCl/KCl (aq.)	?	0.8 °C	0.302 +/- 0.005	alpha-beta-protomer	30
ATPase	NaCl/KCl (aq.)	?	0.8 °C	0.279 +/- 0.002	alpha-beta-diprotomer	30
Basic fibroblast growth factor	Water/acetonitrile	?	?	0.175 +/- 0.004	Independent of the composition of the mobile phase	31
beta-Lactoglobulin A	Phosphate buffer (aq.)	633	?	0.166		32
Bovine alpha--chymotrypsinogen	Phosphate buffer (aq.)	?	20 °C	0.171		33
Bovine Fibrinogen	Aq., I = 0.1 M	546		0.1933		34
Bovine Fibrinogen	Aq., I = 0.2 M	546		0.194		34
Bovine Fibrinogen	Aq., I = 0.3 M	546		0.1935		34
Bovine Fibrinogen	Aq., I = 0.5 M	546		0.1987		34
Bovine Fibrinogen	Glycine buffer	546	25	0.1949	I = 0.45 M	35
Bovine Fibrinogen	Glycine buffer	546	25	0.1898	I = 0.45 M, 0.5 M HMG	35
Bovine Fibrinogen	0.3 M NaCl	546	25	0.197		35
Bovine Fibrinogen	Phosphate buffer	546	25	0.1953	I = 0.45 M	35
Bovine Fibrinogen	Phosphate buffer	546	25	0.1953	I = 0.45 M, 0.5 M HMG	35

Substance	Solvent	Wavelength / nm	Temperature	dn/dc / mL/g	Remarks	Reference
Bovine gamma-globulin thyroglobulin	Phosphate buffer (aq.)	?	20 °C	0.170		33
Bovine serum albumin	Imidazole buffer (aq.)	633	25 °C	0.187	in presence of 0.1% octaethyleneglycol n-dodecylether	7
Bovine serum albumin	Phosphate buffer (aq.)	633	?	0.168		32
Bovine serum albumin	Phosphate buffer (aq.)	633	?	0.166	pH 6.8	36
Bovine serum albumin	Phosphate vuffer (aq.)	?	?	0.174	0.1 M	199
Bovine thyroglobulin	Phosphate buffer (aq.)	?	20 °C	0.170		33
Capsular pneumococcal	Phosphate buffer (aq.)	633	30 °C	0.130 - 0.139		37
Carbonic anhydrase	Imidazole buffer (aq.)	633	25 °C	0.187	in presence of 0.1% octaethyleneglycol n-dodecylether	7
Carboxymethyl--cellulose	NaCl (aq.)	?	?	0.147	0.1 M	38
Carboxymethyl-cellulose	NaNO3 (aq.)	632.8	25°C	0.163	0.1 M. Independent of degree of substitution.	197
Carrageenan	LiNO3 (aq.)	?	?	0.155	0.1 M	39
Carrageenan (κ)	Water	?	?	0.140		198
Carrageenan (κ)	NaCl (aq.)			0.126	0.1 M	198
Casein	0.25N KOH (aq.)	589	25	0.149		40
Casein	0.25N KOH/25% EtOH (aq.)	589	25	0.158		40
Casein	0.25N KOH/50% EtOH (aq.)	589	25	0.149		40
Casein	0.25N KOH/75% EtOH (aq.)	589	25	0.125		40
Cellulose	DMAc/0.5% LiCl	?	?	0.163		41
Cellulose	Acetone	546	25 °C	0.111		42

Substance	Solvent	Wavelength / nm	Temperature	dn/dc / mL/g	Remarks	Reference
Cellulose actetate	Water	546	?	0.131	D.S. = 0.49	43
Cellulose carbanilate	Ethyl acetate	?	?	0.180	D.S. = 1.6-2.3	44
Cellulose diacetate	Acetone	546	25 °C	0.112		45
Cellulose nitrate	Acetone	546	25 °C	0.1151	12.9 % N	46
Cellulose nitrate	Acetone	436	25 °C	0.09	13.96 % N	47
Cellulose propionate	Acetone	632.8	25 °C	0.111		48
Cellulose propionate	MEK	632.8	25 °C	0.096		48
Cellulose triacetate	Chloroform	?	25 °C	0.0406		49
Cellulose tributyrate	DMF	546	41 °C	0.0442		50
Cellulose tricaproate	DMF	546	41 °C	0.0442		50
Cellulose tricarbanilate	Acetone	546	27 °C	0.2176		50
Cellulose tricarbanilate	Dioxane	546	25 °C	0.1651		51
Cellulose trinitrate	Acetone	546	25 °C	0.1116		46
Cellulose trinitrate	Ethyl acetate	546	30 °C	0.102		52
Cellulose xanthate	NaOH (aq.)	436	?	0.212		53
Chitosan	Acetate buffer	?	?	0.163		54
Chitosan	Acetate buffer (aq.)	633	25 °C	0.181		55
CHO derived SCF	10 mM Phosphate (aq.)	633	?	0.263	0.15 M NaCl, pH 7.0	56
α-Chymotrypsin	Phosphate buffer (aq.)	436	?	0.187	I = 0.2 M, pH 6.1	57
α-Chymotrypsinogen A	5 mM Bis-Tris (aq.)	633	?	0.168		58
Chymotrypsinogen	0.05 M Tris (aq.)	589	?	0.178	0.2 M NaCl, pH 6.0	59
Collagen	Acetate buffer (aq.)	?	25 °C	0.185		60
Conalbumin	Water	546	?	0.192		61
Crescormon	Acetonitril/water	630	20 °C	0.149	80:20 - 20:80	62

Substance	Solvent	Wavelength / nm	Temperature	dn/dc / mL/g	Remarks	Reference
Crescormon	Phosphate buffer (aq.)	630	20 °C	0.160		62
Crescormon	Phosphate buffer (aq.)	633	?	0.168		32
Crescormon	Protein buffer	630	20 °C	0.160		62
Croglobulin	Water	546	37	0.19		63
Dextran	Acetate buffer (aq.)	633	25 °C	0.150		55
Dextran	Water	436	25 °C	0.1518		14
Dextran	NaCl (aq.)	436	25 °C	0.1361		65
Dextran	0.5 M NaCl (aq.)	546	25 °C	0.147		66
Dextran	1.0 M NaCl (aq.)	546	25 °C	0.1435		66
Dextran	Water	546	20 °C	0.15		67
DNA	NaCl (aq.)	633	25 °C	0.168	0.1 M	68
E. coli derived SCF	10 mM phosphate (aq.)	633	?	0.192	0.15 M NaCl, pH 7.0	56
Edestin	0.02 N KOH (aq.)	589	17.5 °C	0.179		69
Edestin	0.05 N KOH (aq.)	589	17.5 °C	0.179		69
Edestin	0.1 N KOH (aq.)	589	17.5 °C	0.174		69
Egg Albumin	Salt Free (aq.)	589	?	0.1874		70
Enolase	Imidazole buffer (aq.)	633	25 °C	0.187	in presence of 0.1% octaethyleneglycol n-dodecylether	7
Ethyl cellulose	Methanol	546	25 °C	0.13		71
Ethyl cellulose	Water	546	?	0.154		72
Galactomannan	Ammonium nitrate (aq.)	red light	?	0.150	0.1 M	73
Gelatin	NaAc (aq.)	514.5	40 °C	0.18	0.001 M - 0.1 M	74
Gelatin	100% Formic acid	546	25.5 °C	0.1765		75
Gelatin	80% Formic acid + 20% DMF	546	25.5 °C	0.1515		75
Gelatin	60% Formic acid + 40% DMF	546	25.5 °C	0.1423		75

Substance	Solvent	Wavelength / nm	Temperature	dn/dc / mL/g	Remarks	Reference
Gelatin	40% Formic acid + 60% DMF	546	25.5 °C	0.1267		75
Gelatin	10% Formic acid + 90% DMF	546	25.5 °C	0.1223		75
Gelatin	1.0 M KCNS (aq.)	546	30 °C	0.172		76
Gelatin	0.05 M Phosphate (aq.)	546	30 °C	0.188		76
Gelatin	Water	546	25 °C	0.191		77
Gelatin	Water	589	25 °C	0.184		77
Gelatin	Water	436	25 °C	0.186		77
Gliadine	1.0 N Acetic acid	589	25 °C	0.159		78
Gliadine	25% Aq. acetone	589	25 °C	0.172		78
Gliadine	50% Aq. acetone	589	25 °C	0.144		78
Gliadine	60% Aq. ethanol	589	25 °C	0.144		78
Gliadine	0.1 N KOH (aq.)	589	25 °C	0.162		78
Globins	Aq. acetate pH 5.6	589	0 °C	0.185		79
Globins	Aq. phosphate pH 7.7	589	0 °C	0.1778		79
Globins	Water	436	15 °C	0.19		80
Glucan	NaN3 (aq.)	632.8	?	0.145	beta-Glucan	81
Glucan	Water	488	25 °C	0.151	beta-Glucan	82
Glucan phosphate	Aqueous solution	?	?	0.145		83
Glutamate dehydrogenase	Imidazole buffer (aq.)	633	25 °C	0.187	in presence of 0.1% octaethyleneglycol n-dodecylether	7
Glutaraldehyde-3-phosphate dehydrogenase	Aq. phosphate buffer	546	?	0.19		84
Glutaraldehyde-3-phosphate dehydrogenase	Aq. phosphate buffer	436	?	0.185		84
Glutaraldehyde-3-phosphate dehydrogenase	Aq. phosphate buffer	546	20 °C	0.188	rabbit muscle, pH 7.0	85

Substance	Solvent	Wavelength / nm	Temperature	dn/dc / mL/g	Remarks	Reference
Glutaraldehyde-3-phosphate dehydrogenase	Aq. phosphate buffer	436	20 °C	0.182	rabbit muscle, pH 7.0	85
Glycogen	Water	546	?	0.136		86, 87
Glycogen	8 M GHCl (aq.)	546	?	0.131		88
Glycogen	8 M urea (aq.)	546	?	0.102		88
Guaran triacetate	Acetonitrile	436	22.5 °C	0.12		89
Gum arabic	HCl (aq.)	436	25 °C	0.152		14
Gum arabic	Water	436	?	0.145		14
Hemicellulose	0.5 M NaCl (aq.)	436	?	0.145		90
Hemocyanin	0.2 N Acetate	546	25 °C	0.1991	pH 5.05	9
Hemocyanin	0.2 N Acetate	589	25 °C	0.1908	pH 5.05	9
Hemocyanin	0.2 N Acetate	436	25 °C	0.1905	pH 5.05	9
Hemocyanin	0.2 N Acetate	643	25 °C	0.1872	pH 5.05	9
Hemocyanin	Water	589	24 °C	0.194		91
α-Hemocyanin	0.1 M Acetate, pH 5.7	546	?	0.191	*Helix pomatia*	92
Hemocyanin	0.1 M Acetate, pH 5.7	546	?	0.194	*Lunatia heros*	93
Hemocyanin	0.1 M Acetate, pH 5.7	546	?	0.194	*Littorina littorea*	93
Hemocyanin	0.1 M Tris (aq.)	546	?	0.194	0.05 M Mg^{2+}, 0.01 M Ca^{2+}, pH 7.4, *Octopus bimaculoides*	94
Hemoglobin	Water	?	?	0.170 - 0.190	Depending on the amount of glucoproteins	95
Hemoglobin	Water	633	?	0.196		96
Hemoglobin	0.05 M Na-phosphate	633	?	0.192	pH 7.0	96
Heparin	Acetate buffer	690 nm	25 °C	0.129 - 0.134	Depending on manufacturer	97

Substance	Solvent	Wavelength / nm	Temperature	dn/dc / mL/g	Remarks	Reference
Heparin	Water	546	?	0.121		98
Heparin	Water	436	?	0.150		99
Horse serum albumin	0.1 M Acetate-acetic acid buffer	546	25 °C	0.1912	pH 4.8	100
Horse serum albumin	0.1 M Acetate-acetic acid buffer	436	25 °C	0.1844	pH 4.8	100
Horse serum globulin	Aq. phosphate	589	17.5 °C	0.1815	pH 5.35	79
Human fibrinogen	Aq. NaCl	546	20 °C	0.1958	I = 0.1 M	34
Human growth hormone	Phosphate buffer	630	20 °C	0.160		101
Human growth hormone (hGH)	Water	488	?	0.190		102
Human IgM monoclonal antibody (4B9)	Phosphate buffer (aq.)	?	?	0.18		103
Human serum albumin	Phosphate buffer (aq.)	?	20 °C	0.165		33
Human serum albumin	Water	546	?	0.1938		104
Human serum albumin	Water	578	?	0.1854		104
Human serum albumin	Water	436	?	0.1863		104
Human serum globulin	Water	546	25 °C	0.188		77
Human serum globulin	Water	578	25 °C	0.180		77
Human serum globulin	Water	436	25 °C	0.186		77
Hyaluronan	NaCl (aq.)	633	20 °C	0.165	0.05 M	196
Hyaluronic acid	Ammonium nitrate (aq.)	?	?	0.155 +/- 0.008	0.1 M	105
Hyaluronic acid	NaOH (aq.)	?	?	0.176		106
Hyaluronic acid	NaOH (aq.)/DMSO	?	?	0.176	80/20 vol.	106
Hyaluronic acid	Water	?	?	0.155		107
Hyaluronic acid	Water	546	25 °C	0.166 - 0.17		14

Substance	Solvent	Wavelength / nm	Temperature	dn/dc / mL/g	Remarks	Reference
Hydroxyethyl cellulose	NaCl (aq.)	?	?	0.159	0.1 M	38
Hydroxypropyl cellulose	Water	546	25 °C	0.146		108
Hydroxypropyl cellulose	Water	578	25 °C	0.143		108
Hydroxypropyl starch	Water	546	20 °C	0.152	D.S. = 0.5	109
Hydrolyzed waxy maize starch	0.1 M KCl (aq.)	436	?	0.155		110
Hydrolyzed waxy maize starch	0.5 M KCl (aq.)	436	?	0.152		110
Hydrolyzed waxy maize starch	Water	546	20 °C	0.152		109
Insulin	0.1 M KCl	546	?	0.202	pH 2.0	111
Iodinated fibrinogen	Aq. NH_4OH	546	?	0.195	pH 7.35	112
iota-Carrageenan	Aqueous solution	633 nm	?	0.127 +/- 0.003		113
kappa-Carrageenan	LiCl (aq.)	633	25 °C	0.111	0.1 M	114
kappa-Carrageenan	LiCl (aq.)	633	60 °C	0.115	0.1 M	114
α-Keratose	Phosphate buffer (aq.)	436	?	0.182	I = 0.2 M, pH = 6.7	110
α-Keratose	Dichloroacetic acid	436	?	0.088		115
α-Keratose	Formic acid	436	?	0.156		115
Krestin	Aqueous solution	?	?	0.145		83
Krestin	Sodium nitrite (aq.)	?	30 °C	0.146		116
α-Lactalbumin	Water	546	25 °C	0.195		77
α-Lactalbumin	Water	589	25 °C	0.188		77
α-Lactalbumin	Water	436	25 °C	0.198		77
Lactate dehydrogenase	Imidazole buffer (aq.)	633	25 °C	0.187	in presence of 0.1% octaethyleneglycol n-dodecylether	7

Substance	Solvent	Wavelength / nm	Temperature	dn/dc / mL/g	Remarks	Reference
α-Lactoglobulin	10 mM Sodium phosphate	633	?	0.164		58
α-Lactoglobulin	Phosphate buffered saline	633	?	0.166		117
β-Lactoglobulin	0.1 M NaCl	546	25 °C	0.189		118
β-Lactoglobulin	0.1 M NaCl	436	25 °C	0.183		118
lambda-Receptor protein	Imidazole buffer (aq.)	633	25 °C	0.259	in presence of 5 mM octaethyleneglycol	7
Lecithin	Ethanol	546	20 °C	0.1233		119
Lecithin	Water	546	20 °C	0.1245		119
Legumin	Aq. phosphate buffer	?	?	0.197		120
Legumin	Water	436	?	0.198		28
Lentinan	Aqueous solution	?	?	0.145		83
LiCl	Water	633	60 °C	0.1879		114
Lignin	$NaHCO_3$ (aq.)	436	25 °C	0.218	pH 9.65	121
Lipopolysaccharide	Water	546	?	0.151		
β-Lipoproteins	Water	578	?	0.171		122
Liposome	Water	?	?	0.16	Phospholipid vesicles	123
Lysozyme	0.1 M NaCl	546	25 °C	0.1955	pH 6.2	100
Lysozyme	0.1 M NaCl	436	25 °C	0.1888	pH 6.2	100
Lysozyme	Water	436	20 °C	0.1888		124
Lysozyme	Water	589	25 °C	0.184		77
Mannan	Acetone	546	room	0.102		125
Methyl cellulose	Water	546	?	0.154		72
Mucopolysaccharides	Water	?	?	0.181		126
Myosin	Aq. dialysate	546	3 °C	0.192		127
Myosin	Water	546	20 °C	0.206		128

Substance	Solvent	Wavelength / nm	Temperature	dn/dc / mL/g	Remarks	Reference
γ-Myosin	Water	546	20 °C	0.195		129
Nylon 12	Hexafluoroisopropanole	633	?	0.2212	n-dodecylether	130
Octaethyleneglycol n-dodecylether	Imidazole buffer (aq.)	633	25 °C	0.135		7
Ovalbumin	Imidazole buffer (aq.)	633	25 °C	0.187	in presence of 0.1% octaethyleneglycol n-dodecylether	7
Ovalbumin	Phosphate buffer (aq.)	633	25 °C	0.374	in presence of SDS	131
Ovalbumin	0.1 M NaCl	546	25 °C	0.1883	pH 4.8	100
Ovalbumin	0.1 M NaCl	436	25 °C	0.182	pH 4.8	100
Pepsin	Water	546	25 °C	0.188		77
Pepsin	0.2 M Acetate buffer	546	25 °C	0.1905	pH 4.5	132
Phosphofructokinase-1	Phosphat buffer (aq.)	?	?	0.170		133
Phycocyanin	Aq. I = 0.1	436	25 °C	0.180	pH 6.8	134
Platelet derived growth factor (PDGF)	Acetate buffer	?	?	0.19		135
Poly(2-vinylpyridine)	Sodium nitrate (aq.)	690	?	0.250	0.05 m	136
Poly(4-(acetoxymethyl) styrene)	Toluene	632.8	25 °C	0.0643		137
Poly(4-t-butylstyrene)	THF	632.8	?	0.140		138
Poly(acrylamide)	Acetic acid	436	25 °C	0.199		14
Poly(acrylamide)	Acetic acid	633	25 °C	0.192		14
Poly(acrylamide)	DMSO	436	25 °C	0.091		14
Poly(acrylamide)	DMSO	633	25 °C	0.089		14
Poly(acrylamide)	Ethylene glycol	436	25 °C	0.117		14
Poly(acrylamide)	Ethylene glycol	633	25 °C	0.111		14
Poly(acrylamide)	Formamide	436	25 °C	0.109		14

Substance	Solvent	Wavelength / nm	Temperature	dn/dc / mL/g	Remarks	Reference
Poly(acrylamide)	Formamide	633	25 °C	0.109		14
Poly(acrylamide)	Formic acid	436	25 °C	0.172		14
Poly(acrylamide)	Formic acid	633	25 °C	0.166		14
Poly(acrylamide)	Na2SO4 (aq.)	632.8	25 °C	0.1869	0.02 M	139
Poly(acrylamide)	NaCl (aq.)	633	25 °C	0.156 - 0.159	1 M	14
Poly(acrylamide)	Water	632.8	23 °C	0.146		64
Poly(acrylamido methylpropanesulfonat	NaAc (aq.)	514.5	40 °C	0.14 - 0.135	0.1 M - 0.5 M, Poly(2-acralamido-2-methylpropane sulfonate)	74
Poly(acrylamido methylpropanesulfonat	NaAc (aq.)	514.5	40 °C	0.145	0.001 M - 0.1 M, Poly(2-acralamido-2-methylpropane sulfonate)	74
Poly(acrylic acid)	CsCl (aq.)	633	25 °C	0.179	0.3 M	140
Poly(acrylic acid)	KCl (aq.)	633	25 °C	0.159	0.3 M	140
Poly(acrylic acid)	LiCl (aq.)	633	25 °C	0.153	0.3 M	140
Poly(acrylic acid)	NaBr (aq.)	633	25 °C	0.155	0.3 M	140
Poly(acrylic acid)	NaCl (aq.)	633	25 °C	0.147	0.5 M	140
Poly(acrylic acid)	NaCl (aq.)	633	25 °C	0.159	0.3 M	140
Poly(acrylic acid)	NaF (aq.)	633	25 °C	0.170	0.3 M	140
Poly(acrylic acid)	NaI (aq.)	633	25 °C	0.144	0.3 M	140
Poly(acrylic acid)	Phosphate buffer (aq.)	633	25 °C	0.143	0.3 M	140
Poly(acrylic acid)	Sodium nitrate (aq.)	633	25 °C	0.162	0.3 M	140
Poly(acrylic acid)	TRIS (aq.)	633	25 °C	0.180	0.08 M + 0.3 M NaCl	140
Poly(acrylic acid)	TRIS (aq.)	633	25 °C	0.296	0.08 M	140
Poly(acrylic acid)	TRIS (aq.)	633	25 °C	0.195	0.08 M + 0.15 M NaCl	140
Poly(allylamine)	Sodium nitrate (aq.)	690	?	0.195	0.05 M	136

Substance	Solvent	Wavelength / nm	Temperature	dn/dc / mL/g	Remarks	Reference
Poly(benzyl acrylate)	Benzene	436	20 °C	0.062		14
Poly(benzyl acrylate)	DMF	436	20 °C	0.124		14
Poly(benzyl acrylate)	DMF	644	20 °C	0.116		14
Poly(benzyl acrylate)	MEK	436	20 °C	0.176		14
Poly(benzyl acrylate)	MEK	644	20 °C	0.1632		14
Poly(butadiene)	Cyclohexane	633	30 °C	0.111	1,4	14
Poly(butadiene)	Dioxane	546	25 °C	0.110		141
Poly(butadiene)	THF	488	30 °C	0.133		142
Poly(butadiene)	THF	633	23 °C	0.130	1,4	14
Poly(butadiene)	Toluene	?	?	0.040	cis-1,4	143
Poly(caprolactone)	Butanone	488	25 °C	0.108		144
Poly(caprolactone)	Chloroform	488	25 °C	0.060		144
Poly(caprolactone)	Ethylacetate	488	25 °C	0.110		144
Poly(caprolactone)	THF	488	25 °C	0.079		144
Poly(chloroprene)	Carbon tetrachloride	436	25 °C	0.0976		14
Poly(chloroprene)	MEK	436	25 °C	0.162		14
Poly(chloroprene)	n-Butylacetate	436	25 °C	0.146		14
Poly(chlorostyrene)	Toluene	632.8	25 °C	0.0844 - 0.0889	Poly(p-chlorostyrene)	145
Poly(cyanostyrene)	THF	632.8	25 °C	0.2233	Poly(p-cyanostyrene)	145
Poly(cyclopentadiene)	Benzene	546	21 °C	0.0394		14
Poly(cyclopentadiene)	Carbon tetrachloride	546	21 °C	0.125		14
Poly(ethenylformamide)	Sodium nitrate (aq.)	488	?	0.155	0.05 M	136
Poly(ethyl acrylate)	Acetone	436	20 °C	0.109		14
Poly(ethyl acrylate)	Benzene	546	25 °C	-0.042		14
Poly(ethyl acrylate)	Chloroform	546	25 °C	0.0363		14

Substance	Solvent	Wavelength / nm	Temperature	dn/dc / mL/g	Remarks	Reference
Poly(ethyl acrylate)	Dichloroethane	546	25 °C	0.023		14
Poly(ethyl acrylate)	DMF	546	25 °C	0.032		14
Poly(ethyl acrylate)	Ethyl acetate	546	25 °C	0.0916		14
Poly(ethyl acrylate)	MEK	488	30 °C	0.088		14
Poly(ethyl acrylate)	MEK	644	20 °C	0.0852		14
Poly(ethyl acrylate)	Water	?	25 °C	0.131		14
Poly(ethyl methacrylate)	2-Methoxyethanol	546	25 °C	0.076		141
Poly(ethyl methacrylate)	Ethylacetate	436	?	0.109		14
Poly(ethyl methacrylate)	MEK	546	23 °C	0.104		14
Poly(ethyl methacrylate)	Toluene	436	25 °C	-0.009		14
Poly(ethylene glycol)	Water	630	20 °C	0.134		146
Poly(ethylene terephthalate)	Butanone	488	25 °C	0.194		144
Poly(ethylene terephthalate)	Chloroform	488	25 °C	0.143		144
Poly(ethylene terephthalate)	Ethylacetate	488	25 °C	0.200		144
Poly(ethylene terephthalate)	THF	488	25 °C	0.165		144
Poly(ethylene)	1,2,4-Trichlorobenzene	436	135 °C	-0.125		14
Poly(ethylene)	1,2,4-Trichlorobenzene	632.8	135 °C	-0.104		147
Poly(ethylene)	1,2,4-Trichlorobenzene	632.8	135 °C	-0.104 +/- 0.001	HDPE	148
Poly(ethylene)	1,2,4-Trichlorobenzene	632.8	135 °C	-0.091 +/- 0.002	LDPE	148
Poly(ethylene)	1,2,4-Trichlorobenzene	632.8	145 °C	-0.104 +/- 0.002		149

Substance	Solvent	Wavelength / nm	Temperature	dn/dc / mL/g	Remarks	Reference
Poly(ethylene)	1,2,4-Trichlorobenzene	633	135 °C	-0.097		150
Poly(ethylene)	alpha-Chloronaphthalene	632.8	135 °C	-0.177 +/- 0.002	HDPE	148
Poly(ethylene)	Bromobenzene	436	135 °C	-0.101		14
Poly(ethylene)	Bromobenzene	633	135 °C	-0.083		14
Poly(ethylene)	n-Decan	633	135 °C	0.116		14
Poly(ethylene)	n-Decan	633	135 °C	0.112		14
Poly(ethylene)	o-Dichlorobenzene	632.8	135 °C	-0.056 +/- 0.002	HDPE	148
Poly(ethylene)	o-Dichlorobenzene	633	135 °C	-0.078		14
Poly(ethylene)	Tetralin	436	135 °C	-0.087		14
Poly(ethylene)	Tetralin	633	135 °C	-0.074		14
Poly(galacturonate acid)	Ammonium nitrate (aq.)	?	?	0.155	0.1 M	151
Poly(galacturonic acid)	NH4Cl (aq.)	?	?	0.1757	0.35 M	152
Poly(hydroxybutyrate)	2,2,2-Trifluoroethanole	?	35 °C	0.149		153
Poly(hydroxyethyl methacrylate)	2-Methoxyethanol	546	25 °C	0.095	Poly(2-hydroxyethyl methacrylate)	141
Poly(hydroxyethyl methacrylate)	Isopropanol	436	25 °C	0.125	Poly(2-hydroxyethyl methacrylate)	141
Poly(imide)	N-Methylpyrrolidone	632.8	25 °C	0.144		154
Poly(isobutylene)	THF	488	30 °C	0.125		142
Poly(isoprene)	THF	488	30 °C	0.129		142
Poly(isoprene)	Toluene	633	25 °C	0.108 +/- 0.004	Mw > 40 kDa, independent of branching ratio	155
Poly(isoprene)	Toluene	633	25 °C	0.104	Mn = 6.44 kDa	155
Poly(isoprene)	Toluene	633	25 °C	0.103	Mn = 2.61 kDa	155
Poly(isoprene)	Toluene	633	25 °C	0.093	Mn = 0.90 kDa	155

Substance	Solvent	Wavelength / nm	Temperature	dn/dc / mL/g	Remarks	Reference
Poly(isoprene)	Toluene	633	25 °C	0.098	Mn = 1.67 kDa	155
Poly(isoprene)	Toluene	633	25 °C	0.096	Mn = 1.22 kDa	155
Poly(isoprene)	Toluene	633	25 °C	0.106	Mn > 20.0 kDa	155
Poly(isoprene)	Toluene	633	25 °C	0.105	Mn = 10.1 kDa	155
Poly(methacrylic acid)	Ethanol	436	25 °C	0.154		14
Poly(methacrylic acid)	Methanol	546	25 °C	0.134		14
Poly(methacrylic acid)	Water	546	25 °C	0.175		14
Poly(methacrylic acid)	Water/Dioxan	546	25 °C	0.139	50/50 vol.	14
Poly(methoxystyrene)	Toluene	632.8	25 °C	0.0967	Poly(p-methoxy styrene)	145
Poly(methyl methacrylate)	Butanone	546	25 °C	0.112		141
Poly(methylacrylate)	Acetone	436	20 °C	0.113		14
Poly(methylacrylate)	Acetonitrile	436	25 °C	0.120		14
Poly(methylacrylate)	Acetonitrile	546	25 °C	0.118		14
Poly(methylacrylate)	Benzene	436	30 °C	-0.019		14
Poly(methylacrylate)	Dioxane	436	25 °C	0.0503		14
Poly(methylacrylate)	Dioxane	546	25 °C	0.0497		14
Poly(methylacrylate)	Ethylacetate	436	19.5 °C	0.0940		14
Poly(methylacrylate)	Ethylacetate	546	19.5 °C	0.0920		14
Poly(methylacrylate)	MEK	436	20 °C	0.0938		14
Poly(methylacrylate)	MEK	644	20 °C	0.0915		14
Poly(methylacrylate)	o-Chlorophenol	436	30 °C	-0.056		14
Poly(methylacrylate)	Tetrafluoropropanol	436	30 °C	0.126		14
Poly(methylacrylate)	Toluene	436	30 °C	-0.009		14

Substance	Solvent	Wavelength / nm	Temperature	dn/dc / mL/g	Remarks	Reference
Poly(methyl methacrylate)	Chloroform	632.8	?	0.0627		156
Poly(methylmeth acrylate)	Ethylbenzoate	633	40 °C	0.005		157
Poly(methylmeth acrylate)	Ethylbenzoate	633	23 °C	-0.008		157
Poly(methylmeth acrylate)	Ethylbenzoate	633	15 °C	0.000		157
Poly(methylmeth acrylate)	Ethylbenzoate	633	20 °C	0.001		157
Poly(methylmeth acrylate)	Ethylbenzoate	633	30 °C	0.003		157
Poly(methylmeth acrylate)	Ethylbenzoate	633	25 °C	0.002		157
Poly(methylmeth acrylate)	MEK	632.8	25 °C	0.113		158
Poly(methylmeth acrylate)	Methylbenzoate	633	23 °C	0.002		157
Poly(methylmeth acrylate)	o-Xylene	633	-2 °C	0.001		157
Poly(methylmeth acrylate)	o-Xylene	633	5 °C	0.003		157
Poly(methylmeth acrylate)	o-Xylene	633	15 °C	0.005		157
Poly(methylmeth acrylate)	o-Xylene	633	25 °C	0.007		157
Poly(methylmeth acrylate)	THF	488	30 °C	0.089		142
Poly(methylmeth acrylate)	THF	633	?	0.089		159
Poly(methylmeth acrylate)	THF	633	25 °C	0.086		14

Substance	Solvent	Wavelength / nm	Temperature	dn/dc / mL/g	Remarks	Reference
Poly(methylmeth acrylate)	Toluene	633	15 °C	0.012		157
Poly(methylmeth acrylate)	Toluene	633	25 °C	0.014		157
Poly(methylstyrene)	THF	632.8	25 °C	0.1326 - 0.1570	Poly(p-methylstyrene)	145
Poly(methylstyrene)	Toluene	632.8	25 °C	0.0967 - 0.0980	Poly(p-methylstyrene)	145
Poly(n-butyl acrylate)	Acetone	436	20 °C	0.112		14
Poly(n-butyl acrylate)	Benzene	546	30 °C	-0.0292		14
Poly(n-butyl acrylate)	Chlorobenzene	546	30 °C	-0.0525		14
Poly(n-butyl acrylate)	Cyclohexanone	488	30 °C	0.021		14
Poly(n-butyl acrylate)	Dioxane	488	30 °C	0.043		14
Poly(n-butyl acrylate)	n-Hexane	546	30 °C	0.0885		14
Poly(n-butyl acrylate)	THF	546	30 °C	0.0651		14
Poly(n-butyl methacrylate)	Acetone	436	25 °C	0.1249		14
Poly(n-butyl methacrylate)	Acetone	546	25 °C	0.1236		14
Poly(n-butyl methacrylate)	Benzene	436	25 °C	-0.023		14
Poly(n-butyl methacrylate)	Benzene	546	25 °C	-0.014		14
Poly(n-butyl methacrylate)	Bromobenzene	436	25 °C	-0.084		14
Poly(n-butyl methacrylate)	Bromobenzene	546	25 °C	-0.073		14
Poly(n-butyl methacrylate)	Carbon tetrachlorid	436	25 °C	0.026		14
Poly(n-butyl methacrylate)	Carbon tetrachlorid	546	25 °C	0.027		14

Substance	Solvent	Wavelength / nm	Temperature	dn/dc / mL/g	Remarks	Reference
Poly(n-butyl methacrylate)	DMF	633	20 °C	0.016		14
Poly(n-butyl methacrylate)	Isopropanol	436	23 °C	0.102		14
Poly(n-butyl methacrylate)	Isopropanol	546	23 °C	0.102		14
Poly(n-butyl methacrylate)	MEK	436	25 °C	0.103		14
Poly(n-butyl methacrylate)	MEK	546	25 °C	0.102		14
Poly(n-butyl methacrylate)	MEK	633	20 °C	0.097		14
Poly(n-butyl methacrylate)	Tetrafluoropropanol	633	20 °C	0.067		14
Poly(n-butyl methacrylate)	Toluene	436	25 °C	-0.017		14
Poly(n-butyl methacrylate)	Toluene	633	20 °C	-0.024		14
Poly(n-decyl methacrylate)	Cyclohexane	633	30 °C	0.054		14
Poly(n-decyl methacrylate)	Ethylacetate	436	25 °C	0.115		14
Poly(octadecyl methacrylate)	THF	488	30 °C	0.075		142
Poly(octene-1)	1,2,4-Trichlorobenzene	633	135 °C	-0.10		160
Poly(phenyleneethynylene)	CHCl3	?	?	0.136		161
Poly(phenyleneethynylene)	THF	?	?	0.163		161
Poly(propylene)	1,2,4-Trichlorobenzene	436	135 °C	-0.121		14

Substance	Solvent	Wavelength / nm	Temperature	dn/dc / mL/g	Remarks	Reference
Poly(propylene)	1,2,4-Trichlorobenzene	632.8	145 °C	-0.093 +/- 0.001		149
Poly(propylene)	1,2,4-Trichlorobenzene	633	135 °C	-0.102		14
Poly(styrene)	1,2,4-Trichlorobenzene	632.8	140 °C	0.052		162
Poly(styrene)	1,2,4-Trichlorobenzene	633	135 °C	0.046		160
Poly(styrene)	Benzene	436	25 °C	0.111		14
Poly(styrene)	Benzene	633	25 °C	0.105		14
Poly(styrene)	Bromobenzene	436	25 °C	0.043		14
Poly(styrene)	Bromobenzene	546	25 °C	0.042		14
Poly(styrene)	Carbon tetrachloride	436	25 °C	0.160		14
Poly(styrene)	Carbon tetrachloride	633	30 °C	0.156		14
Poly(styrene)	Chlorobenzene	436	20 °C	0.082		14
Poly(styrene)	Chlorobenzene	546	25 °C	0.079		14
Poly(styrene)	Chloroform	436	25 °C	0.161		14
Poly(styrene)	Chloroform	632.8	?	0.1608		156
Poly(styrene)	Chloroform	?	35°C	0.145		200
Poly(styrene)	Cyclohexane	?	25 °C	0.164-0.167		163
Poly(styrene)	Cyclohexane	436	25 °C	0.181		14
Poly(styrene)	Cyclohexane	514.5	40 °C	0.1787 +/- 0.0009		164
Poly(styrene)	Cyclohexane	514.5	30 °C	0.1728 +/- 0.0008		164
Poly(styrene)	Cyclohexane	514.5	20 °C	0.1700 +/- 0.0007		164
Poly(styrene)	Cyclohexane	633	?	0.163		14
Poly(styrene)	Decaline	436	25 °C	0.120		14
Poly(styrene)	Decaline	633	20 °C	0.120		14
Poly(styrene)	DMF	436	20 °C	0.1739		14

Substance	Solvent	Wavelength / nm	Temperature	dn/dc / mL/g	Remarks	Reference
Poly(styrene)	DMF	633	20 °C	0.165		14
Poly(styrene)	MEK	436	20 °C	0.229		14
Poly(styrene)	MEK	633	20 °C	0.214		14
Poly(styrene)	THF	488	30 °C	0.199		142
Poly(styrene)	THF	632.8	40 °C	0.184		147
Poly(styrene)	THF	632.8	30 °C	0.184		147
Poly(styrene)	THF	633	?	0.195		165
Poly(styrene)	Toluene	436	20 °C	0.112		14
Poly(styrene)	Toluene	546	25 °C	0.110		141
Poly(styrene)	Toluene	546	25 °C	0.109	linear and branched	166
Poly(styrene)	Toluene	632.8	25 °C	0.1028		145
Poly(styrene)	Toluene	633	25 °C	0.102	Mn = 4.00 kDa	155
Poly(styrene)	Toluene	633	25 °C	0.099	Mn = 1.72 kDa	155
Poly(styrene)	Toluene	633	25 °C	0.081	Mn = 0.725 kDa	155
Poly(styrene)	Toluene	633	25 °C	0.082	Mn = 0.932 kDa	155
Poly(styrene)	Toluene	633	25 °C	0.101	Mn = 2.90 kDa	155
Poly(styrene)	Toluene	633	?	0.105		165
Poly(styrene)	Toluene	633	20 °C	0.111		14
Poly(styrene)	Toluene	633	25 °C	0.107 +/- 0.001	Mn > 10.0 kDa	155
Poly(styrene)	Toluene	633	25 °C	0.105 +/- 0.002	Mw > 25 kDa, independent of branching ratio	155
Poly(styrene)	Toluene	633 nm	22 °C	0.108		167
Poly(styrene), sulfonated	Sodium nitrate (aq.)	630	?	0.195		168
Poly(styrene), sulfonated	Water	?	?	0.189		169

Substance	Solvent	Wavelength / nm	Temperature	dn/dc / mL/g	Remarks	Reference
Poly(styrene), sulfonated	Water	?	?	0.189		107
Poly(styrenesulfonate)	NaAc (aq.)	514.5	40 °C	0.18	0.001 M - 0.1 M	74
Poly(t-butyl acrylate)	MEK	488	30 °C	0.088		14
Poly(tetramethylene oxide)	THF	?	?	0.063 +/- 0.002		170
Poly(tetramethylene oxide)	THF	632.8	25 °C	0.066		171
Poly(urethane)	THF	?	?	0.23 - 0.25	Depending on composition	170
Poly(urethane)	THF	632.8	25 °C	0.68 - 0.90	Depending on composition	171
Poly(vinyl alcohol)	Sodium nitrate (aq.)	?	?	0.143	partially hydrolyzed	172
Poly(vinyl alcohol)	Sodium nitrate (aq.)	?	?	0.150	fully hydrolyzed	172
Poly(vinylacetate)	Acetone	436	25 °C	0.104		14
Poly(vinylacetate)	Acetone	546	25 °C	0.104		14
Poly(vinylacetate)	Benzene	546	30 °C	-0.0225		14
Poly(vinylacetate)	Chlorobenzene	436	25 °C	-0.049		14
Poly(vinylacetate)	Chlorobenzene	546	30 °C	-0.0426		14
Poly(vinylacetate)	MEK	436	25 °C	0.080		14
Poly(vinylacetate)	MEK	632	?	0.075		14
Poly(vinylacetate)	Methanol	436	25 °C	0.130		14
Poly(vinylacetate)	Methanol	633	?	0.119		14
Poly(vinylacetate)	THF	610	24 °C	0.0480		173
Poly(vinylacetate)	THF	632	25 °C	0.054		14
Poly(vinylacetate)	Toluene	610	24 °C	-0.0183		173
Poly(vinylalcohol)	Water	436	30 °C	0.168		14

Substance	Solvent	Wavelength / nm	Temperature	dn/dc / mL/g	Remarks	Reference
Poly(vinylalcohol)	Water	546	30 °C	0.164		14
Poly(vinylalcohol)	Water/n-Propanol	436	40 °C	0.145		14
Poly(vinylalcohol)	Water/n-Propanol	436	25 °C	0.134	98/2 wt.	14
Poly(vinylalcohol)	Water/n-Propanol	436	70 °C	0.158		14
Poly(vinylalcohol)	Water/n-Propanol	546	70 °C	0.160		14
Poly(vinylalcohol)	Water/n-Propanol	546	40 °C	0.147		14
Poly(vinylchloride)	Acetone	546	20 °C	0.138		14
Poly(vinylchloride)	Cyclohexanone	436	20 °C	0.0723		14
Poly(vinylchloride)	Cyclohexanone	633	20 °C	0.075		14
Poly(vinylchloride)	Dioxane	436	25 °C	0.107		14
Poly(vinylchloride)	Dioxane	586	25 °C	0.107		14
Poly(vinylchloride)	DMF	436	25 °C	0.0816		14
Poly(vinylchloride)	DMF	578	25 °C	0.0813		14
Poly(vinylchloride)	THF	436	20 °C	0.1124		14
Poly(vinylchloride)	THF	632.8	23 °C	0.105		64
Porin	Imidazole buffer (aq.)	633	25 °C	0.303	in presence of 0.1% octaethyleneglycol n-dodecylether	7
Porin	Phosphate buffer (aq.)	633	25 °C	0.328	in presence of SDS	131
Protropin	Acetonitril/water	630	20 °C	0.149	80:20 - 20:80	62
Protropin	Phosphate buffer (aq.)	630	20 °C	0.160		62
Protropin	Phosphate buffer (aq.)	633	?	0.166		32
Protropin	Protein buffer	630	20 °C	0.160		62
Pullulan	DMAc/0.5% LiCl	?	?	0.163		41
Pullulan	LiCl (aq.)	?	?	0.147	0.1 M	174
Pullulan	NaCl (aq.)	?	?	0.145		175

Substance	Solvent	Wavelength / nm	Temperature	dn/dc / mL/g	Remarks	Reference
Pullulan	Phosphate buffer (aq.)	633	30 °C	0.137		37
Pullulan	Sodium nitrate (aq.)	630	?	0.152	0.01 M - 1 M	176
Pullulan, oxidized	Sodium nitrate (aq.)	630	?	0.143	0.01 M - 1 M	176
Ribonuclease A	Imidazole buffer (aq.)	633	25 °C	0.187	in presence of 0.1% octaethyleneglycol n-dodecylether	7
Ribonuclease A	Phosphate buffer (aq.)	633	?	0.174		32
Ribonuclease	Water	546	25 °C			
Ribonuclease	Water, phosphate buffer	436	20 °C	0.187	pH 7.0	85
Rubber	Chloroform	546	25 °C	0.1		177
Rubber	Cyclohexane	546	25 °C	0.1305		178
Rubber	n-Hexane	546	25 °C	0.1886		177
Rubber	THF	436	20 °C	0.128		179
Rubber	Toluene	546	25 °C	0.0308		177
Schizophyllan	LiNO3 (aq.)	?	?	0.143	0.1 M	180
Schizophyllan	Water	546	25 °C	0.145		181
Scleroglucan	Sodium nitrite (aq.)	?	?	0.145		182
Shizophyllan	Aqueous solution	?	?	0.145		83
Sodium carboxymethyl amylose	0.35 M NaCl (aq.)	546	35 °C	0.1325		183
Sodium carboxymethyl cellulose	NaCl (aq.)	546	?	0.136		184
Sodium cellulose xanthate	1.0 N NaOH (aq.)	546	?	0.425	D.S. 0.91	185
Src homology 2	Phosphate buffer (aq.)	?	?	0.185		186
Starch	Aqueous solution	?	?	0.146		12

Substance	Solvent	Wavelength / nm	Temperature	dn/dc / mL/g	Remarks	Reference
Starch	Water	?	?	0.151		187
Starch	DMSO (+50mM LiBr)	?	?	0.066		201
Thyroglobulin	Water	546	23 °C	0.1949		188
Tropomyosin (guanidated)	Water	436	25 °C	0.188		189
Tropomyosin	Water	546	?	0.18		190
Trypsin	Water	546	?	0.193		191
Trypsinogen	BIS-TRIS (aq.)	633	?	0.171 +/- 1.75%	0.005 M	192
Xanthan	Ammonium nitrate (aq.)	633	?	0.155		193
Xanthan	$LiNO_3$ (aq.)	?	?	0.143	0.1 M	180
Xylan	DMSO	?	?	0.064		194
Xylan	Ethyl acetate	436	?	0.97		195

1 Steiner, R. F. Laki. K. and Spicer, S., J. Polymer Sci. 8, 23-33 (1952).

2 Ooi, T. J., Phys. Chem. **64,** 984-988 (1960).

3 Mommaerts, W. F. H. M., J. Biol. Chem. **198,** 445-457 (1952).

4 Wasserman, A. and Harkness, M. L. R., Nature **173,** 167-168 (1954a).

5 Wasserman, A. and Harkness, M. L. R., J. Chem. Soc. 1344-1356 (1954b).

6 Gergely, J., J. Biol. Chem. **220,** 917-926 (1956).

7 Maezawa, S., Hayashi, Y. Biochim. Biophys. Acta, **747,** 291 (1983).

8 Buchner, P., Cooper, R. E. and Wasserman, A., J. Chem. Soc. 3974-3983 (1961).

9 Putzeys, P. and Brosteaux, J., Bull. Soc. Chem. Biol. **18,** 1681-1703 (1936).

10 Kratohvil, J., Ajdukovic, D.J.., Croat. Chem. Acta **30,** 173-180 (1958).

11 Tomski, S. J., Murphy, R. M., Arch. Biochem. Biophys. **294,** 630-638 (1992).

12 Park, J. T., Rollings, J. E., , Biotechnologa and Bioengineering, **44,** 792 (1994).

13 Millard, M. M., Dintzis, F. R., , Cereal Chemistry, **74,** 687 (1997).

14 Huglin, M. B., *Specific refractive index increments of polymers in dilute solution*, **in:** Brandrup, J., Immergut, E. H., Polymer Handbook 3rd Edition, (John Wiley & Sons, New York, 1989).

15 Erlander, S. R. and Griffin, H. L., Stärke **19,** 134-138 (1967a).

16 Stacy, C. J. and Foster, J. F., J. Polymer Sci. **20,** 57-65 (1956).

17 Witnauer, L. P., Senti, F. R. and Stern, M. D., J. Polymer Sci. **16,** 1-17 (1955).

18 Greenwood, C. T. and Hourston, D. J., Stärke **19,** 243-246 (1967).

19 Jordan, R. C. and Brant, D. A., Macromolecules **13,** 345 (1980).

20 Roger, P., Colonna, PCarbohydr. Polym., **21,** 83 (1993).

21 Griffin, H. L., Erlander, S. R. and Senti, F. R., Stärke **19,** 8-17 (1967).

22 Paschall, E. F. and Foster, J. F., J. Polymer Sci. **9,** 85-92 (1952).

23 Banks, W. and Greenwood, C. T., Stärke **19,** 394-398 (1967).

24 Cowie, J. M. G. and Maconnachie, A., Eur. Polym. J. **10,** 367 (1974).

25 Burchard, W. and Husemann, E., Makromol Chem. **44,** 358-387 (1961).

26 Tomimatsu, Y., Palmer, K. J., Goodban, A. E. and Ward, W. H., J. Polymer Sci. **36,** 129-139 (1959).

27 Goring, D. A. I. and Johnson, P., Trans. Faraday Soc. **48,** 367-379 (1952).

28 Brand, B. P., Goring, D. A. I. and Johnson, P., Disc. Faraday Soc. **51,** 872-876 (1955).

29 Hayashi, Y., Takagi, T., *(More authors!)* Biochim. Biophys. Acta, **748,** 153 (1983).

30 Hayashi, Y., Mimura, K*(More authors!)* Biochim. Biophys. Acta, **983,** 217 (1989).

31 Astafieva, I. V., Eberlein, G. A., *(More authors!)*, J. Chromatogr., **740,** 215 (1996).

32 Stuting, H. H., Krull, I. S., , Anal. Chem., **62,** 2107 (1990).

33 Flapper, W., van den Oetelaar, P. J. M., *(More authors!)* Clin. Chem., **32,** 363 (1986).

34 Sowinski, R., Oharenko, L. and Koenig, V. L., J. Am. Chem. Soc. **81,** 6193-6198 (1959).

35 Casassa, E. F., J. Phys. Chem. **60,** 926-933 (1956).

36 Odaka, M., Inagaki, F.. Protein, Nucleic Acid & Enzyme, **39,** 1161 (1994).

37 Bednar, B., Hennessey, J. P., Carbohydr. Res., **243,** 115 (1993).

38 Picton, L., Merle, L., , Int. J. Polymer Analysis & Characterization, **2,** 103 (1996).

39 Capron, I., Yvon, M., *Molecular size analysis of capsular polysaccharide preparations from Streptococcus pneumoniae*, Food Hydrocolloids, **10,** 239 (1996).

40 Robertson, T. B., J. Biol. Chem. **8,** 507-511 (1910-1911 b).

41 Striegel, A. M., Timpa, J. D., **in:** Potschka, M., Dubin, P. L., Strategies in Size Exclusion Chromatography (ACS Symposium Series, Washington, D. C., 1996).

42 Marx-Figini, M. and Penzel, E., Makromol. Chem. **87,** 307-315 (1965).

43 Kamide, K., Saito, M., Abe, T., Polym. J. **13,** 421 (1981).

44 Tsvetkov, V. N., Rjumtsev, E. I., Andreeva, L.N., Pogodina, N. V., Lavrenko, P. N. and Kutsenko, L. I., Eur. Polym. J. **10,** 563 (1974).

45 Suzuki, H., Miyazaki, Y. and Kamide, K., Eur. Polym. J. **16,** 703 (1980).

46 Schulz, G. V. and Penzel, E., Makromol. Chem. **112,** 260-280 (1968).

47 Badger, R. M. and Blaker, R. H., J. Phys. Colloid Chem. **53,** 1056-1069 (1949).

48 Casay, G. A., George, N., *(More authors).*, , J. Polym. Sci., **33,** 1537 (1995).

49 Sharples, A. and Swinton, F. L., J. Polymer Sci. **50,** 53-64 (1961).

50 Krigbaum, W. R. and Sperling, L. H., J. Phys. Chem. **64,** 99-108 (1960).

51 Ohman, J., Arkiv. Kem. **31,**125-136 (1969).

52 Hunt, M. L., Newman, S., Scheraga, H. A. and Flory, P. J., J. Phys. Chem. 60, 1278-1290 (1956).

53 Tait, C. W., Vetter, R. J., Swanson, J. M. and Debye, P., J. Polymer Sci. 7, 261-276 (1951).

54 Rinaudo, M., Milas, M., *(More authors).*, Int. J. Biol. Macromol., **15,** 281 (1993).

55 Beri, R., Walker, G. J., *(More authors).*,, Carbohydr. Res., **238,** 11 (1993).

56 Arakawa, T., Langley, K. E., Kameyama, K., Takagi, T., Anal. Biochem. **203,** 53-57. (1992) (TSK Model RI-8011 differential refractometer).

57 Sarfare, P. S., Kegeles, G. and Kwon-Rhee, S. J., Biochem. **5,** 1389-1393 (1966).

58 Mhatre, R. M., Krull, L. S., J. Chromatogr. **591,** 139-148 (1992) (KMX-16 633nm laser based differential refractometer).

59 Kock, R., Greiling, H., Fresenius J. Anal. Chem. **343,** 76-77 (1992).(Milton Roy refractive index detector)

60 Taravel, M. N., Domard, A.. Biomaterials, **14,** 930 (1993).

61 Timasheff, N. and Tinoco, I., Arch. Biochem. Biophys. 66, 427-437 (1957).

62 Stuting, H. H., Krull, I. S., J. Chromatogr., **539,** 91 (1991).

63 Guinand, S., J. Polymer Sci. **29,** 497-503 (1958).

64 McConnell, M. L., Am. Lab., **10 (5),** 63, (1978).

65 Jackson, C., Nilsson, L. M., Wyatt, P. J., J. Appl. Polym. Sci. **43,** 99 (1989).

66 Vink, H. and Dahlstrom, G., Makromol. Chem. **109,** 249-252 (1967).

67 Antonini, E., Bellelli, L., Bruzzesi, M. R., Caputo, A., Chiancone, E. and Rossi, ?, Fanelli, A., Biopolymers **2,** 27-34 (1964).

68 Nicolai, T., van Dijk, L., *(More authors).*,, J. Chromatogr., **389,** 286 (1987).

69 Schmidt, C. L. A., J. Biol. Chem. **23,** 487-493 (1915).

70 Perlman, G. E. and Longworth, L. G., J. Am. Chem. Soc. **70,** 2719-2724 (1948).

71 Scherer, P. C., Tannenbaum, A. and Levi, D. W., J. Polymer Sci. **43,** 531-535 (1960).

72 Neely, W. B., J. Polymer Sci. **A-1,** 311-320 (1963).

73 Kapoor, V. P., Milas, M., *(More authors).*, Carbohydr. Polym., **25,** 79 (1994).

74 Bowman, W. A., Rubinstein, M., *(More authors).*, Macromolecules, **30,** 3262 (1997).

75 Veis, A. and Anesey, J., J. Phys. Chem. **63,** 1720-1725 (1959).

76 Gouinlock, E. V., Jr., Flory, P. J. and Scheraga, H. A., J. Polymer Sci. **16,** 383-395 (1955).

77 McMeekin, T. M., Groves, M. L. and Hipp, N. J., Advan. Chem. Ser. **44,** 54-66 (1964).

78 Robertson, T. B. and Greaves, J. E., J. Biol. Chem. **9,** 181-184 (1911).

79 Adair, G. S. and Robinson, M. E., Biochem. J. **24,** 933-1011 (1930).

80 Rossi-Fanelli, A., Antonini, E. and Caputo, A., J. Biol. Chem. **234,** 2906-2910 (1959).

81 Knuckles, B. E., Yokoyama, W. H*(More authors).*, Cereal. Chem., **74,** 599 (1997).

82 Gomez, C., Navarro, A., *(More authors).*, Carbohydr. Polym., **32,** 7 (1997).

83 Williams, D. L., Pretus, H. A., *(More authors).*, International GPC Symposium '91 Waters (Division of Millipore), 1991.

84 Dandliker, W. B. and Fox, J. B., Jr., J. Biol. Chem. **214,** 275-283 (1955).

85 Jaenicke, R., Schmid, D. and Knof, S., Biochem. **7,** 919-926 (1968).

86 Putzeys, P. and Verhoeven, L., Rec. Trav. Chim. **68,** 817-826 (1949).

87 Holme, T., Laurent, T. and Palmstierna, H., Acta Chem. Scand. **11,** 757-762 (1957).

88 Greenwood, C. T. and Hourston, D. J., Polymer **16,** 474 (1975)

89 Koleske, G. V. and Kurath, S. F., J. Polymer Sci. **A-2,** 4123-4149 (1964).

90 Swenson, H. A., Kaustinen, H. M., Kaustinen, O. A. and Thompson, N. S., J. Polymer Sci. A-2, **6,** 1593-1606 (1968).

91 Redfield, A. C., Biol. Rev. **9,** 175-212 (1934).

92 Herskovits, T. T., Russell, M. W., Biochemistry **23,** 2812-2819 (1984) (Wood mfg. Co. photometer of Brice's design).

93 Herskovits, T. T., Mazella, L. J., Villanueva, G. B., Biochemistry **24,** 3862-3870 (1985) (Wood manufacturing Co. Instrument of Brice's design, 436nm).

94 Herskovits, T. T., Villaneuva, G. B., Biochemistry **25,** 931-939 (1986) (Wood manufacturing Co. Instrument of Brice's design, 436nm).

95 Zal, F., Lallier, F. H., *(More authors)*., J. Biol. Chem., **271,** 8869 (1996).

96 Noren, I. B. E., Ho, C., Casassa, E. F., Biochemistry **10,** 3222-3229 (1971) (Brice-Phoenix)

97 Knobloch, J. E., Shaklee, P. N. Anal. Biochem., **245,** 231 (1997).

98 Barlow, G. T., Sanderson, N. D. and McNeill, P. G., Arch. Biochem. Biophys. **94,** 518-525 (1961).

99 Peitzsch, R. M., Burt, M. J., Reed, W. F., Macromolecules, **25,** 806 (1992).

100 Halwer, M., Nutting, G. C. and Brice, B. A., J. Am. Chem. Soc. **73,** 2786-2790 (1951).

101 Stuting, H. H., Krull, I. S., J. Chromatogr., **539,** 91 (1991).

102 DeFelipis, M. R., Kilcomons, M. A., *(More authors)*.,, Biochim. Biophys. acta, **1247,** 35 (1995).

103 Gombotz, W. R., Pankey, S. C*(More authors)*., Pharm. Res., **11,** 624 (1994).

104 Perlman, G. E. and Longworth, L. G., J. Am. Chem. Soc. **70,** 2719-2724 (1948).

105 Reed, W. F., Macromol. Chem. Phys., **196,** 1539, (1995).

106 Ghosh, S., Kobal, I., *(More authors)*., Macromolecules, **26,** 4685 (1993).

107 Norwood, D. P., Benmouna, M., *(More authors)*.,, Macromolecules, **29,** 4293 (1996).

108 Rymden, R. and Calfors, J., Polym. Commun. **24,** 114 (1983).

109 Granath, K. A., Strömberg, R. and de Belder, A. N., Stärke, 251-256 (1969).

110 Harrap, B. S. and Woods, E. F., Austral. J. Chem. **11,** 581-591 (1958a).

111 Doty, P., Gellert, M., Rabinovitch, B., J. Am. Chem. Soc. **74,** 2065-2069 (1952).

112 Laki, K. and Steiner, R. F., J. Polymer Sci. **8,** 457-465 (1952).

113 Viebke, C., Borgström, J., *(More authors)*.,, Carbohydr. Polym., **27,** 145 (1995).

114 Singh, S. K., Jacobsson, S. P., Carbohydr. Polym., **23,** 89 (1994).

115 Harrap, B. S. and Woods, E. F., Austral. J. Chem. **11,** 592-606 (1958b).

116 Williams, D. L., Pretus, H. A*(More authors)*.,, J. Liq. Chrom., **15,** 2297 (1992).

117 Stuting, H. H., Krull, L. S., Anal. Chem. **62,** 2107-2114 (1990) (KMX-16 633nm laser based differential refractometer).

118 Halwer, M. and Brice, B. A., J. Colloid Sci. **4,** 439-440 (1949).

119 Robinson, N., Trans. Faraday Soc. **56,** 1260-1264 (1960).

120 Brand, B. P., Quoted in Goring and Johnson (1952).

121 Gupta, P. R. and Goring, D. A. I., Canad. J.Chem. **38,** 270-279 (1960).

122 Armstrong, S. H., Budka, M. J. E., Morrison, M. J. E. and Hasson, M., J. Am. Chem. (1949).

123 van Zanten, J., Monbouquette, H. GJ. Coll. Int. Sci., **146**, 330 (1991).

124 Bruzzesi, M. R., Chiancone, E. and Antonini, E., Biochem. **4**, 1796-1800 (1965).

125 Mackie, W. and Sellen, S. B., Polymer **10**, 621-632 (1969).

126 Mathews, M. B., Biochim. Biophys. Acta **35**, 9-17 (1959).

127 Gellert, M. F. and Englander, S. W., Biochem. **2**, 39-42 (1963).

128 Ellenbogen, E., Iyengar, R., Stern, H. and Olson, R. E., J. Biol. Chem. **235**, 2642-2648 (1960).

129 Kay, C. M. and Pabst, H. F., J. Biol. Chem. **237**, 727-732 (1962).

130 Ogawa, T., Sakai, M., , J. Polym. Sci. Polym. Phys. Ed., **23**, 1109 (1985).

131 Kameyama, K., Nakae, T., *(More authors).*,, Biochim. Biophys. Acta, **706**, 19 (1982).

132 Kronman, M. G. and Stern, M. D., J. Phys. Chem. **59**, 969-973 (1955).

133 Kopperschläger, G., Naumann, M., , Int. J. Biol. Chem., **2**, 269 (1997).

134 Iso, N., Mizuno, H., Saito, T., Nitta, N. and Yoshikazi, K., Bull. Chem. Soc. Japan **50**, 2892 (1977).

135 Kenney, W., Haniu, M., *(More authors).*,, J. Biol. Chem., **269**, 12351 (1994).

136 Nagy, D. J, J. Appl. Polym. Sci., **59**, 1479, (1996).

137 Siemens, R., Cotts, P. M., , International GPC Symposium '91 Waters (Division of Millipore), 1991.

138 Pille, L., Jhingran, A. G., *(More authors).*,, Polymer, **37**, 2459 (1996).

139 Hunkeler, D., Hamielec, A. E., , J. Appl. Polym. Sci., **35**, 1603 (1988).

140 Brüssau, R., Goetz, N*(More authors).*,, Tenside Surf. Det., **28**, 396 (1991).

141 Kratochvil, P., *Classical Light Scattering from Polymer Solutions*, **in:** Jenkins, A. D., Polymer Science Library 5, (Elsevier, Amsterdam, 1987).

142 Jackson, C., Chen, Y.-J., *(More authors).*,, J. Appl. Polym. Sci., **61**, 865 (1996).

143 Dayal, U., Mehta, S. K., J. Liquid Chrom., **17**, 303 (1994).

144 Wu, C., Woo, K. F., *(More authors).*, Macromolecules, **27**, 6055 (1994).

145 Dammert, R., Jussila, M*(More authors).*,, Polymer, **38**, 6273 (1997).

146 Hasse, H., Kany, H.-P*(More authors).*,, Macromolecules, **28**, 3540 (1995).

147 Jeng, L., Balke, S. T*(More authors).*,, J. Appl. Polym. Sci., **48**, 1359 (1993).

148 MacRury, T. B., McConnell, M. L.,

149 J. Appl. Polym. Sci., **24**, 651 (1979).

149 Grinshpun, V., Rudin, A., , Makromol. Chem., Rapid Comm., **6**, 219 (1985).

150 Housaki, T., Satoh, K., , Makromol. Chem., Rapid Comm., **9**, 257 (1988).

151 Malovikova, A., Rinaudo, M., *(More authors).*, Carbohydr. Polym., **22**, 87 (1993).

152 Cheng, L., Kindel, P. K., Carbohydr. Res., **301**, 205 (1997).

153 Sim, S. J., Snell, K. D., *(More authors).*,, Nature Biotechnol., **15**, 63 (1997).

154 Kim, S. H., Cotts, P. M*(More authors).*, J. Polym. Sci, Polym. Phys. Ed., **30**, 177 (1992).

155 Hadjichristidis, N., Fetters, L. J., , J. Polym. Sci., **20**, 2163 (1982).

156 Ouano, A. C., Kaye, W., , J. Polym. Sci., **12**, 1151 (1974).

157 Kent, M. S., Tirrell, M. (More authors) (More authors), Polymer, **32**, 314 (1991).

158 Dotson, N. A., Diekmann, T., (More authors) *Non-idealities exhibited by cross-linking free-radical copolymerization*, Polymeric Materials Science and Engineering Meeting, 1992. Town, Publisher?

159 Radke, W., Simon, P. F. W., (More authors) Macromolecules, **29**, 4926 (1996).

160 Rooney, J. G., Ver Strate, G., (More authors), **in:** Cazes, J., Liquid Chromatography of Polymers and Related Materials III, (Marcel Dekker, Inc., New York, 1981).

161 Cotts, P. M., Swager, T. M., (More authors) Macromolecules, **29**, 7328 (1996).

162 Kaspárková, V., Ommundsen, E., , Polymer, **34**, 1765 (1993).

163 Zhong, X. F., Eisenberg, A., , Macromolecules, **27**, 1751 (1994).

164 Philipps, Th., Borchard, WEur. Polym. J., **26**, 1289 (1990).

165 Frater, D. J., Mays, J. W., (More authors) J. Polym. Sci, Polym. Phys. Ed., **35**, 141 (1997).

166 Procházka, O., Tuzar, Z., (More authors) Makromol. Chem., **184**, 2097 (1983).

167 Yunan, W., Zhongade, X., (More authors) J. Appl. Polym. Sci., **49**, 967 (1993).

168 Thielking, H., Kulicke, W.-M., Anal. Chem., **68**, 1169 (1996).

169 Reed, W. F., *Coupled Multiangle Light-Scattering and Viscosimetric Detectors for Size Exclusion Chromatography with Application to Polyelectrolyte Characterization*, **in:** Strategies in Size Exclusion Chromatography, (ACS Symposium Series, Washington, D. C., 1996).

170 Lee, D., Speckhard, T. A., (More authors), Macromolecules, **19**, 2383 (1986).

171 Zigon, M., Mirceva, A., (More authors) J. Liquid. Chrom., **16**, 3813 (1993).

172 Nagy, D. J. Am. Lab., **27 (4)**, 47J, (1995).

173 Hamielec, A. E., Ouano, A. C., (More authors) J. Liq. Chrom., **1**, 527 (1978).

174 Picton, L., Mocanu, G., (More authors), Carbohydr. Polym., **28**, 131 (1995).

175 Jackson, C., Nilsson, L. M., (More authors), J. Appl. Polym. Sci., **43**, 99 (1989).

176 de Nooy, A. E. J., Besemer, A. C(More authors) Macromolecules, **29**, 6541 (1996).

177 Schulz, G. V., Altgelt, K. and Cantow, H.-J., Makromol. Chem. **21**, 13-36 (1956).

178 Altgelt, K. and Schulz, G. V., Makromol Chem. **36**, 209-219 (1959).

179 Vavra, J., J. Polymer Sci. C, **16**, 1103-1111 (1967).

180 Capron, I., Grisel, M(More authors), Int. J. Polymer Analysis & Characterization, **2**, 9 (1995).

181 Norisuye, T., Yanaki, T. and Fujita, H., J. Polym. Sci. Polym. Phys. Edn. **18**, 547 (1980).

182 Pretus, H. A., Ensley, H. E., (More authors), J. Pharm. Exp. Ther., **257**, 500 (1991).

183 Patel, J. R., Patel, C. K. and Patel, R. D., *Starke* **19**, 330-335 (1967).

184 Trap, H. J. L. and Hermans, J. J., J. Phys. Chem. **58**, 757-761 (1954).

185 Das, B. and Choudhury, P. K., J. Polymer Sci. A-1, **5**, 769-777 (1967).

186 Farrow, N. A., Muhandiram, R., (More authors), Biochemistry, **33**, 5984 (1994).

187 Hanselmann, R., Ehrat, M., (More authors) Starch, **47**, 345 (1995).

188 Edelhoch, H., J. Biol. Chem. **235**, 1326-1334 (1960).

189 Kay, C. M. and Bailey, K., Biochim. Biophys. Acta **40**,149-156 (1960).

190 Ooi, T., Mihashi, K. and Kobayashi, H., Arch. Biochem. Biophys. **98**, 1-11 (1962).

191 Steiner, R. F., Arch. Biochem. Biophys. **49**, 71-92 (1954).

192 Mhatre, R. M., Krull, I. S. J. Chromatogr., **591**, 139 (1992).

193 Milas, M., Reed, W. F. Int. J. Biol. Macromol., **18**, 211 (1996).

194 Goring, D. A. I. and Timell, T. E., J. Phys. Chem. **64**, 1426-1430 (1960).

195 Mackie, W. and Sellen, D. B., Biopolymers **10**, 1 (1971).

196 Lavrenko, P.N., Linow, K.J. and Gornitz, E. **In:** Analytical Ultracentrifugation in Biochemistry and Polymer Science 558 (1992).

197 Hoogendam, C.W., de Keizer, A., Cohen Stuart, M. A., Bijsterbosch, B. H., Smit, J. A. M., van Dijk, J. A. P. P., van der Horst, P. M. and Batelaan, J. G., Macromolecules, 31, 6297 (1998).

198 Wittgren, B., Borgström, J., Piculell, L., Wahlund, K.-G., Biopolymers, 45, 85 (1998).

199 Wagoner, D. B., Christman, R. F. Acta Hydrochim. Hydrobiol., 26, 191 (1998).

200 Collins, J. E., Fraser, C. L. Macromolecules, 31, 6715 (1998).

201 Yokoyama, W., Renner-Nantz, J. J., Shoemaker, C. F., Cereal. Chem., 75, 530 (1998).

Appendix II

Publications